PHYSICAL REGULATION OF LAND-OCEAN CNP FLUX AND RELATIONSHIPS TO MACROALGAL BLOOMS ACROSS COASTAL ZONES OF MAUI, HAWAI'I

A DISSERTATION SUBMITTED TO THE GRADUATE DIVISION OF THE UNIVERSITY OF HAWAI'I IN PARTIAL FULFILLMENT OF THE REQUIREMENTS FOR THE DEGREE OF

DOCTOR OF PHILOSOPHY

IN

OCEANOGRAPHY

DECEMBER 2011

By
Iuri Herzfeld

Dissertation Committee:

Francis J. Sansone, Chairperson
Margaret A. McManus
Kathleen C. Ruttenberg
Fred T. Mackenzie
Celia M. Smith

DEDICATION

To Lenna

ACKNOWLEDGEMENTS

I would like to thank Frank Sansone whom without this path of my life's journey would have not been possible. Thank you for providing me with a parent-like hand throughout the process of learning about the present. I thank you mostly for helping me develop awareness of my actions and wisdom.

I also like to extend my most sincere thanks to the rest of my PhD committee: Margaret McManus, Celia Smith, Kathleen Ruttenberg, and Fred Mackenzie for believing in my promises. During this journey I have experienced many different kinds of emotions, and I thank you for your encouraging words and wise advice during times of transition.

I like to thank my entire family for always being supportive of my chosen life path. I know you know my essence will never change, even during changing life conditions. It has been your continued reassurance that has helped me trust myself throughout this process. I would like to specially thank my mother and father both of who have always served as guiding lights to the eternal.

I would also like to thank my dear friends Rachel Kennison, David Harris, and Kelkyra Fragueiro, all of whom appeared in my life like a guiding light in a moment of darkness. Thank you for being such wonderful friends, here and now, always.

Lastly, I would like to thank Ilsa Kuffner for nourishing our daughter, Lenna Marie Herzfeld, throughout the last few years with minimal financial contributions from me, and for your understanding and support during the early stages of my PhD experience. Mostly I thank you for being such a good mother. Knowing that our little one is safe and loved while I am away always gives me peace in my heart. Lenna, you are my sunshine, and I thank you for proving to me that the cosmos dance.

Shalom

L'chaim

ABSTRACT

Physical factors can enhance the exchange between dissolved inorganic nutrient reservoirs within the coastal zone and can control their residence times. This dissertation aims to understand the contribution of sedimentary nutrient subsidies to rapid macroalgal growth being experienced off West Maui, Hawaii. Field-based sediment porewater data are used with a porefluid hydrodynamic model to estimate groundwater nutrient fluxes; these results indicate that, under typical wave heights, 100 % of the macroalgal-biomass P and less than <5 % of the N can be supplied by sedimentary pools. Sedimentary N flux must have either been supplemented by other sources (e.g., N-fixation, or wastewater inputs), or retained for longer time periods within the coastal zone. Historical records of wind, rainfall, and wave data, used as proxies for water residence time and groundwater nutrient inputs to our site, suggest that episodes of high macroalgal growth are the result of increased nutrient residence time within the region, inversely related to the Pacific Decadal Oscillation Index.

Moreover, time-series data on dissolved nutrient concentrations were collected along nine distinct coastal sites along the southwest facing shorelines of Maui, Hawaii that have historically experienced different degrees of chronic macroalgal growth. Near-synchronous time-series measurements performed along these sites demonstrated that the spatiotemporal variability of dissolved nutrients originate from heterogeneous interactions between tides and coastal geomorphology, which regulate wave penetration and subsequently the transport and discharge of submarine groundwater to the coastal zone. The results indicate that nutrient enrichments within the coastal zone are temporally variable, but spatially coherent, along human-impacted sections of the coast.

Lastly, this dissertation explores the temporally-heterogeneous interactions between wind, waves, currents, and tides on groundwater flux, water residence time, and net ecosystem metabolism (NEM) at two coastal sites in Maui, Hawaii. Groundwater flux, CO_2 flux, water residence time, and NEM are highly variable over hourly timescales and (on average) over different times of the year. It is evident that the net autotrophy observed at our Kihei site is the result of enhanced discharge of nutrient-rich groundwater to the coastal zone.

TABLE OF ABBREVIATIONS

PO_4	–	PO_4^{3-}
Si	–	$Si(OH)_4$
NH_4	–	NH_4^+
NO_2	–	NO_2^-
NO_3	–	NO_3^-
DIN	–	NO_2+NO_3+NH_4
LOICZ	–	Land-Ocean Interactions in the Coastal Zone
SWI	–	Sediment Water Interface
CNP	–	Carbon, Nitrogen, and Phosphorus
SGD	–	Submarine Groundwater Discharge
BI	–	Bloom Index
KWWRF	–	Kihei Wastewater Reclamation Facility
PCA	–	Principal Components Analysis
DO	–	Dissolved Oxygen
PAR	–	Photosynthetically Active Radiation

TABLE OF CONTENTS

LIST OF TABLES

sample means not significantly different from each other at the 0.05 significance level.

Table 3.3 - Water currents along the proximal coastal zone. Negative current denotes either south or west flows depending on the site orientation along the coast. AS= along-shore current velocity, XS= cross-shore current velocity.

Table 3.4 –Mean (stdev) of dissolved nutrient (in μM) and salinity data from synoptic diurnal observations. Superscripts denote results of Student's t-test multiple comparisons: entries with the same letter have sample means not significantly different from each other at the 0.05 significance level. †Data from Herzfeld (2011), * Data from Hunt (2006).

Table 3.5 – Summary of sites with significant correlation coefficients (r) between measured variables at alpha = 0.05. An underlined site denotes a significant negative correlation coefficient.

Table 3.6 – Radionuclide data for the 24-hr near-shore surface water time-series. Mean of diurnal radio-isotopic data are shown in boldface with standard deviation, and number of observations (n) in parentheses. Superscripts denote results of Student's t-test multiple comparisons: entries with the same letters have sample means not significantly different from each other at the 0.05 significance level. AR = Activity ratio.

Table 3.7 – Radionuclide data for 24-hr Mn-fiber equilibration deployments. AR = Activity ratio

Table 3.8 - Mean solute fluxes and calculated groundwater outflow velocities (V_{SGD}) using different tracers; standard deviations are given in parentheses. Superscripts denote results of Student's t-test multiple comparisons: entries with the same letters have sample means not significantly different from each other at the 0.05 significance level. We exempt V_{SGD} calculations using PO_4 due to significant bias introduced by adsorptive processes during transition across the land-ocean interface (Charette and Sholkovitz 2006).

Table 3.9 - Ranges of solute fluxes and calculated groundwater outflow velocity (VSGD) using different tracers

Table 3.10 – Literature estimates of groundwater discharge rate induced by waves, density gradients, and total submarine groundwater discharge. For comparison purposes, original units have been converted to discharge volume assuming discharge rate across a 1 m^2 of seafloor.

Table 4.1 – Summary of physical data collected at Waipuilani during all observation periods. N = sample count; Q1 = 25% quartile; Q3 =75% quartile.

Table 4.2 – Summary of surface water salinity and dissolved nutrient data collected at Waipuilani during all observation periods. N = sample count; Q1 = 25% quartile; Q3 =75% quartile.

Table 4.3 – Summary of collected (pH, DIC, and TA) and computed (pCO_2 and Ω) surface water carbonate chemistry at Waipuilani during all observation periods. N = sample count; Q1 = 25% quartile; Q3 =75% quartile. pH sensor failed during January 2006 field deployment.

Table 4.4 - Summary of 7 cm well porewater salinity and dissolved nutrient data collected at Waipuilani during all observation periods. N = sample count; Q1 = 25% quartile; Q3 =75% quartile.

Table 4.5 - Summary of collected (DIC and TA) and computed (pCO_2 and Ω) 7 cm porewater carbonate chemistry data collected at Waipuilani during all observation periods. N = sample count; Q1 = 25% quartile; Q3 =75% quartile.

Table 4.6 - Summary of 25 cm porewater salinity and dissolved nutrient data collected at Waipuilani during all observation periods. N = sample count; Q1 = 25% quartile; Q3 =75% quartile.

Table 4.7 - Summary of collected (DIC and TA) and computed (pCO_2 and Ω) 25 cm porewater carbonate chemistry data collected at Waipuilani during all observation periods. N = sample count; Q1 = 25% quartile; Q3 =75% quartile.

Table 4.8 - Summary of all data collected at Ukumehame during the March 07 observation period. pH (calc) is the pH calculated from CO2SYS model using TA and DIC data. N = sample count; Q1 = 25% quartile; Q3 =75% quartile.

Table 4.9 - Summary of inland groundwater well data for WAI and UKU, and mean coastal water chemistry. Salinity and nutrient data were obtained from Herzfeld (unpublished data). Offshore DIC, TA, and pCO_2 data are the long-term average surface water chemistry at station ALOHA (Keeling et al. 2004); pH at Waipuilani, and offshore $\Omega_{calcite}$ and $\Omega_{aragonite}$ were calculated using CO2SYS software and DIC and TA with carbonate dissociation constants from Mehrbach (1973), refit by Dickson and Millero (1987), and K_{SO4} from Dickson (1990) (seawater scale) at 25^{o} C. Asterisks denote missing data.

LIST OF FIGURES

CHAPTER I – INTRODUCTION

Increased human demand for food, space, and shelter in the past 100 years has dramatically affected land-based nutrient loading rates to the coastal zone (Mackenzie et al. 1998; Ver et al. 1999; Mackenzie et al. 2002). Highest loading rates have occurred during the last 60 years (post World War II) when the world population experienced its highest annual rates of change (Mackenzie et al. 2002; UN 2004). Given that approximately 40% of the human population (~6.8 billion total x 0.4 = 2.72 billion) (US Census Bureau 2010) chooses to live within 100 km of the coast (Cohen and Small 1998; Small and Nicholls 2003), and that their choices are not expected to change as world population is projected to stabilize between 7.4 and 10.6 billion by the year 2050 (UN 2004), further intensification of human impacts to all aspects of the biosphere seem inevitable (Vitousek et al. 1997).

Anthropogenic impacts to the biosphere intensify along the coastal zone because it is here where a great assortment of water-borne terrestrial inputs (e.g., suspended particles and dissolved nutrients in runoff and groundwater discharge) enter the sea (Mackenzie et al. 1998; Crossland et al. 2005), resulting in offshore gradients throughout this region (Dollar and Atkinson 1992; Moore 1996; Laws et al. 1999). Eutrophication (Lapointe and O'Connell 1989; Lapointe and Clark 1992; Howarth and Marino 2006), overfishing (Done 1992; Jackson 1997; Friedlander and DeMartini 2002), drastic thermal changes due to the rise in global temperature (GESAMP 2001; Crossland et al. 2005), and ocean acidification due to increased atmospheric CO_2 concentrations (Feely et al. 2004; Orr et al. 2005; Doney et al. 2007; Kuffner et al. 2008) have all been shown to impact the ecology and the biogeochemical processing of carbon, nitrogen, and phosphorus (CNP)

within the coastal zone. Nutrient loads to the coastal zone have been shown to lead to unwanted ecological cascades (Valiela et al. 1990; Pandolfi et al. 2005) driven by changes in net ecosystem primary production (Smith et al. 1981; Rabalais et al. 2002a; Rabalais et al. 2002b; Valiela et al. 1992; Valiela et al. 1997) and coral-microbe competition (Kline et al. 2006; Smith et al. 2006; Ritchie 2006). Synergistic interactions occurring within the coastal zone can further exacerbate the effects of any single stressor (Wooldridge 2009; Wooldridge and Done 2009).

Primary production in the coastal zone responds greatly to the addition of nutrients (N and P) (Howarth and Marino 2006; Valiela et al. 1990; Valiela et al. 1992; Valiela et al. 1997). Moreover, physical forces such as wind, waves, currents, and tides can readily affect the water column and how it interacts with nearshore coastal nutrient reservoirs such as sediments (Entsch et al. 1983; Tribble et al. 1990; Haberstroh 1994; Szumant and Forrester 1996; Falter 1998; Haberstroh and Sansone 1999; Oldham and Lavery 1999; Falter and Sansone 2000; Slomp and Van Capellen 2004), and shallow unconfined aquifers (D'Elia et al. 1981; Li et al. 1999; Laws et al. 1999; Kim et al. 2003; Johnson et al. 2008). Therefore, understanding of nutrient dynamics and the factors that affect their distributions are important if we are to understand the spatiotemporal mosaic of primary production along the coastal zone.

Sediment to water-column nutrient exchange has been linked to processes that are related to wave activity (Webb and Theodor 1968; Falter and Sansone 2000a; Webster 2003), turbulence induced by diurnal wind patterns (Oldham and Lavery 1999), recirculation and enhanced transport of fluids from the confined aquifer at the beach face via wave run-up (Li et al. 1999), and aquifer recharge rate (Capone and Slater 1990).

Moreover, in theoretical analyses (Webster et al. 1996; Boudreau 2000; Webster 2003), and laboratory flume experiments (Huettel et al. 1996; Huettel et al. 1998; Huettel and Webster 2001; Huettel et al. 2003) it has been demonstrated that physical forces acting on the permeable sediments typical of reef environments can significantly affect the rates at which sediment nutrients become transported to the water column. Similarly, waves propagating through these systems can induce pressure gradients at the sediment surface, generating flow of fluids through the sediment pores (Webster and Taylor 1992; Precht and Huettel 2003; Webster 2003; Precht and Huettel 2004). Waves and diurnal wind patterns can also generate oscillatory currents that interact with sand ripples and lead to characteristic fluid transport into ripple troughs and out of ripple crests (Huettel et al. 1998; Huettel et al. 2003). Furthermore, diurnal wind velocity patterns, mainly driven by island heating due to land insolation, have been observed to possess energy sufficient to induce thorough mixing of the water column and to re-suspend bottom sediments and transport pore fluids (Storlazzi et al. 2004; Herzfeld et al. 2006). This active exchange and rapid remineralization of dissolved and particulate organic matter (Wild et al. 2004a; Wild et al. 2004b; Rusch et al. 2006) has earned the term "biocatalytic filters" for these coarse-grained coastal sediments (Huettel et al. 1998; Precht and Huettel 2003).

Physical forces can affect the discharge of submarine groundwater (fresh, recirculated brackish, or saline; Burnett et al. 2003) and this, in turn, can significantly affect the nutrient delivery to the coastal zone. However, although literature documenting the exchange of solutes between submarine groundwater and nearshore ecosystems is extensive (Moore 1996; Kim and Hwang 2002; Taniguchi 2002; Taniguchi et al. 2002; Moore 2003; Burnett et al. 2003; Burnett and Dulaiova 2003; Dulaiova and Burnett

2007), and although the processes that enhance exchange within permeable coastal margins have been studied extensively (Van Der Loeff 1981; Van Der Loeff et al. 1981; Moore 2000a; Moore 2000b; Huettel and Webster 2001; Precht and Huettel 2003; Webster 2003; Precht and Huettel 2004; Reimers et al. 2004; Wild et al. 2004a; Wild et al. 2004b), studies that combine field-based observations of physical oceanographic conditions and nutrient dynamics in coastal water column/sediment porewater system are still lacking.

This dissertation attempts to address this absence of integrated studies and strives to elucidate the major mechanisms affecting land-ocean exchange of groundwater nutrients and its relationship to primary production within the coastal zone. Given that forces affecting nutrient dynamics in the coastal zone can be spatiotemporally heterogeneous, an important goal of this dissertation was to elucidate the variance of their interplay at different temporal and spatial scales. Increasing our understanding of factors that enhance the exchange between high-nutrient reservoirs (i.e. sediments, unconfined aquifers) and the nearshore water column can increase our understanding of the spatiotemporal distribution of primary production (e.g., macroalgal blooms) along the coastal zone.

The study described here examines the physico-chemical factors affecting nutrient dynamics and their relationship to episodic and chronic nuisance macroalgal blooms at sites on Maui, Hawaii, an island with various degrees of land alteration, nutrient loading, groundwater contamination, and varied coastal geomorphology. Although we hypothesize that sediments and submarine groundwater discharge can account for most of the nutrient inputs affecting the water column nutrient inventories of these areas, we

found that it is critical to consider local and regional physical factors that can enhance the retention of nutrients within the coastal zone if we are to understand the episodic nature of macroalgal blooms. **Chapter 2** explores the occurrence of episodic macroalgal blooms on West Maui, Hawaii, and the local and regional physical processes that can regulate them over various time-scales. In this chapter I illustrate how factors that enhance the exchange of solutes between reservoirs (and the retention within these reservoirs) can greatly influence the temporal distribution of nutrients within the coastal zone and can potentially explain episodic macroalgal blooms in the region is described.

Moreover, although evidence suggests that nutrients can be highly dynamic on timescales of hours in shallow coastal systems exposed to wave energy, no study to date has simultaneously quantified nutrient fluxes across multiple locations under similar physical forcing across various coastal geomorphological settings (e.g., exposed coastlines with/without shallow shelves). **Chapter 3** presents the spatiotemporal variability of dissolved inorganic nutrients within the West Maui proximal coastal zone and the variability's relationship to physical forcing, coastal geomorphology, and land alterations by humans.

Processes affecting the biogeochemistry of carbon, nitrogen, and phosphorous within the coastal zone are highly variable and dependent on their conservative and non-conservative behavior, and these, in turn, are regulated by physical constrains that affect the time a water mass resides along the coast. In **Chapter 4** I present multiple time-series observations of CNP biogeochemistry within two coastal sites on Maui that are characterized by similar geomorphology and physical forcing, but which are affected by different degrees of nutrient loading on land. In addition, I estimate conservative and

non-conservative nutrient fluxes along the coastal zone using box-models. My modeling approach is similar to that utilized by the Land-Ocean Interactions in the Coastal Zone (LOICZ) program (Gordon et al. 1996). However, LOICZ-style modeling was designed for coastal systems with simple hydrodynamics, and this is not the general situation along sites occupied during this study. Use of this modeling approach with my coastal setting necessitated adjustments to account for the water residence time over the time scales of my measurements (hours). My study uses radio-isotopic measurements (radium and radon), acoustic Doppler current measurements, and salt balances to constrain water residence time estimates along the shelf to allow for the water residence time parameterization of the LOICZ modeling approach. Better water residence time parameterization permits better estimation of time-variant non-conservative CNP fluxes, and the net metabolic state of the proximal coastal zone. Thus, Chapter 4 examines the time-variant net metabolic state of the coastal zone under different physical forcing.

In summary, this dissertation aims primarily to understand the underlying cause for the spatiotemporal variability of nutrient fluxes to the coastal zone and their relationship to macroalgal blooms that occur throughout the south-facing shores of Maui. Secondarily, this study aims to characterize how coastal geomorphology and human alteration of the landscape affect nutrient fluxes to the coastal zone. Lastly, I attempt to elucidate how temporally variable interactions between physical factors can affect dissolved nutrient dynamics and net ecosystem metabolism in the coastal zone.

LITERATURE CITED

Boudreau, B.P. 2000. The mathematics of early diagenesis: form worms to waves. Reviews of Geophysics, 38(3): 389-416.

Burnett, W.C. et al. 2003. Groundwater and pore water inputs to the coastal zone. Biogeochemistry, V66 (1): 3-33.

Burnett, W.C. and H. Dulaiova. 2003. Estimating the dynamics of groundwater input into the coastal zone via continuous radon-222 measurements. Journal of Environmental Radioactivity, 69: 21-35.

Capone, D. and J. Slater. 1990. Inter-annual patterns of water table height and groundwater derived nitrate in nearshore sediments. Biogeochemistry, 10(3, Groundwater Inputs to Coastal Waters): 277-288.

Crossland, C.J. et al. 2005. The Coastal Zone - a Domain of Global Interactions. In: C.J. Crossland, H.H. Kremer, H.J. Lindeboom, J.I. Marshall Crossland and M.D.A. Le Tissier (Editors), Coastal Fluxes in the Anthropocene. Springer-Verlag, Berlin Heidelberg, pp. 239.

D'Elia, C.F., K.L. Webb, and J.W Porter. 1981. Nitrate-rich groundwater inputs to Discovery Bay, Jamaica: a significant source of N to local coral reefs? Bulletin of Marine Science, 31: 903-910.

Dulaiova, H. and W.C. Burnett. 2007. Evaluation of the flushing rates of Apalachicola Bay, Florida via natural geochemical tracers. Marine Chemistry, doi:10.1016/j.marchem.2007.09.001.

Entsch, B. et al. 1983. Phosphorous and nitrogen in coral reef sediments. Limnology and Oceanography, 28(3): 465-476.

Falter, J.L. 1998. Time-variant diagenesis within the redox transition zone of an advectively driven sediment. Master's Thesis, University of Hawai'i at Manoa, Honolulu, Hawaii, 101 pp.

Falter, J.L. and F.J. Sansone. 2000. Hydraulic control of porewater geochemistry within the oxic-suboxic zone of a permeable sediment. Limnology and Oceanography, 45(3): 550-557.

GESAMP 2001. The state of the marine environment. Group of Experts on the Scientific Aspects of Marine Pollution, Regional Seas Reports and Studies. UNEP, Nairobi

Gordon, D.C.J. et al. 1996. LOICZ Biogeochemical modeling guidelines. LOICZ/R&S/95-5, VI +96 PP., Netherlands.

Haberstroh, P.R. and F.J. Sansone. 1999. Reef framework diagenesis across wave-flushed oxic-suboxic-anoxic transition zones. Coral Reefs, 18: 229-240.

Herzfeld, I. et al. 2006. Diurnal nutrient dynamics associated with a nuisance algal bloom on south Maui, Hawaii, Ocean Sciences Meeting - TOS AGU ASLO, Honolulu, Hawaii.

Howarth, R.W. and Marino, R., 2006. Nitrogen as the limiting nutrient for eutrophication in coastal marine ecosystems: Evolving views over three decades. Limnology and Oceanography, 51(1): 364-376.

Huettel, M. et al. 2003. Hydrodynamical impact on biogeochemical processes in aquatic sediments. Hydrobiologia, 494: 231-236.

Huettel, M. and I.T. Webster. 2001. Porewater flow in permeable sediments. In: B.P. Boudreau and B.B. Jorgensen (Editors). The benthic boundary layer. Oxford University Press, pp. 144-179.

Huettel, M., W. Ziebis, and S. Forster. 1996. Flow-induced uptake of particulate matter in permeable sediments. Limnology and Oceanography, 41(2): 309-322.

Huettel, M. et al. 1998. Advective transport affecting metal and nutrient distributions and interfacial fluxes in permeable sediments. Geochimica et Cosmochimica Acta, 62(4): 613-631.

Johnson, A.G. et al. 2008. Aerial infrared imaging reveals large nutrient-rich groundwater inputs to the ocean. Geophysical Research Letters, 35: L15606, doi:10.1029/2008GL034574.

Kim, G. and D.-W. Hwang. 2002. Tidal pumping of groundwater into the coastal ocean revealed from submarine ^{222}Rn and CH_4 monitoring. Geophysical Research Letters, 29(14): 1678, doi: 10.1029/2002GL015093.

Kim, G. et al. 2003. Large submarine groundwater discharge (SGD) from a volcanic island. Geophysical Research Letters, 30(21): 2098, doi: 10.1029/2003GL018378.

Kline, D.I. et al. 2006. Role of elevated organic carbon levels and microbial activity in coral mortality. Marine Ecology Progress Series, 314: 119-125.

Krest, J.M. and J.W. Harvey. 2003. Using natural distributions of short-lived radium isotopes to quantify groundwater discharge and recharge. Limnology and Oceanography, 48(1): 290-298.

Laws, E.A., D. Ziemann, and D. Schulman. 1999. Coastal water quality in Hawaii: the importance of buffer zones and dilution. Marine Environmental Research, 48: 1 - 21.

Li, L. et al. 1999. Submarine groundwater discharge and associated chemical input to a coastal sea. Water Resources Research, 35(11): 3253-3259.

Mackenzie, F.T., A. Lerman, and L.M. Ver. 1998. Role of the continental margin in the global carbon balance during the past three centuries. Geology, 26(5): 423-426.

Mackenzie, F.T., L.M. Ver, and A. Lerman. 2002. Century-scale nitrogen and phosphorus controls of the carbon cycle. Chemical Geology, 190(1 - 4): 13-32.

Moore, W.S. 1996. Large groundwater inputs to coastal waters revealed by ^{226}Ra enrichments. Nature, 380(6575): 612-614.

Moore, W.S. 2000. Ages of continental shelf waters determined from ^{223}Ra and ^{224}Ra. Journal of Geophysical Research, 105(C9): 22,117-22,122.

Moore, W.S. 2000. Determining coastal mixing rates using radium isotopes. Continental Shelf Research, 20: 1993-2007.

Moore, W.S. 2003. Sources and fluxes of submarine groundwater discharge delineated by radium isotopes. Biogeochemistry, 66: 75-93.

Moore, W.S. 2006. Radium isotopes as tracers of submarine groundwater discharge in Sicily. Continental Shelf Research, 26(7): 852-861.

Oldham, C.E. and P.S. Lavery. 1999. Porewater nutrient fluxes in a shallow fetch-limited estuary. Marine Ecology Progress Series, 183: 39-47.

Pandolfi, J.M. et al. 2005. Are U.S. coral reefs on the slippery slope to slime? Science, 307(5716): 1725-1726.

Precht, E. and M. Huettel. 2003. Advective pore-water exchange driven by surface gravity waves and its ecological implications. Limnology and Oceanography, 48(4): 1674-1684.

Precht, E. and M. Huettel. 2004. Rapid wave-driven advective pore water exchange in a permeable coastal sediment. Journal of Sea Research, 51(2): 93-107.

Rabalais, N.N., E.R. Turner, and W.J. Wiseman Jr. 2002. Gulf of Mexico hypoxia, a.k.a. "The Dead Zone". Annu. Rev. Ecol. Syst., 33: 235-263.

Rabalais, N.N. et al. 2002. Nutrient-enhanced productivity in the northern Gulf of Mexico: past, present and future. Hydrobiologia, 475/476: 39-63.

Reimers, C.E. et al. 2004. In situ measurements of advective solute transport in permeable shelf sands. Continental Shelf Research, 24(2): 183-201.

Ritchie, K.B. 2006. Regulation of microbial populations by coral surface mucus and mucus-associated bacteria. Marine Ecology Progress Series, 322: 1-14.

Rusch, A., M. Huettel, C. Wild, and C.E. Reimers. 2006. Benthic oxygen consumption and organic matter turnover in organic-poor, permeable shelf sands. Aquatic Geochemistry, 12: 1-19.

Small, C. and R.J. Nicholls. 2003. A global analysis of human settlement in coastal zones. Journal of Coastal Research, 19(3): 584-599.

Smith, J.E. et al. 2006. Indirect effects of algae on coral: algae-mediated, microbe-induced coral mortality. Ecology Letters, 9: 835-845.

Smith, S.V. et al. 1981. Kaneohe Bay sewage diversion experiment: perspectives on ecosystem responses to nutritional perturbation. Pacific Science, 35(4): 279-395.

Storlazzi, C.D. et al. 2004. Wave- and tidally-driven flow and sediment flux across a fringing coral reef: Southern Molokai, Hawaii. Continental Shelf Research, 24: 1397-1419.

Taniguchi, M. 2002. Tidal effects on submarine groundwater discharge into the ocean. Geophysical Research Letters, 29(12).

Taniguchi, M. et al. 2002. Investigation of submarine groundwater discharge. Hydrological Processes, 16(11): 2115-2129.

Tribble, G.W., F.J. Sansone, and S.V. Smith. 1990. Stoichiometric modeling of carbon diagenesis within a coral reef framework. Geochimica et Cosmochimica Acta, 54: 2439 - 2449.

United Nations (UN). 2004. World population to 2300. United Nations. Department of economic and social affairs, pp. 240.

U.S. Census Bureau 2010. http://www.census.gov/main/www/popclock.html. Accessed May 2010.

Valiela, I. et al., 1990. Transport of groundwater-borne nutrients from watersheds and their effects on coastal waters. Biogeochemistry, 10: 177-197.

Valiela, I. et al. 1992. Couplings of watersheds and coastal waters: sources and consequences of nutrient enrichment in Waquoit Bay, Massachusetts. Estuaries, 15(4): 443-457.

Valiela, I. et al. 1997. Macroalgal blooms in shallow estuaries: Controls and ecophisiological and ecosystem consequences. Limnology and Oceanography, 42(5, part 2): 1105-1118.

Van Der Loeff, M.M.R. 1981. Wave effects on sediment water exchange in a submersed sand bed. Netherlands Journal of Sea Research, 15(1): 100-112.

Van Der Loeff, M.M.R. et al. 1981. Sediment water exchanges of nutrients and oxygen on tidal flats in the EMS-Dollard estuary. Netherlands Journal of Sea Research, 15(1): 113-129.

Ver, L.M., F.T. Mackenzie, and A. Lerman. 1999. Carbon cycle in the coastal zone: effects of global perturbations and change in the past three centuries. Chemical Geology, 159: 283-304.

Vitousek, P.M. et al. 1997. Human domination of Earth's ecosystems. Science, 227: 494-499.

Webb, J.E. and J. Theodor. 1968. Irrigation of submerged marine sands through wave action. Nature, 220: 682-683.

Webster, I.T. 2003. Wave enhancement of diffusivities within surficial sediment. Environmental Fluid Dynamics, 3: 269-288.

Webster, I.T., S.J. Norquay, F.C. Ross, and R.A. Wooding. 1996. Solute exchange by convection within estuarine sediments. Estuarine, Coastal and Shelf Science, 42: 171-183.

Webster, I.T. and J.H. Taylor. 1992. Rotational dispersion in porous media due to fluctuating flows. Water Resources Research, 28(1): 109-119.

Wild, C. et al.. 2004. Degradation and mineralization of coral mucus in reef environments. Marine Ecology Progress Series, 267: 159-171.

Wild, C., R. Tollrian, and M. Huettel. 2004. Rapid recycling of coral mass-spawning products in permeable sediments. Marine Ecology Progress Series, 271: 159-166.

Wooldridge, S.A. 2009. Water quality and coral bleaching thresholds: formalizing the linkage for the inshore reefs of the Great Barrier Reef, Australia. Marine Pollution Bulletin, 58: 745-751.

Wooldridge, S.A. and T.J. Done. 2009. Improved water quality can ameliorate effects of climate change on corals. Ecological Applications, 19(6): 1492-1499.

CHAPTER II - PHYSICAL CONTROLS ON COASTAL-ZONE NUTRIENTS AND THEIR POTENTIAL RELATIONSHIP TO EPHEMERAL MACROALGAL BLOOMS OFF WEST MAUI, HAWAIʻI

2.1 ABSTRACT

Several episodes of large *Cladophora sericea* overgrowth have occurred along West Maui coastal regions during the past few decades, but only one of them (summer of 2001) has been quantitatively studied. This study couples field-based sediment porewater nutrient data to a hydrodynamic model in order to estimate potential sediment nutrient contributions to the 2001 macroalgae bloom. Results show that sediment pools of nitrogen may account for ~15% of total bloom requirements, whereas mobilization of sediment phosphate (P) pools can account for more than 100 % of total bloom P requirements. Rapid pore fluid velocities estimated for these sediments suggest that changes in sediment deposition rate can affect the sediment nutrient concentration profiles and fluxes.

Numerical analysis of historical physical data suggests that the synergistic effects of wind, waves, and rainfall increase the probability of *Cladophora sericea* blooms along West Maui. Wind and wave physical conditions effective over the main Hawaiian Islands appear to facilitate local macroalgal blooms via (1) increases in water column nutrient residence time, and (2) the episodic transport of particulate matter from deeper sites to shallow sedimentary environments, where rapid remineralization of particulate organic matter can lead to enhanced, sustained dissolved nutrient release.

KEY WORDS: algal blooms, sediments, nutrients, waves, dynamics, coral reefs

2.2 INTRODUCTION

The dynamic interactions between dissolved nutrients and macroalgae blooms within fringing coral reefs along tropical high islands are complex. Although there is an active debate as to whether ecological shifts from coral- to macroalgal-dominated benthos are due to herbivore population dynamics (e.g., Done 1992; Hughes 1994; Jackson 1997), or coastal eutrophication (e.g., Lapointe and Clark 1992; Lapointe et al. 1997), both, most likely, influence ecological dynamics at different temporal and spatial scales (Menge et al. 2003). In contrast to gradual ecological shifts, rapid macroalgal blooms can be the result of episodic optimal conditions for macroalgal growth.

In the last two decades, episodic blooms of *Cladophora sericea* (G. Hudson) have occurred in coastal regions of West Maui, Hawaii, some of which have led to significant die-off of coral colonies in the region (Wiltse 1996; Dollar and Andrews 1997; Smith et al. 2005; Bennett and Keuper-Bennett 2009), posing a threat to local communities who depend on the reefs for food and tourism income. *Cladophora sericea*, a green filamentous algae that lives in the lower intertidal to subtidal regions of the Maui coastline, is abundant in cool and warm temperate regions worldwide (Huisman et al. 2007), and able to withstand a wide range of salinities (Lee 2008). On Maui, *C. sericea* is usually found at depths greater than 30 m, associated with *Halimeda sp.* meadows (H. Spalding, personal communication), and often colonized by epiphytes. *Cladophora sericea* is able to withstand some unidirectional flow and wave action, though its fragile structure makes it prone to shedding fragments that can be transported across regions of seascape (R. Kennison, personal communication; Dierssen et al. 2009).

Although uncertainty remains as to what may trigger ephemeral coastal zone macroalgal blooms in this region, evidence suggests that their persistence may be sustained by several factors, including frequent nutrient inputs via submarine groundwater discharge (SGD) near the coast (Dollar and Andrews 1997; Laws et al. 2004; Hunt 2006; Herzfeld 2010), frequent sediment re-suspension in the shallow reef flats, which could release pore water nutrients and maintain them at high levels in the water column (Laws et al. 2004; Ogston et al. 2004; Storlazzi and Jaffe 2008), and the decline of herbivorous fish (Williams et al. 2008). Due to the rapidly sloping sea-floor and fairly rapid ocean circulation off West Maui, low temperature, low salinity, nutrient-enriched ground water has only been observed entering the Hawaiian coastal zone close to shore (Bienfang 1980; Dollar and Andrews 1997; Garrison et al. 2003; Laws et al. 2004; Herzfeld et al. 2006; Paytan et al. 2006; Johnson et al. 2008). The cross-shore extent of such nearshore nutrient enrichments depends on groundwater flow, the degree of nutrient enrichment in coastal aquifers, oceanographic mixing, and biological uptake along the coast (Bienfang 1980; Dollar and Andrews 1997; Dollar and Atkinson 1992; Laws et al. 2004; Paytan et al. 2006; Storlazzi et al. 2006).

In the fractured basaltic aquifers of Maui, Hawaii, with their high hydraulic conductivity (Rotzoll et al. 2008), groundwater flows can be readily affected by aquifer recharge water from percolating rainfall, crop irrigation, or municipal wastewater. Moreover, such conduit-rich rock could facilitate quick discharge of natural and anthropogenicaly enriched groundwater to the near shore coastal zone (Soicher and Peterson 1997; Hunt 2006). Indeed, studies along coastal Maui have shown that groundwater around the islands can contain nitrate (10 - >200 µM) and phosphate (2.7 –

4.0 μM) concentrations well above those typical of offshore waters (Laws et al. 2004; Herzfeld et al. 2008). Thus, due to the high transport potential though local aquifers, and the low adsorptive nature of nitrate (Burdige 2006), which facilitates its transport across soils and aquifers, the occurrence of nitrate inputs to the nearshore coastal zone via submarine groundwater discharge are not surprising in this region. On the other hand, phosphate has been shown to be strongly retained at land-ocean transition zones (i.e., a coastline band several hundred meters wide) via adsorption/precipitation and redox processes related to iron (Charette and Sholkovitz 2002; Testa et al. 2002).

Site-specific studies along coastal Maui have, in fact, documented nitrate-rich, phosphate-poor submarine groundwater discharge at the coastline (Dollar and Andrews 1997; Laws et al. 2004). Thus, although nitrogen loads from land could possibly help meet the nitrogen requirements of blooming macroalgae, an alternative phosphorus source must exist.

Alternative nutrient sources for blooming algae

Further offshore, away from direct land-based inputs, nutrient sources to the water column are usually less diverse than close to shore, and remineralization of particulate organic matter within sediments likely plays a greater role in benthic nutrient dynamics (Froelich et al. 1979; Berner 1980; Tribble et al. 1990; Burdige 2006). This notion is supported by the fact that reef sediments are typically characterized by enriched dissolved inorganic nutrients (ammonium and phosphate) in relation to the water column as a result of organic matter catabolism (Haberstroh 1994; Falter 1998; Haberstroh and Sansone 1999; Falter and Sansone 2000a), and that offshore sediment pore water salinities are near ocean water column levels.

Due to the shallow water depth typical of fringing reef ecosystems and their characteristically highly energetic conditions (i.e., strong winds, high waves, currents, and tides), which can readily induce turbulence in the water column, sediment-water column exchange processes are very dynamic. For example, the extent of sediment-water column exchange within permeable sediments has been linked to processes that are related to wave activity (Webb and Theodor 1968; Falter and Sansone 2000a; Webster 2003), turbulence induced by diurnal winds (Oldham & Lavery 1999), sediment re-suspension (Walker and O'Donnell 1981; Laws et al. 2004; Herzfeld et al. 2006), and aquifer recharge rate (Capone and Slater 1990). In particular, waves can significantly affect fluid flows through the rippled sediment bed (Webster and Taylor 1992; Precht and Huettel 2003; Webster 2003; Precht and Huettel 2004) by inducing (hydrostatic and velocity induced) pressure gradients at the sediment surface.

In theory (Webster et al. 1996; Boudreau 2000; Webster 2003), and in laboratory and flume experiments (Huettel et al. 1996; Huettel et al. 1998; Huettel and Webster 2001; Huettel et al. 2003), it has been shown that physical forces (waves, currents) interacting with rippled permeable sediments typical of reef environments can significantly affect the rates at which suspended particulate matter can be entrained into sediments (Huettel et al. 1996; Precht and Huettel 2003; Wild et al. 2004a; Wild et al. 2004b; Rusch et al. 2006), and dissolved porewater nutrients can be transported out to the water column. Therefore, physical forces acting on "shallow" (<30 m) environments dominated by permeable sediments are capable of inducing enhanced sediment porewater transport (Huettle et al. 1998; Reimers et al. 2004; Rusch and Huettel 2000; Precht and Huettel 2003; Precht et al. 2004). The depth to which sediment pore fluids experience rapid transport is a function

of particle size and sorting, sediment ripple wavelength, water depth, wave amplitude, and wave period (Shum 1993, Webster 2003). Mobilization of sediment porewater from the surface sediment layers over large spatial expanses can lead to significant fluxes of dissolved nutrients to the water column and, presumably, subsidized biomass production by opportunistic primary producers (Valiela et al. 1990; Slomp and Van Capellen 2004).

The purpose of our study was to determine the potential contribution of sediment dissolved nutrient pools to nutrient requirements of an ephemeral benthic macroalgal bloom in the coastal environment. I investigated the functional role of sediments in the onset and continued release of N and P to subsidize such a bloom, and ask the question: can the mobilization of sediment dissolved nutrients (due to physically enhanced sediment porewater transport) subsidize the growth requirements of blooming macroalgae? Secondly, to address the timescale of bloom formation, I utilized a numerical model to predict sediment-to-water column dissolved inorganic N and P transport (fluxes) under different wave conditions. I further examined historical meteorological (rainfall, wind, and waves) data and speculate about the role these factors may have on regional (i.e., processes that occur within 10s of km scales) nutrient residence times in an attempt to explain the episodic nature of the observed ephemeral *C. sericea* blooms off Kahekili, West Maui, Hawaii.

2.3 MATERIALS AND METHODS

2.3.1 Study location

The Kahekili area, located north of the town of Lahaina (estimated population 2000 census ~9,000), is one of the principal tourist destinations on the island of Maui (Figure 2.1). Kahekili lies within the wind shadow of the West Maui Mountains that blocks the prevailing northeasterly trade winds. Diurnal wind patterns along this coastline are

driven by land insolation, with light early morning and late evening breezes, and relatively calm wind conditions throughout the day (personal observation). Watersheds along this region are dominated by urban sprawl, sugarcane and pineapple plantations at lower elevations, and steeply sloping mountains that receive much of the regional rainfall at higher elevation.

The regional wave climatology affecting the Main Hawaiian islands is the result of Trade Winds, cyclonic activity, and southern hemisphere storms (Moberly and Chamberlain 1964; Caldwell 2007; Caldwell and Aucan 2007). Although wave height records have not been collected as frequently in Maui as in Oahu, similar seasonal wave regimes can be observed affecting both islands. Typical wave climate within the surf zone along the southern shores of Oahu, Hawaii (Caldwell 2007) indicates that wave heights <1.8 m are frequent, whereas wave heights between 2.5 – 3 m are less frequent, and between 3 – 5 m are infrequent. The largest wave event (9 m) was observed during the arrival of Hurricane Iniki (September 1992), however waves larger than 5 m were highly infrequent during the entire 34 yr (1973 – 2006) observation period on record (Caldwell 2007). Although wave shadowing by the surrounding islands (Lanai, Molokai, and Kaho'olawe) can drastically affect the wave direction and energy affecting the coast at our site, a similar wave climate has been reported by Storlazzi and Jaffe (2008) at a nearby site (Kahana, Maui; Figure 2.1).

2.3.2 Water sampling design

Water column and sediment interstitial water samples at 3, 9, 18, and 27 m water depth were collected over two days on five occasions by SCUBA divers offshore from Kahekili, Maui during 2003-2005 (Figure 2.1, panel 4). Water column samples were

collected 0 and 2 m above the sediment water interface (SWI) and slightly up-current from sediment interstitial water sampling locations. Sediment interstitial water was collected using a modified version the porewater sampling device described by Falter and Sansone (2000b). At each site, six separate sediment interstitial water wells were installed and arranged within a 20 x 30 cm rectangular area in such a way that porewater sampling spheres did not overlap (volume sampled = 240 cc, average sediment porosity = 0.4, radius of sampling sphere = 5.2 cm). Wells consisted of ¼ inch (0.635 cm) schedule 80 PVC pipes with small openings drilled at sampling depths (7, 15, 25, 35, 50, and 70 cm). Sediment porewater was sampled at each depth with a separate well. Wells were fitted at the top (above the sediment water interface) with a barbed connector that connected to Tygon tubing which ended at a three-way stopcock for ease of sampling. Wells were capped and left in place between samplings.

Sampling of sediment porewater was performed using clean 160-cc plastic syringes fitted with a three-way stopcock. At each station, divers flushed each well by withdrawing and discarding first 30-cc and then 60-cc to the water column, followed by a final 150-cc draw of porewater sample that was sealed inside the syringe with a 3-way stopcock. Samples were kept on ice upon return to the research vessel. All samples for dissolved nutrient analysis were filtered through pre-combusted (550˚ C) GF/F glass fiber filters into HCl-cleaned HDPE sample bottles immediately upon return to the field laboratory (less than 6 hours after collection), and kept frozen until analysis. Dissolved inorganic nutrients (phosphate, nitrate, nitrite, ammonium, and silicate) were analyzed colorimetrically at the University of Washington Oceanography Technical Services using standard methods (Gordon et al. 1993) in a segmented flow analyzer. Salinity was

analyzed in the laboratory at University of Hawaii Manoa using a Metler Toledo Seven Multi bench top meter equipped with an InLab®731 conductivity probe.

2.3.3 Solid Phase Sampling and Analysis

Sediment cores and surface grab samples were collected at most stations. Sediment coring at the shallowest (3 m) site was not possible due to the presence of a hard bottom within the top 10 cm, hence only surface sediment grabs were obtained. Sediment core collection was performed by SCUBA divers driving a 90-cm long, 7.62-cm i.d. polycarbonate cylinder into the sediment until hard substrate or 75 cm depth was reached. Sediment compaction during coring (as visually assessed by the location of the sediment-water interface inside and outside of the coring tube) was minimal. Sediment cores were collected, brought up to the research vessel, and transported to the shore laboratory where they were extruded at 4-cm intervals under atmospheric conditions. Sediment sections were weighed, dried, and sieved using sequential sieves (2 mm, 1 mm, 500 µm, 250 µm, 125 µm, 63 µm, and <63 µm). Particle size statistics are reported as percent of total dry bulk weight. Sediment sub-samples were combusted at 550˚ C for 6 hours, their weight recorded, and sequentially combusted at 1000˚ C for 3 hours and their percent weight loss on ignition (WLOI) recorded. Weight loss on ignition was utilized to calculate percent organic carbon (C_{org}) and percent $CaCO_3$ in the sediments according to Dean (1974), and Heiri et al. (2001), respectively. Porosity was calculated from dry bulk density measurements assuming a (mostly calcite) particle density of 2.71 g/cm^3 (Morse and Mackenzie 1990). Porosity and particle size analysis data from sediment cores were used to predict the sediment permeability (k) using the Carman-Kozeny equation (Webster 2003):

$$k = \frac{\varphi^3}{(1-\varphi)^2} \cdot \frac{r^2}{45} \qquad \text{(EQ. 2.1)}$$

where r is the mean particle radius, and φ is the dimensionless porosity (Webster 2003). Harleman's equation was utilized to calculate sediment permeability for sites where only grab samples were collected (Schwartz and Zhang 2003):

$$k = (6.54x10^{-4})d_{10}^2 \qquad \text{(EQ. 2.2)}$$

where d_{10} is the effective grain size cm (i.e. 90% of particles are greater than effective grain size). We further calculated the sediment hydraulic conductivity, κ, which is a function of the sediment permeability (k, in m^2) and density (1027.81 kg/m^3 at 20˚C), gravitational acceleration (g = 9.81 m/s^2), and dynamic viscosity of water (μ_i, $1.002x10^{-3}$ kg m^{-1} s^{-1}) (Schwartz and Zhang 2003):

$$\kappa = \frac{k\rho g}{\mu_i} \qquad \text{(EQ. 2.3)}$$

2.3.4 Pore fluid hydrodynamic model

We utilized sediment solid phase data from our sites to predict sediment porewater transport using combined models for porewater advection (Shum 1992) and dispersion (Webster 2003). Such combined model assumes surface gravity waves drive faster oscillatory currents across the seabed over sand ripple crests than over sand ripple troughs. The differential in current velocities between ripple troughs and crests (Webb and Theodor 1968; Riedl et al. 1972; Shum 1993; Precht and Huettel 2003; Hebert et al. 2007) results in lower pressure over the crests, thus driving porewater flow from troughs to crests. We modeled this sediment-water interface current-induced pressure along the rippled bottom following Elliott & Brook's (1997a, 1997b) model:

$$P_{surf} = -0.14\rho U_o^2 \left(\frac{a}{0.34H} \right)^{\frac{3}{8}} \cos\left(\frac{2\pi x}{L} \right) \qquad \text{(EQ. 2.4)}$$

where a is sand ripple height, L is sand ripple length, ρ is water density, H is water depth, and for U_o we use the maximum wave orbital velocity, which we calculated from water depth (H), significant wave height (H_s), and dominant wave period (T) using linear wave theory (Stewart 2003). Our model domain is between two ripple crests because there is no lateral pressure gradient and thus no modeled lateral flow across a ripple crest. Ripples are assumed to be long and parallel to shore, which results in no alongshore flow. The bottom boundary is hydrostatic pressure ($\rho g(H+d)$), so it has no lateral pressure gradients, and the bottom location (d) of this boundary is deep enough that porewater velocities less than one ripple wavelength from the SWI are not changed noticeably by moving the bottom location deeper. Porewater advection is calculated from the pressure (P) gradient using Darcy's Law:

$$v = -\frac{\kappa}{\phi\mu} \nabla \overline{P} \qquad \text{(EQ. 2.5)}$$

where v is velocity (cm/day) in the vertical and onshore direction, κ is permeability, Φ is porosity, and μ is dynamic viscosity. We employ a 100x100 cell rectangular Cartesian grid which is mapped to the physical model domain following Malarkey and Davies (2002) approach. Flows are calculated in the Cartesian domain and then mapped to the physical domain based on methods in Shum (1992). We use a parametric equation from Shum (1992) to define the shape of the SWI surface:

$$\mathrm{x} = \mathrm{Lt} - \frac{\mathrm{asin}(2\pi t)}{2}, z = \frac{a\cos(2\pi t)}{2} \qquad \text{(EQ. 2.6)}$$

where a and L are computed from Wiberg and Harris (1994) based on measured H, H_s, T, and median grain size d_{50}. Scalar dispersion in porewater as a function of depth is from Webster (2003) and is a function of H, H_s, T, d_{50}, Φ, μ, and molecular diffusivity.

To calculate porewater transport we followed the path taken by infinitely small (i.e., mimicking dissolved constituents in porefluids) particles we inserted into our physical model domain. The model time step started at 10 seconds and increased exponentially to 1 hour over 30 days so that we could view transport on multiple temporal scales. Multiple scales are important here due to velocity reduction as a function of depth with an e-folding scale of only a few centimeters. During each time step, particle displacements from advection and dispersion were calculated independently and then superimposed. For model runs with ripple migration, onshore ripple migration effects are simulated by moving the particles offshore during each time step at the ripple migration rate. Particles that would advect offshore out of the domain we inject into the onshore side of the domain because the lateral boundary conditions can be considered periodic (e.g., the particles exiting one ripple domain can be visualized to enter an adjacent ripple domain. Because all ripple domains are adjacent to each other and identical, we can use a single model ripple domain and re-inject the exiting particles at the nearshore boundary). We calculate the length of time each porewater parcel has been below the SWI, defined as its age, by running the model backwards in time. To calculate age throughout the domain we initialize the entire domain with particles and then run the model backwards until the particles are ejected out through the ripple crests. The length of time each particle remains in the domain when the model is reversed is the particle's age.

2.3.5 Diffusive and Advective Nutrient Fluxes

2.3.5.1 Diffusive Fluxes (J_i)

Sediment porewater data were used to predict the dissolved nutrient flux direction and magnitude utilizing Fick's First Law and published constants for molecular diffusivity:

$$J_i = -\varphi D_i \frac{\Delta C_i}{\Delta z} \quad \text{(EQ. 2.7)}$$

where φ is sediment effective porosity, D_i is the molecular diffusivity of component *i*, ΔC_i is the concentration difference of component *i* between maxima (or minima) and the sediment surface, and Δz is the distance between the surface and the depth at which maxima (or minima) in component *i* occur. A positive value is a flux from the sediment to the water column.

2.3.5.2 Advective Fluxes (J_o)

We calculate advective sediment-to-water column fluxes (J_o) by multiplying half the modeled ((trough+crest)/2) vertical porefluid velocity (v_{i1cm}) at 1 cm below the SWI, by the difference between exponential or 2nd order polynomial predictions (based on collected pore water profiles) of nutrient porewater concentration 1 cm below the SWI and concentrations in the overlying water column (C_o):

$$J_o = v_{i1cm} \times (C_{i1cm} - C_o) \quad \text{(EQ. 2.8)}$$

In our calculations of advective fluxes we assume that the contributions to the flux from diffusive processes are negligible given the permeable nature of our sediments (Huettel and Gust 1992; Precht and Huettel 2003; Huettel et al. 2003; Precht and Huettel 2004). We report the mean and standard deviation of nutrient flux estimates from each site sampled. Positive advective fluxes represent transport of solutes into the water column, whereas a negative flux represents solute consumption within sediments.

Multiple comparisons of flux rate variances were performed using SAS JMP software. Significance is reported at the alpha = 0.05 level.

2.3.6 Areal extrapolations of sedimentary data

In the calculation of the potential nutrient mass transport from sediments it was assumed that the mean porewater dissolved inorganic nutrient profiles from each depth were representative of a region of seafloor. SHOALS Lidar data (http://shoals.sam.usace.army.mil/hawaii/pages/Hawaii_Data.htm), in combination with geographic information system software (ESRI, ArcGis 9.2), were utilized to determine the benthic surface area that a given set of sediment porewater data represents. SHOALS Lidar data were interpolated using an ordinary Krigging algorithm. The interpolated surface was then reclassified into 35m intervals, and these converted to polygon features. The 2001 *C. sericea* bloom was recorded to extend between the shore-edge to depths of approximately 34 m (Smith et al. 2005). Thus, the 0 – 35 m polygon was chosen as the region of interest (ROI) for this study. The ROI was converted to a 5 x 5 m grid and assigned a value of 1. SHOALS Lidar interpolated data were then multiplied by this grid layer to obtain the water depths along our ROI. Water depth grid data within our ROI were then reclassified between 0-7.5, 7.5-15, 15-25, 25-35 m to reflect representative areas to our sampled porewater depths (3, 9, 18, and 27m, respectively). Counts of grid cells belonging to each depth interval class were made and converted to a measure of surface area (area (m^2) = cell count x 25 m^2/cell). Our spatial analysis yielded estimates of the area represented by the 3, 9, 18, and 27 m wells along the region of interest of 1.89, 1.08, 0.75, and 2.24 x 10^6 m^2, respectively.

2.3.7 Statistical analyses

All statistical analyses were performed using either Matlab or SAS JMP software. Multiple comparisons of one-way analysis of variance between populations are reported as significantly different if $p < 0.05$. Correlation-based principal components analysis was performed using SAS JMP software. All time-series analysis and modeling was performed using Matlab software.

2.4 RESULTS

2.4.1 Sediment physicochemical characteristics

Key physicochemical characteristics of sediments at Kahekili are summarized in Table 2.1. Sediment porewater phosphate (PO_4^{3-}), silicate (Si), ammonium (NH_4), nitrate plus nitrite (N+N), and salinity (Sal) profiles for all sampling periods are shown in Figures 2.2, 2.3, and 2.4. Mean and standard deviations of water column and sediment porewater nutrient concentrations and nutrient ratios are summarized in Tables 2.2 and 2.3, respectively.

Dissolved N+N decreased with depth into the sediments as expected (Froelich et al. 1979) due to the high demand of nitrate as an electron acceptor by facultative anaerobic microbial communities. A large subsurface region of low salinity, high N+N porewater was observed in July 2003 at the 3-m site only. Nitrate plus nitrite levels were low (< 0.5µM, except in July 2003) at all depths during all sampling dates. Mean N+N concentrations in the water column at the 3-m site were significantly higher ($F= 3.19$, $p=0.03$) than at other sites, suggesting greater N+N enrichment close to shore. Water column PO_4, Si, and NH_4 were close to detection limits and not significantly different across water sampling sites.

Porewater silicate profiles for September 2004, March 2005, and July 2005 showed striking differences to the other two sampling dates at all depths (Fig. 2.2), that could not be attributed to a salinity anomaly (Fig. 2.4). The lack of a salinity anomaly, and enrichment in Si compared to NH_4 and PO_4, suggests catabolism and dissolution of entrapped diatom particles within sediments, rather than intrusion of SGD. The porewater Si enrichment appears to penetrate 15 and 20 cm into sediments at the 18- and 27-m sites, respectively, and deeper (between 35- and 50-cm) at the 9- and 3-m sites.

A general feature of most porewater nutrient profiles was a subsurface enrichment between 0 and 20 cm followed by a slight decrease and finally another enriched section between 40- and 70-cm below the SWI. The first subsurface maxima might have resulted from particle entrapment and remineralization, whereas the lower maxima might be the result of the sum total of catabolism and dissolution processes under a diffusive environment. Thus, the top layer of the sediments (~0 – 25cm) can be recognized as a layer where active porefluid transport occurs (i.e. advection is responsible for solute transport); whereas the bottom layer can be recognized as being a stagnant region, where diffusive processes are mainly responsible for solute transport.

Percent organic carbon (%OC) data indicate that most of the incoming sediment organic matter is remineralized within the top layers of sediment at all sites (Tables 2.1 & 2.4). Multiple comparisons of one-way analysis of variance show that the % OC of particles reaching all sites are not significantly different ($F=1.06$, $p=0.3842$). Mean sedimentation rates, although not significantly different ($F=1.42$, $p=0.2595$), appear to decrease with water depth (Table 2.4).

2.4.2 Sediment porefluid dynamics under different wave regimes

Model results predicting porefluid age decrease exponentially over model run times (Figure 2.5). Porewater age results greater than 28 days (4 weeks) were not considered as they are thought to be beyond the time scales of our blooms. We report the first two days of model output as the largest model response was observed during this time period. Our model estimates porewater fluid velocity under constant wave amplitude. Under such hypothetical, instantaneous conditions, the length scale of turbulent flow penetration rapidly increases from approximately 0 to 25 cm at all depths under all wave regimes considered, under both ripple trough and crest (Figure 2.6). The rate of penetration beneath troughs under different wave regimes decreases isotonically after this initial pulse, and stabilizes at a value of approximately 30 cm within 2 days. Rate of penetration under large (5 m significant wave height) waves is faster and does not stabilize within the model run times (data not shown). Our model indicates rapid porewater fluid flows down to 25 cm below the SWI are achievable at all water column depths, with typical Trade-Wind wave conditions (Figure 2.6), within a few days.

2.4.3 Nutrient Fluxes

2.4.3.1 Diffusive Fluxes

A summary of calculated sediment to water column diffusive nutrient fluxes are presented in Table 2.5. Significantly higher phosphate and silicate, and lower ammonium fluxes are expected at the 27 m site compared to all other locations. Phosphate fluxes at the 27 m site were approximately 4 times those at other sites. Compared to all other sites, silicate fluxes were 10 times higher at the 27 m site. Diffusive fluxes of nitrate and nitrite are minimal at all depths sampled. Ammonium fluxes were highest at the 3, 9, and 18 m sites, and significantly higher than those calculated for the 27 m site.

2.4.3.2 Advective Fluxes

Results for calculated advective fluxes are reported in Table 2.6. Phosphate fluxes were significantly higher at 9 m compared to other sites. Silicate fluxes at the 9 and 18 m sites were significantly higher than at the 3m site, but not significantly different from the 27 m site. Nitrate fluxes at most sites were negative, indicating active denitrification within sediments. A slight positive nitrate flux was predicted for the 9 m site, but it is not significantly different from fluxes at other sites. Nitrite fluxes were lower than nitrate (except at the 9 m site) and not significantly different across sites. Significantly higher ammonium and dissolved inorganic nitrogen (DIN = (N+N)+NH_4) fluxes were observed at the 9 m site, indicating significantly higher ammonification rates within sediments at this site. Ammonium and DIN fluxes at 3 and 27 m are significantly different from those of the 9 m site, but not significantly different from those of the 18 m site.

2.4.3.3 Sediment dissolved nutrient inventories

Tabulated depth-integrated sediment porewater nutrient inventories per square meter (Table 2.7) show significant phosphate and silicate enrichment at the 27 m site. Integrated phosphate and silicate standing stocks within the top 50 cm at the 27 m site are equal or greater to the total whole-sediment column integrated standing stocks at all other sites combined. Integrated ammonium standing stocks at the 9 m site are an order of magnitude higher than at other sites. Integrated ammonium standing stock between 30 and 50 cm below the SWI at the 9 m site are equal or greater than the sum of all integrated ammonium standing stocks from all other sites combined.

2.5 DISCUSSION

2.5.1 The 2001 Cladophora sericea bloom nutrient requirements

Smith and co-workers (2005) reported benthic biomass surveys and tissue CNP values from the 2001 *Cladophora sericea* bloom. Although the 2001 bloom was reported to extend from Kahana to Lahaina (Figure 2.1), we present calculations of bloom requirements for only a portion of this coastline (the approximately 7-km section from Kahana to Black Rock, just south of Kahekili) given our limited geochemical sediment porewater sampling along the region of interest (ROI, Figure 2.1). According to Smith and co-workers (2005), average abundance of *C. sericea* from 3 m to 34 m was 23.1 % cover, and mean percent tissue C, N, and P were approximately 36%, 1.5%, and 0.02%, respectively. We calculate the total moles of C, N, and P in the bloom biomass from these data and the assumptions that: (1) the average *C. sericea* algal fragment height was ~ 20 cm (Huisman et al. 2007), and (2) the macroalgal wet biomass was ~ 5 times the % cover, and the dry biomass was ~ 15% of the wet biomass (J. Smith, unpublished algal conversions from benthic surveys of *Hypnea musciformis* and *Ulva fasciata*).

The sediment area affected by the macroalgal bloom can be approximated as 6.0×10^6 m^2, and the wet-biomass, dry-biomass, and bloom molar C, N and P content as 460, 69, 25, 1, and 0.01 g/m^2, respectively. On an areal basis this translates to a 4.1×10^8 g-dry biomass, and 1.2×10^7, 4.4×10^5, and 2.7×10^3 total moles of C, N, and P required, respectively, by the algae in the bloom region. The bloom requirement calculations are summarized in Table 2.8.

2.5.2 Potential sediment contributions to the 2001 C. sericea macroalgal bloom

Sediment nutrient pools may contribute significant DIN and PO_4 subsidies to blooming macroalgae. We calculated the depth-integrated (layer by layer) sediment

porewater inventories and multiplied them by the estimated 2001 *C. sericea* bloom area to estimate the mean total sediment standing stocks of nutrients in the region of interest. Molar nutrient requirements of the 2001 *C. sericea* bloom were divided by the depth-integrated dissolved DIN and PO_4 nutrient standing stocks over the representative regions of each depth profile to obtain estimates of the potential bloom percentage of DIN (PB% DIN) and PO_4 (PB% PO_4) potentially supplied by sediment standing stocks (Figure 2.7 A and B). Although variability is high, the mean PB% DIN from sediments is on the order of 0 - 11 %, with the largest contribution observed at the 9 m site. On the other hand, the PB% PO_4 from sediments potentially accounts for greater than 100 % of the PO_4 required for the bloom. In particular, sediments from the 27 m site have the highest potential PO_4 mass transport to the water column due to its high inventories (Table 2.7). Cumulative contributions profiles (area weighed total mean potential % contribution if the length scale of porefluid transport within sediments from all depths are similar) show maximal DIN PB% of 11 % at 70 cm below the SWI, and PB% PO_4 of 215 % also at 70 cm below the SWI. Under typical length scales of advective porewater transport, (~25–35 cm, Figure 2.6) we predict that sediments could provide ~4 % of the DIN and 126 % of the PO_4 requirements to blooming macroalgae.

Fluid flow through sediment interstitial spaces (as calculated by our porefluid hydrodynamic model) under typical (0.8 m) and slightly elevated (1.5 – 2.5 m) wave regimes can potentially transport significant quantities of sediment PO_4 to the water column. Porefluid transport down to 25 cm could account for approximately 72 % of the PO_4 required by the bloom, and transport of the top 35 cm of sediment pore fluids could provide PO_4 in excess of the bloom requirements (~126 %). Higher waves (1.5 - 5m)

could induce higher pore fluid flows deeper in the sediment column. In particular, small shifts in the penetration depth (25 to 45 cm) at the 27 m site could potentially lead to a significant further increase in PO_4 transport to the water column.

2.5.3 Time required for the 2001 Cladophora sericea bloom development

Cladophora sericea nutrient uptake rates (Thybo-Christesen et al. 1993) were used to estimate the time it would take *C. sericea* to achieve the estimated observed bloom biomass. We utilize the term "Bloom Development Time" to refer to the estimated macroalgal bloom outgrowth time (Table 2.8). According to the bloom molar mass estimates and published in-field growth rates (Thybo-Christesen et al. 1993), it would take approximately 1394, 577, and 17 days for the NO_3, NH_4, and PO_4 bloom requirements to be satisfied, respectively.

Similarly, data from an independent study performed along the Kahana coast of Maui (Paytan et al. 2006) indicated that the total inorganic nitrogen (TIN) load via SGD along this region was 82 mmol TIN/m/hr. Unfortunately, no phosphate loading estimates were reported in that study. Based on the N loading estimate of Paytan et al. (2006), submarine groundwater discharge along our study coastline is predicted to supply the total N needed by the bloom in approximately 32 days.

Results from our study indicate that advective nutrient transport from the top layer of sediment can lead to mass transfer of bloom-required dissolved inorganic nitrogen (99% ammonium) and phosphate in ~42 and 4 days, respectively (Table 2.8). The bloom timeline estimates from our advective flux calculations fall at the upper (using N) and lower (using P) boundaries of the previous two independent estimates. The higher estimates of bloom development time based on N are the result of our conservative

approach in calculating advective fluxes: we only consider the top centimeter of sediment to exchange solutes with the overlying water. This suggests that thicker sections of sediment (perhaps the top 20cm) can act as an advective layer (Figure 2.6). However, rapid mass transfer of solutes (mainly phosphate and ammonium) from deeper sedimentary pools would further reduce our estimated time necessary for bloom nitrogen and phosphorus subsidy from sediments. Although we can accept such a scenario, our modeling approach is not capable of testing such a hypothesis at this point. Rapid redox shifts, adsorption, and possibly precipitation reactions within dynamic surficial sediments limits our ability to conclude that advective water flow transports solutes from the top 20 cm of sediments to the water column.

We conclude that nutrients required by the 2001 *C. sericea* bloom could have been supplied by a variety of sources (e.g., sediments or fresh water SGD) within 4 to 42 days. Loading rates of land-based SGD nitrogen sources (Paytan et al. 2006) are capable of supplying the entire required N to blooming macroalgae within observed bloom timelines (i.e., a few weeks) (Bennett and Keuper-Bennett 2009). However, predictions from algal physiological studies (Thybo-Christesen et al. 1993) indicate that long time periods would be required for bloom development if only nitrogen uptake mechanisms are considered. Although Smith and co-workers (2005) argue that elevated algal N uptake rates occur under higher nitrogen enrichment, such N uptake rates would have to be 50 - 100 times those observed by Thybo-Christensen and coworkers (1993) for the *C. sericea* bloom time-scales (weeks) to match uptake timeline predictions (months) (Table 2.8), an unlikely occurrence. Therefore, the combined N and P input sources to the nearshore

coastal zone can supply the needed nutrients to the 2001 *C. sericea* bloom, but phosphorus uptake and availability may ultimately regulate bloom timelines.

The potential role of sediment nutrient stocks in providing a bloom with dissolved nutrients will further increase with elevated wave heights as indicated by our modeled porefluid transport velocities (Figure 2.5). Thus, advective sediment phosphate fluxes can potentially provide the required "new" phosphate to blooming macroalgae that land-based SGD does not appear to provide.

2.5.4 New nutrients in the shallows: Cladophora sericea transport from depth

Cladophora sericea has not been observed undergoing bloom phases at depths between 30 – 120 m, but large clumps have been seen being transported from/to these depths by swift currents within the region (H. Spalding personal communication). Although *C. sericea* communities at deep sites appear healthy, low porewater N inventories (Table 2.7), and consequently low sediment to water-column fluxes (Table 2.5) suggest these algal communities may be nitrogen poor.

Seasonal large wave events (> 3 m) in the region are known for their capability to translocate shallow (< 30 m) algal biomass to deeper depths offshore (personal observation). Conversely, periods of low wave (<0.8 m) activity can be expected to result in algal biomass buildup due to a lack of physical removal, exacerbated by the reduced herbivory (see below). Under increasing water column currents, induced by meso-scale intensification of oceanic currents or by regionally intensified wind fields, algal biomass could break off from the benthos. Down-current transport of algal fragments could translocate large amounts of "new" nutrients to calmer (wind-shadowed) regions of coastline, such as our region of interest. However, particulate organic matter

loads would need to be mineralized in order for available nutrients to fuel primary production in the shallow coastal zone. The impact of such nutrients would depend on physical processes that control their residence time within the system, as discussed below.

2.5.5 Physical controls of coastal-zone nutrient residence time

2.5.5.1 Role of sediment hydrodynamics

Due to the high permeability, and therefore high hydraulic conductivity of sediments at our study site, physical forces are expected to exert great influence on particulate organic matter entrainment and fluid transport through sediments. Shum (1993) presents an approximation of the Peclet number (P) as appropriate for distinguishing when diffusive or advective processes dominate a sedimentary environment:

$$P \approx \frac{\kappa H^2}{4h\mu} \qquad \text{(EQ. 2.9)}$$

where κ is the hydraulic conductivity (m/s), H is the wave height (m), h is the water depth (m), and μ is the diffusivity (m^2/s). Under typical conditions observed at our study coastline (see below), the Peclet number ranges between $1.3 \times 10^5 – 6.7 \times 10^6$, indicating that advective conditions dominate sediment porefluid dynamics.

From flume and field data, and models of porefluid transport in rippled sandy sediments, it has been observed that pore fluids follow a hemi-elliptical path from ripple trough to ripple crest (Shum 1993; Huettel et al. 1998; Huettel et al. 2003). This directional transport of pore fluids represents a non-random process. The sandy nature of our sediments further indicates that surface sediment layers at our sites can function under an advective regime. In fact, results from our modeled pore fluid flows indicate

porewater fluid velocities in the top of sediments can range between 0.08 and 21 cm/day, and fall in the range of those observed at other sites (Table 2.9).

Oscillations in the sediment porewater nutrient concentration profiles could reflect the response to oscillations in the delivery of organic particles to the sediment. From our sediment deposition rates (Table 2.4) it is apparent that higher particle (and subsequently organic matter) deposition rates are characteristic of shallow regions of the study site. Organic matter deposition rates, in combination with the predicted sediment porefluid velocities and the low percent organic carbon of the sediments (Table 2.1), indicates that sedimentary dissolved nutrient pools in the top layer of sediment are mostly the result of active remineralization of organic matter from the water column. Therefore, in the highly permeable sediments of our study site, where porewater transport is enhanced by wave action by a factor of 10^3 to 10^6 times molecular diffusion, the time scale of non-steady state sediment porewater variability can on the order of hours to days. However, general stability of sediment porefluid nutrient profiles across temporal measurements (Figures 2.2 and 2.3) suggests particle loading rates are fairly constant throughout the year.

Presumably rapid organic matter remineralization rates (Wild et al. 2004a; Wild et al. 2004b; Rusch et al. 2006) and high transport rates of dissolved constituents in the pore fluids to the water column, suggest that large input pulses of particulate organic matter to our site could lead to rapid increases in dissolved nutrients in the water column. Rapid uptake by benthic primary producers could, in turn, readily return nutrient pools to the sediments. Thus, the cycle of production, senescence, remineralization, and production could be sustained as long as the biological communities are not physically removed from the site.

2.5.5.2 Oceanographic controls

Although the regional oceanic currents around the main Hawaiian Islands are greatly dependent on tides, wind fields, meandering of the North Equatorial Current (NEC) (Firing 1996; Qiu et al. 1997; Bingham 1998; Qiu and Durland 2002), and mesoscale eddies (Firing and Merrifield 2004), local circulation near our region of interest is mainly dependent on tides, wind fields, and incident waves (Storlazzi and Jaffe 2003; Storlazzi et al. 2003; Storlazzi et al. 2006; Storlazzi and Jaffe 2008). Results from one study near our study site indicates that nearshore (0 – 10 m depth) flows are highly dependent on incident waves, whereas flows outside of the 10-m isobath are dominated by tidal currents (Storlazzi et al. 2003). Modulation of mean currents by tides at shallow (2-10 m) depths along our study region can range between 0.17 ± 0.10 m/s and 0.05 ± 0.06 m/s at 10 and 2 m water depths, respectively (Storlazzi and Jaffe 2003). Moreover, Storlazzi et al. (2003) have shown that tidal currents (measured along the 20-m isobath) are modulated by the lunar phase, with higher and lower flows during spring and neap tides, respectively. Mean net alongshore tidally induced currents (along the 20-m isobath) were 0.25 m/s, directed NNE. The high tidally induced mean current reported by Storlazzi et al. (2003) needs to be taken with some caution, however, as it may have been affected by an extreme sea-level event caused by a meso-scale eddy passing through the region (see Firing and Merrifield 2004, Figure 2.2).

Data from moored instruments along Kahana, Maui (Storlazzi and Jaffe 2008) indicate that currents close to shore (<10 m isobath) are greatly dependent on wind strength. Storlazzi and Jaffe (2008) report that a strong (~0.10 m/s) northerly transport is observed at the 10-m isobath during the relaxation of Trade Winds, whereas reduced current speeds

are common during ‘normal’ Trade Wind conditions, and a small northerly transport occurs during the passage of local storms to the south.

The wave regime in this region is dominated by low frequency trade-wind waves that wrap around the island and arrive at the coastline from the NW/NNW (Moberly and Chamberlain 1964). Under these ‘normal’ Trade Wind conditions, and during large swell episodes, alongshore currents are slow (0 – 0.05 m/s) in a southerly direction. Data from previous studies along our study region (Vitousek 2007; Storlazzi and Jaffe 2008) have shown that, under similar tidal and wind forcing, small waves (maximum significant wave height < 0.6 m) tend to increase near-bed onshore flow in the fore-reef, whereas the mean flow on the reef flat is more variable and downwind. Under bigger waves (> 2.5 m) moderate near-bed cross-shore currents (> 0.5 m/s) developed on the fore reef, and stronger than typical cross-shore flows (> 0.1 m/s) developed on the reef flat close to shore (Vitousek 2007). Extreme wave episodes (>5 m) are expected to lead to even greater cross-shore flows which enhance physical removal of algal biomass and coral reef. However, extreme wave events along this coastline are rare.

Overall, the general circulation at a site close (~5 km north) to our study region is characterized by southerly flow close to shore and northward flow further offshore, with mean (±1 stdev) current speeds along the region of 0.24 ± 0.23 m/sec, ranging between <0.01 and 1.96 m/sec depending on wind and wave conditions (Storlazzi et al. 2003). From the limited physical oceanographic information available, it may be reasonable to conclude that the interaction of wind and waves with tides affects the residence time of water along the coastal margin of our study site. Increases in nearshore water residence time (lower currents), as brought about by wind intensification and/or lower mean

incident wave height will, in turn, increase dissolved nutrient (natural and anthropogenic) residence times. Thus, the availability of nutrients along the nearshore zone of our region of interest is a function of inputs and outputs, as controlled by both regional (i.e., wind fields) and local (i.e., wave-enhanced porefluid transport) physical processes.

2.5.6 Predictive model of C. sericea bloom periodicity: the Bloom Index.

2.5.6.1 Conceptual formulation

In the previous section (2.5.5.2) of this paper we examined the synergistic physicochemical controls of coastal zone nutrient exchange between the ocean and the land/sediment system and concluded that net currents are dependent on wind and waves (Storlazzi and Jaffe 2008), whereas nutrient delivery from land may be a function of both wave-enhanced porefluid transport and rainfall. Therefore, we now explore historical rainfall, wind speed, and significant wave height data in an attempt to synthesize the relationship between these physical factors and coastal zone nutrient exchange. Our numerical analysis targets the generation of a measure of the likelihood for macroalgal blooms to occur along the region of interest.

We utilized several types of data to determine the basic relationship between waves, wind, and rainfall, and their presumed effect on coastal hydrodynamics and nutrient residence time. First, Storlazzi and Jaffe (2008) reported that under "normal" intensified trade-wind conditions, net transport through the coast at Kahana was close to zero, whereas under wind relaxation (low trade winds) a large northward transport was observed along this region. Although the exact mechanism regulating flow in this region is not fully understood, our simplistic model proposes that wind intensification increases nutrient residence time along this region via decreased net flows close to shore.

Secondly, rainfall at Puʻu Kukui is thought to represent the main freshwater recharge to the West Maui Mountain aquifers. Groundwater in the West Maui Mountains are nutrient rich (Dollar and Andrews 1997; Laws et al. 2004; Herzfeld 2010), and an increase in rainfall-driven aquifer recharge can lead to increased SGD nutrient fluxes from land. Rainfall, in our model, serves as a proxy for increased nutrient fluxes at the coastline via surface and subsurface fresh water inputs over seasonal-annual time scales.

Lastly, wave forcing can facilitate remineralization of particulate matter entrained in sediments and nutrient exchange between the sediments and water column, therefore potentially contributing significant quantities of nutrients to the overlying seawater. In our basic model, wave height serves as a proxy for the (1) enhanced advective flux of sedimentary nutrients to the water column, (2) cross-shore mixing, and (3) physical removal of algal biomass from nearshore regions. Optimal algal growth conditions are expected under periods of low to moderate (0.5 – 2.5 m) wave heights, when advective sedimentary fluxes and onshore-cross shore currents are high, and algal removal is low. The model assumes that physical forces can lead to the homogenization of water masses close to shore, creating a nutrient-enriched buffer zone via either enhanced transport of nutrient-rich porefluids to the water column, retention of nutrients discharging into the coastal zone from fresh/brackish groundwater, or both.

2.5.6.2 Data sources

Monthly total rainfall data for the Puʻu Kukui rainfall gauge station (ID 518433, Lat/Lon: 20˚ 54´N/156˚ 35´W) for the period of 1986-2008 were downloaded from the National Climatic Data Center (NCDC) website. The Puʻu Kukui rainfall gauge is

located within the Puʻu Kukui Watershed Preserve at the summit of the Mauna Kahalawai (West Maui Mountains, Fig. 2.1) at an elevation of 1773 m.

Daily mean wind speed and direction data for the Kahului Airport Station (COOPID 512572, Lat. 20° 54" N, Lon. 156° 26" W) for the 1984-2008 period were downloaded from the NCDC website. Average monthly wind speed data were obtained using Matlab.

Hourly wave data were obtained from the US Army Corps of Engineers Coastal and Hydraulics Laboratory Wave Information Studies (WIS) group. The WIS dataset (http://frf.usace.army.mil/cgi-bin/wis/pac/pac_main.html) contains 24 years (1981-2004) of wave hindcast data for 32 stations surrounding the MHI (Figure 2.1). The wave hindcast data are derived from the Wave Watch III model to predict wave amplitude, period, and direction at locations where no physical buoy data exist. In this study we utilized data from 13 virtual buoys surrounding the island of Maui to hindcast the significant wave height over time in the region (Figure 2.1).

Monthly averages for the mean hourly wave and daily wind data were obtained using Matlab algorithms. Historic meteorological data from 1986 to 2005 (Figure 2.8) show the seasonally (and 36-month running mean) variable rainfall, wind, and wave regimes in the region of interest.

General periods of lower rainfall occurred in the 1990's, whereas a general increase in rainfall can be observed since 1997. Wind patterns show typical seasonal variability, with mean monthly summer wind speeds approaching 8 m/s and mean winter relaxations of ~5 m/s. Periods of wind intensification can be observed from 1988 to 1995, with the exception of 1993. Significant wave height predictions from WIS model outputs show

periods of decreased winter mean monthly wave maxima during 1988 to 1990, and 1999 to 2001.

2.5.6.3 The Bloom Index

From the datasets described above, a simple model was developed to describe the inter-relations between these variables in time, with the objective of utilizing such relationships to predict the episodic nature of macroalgal blooms in our region of interest. We name this simplistic model the Bloom Index (BI):

$$BI = \frac{e^{w} * r}{200 * Ho} \qquad \text{(EQ. 2.10)}$$

where *w* is the 36-month running mean (boxcar)-filtered wind velocity (m/s), *r* is the 36-month boxcar-filtered rainfall (m), and *Ho* is the 36-month boxcar-filtered significant wave height (m). Boxcar filtered Bloom Index data was de-meaned in order to show its variability about its long term mean.

Results from our analysis of the inter-relations between rainfall, wind speed, and significant wave height are shown in Figure 2.9. Our results suggest modulations of physical forces are operative at sub-decadal timescales, and are closely related to the inverse of the Pacific Decadal Oscillation (PDO) index (http://jisao.washington.edu/pdo/PDO.latest). Periods with elevated BI values (i.e., BI>0) correspond (four out of six) to years where *C. sericea* accumulations were observed in the region. Principal component analysis (PCA) of monthly data show that 88% of the total variance (λ) can be explained by approximately equal interactions of all three variables (indicated by similar eigenvalues in the first principal component (PC1); see inset table in Figure 2.9).

2.5.7 Bottom-up vs. top-down controls of the 2001 C. sericea bloom

As suggested above, physical forces can regulate the degree of inter-connectedness between biological communities and nutrient resources in space and time. However, the occurrence of macroalgal blooms can also result from other optimal natural and anthropogenic circumstances, as discussed below.

2.5.7.1 Nutrient enriched coastal zones and "new" nutrients

Recent work by Vermeij and co-workers (2009) indicates that the nutrient enrichment (via SGD inputs, wastewater disposal, and rivers) occurring over coastal regions of the island of Maui facilitates growth and survival (and hence, dispersal) of drifting fragments of the invasive algae *H. musciformis*. The authors argue that nutrient-enriched coastal waters can act as corridors facilitating the dispersal of algal fragments via increased survival across large expanses of coastline (kilometer-scale).

We hypothesize that periods of lower winter wave height allow for the build-up of *C. sericea* biomass at deeper depths (30 – 120 m). Furthermore, the combination of increased algal build-up at depth, and the likely increased along-shore water currents offshore driven by wind intensification (Storlazzi and Jaffe 2003; Storlazzi et al. 2006) during the summer months, can lead to the translocation of viable *C. sericea* fragments to shallower, calmer, wind-protected regions, with enhanced survival due to transport along a nutrient enriched coastline (Vermeij et al. 2009). Once at shallower depths, *C. sericea* is able to overcome N limitation (via SGD N inputs) and grow large populations. We further hypothesize that sediments may play a significant role in providing dissolved inorganic phosphorus within the water column, either via direct (rapid remineralization, hours to days), or indirect (see below) interactions with incoming particulate organic matter.

"New" phosphorus could be indirectly liberated to benthic primary producers by the geochemical response of sediments to an upward shift in the redox transition zone (RTZ) due to increased particulate organic matter loading. Weathering of basaltic, iron-rich, rocks leads to the formation of amorphous, highly P-adsorptive, iron oxy-hydroxides, and anthropogenicaly enhanced and natural sedimentation of land-based particles rich in iron oxy-hydroxides can affect the P-sorption capabilities of local sediments. It is well documented that changes in the redox state within sediments can lead to a significant release of iron-bound dissolved phosphorus to sediment porewater (Patrick and Khalid 1974; Colman and Holland 2000; Miller et al. 2001; Pant and Reddy 2001; Slomp et al. 2006). Although this "new" phosphorus is not thought to be readily available, due to the frequently highly oxic conditions in the surface layers of sediments, a large influx of particulate organic matter at our site could temporarily, but significantly, affect the sediment oxygen demand within the surface sediment layers. This, in turn, would lead to an upward shift in the redox transition zone. Liberation of adsorbed phosphorus to porewater, and its subsequent transport to the water column, could thus increase the phosphorus available to the benthic primary producers.

2.5.7.2 Potential role of herbivores

Many studies argue that nutrient inputs to the coastal zone can impact the ability of algae to grow and overcome herbivore grazing pressure, by freeing primary producers from nutrient limitation, thereby stimulating rapid tissue growth (D'Elia & DeBoer 1978; Lapointe & O'Connell 1989; Lapointe & Clark 1992; Lapointe et al. 1997; Smith et al. 2005), although there is no consensus on this issue (Hughes et al. 1999). Nonetheless, several studies indicate that depleting herbivore populations can greatly affect the

delicate balance between primary producers on reefs (Done 1992; Hughes 1994; Jackson 1997; Szumant 2002; Williams et al. 2008).

According to Friedlander & DeMartini (2002) the Main Hawaiian Islands (MHI) are, in general, devoid of top predators and have remarkably similar herbivore populations (see their Figure 2.3), with an average fish biomass similar to other "lightly exploited" coral reefs in the Pacific. Although the herbivore populations have not been extensively studied in the Kahekili region, this region appears to have similar fishing pressure to the rest of the MHI (Friedlander & DeMartini 2002; Williams et al. 2008). Thus, uniformly depleted fish stocks do not seem likely to explain the occurrence of an ephemeral, geographically limited macroalgal bloom, although little is known about short-term temporal variability in fish populations in this region. It appears that factors that may trigger ephemeral macroalgal blooms are not related to stable, regionally depleted, herbivore populations. Instead, herbivore populations may play a more significant role in limiting the duration and extent of episodic large increases in primary production.

2.6 CONCLUSIONS

Our results suggest particulate organic phosphorus transported to shallow sediments can undergo rapid remineralization, releasing inorganic phosphorus. Liberation of inorganic P to an N-enriched coastal region may be an important factor for the enhanced growth by an opportunistic primary producer such as the macroalgae *Cladophora sericea*. We hypothesize that *C. sericea* blooms occur as a result of the interactions between local SGD N inputs and regional meteorological conditions that facilitate particulate organic-P transport to N-enriched regions of coastline. The 2001 *C. sericea* bloom could have been triggered by the rapid remineralization of dislocated *C. sericea* populations from depth,

and sustained by the combined effects of physical oceanographic conditions on nutrient residence time and reduced herbivore populations in the region.

Sediments responsible for rapid remineralization of incoming particulate organic matter could have contributed significant amounts of nutrients to blooming benthic macroalgae (Figure 2.7). New nutrients (additional to SGD sources) required by the 2001 *C. sericea* bloom could have been supplied from deep seed algal communities that were allowed to build biomass due to decreased wave energy in years prior to bloom events, from readily desorbable sediment pools (e.g., iron-bound phosphates), or wastewater inputs (Dailer et al. 2010). Large increases in summer wind forcing could have increased offshore currents along the 20-m isobath, leading to detachment of deep seed algal communities, and the delivery of large amounts of algal fragments to calmer waters of the wind-shadowed regions of Maui. The combined effect of large porefluid transport, particle remineralization, and shifts in sediment redox state could meet phosphorus (but not nitrogen) requirements by the blooming macroalgae. Nitrogen loads from land can explain the source of the macroalgae bloom's N requirements. Predicted bloom timelines from independent N and P flux estimates match closely (days to weeks), suggesting the 2001 *Cladophora sericea* bloom resulted from the synergistic effects of natural and anthropogenic factors. Our Bloom Index suggests bloom forming factors may be cyclical at sub-decadal scales. We conclude that hydrodynamics and sedimentary processes are of fundamental importance to understand ecological change driven by nutrient dynamics in the coastal zone.

2.7 FUTURE WORK

Future work should focus on understanding the hydrodynamic circulation patterns in the region in order to verify hypothesized processes with concrete data. To make better use of our advective flux modeling technique, we need a much more detailed time-series of sediment porewater nutrient data along the vertical and horizontal axes. An understanding of the P-sorption capabilities of sediments and their response to changing redox states is also needed. Finally, an understanding of the regional circulation and the P-flux response of sediments to changing redox states will enhance our understanding of "new P" sources to ephemeral bloom-forming macroalgae.

2.8 ACKNOWLEDGEMENTS

The authors would like to acknowledge Jennifer Smith for providing the macroalgal conversion equations. Special thanks to Heather Spalding, Chris Colgrove, Shawn Fujimoto, and to the crew of Wiki-Wahine for their assistance in the field. This project was partly supported by NOAA ECOHAB Program and NSF award OCE-0327332. Special thanks to James Krest and Christopher D'Elia for providing logistical support during the preparation of this manuscript.

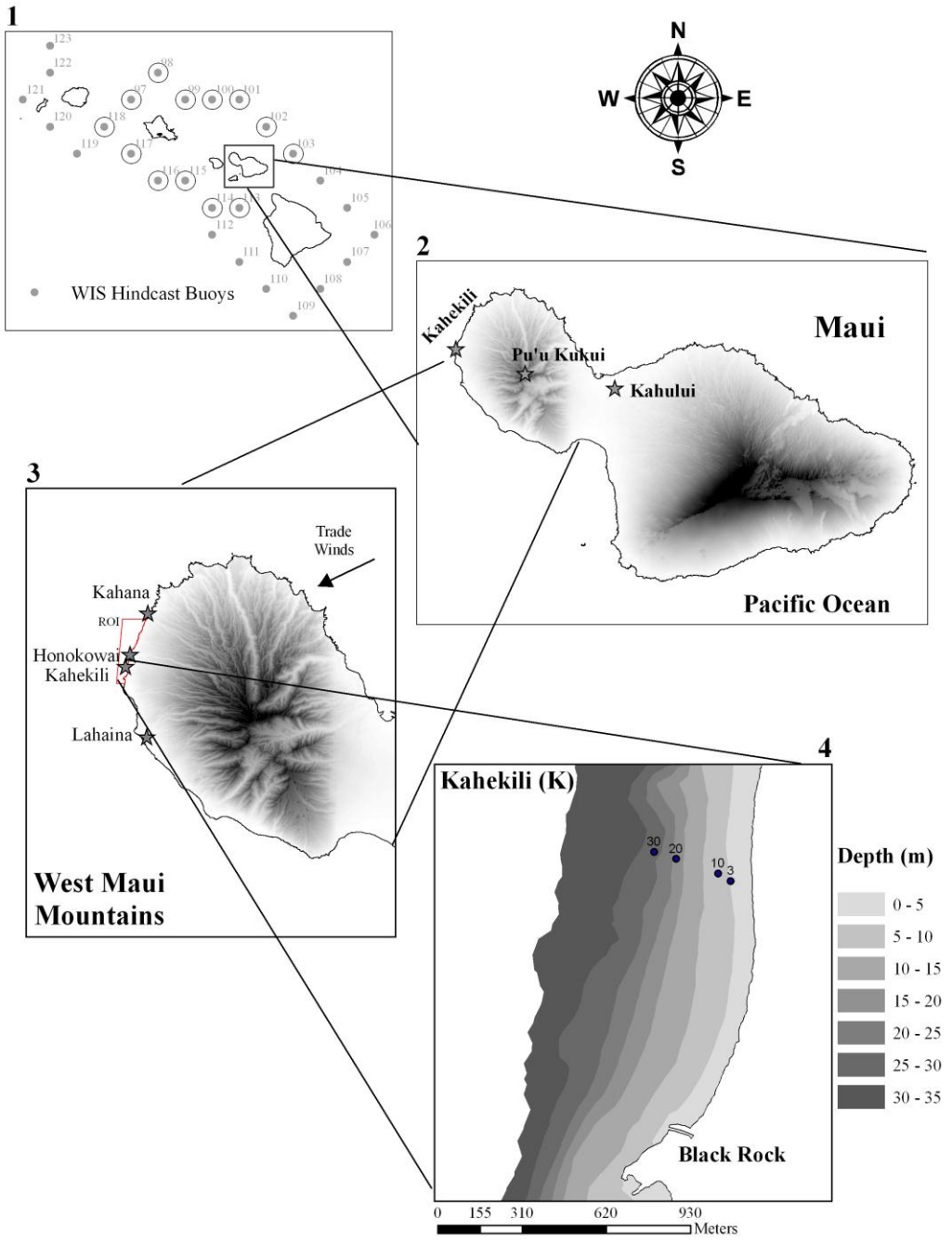

Figure 2.1 – Study region (1) Wave information systems (WIS) data buoy locations utilized in this study in bold, (2) Kahekili study location and sites from which wind and rainfall data were obtained (see text for details), (3) West Maui Mountains showing the location of relevant sites (stars) surrounding this study's region of interest (ROI), and (4) Five meter isobath gray scale contours obtained from analysis of SHOALS Lidar data (see text for more details).

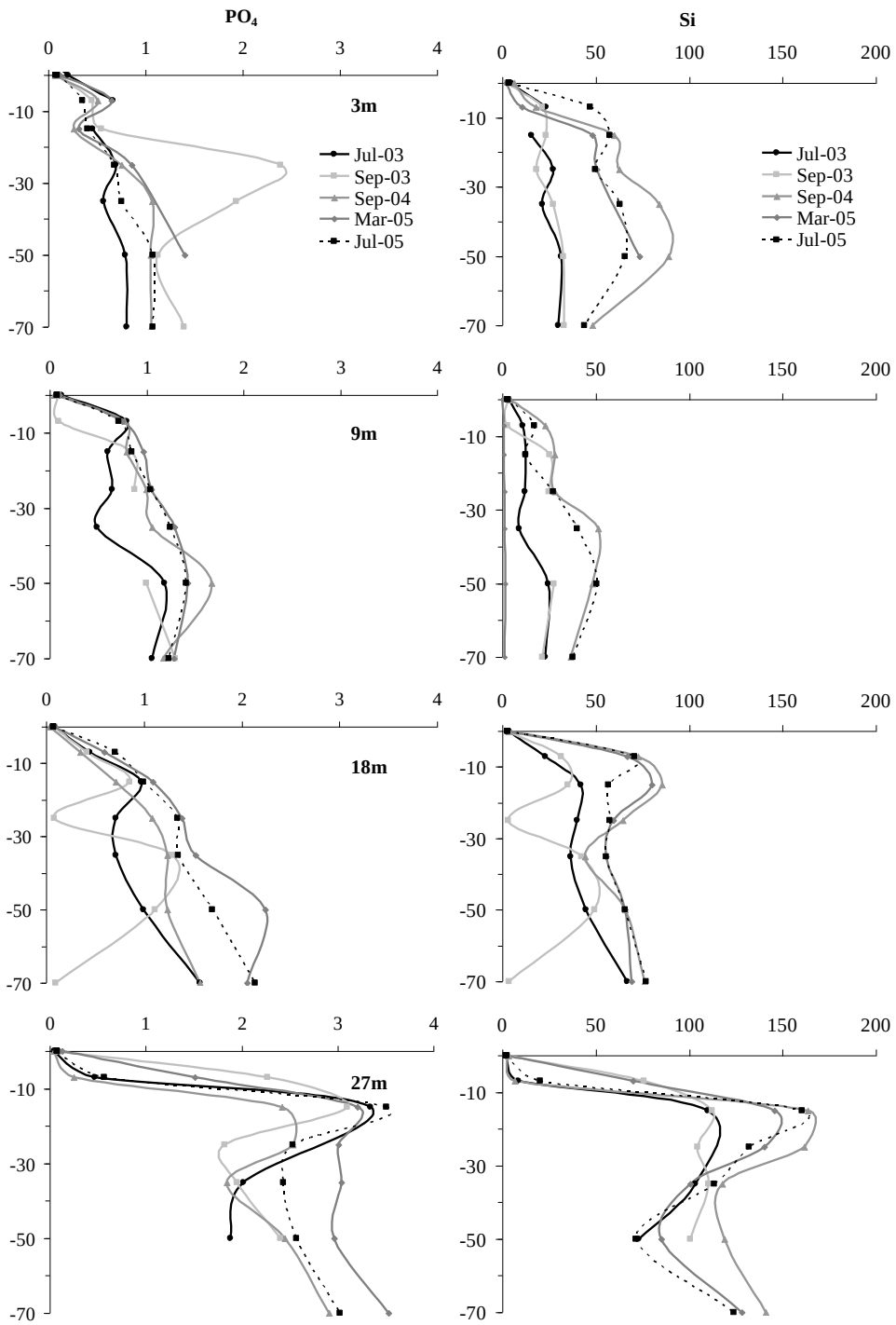

Figure 2.2 – Dissolved inorganic phosphate and silicate in porewater for Kahekili, Maui (various collection dates – abscissa (concentrations) in µmolar and ordinate (sediment depth) in cm below the sediment water interface). A sediment depth of zero (0) represents the concentration in the water column approximately 5 cm above the SWI.

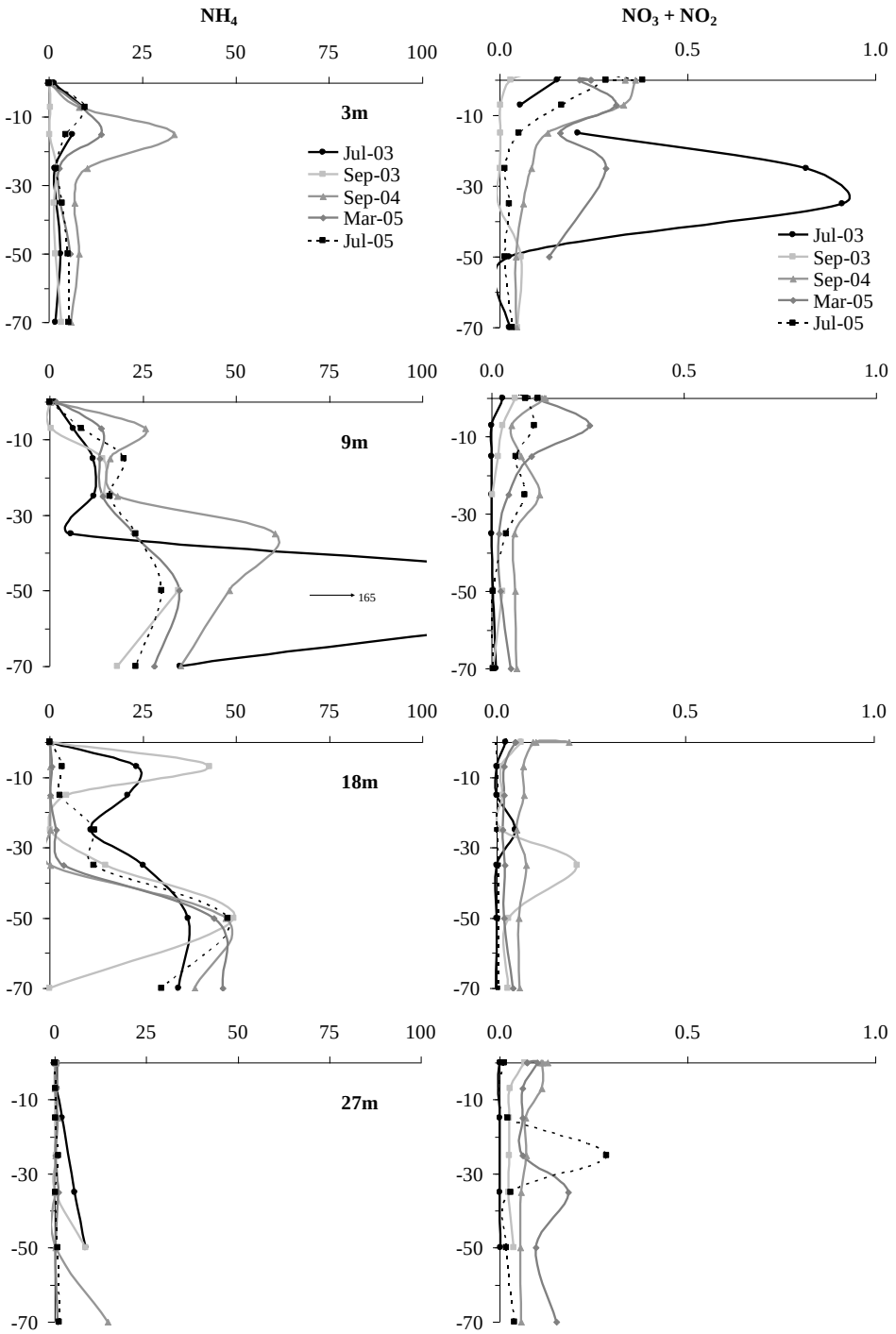

Figure 2.3 – Dissolved inorganic nitrogen species in porewater for Kahekili, Maui (various collection dates - abscissa (concentrations) in µmolar and ordinate (sediment depth) in cm below the sediment water interface). A sediment depth of zero (0) represents the concentration in the water column approximately 5 cm above the SWI.

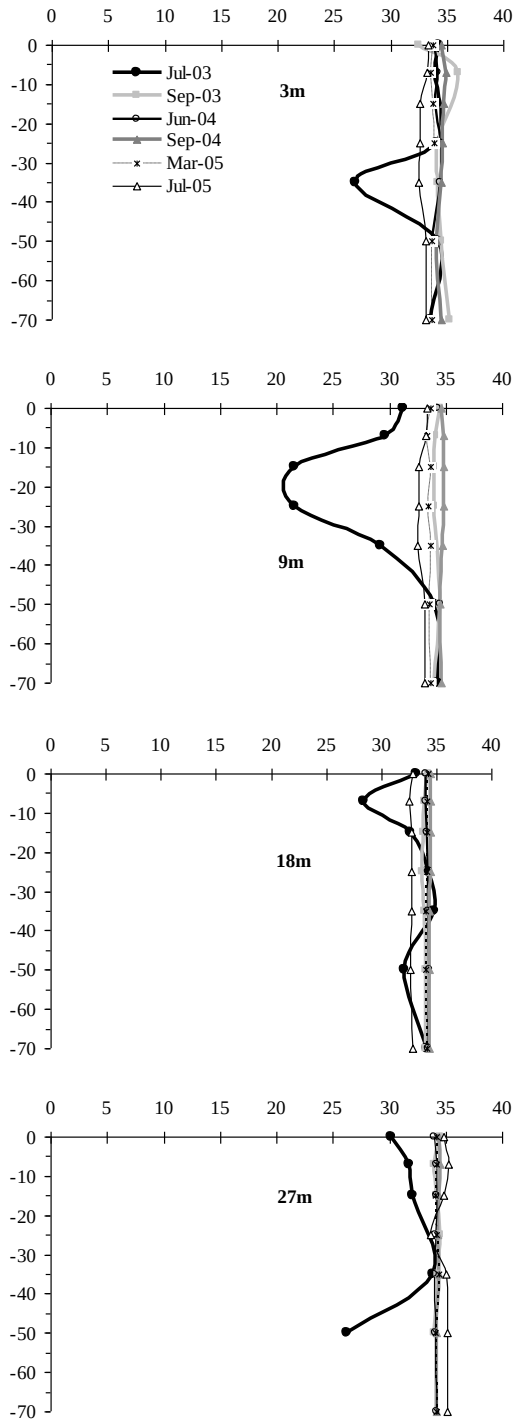

Figure 2.4 - Sediment porewater salinity at Kahekili, Maui (various collection dates - abscissa (salinity) in Practical Salinity Units (PSU) and ordinate (sediment depth) in cm below the sediment water interface. A sediment depth of zero (0) represents the concentration in the water column approximately 5 cm above the SWI.

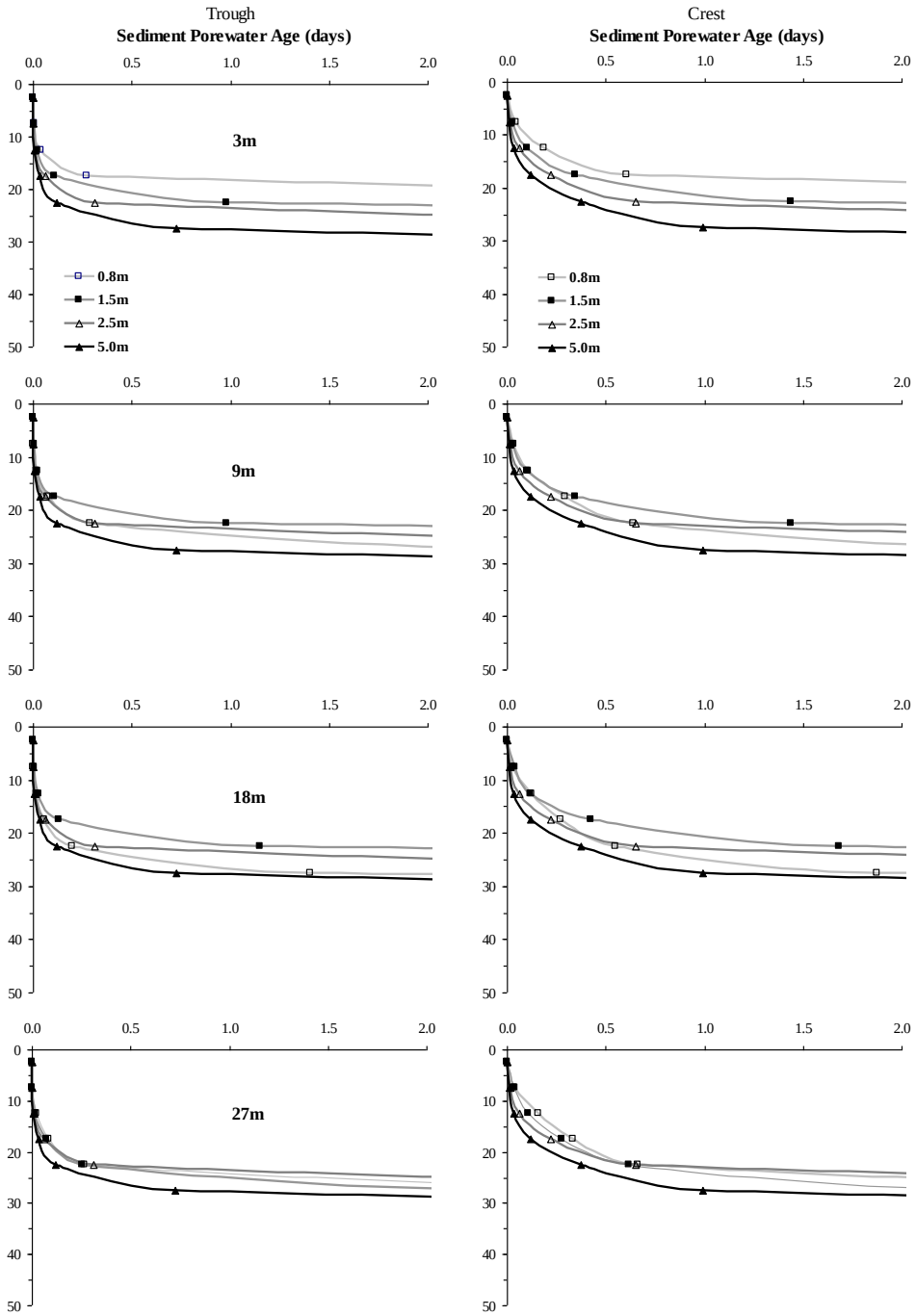

Figure 2.5 – Sediment porewater age (see text for explanation) under sediment ripple trough and crest, after 0.8, 1.5, 2.5, and 5.0 m instantaneous wave conditions are applied to the porefluid hydrodynamic model. Panels show simulations at different water depths, and ordinate axis denotes cm below the SWI.

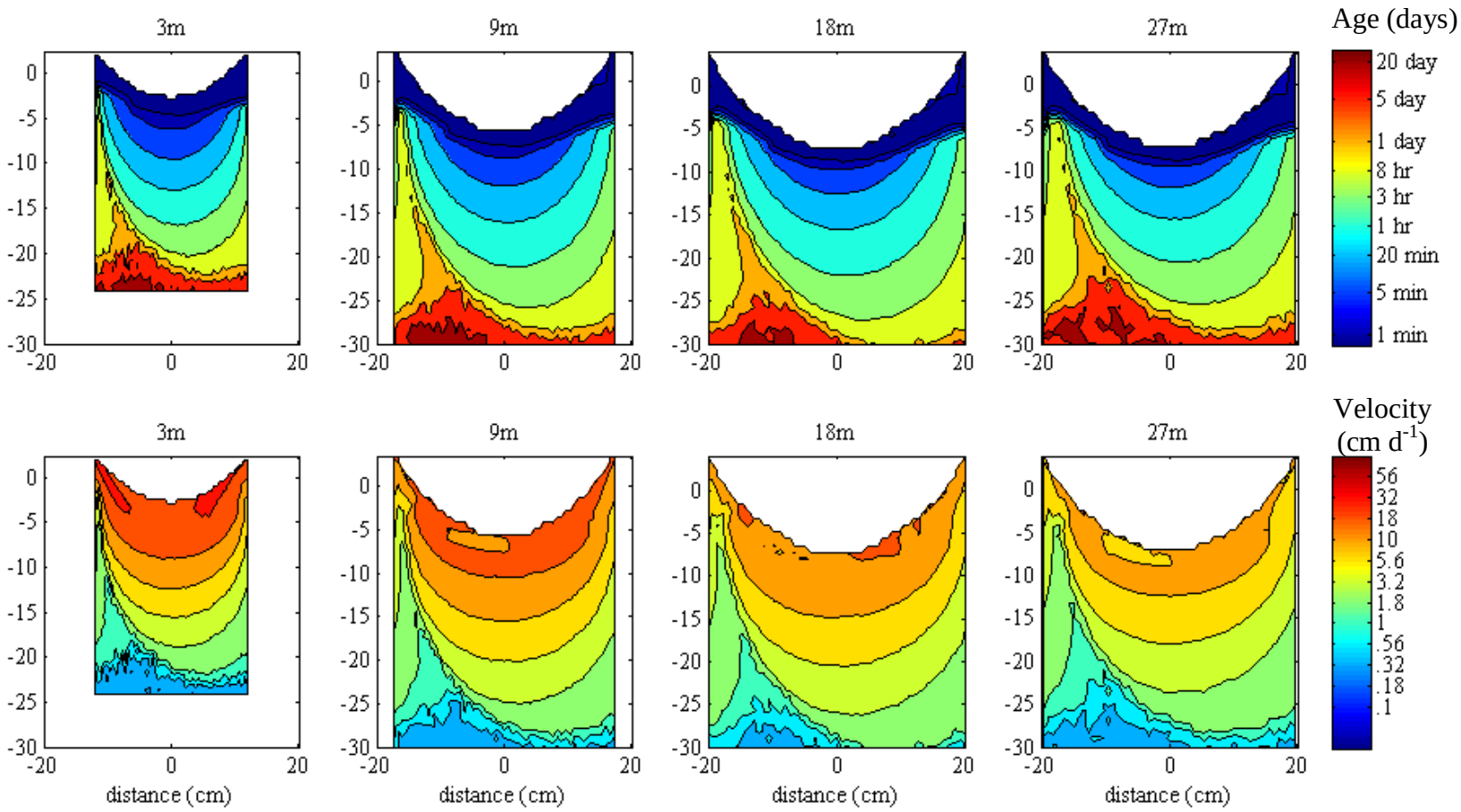

Figure 2.6 – Mean modeled sediment porewater age (top) and velocity (bottom) for the four depths under study under typical significant wave heights (Hs = 0.8 m) at Kahekili, Maui (see text for model details). Younger ages and higher porewater velocities are observed near the sediment-water interface (zero in the y-axis). Contour lines help visualize fluid flows from ripple through to ripple crest.

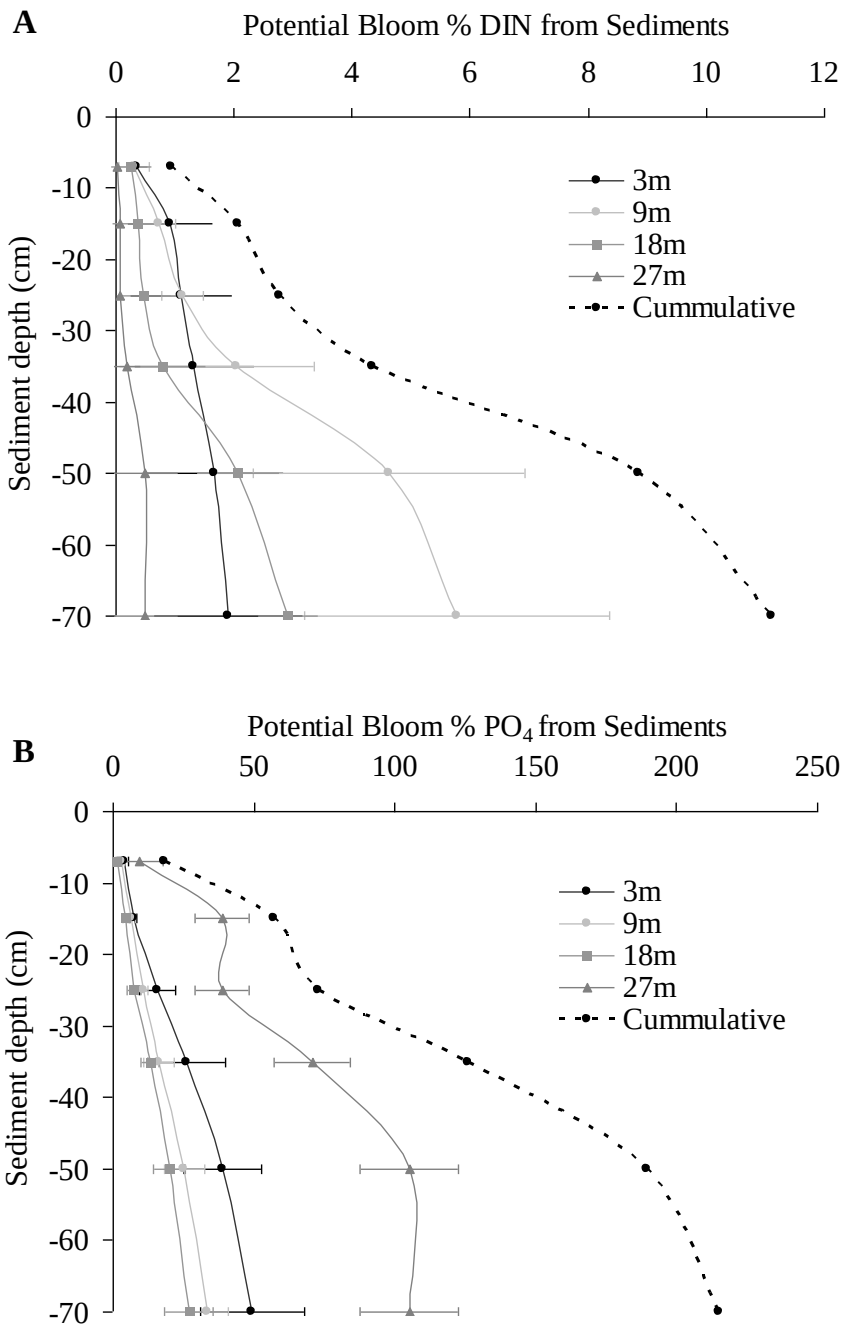

Figure 2.7 - Potential % DIN (A) and PO_4 (B) contribution to C. sericea bloom requirements from mobilized sedimentary porewater inventories as a function of depth. Cumulative potential % contribution assumes mobilization of sediment porewater to an equal depth below the sediment water interface at all water depths.

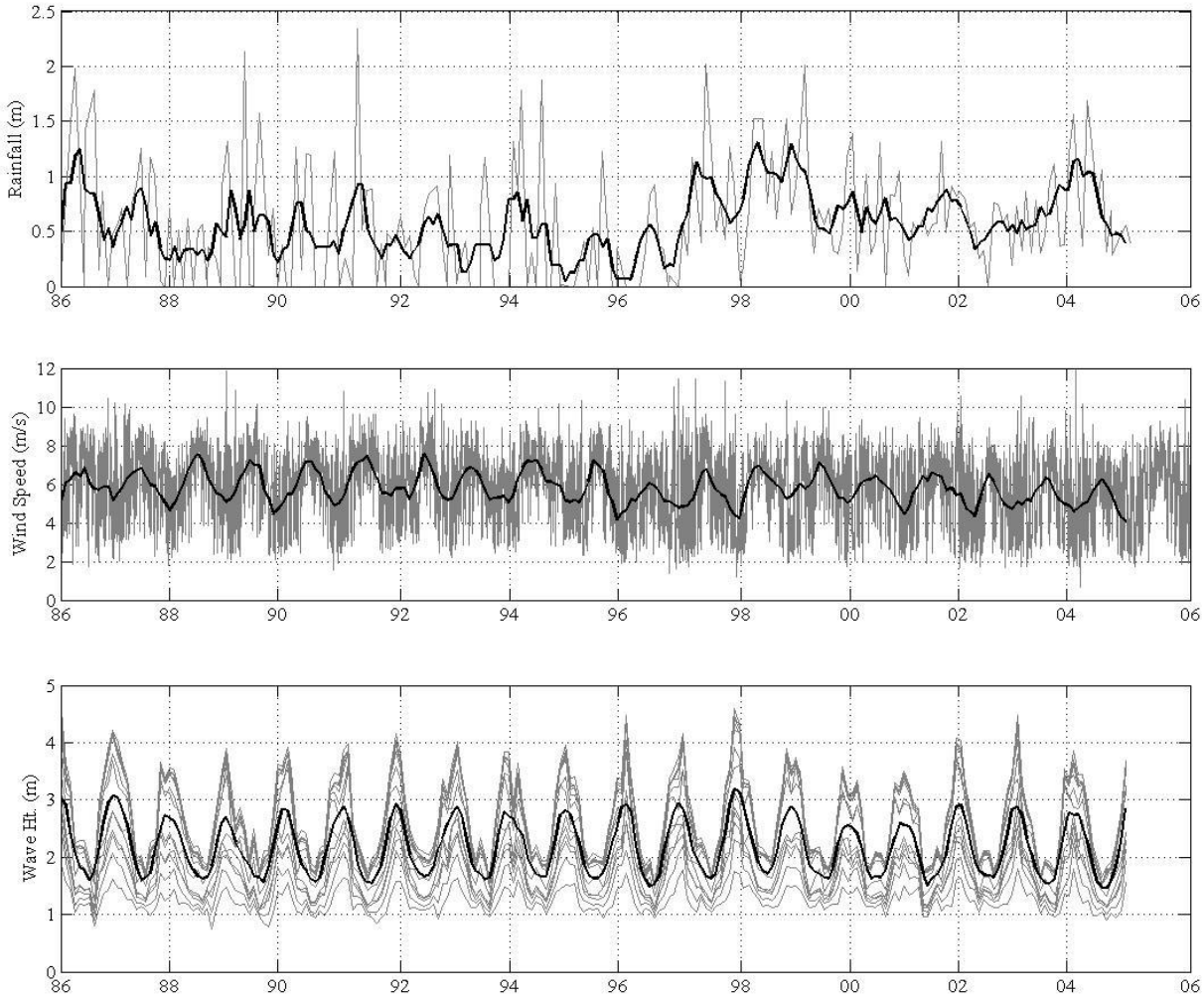

Figure 2.8 - Historical rainfall, wind, and significant wave height data (see text for details). Solid black line in each subplot denotes the 6-, 3-, and 3-month moving means for rainfall, wind speed, and wave height, respectively.

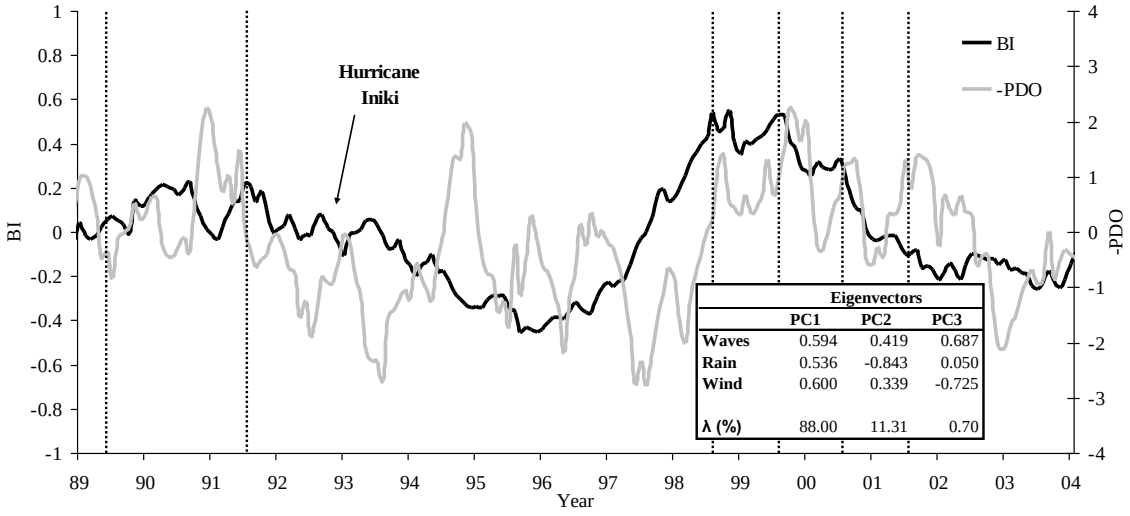

Figure 2.9 - Bloom Index (BI), as calculated from monthly averaged historical meteorological data (see text for details). Dotted lines denote years with records of *C. sericea* bloom in the region of interest. Inset table show results from covariance-based principal components analysis of all data used in the Bloom Index calculation.

Table 2.1 – Mean (standard deviation, number of replicate samples) of physicochemical data for Kahekili surface sediment samples. Depth denotes the depth of the water column above the collected sediments, d is the mean particle diameter, r is the effective radius, Φ is the porosity, k is the sediment permeability, κ is the hydraulic conductivity, and %OC and $\%CaCO_3$ are the mean percent organic carbon and percent $CaCO_3$ in the samples as determined via weight loss on ignition (see text for details). Numbers in parenthesis are the standard deviation and the number of samples analyzed. A denomination of "nan" represents samples for which enough data were not available for statistics.

Depth (m)	d (um)	r (mm)	Φ	k (m^2)	κ (m/s)	% OC	% CaCO3
3	451.74 (nan, n=1)	0.23 (nan, n=1)	*	9.22×10^{-11} (nan, n=1)	9.3×10^{-4} (nan, n=1)	1.90 (0.58, n=2)	90.45 (nan, n=1)
9	710.31 (327.85, n=5)	0.36 (0.16, n=5)	0.44 (0.04, n=3)	4.72×10^{-10} (3.97×10^{-11}, n=3)	3.8×10^{-3} (1.9×10^{-3}, n=4)	2.99 (0.99, n=10)	75.87 (5.73, n=5)
18	509.34 (104.36, n=6)	0.25 (0.05, n=6)	0.47 (0.08, n=6)	2.93×10^{-10} ($2.50 \times^{-10}$, n=8)	2.9×10^{-3} (2.5×10^{-3}, n=8)	3.14 (0.68, n=18)	82.02 (9.55, n=9)
27	*	*	*	*	*	*	*

Table 2.2 - Mean (standard deviation, number of replicate samples) of water column and sediment porewater data for Kahekili, Maui.

SITE	Water Depth (m)	Sediment Depth (cm)	PO_4	Si	NO_3	NO_2	NH_4	DIN
Kahekili	3	200	0.09 (0.02), n = 5	3.25 (0.32), n = 5	0.16 (0.07), n = 5	0.03 (0.01), n = 5	0.19 (0.23), n = 5	0.38 (0.22), n = 5
Kahekili	3	0	0.10 (0.04), n = 10	3.68 (0.04), n = 10	0.23 (1.51), n = 10	0.02 (0.1), n = 10	0.27 (0.01), n = 10	0.52 (0.42), n = 10
Kahekili	3	-7	0.52 (0.13), n = 5	24.05 (13.69), n = 5	0.15 (0.13), n = 5	0.03 (0.03), n = 5	7.23 (3.88), n = 5	7.40 (3.96), n = 5
Kahekili	3	-15	0.40 (0.11), n = 5	40.74 (20.16), n = 5	0.1 0(0.09), n = 5	0.01 (0.01), n = 5	11.68 (13.16), n = 5	11.79 (13.19), n = 5
Kahekili	3	-25	1.07 (0.74), n = 5	41.76 (18.27), n = 5	0.21 (0.33), n = 5	0.02 (0.03), n = 5	3.75 (3.62), n = 5	3.99 (3.53), n = 5
Kahekili	3	-35	1.08 (0.60), n = 4	48.84 (29.81), n = 4	0.25 (0.45), n = 4	0.00 (0.01), n = 4	3.43 (2.51), n = 4	3.68 (2.39), n = 4
Kahekili	3	-50	1.09 (0.22), n = 5	58.45 (25.53), n = 5	0.03 (0.05), n = 5	0.02 (0.02), n = 5	4.78 (2.45), n = 5	4.83 (2.45), n = 5
Kahekili	3	-70	1.09 (0.24), n = 4	38.77 (8.65), n = 4	0.02 (0.02), n = 4	0.02 (0.02), n = 4	4.11 (1.90), n = 4	4.15 (1.90), n = 4
Kahekili	9	200	0.08 (0.01), n = 5	2.77 (0.01), n = 5	0.03 (0.03), n = 5	0.01 (0.01), n = 5	0.29 (0.53), n = 5	0.33 (0.51), n = 5
Kahekili	9	0	0.09 (0.04), n = 13	3.29 (0.94), n = 13	0.11 (0.05), n = 13	0.01 (0.02), n = 13	0.36 (0.58), n = 13	0.48 (0.57), n = 13
Kahekili	9	-7	0.62 (0.30), n = 5	13.71 (7.49), n = 5	0.07 (0.08), n = 5	0.02 (0.02), n = 5	11.01 (9.55), n = 5	11.10 (9.58), n = 5
Kahekili	9	-15	0.81 (0.13), n = 5	18.66 (7.39), n = 5	0.04 (0.04), n = 5	0.01 (0.01), n = 5	15.10 (3.12), n = 5	15.15 (3.14), n = 5
Kahekili	9	-25	0.92 (0.17), n = 5	22.98 (6.42), n = 5	0.04 (0.04), n = 5	0.01 (0.02), n = 5	15.03 (2.34), n = 5	15.08 (2.39), n = 5
Kahekili	9	-35	1.02 (0.37), n = 4	35.25 (18.37), n = 4	0.03 (0.02), n = 4	0.00 (0.00), n = 4	27.99 (23.08), n = 4	28.02 (23.10), n = 4
Kahekili	9	-50	1.34 (0.26), n = 5	39.94 (12.68), n = 5	0.01 (0.01), n = 5	0.01 (0.02), n = 5	62.8 (58.18), n = 5	62.83 (58.17), n = 5
Kahekili	9	-70	1.21 (0.10), n = 5	30.54 (7.85), n = 5	0.02 (0.03), n = 5	0.00 (0.00), n = 5	27.9 (7.47), n = 5	27.93 (7.49), n = 5
Kahekili	18	200	0.08 (0.00), n = 5	2.76 (0.21), n = 5	0.01 (0.01), n = 5	0.01 (0.01), n = 5	0.57 (0.87), n = 5	0.58 (0.88), n = 5
Kahekili	18	0	0.08 (0.03), n = 13	2.95 (0.75), n = 13	0.05 (0.05), n = 13	0.01 (0.02), n = 13	0.10 (0.07), n = 13	0.16 (0.10), n = 13
Kahekili	18	-7	0.50 (0.14), n = 5	52.79 (23.72), n = 5	0.02 (0.03), n = 5	0.00 (0.01), n = 5	14.06 (18.72), n = 5	14.08 (18.71), n = 5
Kahekili	18	-15	0.93 (0.15), n = 5	59.77 (22.39), n = 5	0.02 (0.03), n = 5	0.01 (0.01), n = 5	5.73 (8.73), n = 5	5.75 (8.72), n = 5
Kahekili	18	-25	0.92 (0.54), n = 5	45.00 (25.10), n = 5	0.02 (0.03), n = 5	0.01 (0.01), n = 5	5.04 (6.03), n = 5	5.07 (6.02), n = 5
Kahekili	18	-35	1.23 (0.31), n = 5	46.77 (8.50), n = 5	0.02 (0.04), n = 5	0.05 (0.09), n = 5	11.17 (9.75), n = 5	11.24 (9.74), n = 5
Kahekili	18	-50	1.46 (0.51), n = 5	58.20 (10.35), n = 5	0.01 (0.03), n = 5	0.01 (0.01), n = 5	45.15 (4.85), n = 5	45.17 (4.86), n = 5
Kahekili	18	-70	1.49 (0.82), n = 5	58.36 (31.02), n = 5	0.01 (0.02), n = 5	0.02 (0.02), n = 5	30.03 (17.80), n = 5	30.06 (17.8), n = 5
Kahekili	27	200	0.08 (0.01), n = 5	2.45 (0.53), n = 5	0.01 (0.03), n = 5	0.02 (0.01), n = 5	0.11 (0.07), n = 5	0.13 (0.06), n = 5
Kahekili	27	0	0.07 (0.03), n = 11	2.40 (0.65), n = 11	0.06 (0.05), n = 11	0.01 (0.01), n = 11	0.24 (0.21), n = 11	0.30 (0.21), n = 11
Kahekili	27	-7	1.01 (0.85), n = 5	36.19 (33.94), n = 5	0.02 (0.04), n = 5	0.02 (0.03), n = 5	0.34 (0.22), n = 5	0.38 (0.19), n = 5
Kahekili	27	-15	3.11 (0.42), n = 5	138.36 (25.78), n = 5	0.02 (0.03), n = 5	0.02 (0.03), n = 5	0.72 (0.73), n = 5	0.76 (0.72), n = 5
Kahekili	27	-25	2.48 (0.49), n = 4	134.51 (23.62), n = 4	0.09 (0.13), n = 4	0.02 (0.03), n = 4	0.46 (0.41), n = 4	0.57 (0.52), n = 4
Kahekili	27	-35	2.26 (0.49), n = 5	108.99 (7.10), n = 5	0.02 (0.03), n = 5	0.04 (0.08), n = 5	1.42 (2.29), n = 5	1.48 (2.28), n = 5
Kahekili	27	-50	2.45 (0.39), n = 5	89.76 (20.03), n = 5	0.01 (0.02), n = 5	0.03 (0.04), n = 5	3.65 (4.48), n = 5	3.70 (4.46), n = 5
Kahekili	27	-70	3.16 (0.33), n = 3	130.97 (8.85), n = 3	0.03 (0.03), n = 3	0.05 (0.08), n = 3	5.42 (7.77), n = 3	5.50 (7.75), n = 3

Table 2.3 – Mean (standard deviation, number of replicate samples) water column and sediment nutrient ratios at all water depths.

SITE	WATER DEPTH (m)	SEDIMENT DEPTH (cm)	DIN:DIP	Si:DIP	Si:DIN
Kahekili	3	2	3.98 (1.46), n = 5	36.12 (6.62), n = 5	7.30 (3.51), n = 5
Kahekili	3	0	5.14 (0.39), n = 10	42.59 (3.46), n = 10	5.19 (27.95), n = 10
Kahekili	3	-7	14.72 (9.73), n = 5	53.91 (46.48), n = 5	13.46 (24.33), n = 5
Kahekili	3	-15	39.67 (52.01), n = 5	119.39 (81.13), n = 5	28.16 (51.95), n = 5
Kahekili	3	-25	4.92 (4.97), n = 5	52.55 (30.02), n = 5	13.02 (7.00), n = 5
Kahekili	3	-35	4.24 (2.50), n = 4	53.53 (33.41), n = 4	14.29 (5.64), n = 4
Kahekili	3	-50	4.47 (2.20), n = 5	53.35 (21.23), n = 5	12.84 (3.46), n = 5
Kahekili	3	-70	3.82 (1.73), n = 4	36.71 (9.28), n = 4	10.63 (4.22), n = 4
Kahekili	9	2	4.33 (6.70), n = 5	34.95 (2.41), n = 5	16.34 (9.25), n = 5
Kahekili	9	0	5.38 (5.29), n = 13	43.69 (26.48), n = 13	8.87 (5.15), n = 13
Kahekili	9	-7	15.61 (11.26), n = 5	23.50 (6.95), n = 5	2.23 (1.91), n = 5
Kahekili	9	-15	18.89 (3.59), n = 5	23.26 (9.00), n = 5	1.26 (0.48), n = 5
Kahekili	9	-25	16.52 (1.98), n = 5	24.58 (4.27), n = 5	1.50 (0.27), n = 5
Kahekili	9	-35	26.32 (20.84), n = 4	32.59 (12.50), n = 4	1.47 (0.44), n = 4
Kahekili	9	-50	50.00 (50.78), n = 5	29.51 (5.99), n = 5	1.00 (0.59), n = 5
Kahekili	9	-70	23.60 (7.95), n = 5	25.34 (6.30), n = 5	1.14 (0.35), n = 5
Kahekili	18	2	7.12 (10.63), n = 5	34.89 (1.81), n = 5	28.31 (30.19), n = 5
Kahekili	18	0	2.54 (2.61), n = 13	43.10 (25.17), n = 13	23.74 (22.78), n = 13
Kahekili	18	-7	32.30 (44.89), n = 5	109.35 (59.98), n = 5	69.56 (97.35), n = 5
Kahekili	18	-15	6.04 (8.95), n = 5	66.83 (32.43), n = 5	147.43 (188.51), n = 5
Kahekili	18	-25	5.66 (6.57), n = 5	48.22 (8.90), n = 5	63.70 (109.21), n = 5
Kahekili	18	-35	11.67 (13.88), n = 5	39.34 (7.23), n = 5	25.35 (43.88), n = 5
Kahekili	18	-50	33.57 (9.71), n = 5	42.05 (8.83), n = 5	1.29 (0.19), n = 5
Kahekili	18	-70	16.92 (9.71), n = 5	38.95 (6.26), n = 5	7.61 (12.61), n = 5
Kahekili	27	2	1.65 (0.66), n = 5	30.50(4.44), n = 5	19.20 (6.08), n = 5
Kahekili	27	0	4.78 (3.96), n = 11	40.59 (25.05), n = 11	13.46 (12.12), n = 11
Kahekili	27	-7	0.63 (0.52), n = 5	31.99 (10.41), n = 5	93.63 (83.57), n = 5
Kahekili	27	-15	0.25 (0.22), n = 5	45.59 (13.54), n = 5	348.61 (287.57), n = 5
Kahekili	27	-25	0.24 (0.20), n = 4	54.91 (7.32), n = 4	308.57 (173.40), n = 4
Kahekili	27	-35	0.69 (1.14), n = 5	50.18 (11.47), n = 5	298.23 (260.88), n = 5
Kahekili	27	-50	1.72 (2.16), n = 5	37.13 (8.90), n = 5	155.91 (197.03), n = 5
Kahekili	27	-70	1.87 (2.68), n = 3	41.88 (6.10), n = 3	79.00 (60.96), n = 3

Table 2.4 - Sediment deposition rate (w) and percent organic carbon (%OC) of particles being deposited at each site in Kahekili, Maui.

Depth (m)	ω (mg/day)	%OC
3	407.1 (763.1, n=9)	14.72 (6.17, n=7)
9	161.8 (168.4, n=9)	13.93 (6.55, n=9)
18	36.0 (20.5, n=8)	17.93 (3.85, n=9)
27	16.0 (11.4, n=5)	18.31 (7.36, n=5)

Table 2.5 – Sampled sediment profiles (n) and mean (standard deviation) diffusive nutrient fluxes from sediments off Kahekili, Maui. Superscript letters denote Student's t-test multiple comparisons of 1-way ANOVA. Absence of a letter denotes significant ($p<0.05$) differences amongst groups.

Water Depth (m)	n	Diffusive Flux (µmol/m^2/day)					
		PO_4	Si	NO_3	NO_2	NH_4	DIN
3	5	0.04 (0.04)^a	0.37 (0.19)^a	-0.03 (0.02)^a	0.00 (0.00)^a	3.89 (2.65)^a	3.86 (2.64)^a
9	5	0.01 (0.04)^a	0.13 (0.94)^a	0.01 (0.00)^b	0.00 (0.00)^a	3.92 (2.89)^a	3.92 (2.88)^a
18	5	0.04 (0.01)^a	0.94 (0.83)^b	0.00 (0.00)^b	0.00 (0.00)^a	2.89 (0.50)^a	2.88 (0.50)^a
27	5	0.18 (0.12)^b	3.13 (0.60)^c	0.00 (0.00)^b	0.00 (0.01)^a	0.39 (0.30)^b	0.38 (0.30)^b

Table 2.6 – Sampled sediment profiles (n) and mean (standard deviation) advective nutrient fluxes from the top (1cm) surface sediments off Kahekili, Maui. Superscript letters denote Student's t-test multiple comparisons of 1-way ANOVA. Absence of a letter denotes significant ($p<0.05$) differences amongst groups.

Water Depth (m)	n	Advective Flux (µmol/m^2/day)					
		PO_4	Si	NO_3	NO_2	NH_4	DIN
3	5	2.39 (0.82)^a	89.32 (85.31)^a	-0.16 (0.40)^a	0.02 (0.22)^a	30.59 (24.86)^a	30.45 (24.74)^a
9	5	15.31 (7.86)^b	309.67 (182.16)^b	0.22 (2.03)^a	0.41 (0.90)^a	286.02 (312.59)^b	287.08 (311.38)^b
18	5	1.94 (0.89)^a	291.06 (152.48)^b	-0.15 (0.15)^a	-0.04 (0.07)^a	95.32 (134.68)^{ab}	95.13 (134.65)^{ab}
27	5	3.22 (4.15)^a	123.76 (145.45)^{ab}	-0.15 (0.18)^a	0.07 (0.13)^a	0.39 (1.19)^a	0.32 (1.13)^a

Table 2.7 – Estimated average depth integrated nutrient inventories for sediments at different water depths off Kahekili, Maui

		Depth Integrated Nutrient Inventories (µmoles/m^2)				
Water Depth (m)	**Sediment Depth (cm)**	**PO_4^{3-}**	**$Si(OH)_4$**	**NO_3^-**	**NO_2^-**	**NH_4^+**
3	-7	32.76	1515.15	9.45	1.89	455.49
	-15	57.96	4081.77	15.75	2.52	1191.33
	-25	125.37	6712.65	28.98	3.78	1427.58
	-35	227.43	11328.03	52.61	3.78	1751.72
	-50	330.44	16851.56	55.44	5.67	2203.43
	-70	433.44	20515.32	57.33	7.56	2591.82
9	-7	39.34	869.90	4.44	1.27	698.58
	-15	90.73	2053.88	6.98	1.90	1656.68
	-25	149.11	3511.96	9.52	2.54	2610.33
	-35	246.19	6866.88	12.37	2.54	5274.28
	-50	373.72	10668.17	13.32	3.49	11251.27
	-70	488.88	13574.81	15.23	3.49	13906.65
18	-7	15.53	1639.13	0.62	0.00	436.56
	-15	44.40	3494.99	1.24	0.31	614.48
	-25	72.97	4892.24	1.86	0.62	770.97
	-35	130.25	7070.55	2.79	2.95	1291.21
	-50	198.25	9781.22	3.26	3.42	3394.08
	-70	267.65	12499.33	3.73	4.35	4792.72
27	-7	94.54	3387.38	1.87	1.87	31.82
	-15	385.63	16337.88	3.74	3.74	99.22
	-25	617.76	28928.02	12.17	5.62	142.27
	-35	935.06	44230.21	14.98	11.23	341.64
	-50	1279.04	56832.52	16.38	15.44	854.10
	-70	1722.71	75220.70	20.59	22.46	1615.07

Note: Depth integrated nutrient inventories represent the cumulative mass of solute (C) under 1 m^2 of seabed. Mass of solute C under the seabed was calculated by multiplying the average porewater concentration ([C]) sampled at each depth by its mean sediment porosity, and *d*, the diameter of the sphere of influence represented by our porefluid sampling technique (*[C]*x *porosity* x *d*).

Table 2.8 - Summary of calculations for the 2001 *C. sericea* bloom nutrient and time requirements (see text for details)

Parameter	Value	Units	Source
BLOOM EXTENT			
Coastal distance	7	km	This study - calculated
Distance offshore	850	m	Smith, et al. (2005)
Bloom sediment area	5.96E+06	m^2	This study - calculated
BLOOM BIOLOGICAL PARAMETERS			
Percent benthic area cover	23.1	%	Smith, et al. (2005)
Average algal height	0.2	meters	Huisman, et al. (2007)
Dry biomass (see text for explanation)	4.44E+05	kg	This study - calculated
UPTAKE RATES			
k_{PO4}	0.06	µmol/L/hr	Thybo-Christesen, et al. (1993)
k_{NO3}	0.12	µmol/L/hr	Thybo-Christesen, et al. (1993)
k_{NH4}	0.29	µmol/L/hr	Thybo-Christesen, et al. (1993)
TISSUE CNP CONTENT			
% Carbon	36	%	Smith, et al. (2005)
% Nitrogen	1.5	%	Smith, et al. (2005)
% Phosphorus	0.02	%	Smith, et al. (2005)
TOTAL BLOOM MOLAR ESTIMATE			
C	1.2E+07	mol C	This study - calculated
DIN	4.4E+05	mol N	This study - calculated
PO_4	2.7E+03	mol P	This study - calculated
BLOOM TIMELINE (as per Thybo-Christensen, et al., 1993 uptake rates)			
NO_3	1393.6	days	This study - calculated
NH_4	576.7	days	This study - calculated
PO_4	16.8	days	This study - calculated
BLOOM TIMELINE (as per Paytan, et al., 2006 TIN SGD loading rates)			
TIN loading rate	82	mmol TIN/m/hr	Paytan, et al., 2006
Tiime to bloom (bloom moles/TIN loading rate*coastal distance)	32.0	days	This study - calculated
BLOOM TIMELINE (this study modeled advective fluxes)			
Mean DIN flux (±1 stdev)	1.8	$mmol/m^2/day$	This study - calculated
Mean PO_4 flux (±1 stdev)	0.1	$mmol/m^2/day$	This study - calculated
DIN timeline (bloom DIN moles/(mean flux x sediment area))	41.9	days	This study - calculated
PO_4 timeline (bloom PO_4 moles/(mean flux x sediment area))	3.7	days	This study - calculated

Table 2.9 - Reported porefluid velocities for permeable sediments

Velocity (cm/hr)	Origin and type of sediment	Measurement type	Reference
0.38	Wave amplitude 10cm, water depth 20cm, k=2.9x10^{-11} m^2, wavelength 120cm, median grain = 250 μm	Wave tank	Huettle et al., 2003
0.16 - 2.46	Rhodamine tracer, wave amplitude 6-8 cm, water depth ~20cm, k=1.32 - 2.02 x10^{-11} m^2, wavelength ~80cm, median grain = 100-300 μm	Wave tank	Precht and Huettel, 2003
7.92	Lotic beaches at Onslow Bay, North Carolina (USA)	In-field thermistors	Riedl, 1972
3.2 - 53	Mid-Atlantic Bight (USA), continental shelf sand deposit	Iodide breaktrhough	Reimers et al., 2004
130	Amphioxus coarse sands, LeRacou (Roussillon), France	In- field, flourescein eflux	Webb and Theodor, 1968
0.06 - 26.3	Advection, unidirectional flow	Flourescent tracer using optode technique	Precht and Huettel, 2004
0.13	Advection, unidirectional flow with mounds	Particle tracer on flume	Huettel et al., 1996
20.5 - 40	Coastal sandy sediments, Campese Bay, Giglio Island, Italy	In-field optical sensors detecting neutrally bouyant flourescein	Precht and Huettel, 2004
0.25 - 63	Coastal sandy sediments from Kahekili, Maui. Permeability 2.93x10^{-10} - 9.2x10^{-11}m^2	Modeled sediments from Kahekili, Maui	This study

2.9 LITERATURE CITED

Bennett P, U. Keuper-Bennett. 2009. An underwater history of Honokowai (1988 - 1995: Algae blooms, coral heads, and sea turtles. www.turtles.org/honohist.htm.

Berner R.A. 1980. Early diagenesis: A theoretical approach, Princeton University Press, New Jersey.

Bienfang P. 1980. Water quality characteristics of Honokohau harbor: A subtropical embayment affected by groundwater intrusion. Pacific Science 34:279-291.

Bingham F.M. 1998. Evidence for the existence of a North Hawaiian Ridge Current. Journal of Physical Oceanography 28:991-998.

Boudreau B.P. 2000. The mathematics of early diagenesis: form worms to waves. Reviews of Geophysics 38:389-416.

Burdige D.J. 2006. Geochemistry of marine sediments, Princeton University Press, New Jersey.

Caldwell, P.C., 2007. Spectral density composites for aiding Hawaiian southern shore surf forecasts, International workshop on wave hindcasting and forecasting, Turtle Bay, Oahu. November 13-16.

Caldwell, P.C. and J.P. Aucan. 2007. An empirical method for estimating surf heights from deepwater significant wave heights and peak periods in coastal zones with narrow shelves, steep bottom slopes, and high refraction. Journal of Coastal Research, 23(5): 1237-1244.

Capone D., J. Slater. 1990. Interannual patterns of water table height and groundwater derived nitrate in nearshore sediments. Biogeochemistry 10:277-288.

Charette M.A., E.R. Sholkovitz. 2002. Oxidative precipitation of groundwater-derived ferrous iron in the subterranean estuary of a coastal bay. Geophysical Research Letters 29:85.81 - 85.84.

D'Elia C.F., J.A. DeBoer. 1978. Nutritional studies of two red algae. II. Kinetics of ammonium and nitrate uptake. Journal of Phycology 14:266-272.

Dailer, M., R.S. Knox, J.E. Smith, M. Napier, and C.M. Smith. 2010. Using $d^{15}N$ values in algal tissue to map locations and potential sources of anthropogenic nutrient inputs on the island of Maui, Hawai‘i, USA. Marine Pollution Bulletin, 60(5): 655-671.

Dean W.E., Jr. 1974. Determination of carbonate and organic matter in calcareous sediments and sedimentary rocks by loss of ignition: comparison with other methods. Journal of Sedimentary Petrology 44:242-248.

Dierssen, H.M., R.C. Zimmerman, L.A. Drake, and D.J. Burdige. 1999. Potential export of unattached benthic macroalgae to the deep sea through wind-driven Langmuir circulation. Geophysical Research Letters, 36(L04602, doi:10.1029/2008GL036188): 1-5.

Dollar S.J., C. Andrews. 1997. Algal blooms off West Maui: Assessing causal linkages between land and the coast ocean, National Oceanic and Atmospheric Administration Coastal Ocean Program Office, Honolulu, Honolulu.

Dollar, S.J. and M.J. Atkinson. 1992. Effects of nutrient subsidies from groundwater to nearshore marine ecosystems off the island of Hawaii. Estuarine, Coastal and Shelf Science, 35(4): 409-424.

Done T.J. 1992. Phase shifts in coral reef communities and their ecological significance. Hydrobiologia 247:121-132.

Elliott A.H., N.H. Brooks. 1997a. Transfer of non-sorbing solutes to a streambed with bed forms: Theory. Water Resources Research 33:123-136.

Elliott A.H., N.H. Brooks. 1997b. Transfer of non-sorbing solutes to a streambed with bed forms: Laboratory experiments. Water Resources Research 33:137-151.

Falter J.L. 1998. Time-variant diagenesis within the redox transition zone of an advectively driven sediment. Master's Thesis, University of Hawai'i at Manoa.

Falter J.L., F.J. Sansone. 2000a. Hydraulic control of porewater geochemistry within the oxic-suboxic zone of a permeable sediment. Limnology and Oceanography 45:550-557.

Falter J.L., F.J. Sansone. 2000b. Shallow pore water sampling in reef sediments. Coral Reefs 19:93-97.

Firing E. 1996. Currents observed north of Oahu during the first five years of HOT. Deep Sea Research II: Topical Studies in Oceanography 43:281-303.

Firing Y.L., M.A. Merrifield. 2004. Extreme sea level events at Hawaii: Influence of mesoscale eddies. Geophysical Research Letters 31:1-4.

Friedlander A.M., E.E. DeMartini. 2002. Contrasts in density, size, and biomass of reef fishes between the northwestern and the main Hawaiian Islands: the effects of fishing down apex predators. Marine Ecology Progress Series 230:253-264.

Froelich P.N., G.P. Klinkhammer, M.L. Bender, N.A. Luedtke, G.R. Heath, D. Cullen, P. Dauphin, D. Hammond, B. Hartman, V. Maynard. 1979. Early oxidation of organic matter in pelagic sediments of the eastern equatorial Atlantic: suboxic diagenesis. Geochimica et Cosmochimica Acta 43:1075-1090.

Garrison G.H., C.R. Glenn, G.M. McMurtry. 2003. Measurement of submarine groundwater discharge in Kahana Bay, O'ahu, Hawai'i. Limnology and Oceanography 48:920-928.

Gordon L.I., J. C. Jennings, A.A. Ross, and J.M. Krest. 1993. A Suggested protocol for continuous flow automated analysis of seawater nutrients (phosphate, nitrate, nitrite and silicic acid) in the WOCE Hydrographic Program and the Joint Global Ocean Fluxes Study, College of Oceanic and Atmospheric Sciences, Oregon State University.

Haberstroh P.R. 1994. Wave-forced porewater mixing and nutrient flux in a coral reef framework. PhD. Dissertation, University of Hawai'i at Manoa, Honolulu.

Haberstroh P.R., F.J. Sansone. 1999. Reef framework diagenesis across wave-flushed oxic-suboxic-anoxic transition zones. Coral Reefs 18:229-240.

Hebert, A.B., F.J. Sansone, and G.R. Pawlak. 2007. Tracer dispersal in sandy sediment porewater under enhanced physical forcing. Continental Shelf Research, 27(17): 2278-2287.

Heiri O., A.F. Lotter, G. Lemcke. 2001. Loss on ignition as a method for estimating organic and carbonate content in sediments: reproducibility and comparability of results. Journal of Paleolimnology 25:101-110.

Herzfeld I., F.J. Sansone, C. Colgrove, M. Ross, M. O'Brian, and C. Smith. 2006. Diurnal nutrient dynamics associated with a nuisance algal bloom on south Maui, Hawaii. EOS Trans. AGU, 87(36), Ocean Sci. Meet. Suppl., Abstract OS54J-05, Hawaii.

Herzfeld I., F.J. Sansone, C. Smith, C. Colgrove, M. Ross, M. Dailer, and M. Vermeij 2008. Diurnal dissolved inorganic C, N, P, and Fe dynamics in permeable back-reef sediments of the south shore of Maui, Hawaii Ocean Sciences Meeting, Orlando, Florida. http://www.aslo.org/orlando2008/files/2008osm-abstracts.pdf.

Huettel, M. and G. Gust. 1992. Impact of bioroughness on interfacial solute exchange in permeable sediments. Marine Ecology Progress Series, 89: 253-267.

Huettel M., H. Røy, E. Precht, S. Ehrenhauss. 2003. Hydrodynamical impact on biogeochemical processes in aquatic sediments. Hydrobiologia 494:231-236.

Huettel M., I.T. Webster. 2001. Porewater flow in permeable sediments. In: Boudreau BP, Jorgensen BB (eds) The benthic boundary layer. Oxford University Press, p 144-179.

Huettel M., W. Ziebis, S. Forster. 1996. Flow-induced uptake of particulate matter in permeable sediments. Limnology and Oceanography 41:309-322.

Huettel M., W. Ziebis, S. Forster, G.W. Luther III. 1998. Advective transport affecting metal and nutrient distributions and interfacial fluxes in permeable sediments. Geochimica et Cosmochimica Acta 62:613-631.

Hughes T.P. 1994. Catastrophes, phase shifts, and large-scale degradation of a Caribbean coral reef. Science 265:1547-1551.

Hughes T.P., A.M. Szumant, R. Steneck, R. Carpenter, S. Miller. 1999. Algal blooms on coral reefs: What are the causes? Limnology and Oceanography 44:1583-1586.

Huisman J.M., I.A. Abbott, C.M. Smith. 2007. Hawaiian Reef Plants, University of Hawaii Sea Grant College Program, UNIHI-SEAGRANT-BA-03-02.

Hunt C.D. 2006. Ground-water nutrient flux to coastal waters and numerical simulation of wastewater injection at Kihei, Maui, Hawaii. U.S. Geological Survey Scientific Investigations Report 2006–5283, p 69.

Jackson J.B.C. 1997. Reefs since Columbus. Coral Reefs 16:S23-S32.

Johnson A.G., C.R. Glenn, W.C. Burnett, R.N. Peterson, P.G. Lucey. 2008. Aerial infrared imaging reveals large nutrient-rich groundwater inputs to the ocean. Geophysical Research Letters 35:L15606, doi:15610.11029/12008GL034574.

Lapointe B.E., M. Clark. 1992. Nutrient inputs from the watershed and coastal eutrophication in the Florida Keys. Estuaries 15:465-476.

Lapointe B.E., M.M. Littler, D.S. Littler. 1997. Macroalgal overgrowth of fringing coral reefs at Discovery Bay, Jamaica: Bottom-up versus top-down control Proceedings of the 8th international Coral Reef Symposium. ICRS, Panama, p 927-932.

Lapointe B.E., J. O'Connell. 1989. Nutrient-enhanced growth of *Cladophora prolifera* in Harrington Sound, Bermuda: Eutrophication of a confined, phosphorus-limited marine ecosystem. Estuarine, Coastal and Shelf Science 28:347-360.

Laws E.A., D. Brown, C. Peace. 2004. Coastal water quality in the Kihei and Lahaina districts of the island of Maui, Hawaiian Islands: Impacts from physical habitat and groundwater seepage: Implications for water quality standards. International Journal of Environment and Pollution 22:531-546.

Lee R.E. 2008. Phycology, Cambridge University Press, New York. pp.547.

Malarkey J. and A.G. Davies. 2002. Discrete vortex modeling of oscillatory flow over ripples. Applied Ocean Research 24:127-145.

Martens C.S., R.A. Berner, J. Rosenfeld. 1978. Interstitial water chemistry of anoxic Long Island Sound sediments. 2. Nutrient regeneration and phosphate removal. Limnology and Oceanography 23:605-617.

Menge, B.A. et al. 2003. Coastal oceanography sets the pace of rocky intertidal community dynamics. PNAS v100(21):12229-12234.

Miller A.J., E.A.G. Schuur, and O.A. Chadwick. 2001. Redox control of phosphorus pools in Hawaiian montane forest soils. Geoderma: 219-237.

Moberly, R.M., Chamberlain, T., 1964. Hawaiian Beach Systems. University of Hawaii, Hawaii, Hawaii Institute of Geophysics Technical Report No. 64-2, 95p.

Morse J.W., F.T. Mackenzie. 1990. Geochemistry of sedimentary carbonates. Developments in Sedimentology 48, Elsevier, New York. 707pp.

Ogston A.S., C.D. Storlazzi, M.E. Field, M.K. Presto. 2004. Sediment resuspension and transport patterns on a fringing reef flat, Molokai, Hawaii. Coral Reefs 23:559-569.

Oldham C.E., and P.S. Lavery. 1999. Porewater nutrient fluxes in a shallow fetch-limited estuary. Marine Ecology Progress Series 183:39-47.

Pant H.K., and K.R. Reddy. 2001. Phosphorous sorption characteristics of estuarine sediments under different redox conditions. Journal of Environmental Quality:1474-1480.

Patrick W.H. Jr., and R.A. Khalid. 1974. Phosphate release and sorption by soils and sediments: Effect of aerobic and anaerobic conditions. Science 186:53-55.

Paytan A., et al. 2006. Submarine groundwater discharge: An important source of new inorganic nitrogen to coral reef ecosystems. Limnology and Oceanography 51:343-348.

Precht, E., U. Franke, L. Polerecky, and M. Huettel. 2004. Oxygen dynamics in permeable sediments with wave-driven pore water exchange. Limnol. Oceanogr., 49(3): 693-705.

Precht E., M. Huettel. 2003. Advective pore-water exchange driven by surface gravity waves and its ecological implications. Limnology and Oceanography 48:1674-1684.

Precht E., M. Huettel. 2004. Rapid wave-driven advective pore water exchange in a permeable coastal sediment. Journal of Sea Research 51:93-107.

Qiu B., T.S. Durland. 2002. Interaction between an island and the ventilated thermocline: Implications for the Hawaiian Lee countercurrent. Journal of Physical Oceanography 32:3408-3426.

Qiu B., D.A. Koh, C. Lumpkin, P. Flament. 1997. Existence and formation mechanism of the North Hawaiian Ridge current. Journal of Physical Oceanography 27:431-444.

Reimers C.E., et al. 2004. In situ measurements of advective solute transport in permeable shelf sands. Continental Shelf Research 24:183-201.

Riedl R.J., N. Huang, and R. Machan. 1972. The subtidal pump: a mechanism of interstitial water exchange by wave action. Marine Biology 13:210-221.

Rotzoll K., A.I. El-Kadi, S.B. Gingerich. 2008. Analysis of an unconfined aquifer subject to asynchronous dual-tide propagation. Groundwater 46:239-250.

Rusch, A., and M. Huettel. 2000. Advective particle transport into permeable sediments-evidence from experiments in intertidal sandflats. Limnology and Oceanography 45: 525-533.

Rusch, A., M. Huettel, C. Wild, and C. E. Reimers. 2006. Benthic oxygen consumption and organic matter turnover in organic-poor, permeable shelf sands. Aquatic Geochemistry 12: 1-19.

Schwartz F.W., and H. Zhang. 2003. Fundamentals of groundwater, Vol. John Wiley & Sons, New York. pp 583.

Shum K.T. 1993. The effects of wave-induced pore water circulation on the transport of reactive solutes below the rippled sediment bed. Journal of Geophysical Research 98:10289-10301.

Slomp, C.P. and Van Cappellen, P., 2004. Nutrient inputs to the coastal ocean through submarine groundwater discharge: controls and potential impact. Journal of Hydrology, 295(1-4): 64-86.

Smith J.E., J.W. Runcie, and C.M. Smith. 2005. Characterization of a large-scale ephemeral bloom of the green alga Cladophora sericea on the coral reefs of West Maui, Hawai'i. Marine Ecology Progress Series 302:77-91.

Soicher A.J., and F.L. Peterson. 1997. Terrestrial nutrient and sediment fluxes to the coastal waters of west Maui, Hawai'i. Pacific Science 51:221-232.

Stewart, R.H., 2003. Introduction to Physical Oceanography, Texas A&M University. 344 pp.

Storlazzi C.D., and B.E. Jaffe. 2003. Coastal circulation and sediment dynamics along West Maui, Hawaii. Part I: Long-term measurements of currents, temperature, salinity and turbidity off Kahana, West Maui: 2001-2003 USGS Open File Report 03-482.

Storlazzi C.D., and B.E. Jaffe. 2008. The relative contribution of processes driving variability in flow, shear, and turbidity over a fringing coral reef: West Maui, Hawaii. Estuarine, Coastal and Shelf Science 77:549-564.

Storlazzi C.D., J.B. Logan, M.A. McManus, B.E. McLaughlin. 2003. Coastal circulation and sediment dynamics along West Maui, Hawaii, Part II: Hydrographic survey cruises A-3-03-HW and A-4-03-HW Report on the spatial structure of currents, temperature, salinity and turbidity along Western Maui., U.S. Geological Survey Open-file Report 03-430.

Storlazzi C.D., M.A. McManus, J.B. Logan, B.E. McLaughlin. 2006. Cross-shore velocity shear, eddies and heterogeneity in water column properties over fringing coral reefs: West Maui, Hawaii. Continental Shelf Research 26:401-421.

Szumant A.M. 2002. Nutrient enrichment on coral reefs: is it a major cause of coral reef decline? Estuaries 25:743-766.

Testa J.M., et al. 2002. Dissolved iron cycling in the subterranean estuary of a coastal bay: Waquoit Bay, Massachusetts. Biol. Bull. 203:255-256.

Thybo-Christesen M., M.B. Rasmussen, T.H. Blackburn. 1993. Nutrient fluxes and growth of Cladophora sericea in a shallow Danish bay. Marine Ecology Progress Series 100:273-281.

Tribble G.W., F.J. Sansone, S.V. Smith. 1990. Stoichiometric modeling of carbon diagenesis within a coral reef framework. Geochimica et Cosmochimica Acta 54:2439 - 2449.

Valiela, I. et al., 1990. Transport of groundwater-borne nutrients from watersheds and their effects on coastal waters. Biogeochemistry, 10: 177-197.

Vermeij, M., M. Dailer, and C. Smith. 2009. Nutrient enrichment promotes survival and dispersal of drifting fragments in an invasive tropical macroalgae. Coral Reefs, 28(2): 429-435(7).

Vitousek S. 2007. Nearshore hydrodynamics at Kaanapali, Maui & Hawaii extreme wave statistics. Masters Thesis, University of Hawaii at Manoa.

Walker T.W., G. O'Donnell. 1981. Observations on nitrate, phosphate and silicate in Cleveland Bay, Northern Queensland. Australian Journal of Marine and Freshwater Research 32:877-887.

Webb J.E.,J. Theodor. 1968. Irrigation of submerged marine sands through wave action. Nature 220:682-683.

Webster I.T. 2003. Wave enhancement of diffusivities within surficial sediment. Environmental Fluid Dynamics 3:269-288.

Webster I.T., S.J. Norquay, F.C. Ross, and R.A. Wooding. 1996. Solute exchange by convection within estuarine sediments. Estuarine, Coastal and Shelf Science 42:171-183.

Webster I.T., J.H. Taylor. 1992. Rotational dispersion in porous media due to fluctuating flows. Water Resources Research 28:109-119.

Wiberg P.L., C.K. Harris. 1994. Ripple geometry in wave-dominated environments. Journal of Geophysical Research 99:775-789.

Williams I., R. Sparks, and C. Smith. 2008. Status of Maui coral reefs. In: Initiative HCR (ed). Hawaii Department of Aquatic Resources, p 2.

Wiltse W. 1996. Algal Blooms: Progress report on scientific research. Environmental Protection Agency.

Wild, C., M. Rasheed, U. Werner, U. Franke, R. Johnstone, and M. Huettel. 2004a. Degradation and mineralization of coral mucus in reef environments. Marine Ecology Progress Series 267: 159-171.

Wild, C., R. Tollrian, and M. Huettel. 2004b. Rapid recycling of coral mass-spawning products in permeable sediments. Marine Ecology Progress Series 271: 159-166.

CHAPTER III - LAND-OCEAN INTERACTIONS AND NUTRIENT DYNAMICS IN PROXIMAL COASTAL ZONES OF MAUI, HAWAII

3.1 ABSTRACT

We report results from multiple, simultaneous 24-hour observations of nutrient dynamics at coastal sites on Maui, Hawaii that display a range in coastal geomorphologies. Land-ocean submarine groundwater discharge (SGD) fluxes estimated from various conservative tracer mixing models and radium isotopic measurements show high spatiotemporal variability. Highest variability in SGD and nutrient fluxes along the coastline are found along heavily populated regions, and appear to be altered by site-specific interactions between tides and coastal geomorphology. Principal component analysis shows that dissolved nutrient variability patterns along the coastal region can be quite diverse, even under a similar geomorphologic setting. SGD fluxes along regions with shallow shelves experience tidally regulated wave regimes and correlate positively with tidal height, whereas SGD fluxes at sites where shallow shelves are absent display inverse relationships with tidal height. The existence of different mechanisms of water exchange along the coastline makes it untenable to constrain whole-coastline fluxes using single-point measurements. Although the extent of land alteration, the coastal geomorphology, and morphological effects on wave energy penetration to the beach face are identified as key features explaining the variability of land-ocean exchange of dissolved nutrients along the coast, human alteration of the landscape and natural hydrology are identified as the primary reasons for elevated nutrient loads to the coastal zone.

Key words: nutrients, land-ocean exchange, coastal geomorphology, submarine groundwater discharge, anthropogenic

3.2 INTRODUCTION

The application of synthetic inorganic fertilizer has led to a doubling of the total nitrogen in the biosphere (Galloway and Cowling 2002; Erisman et al. 2008). A large fraction of these new N inputs enter the coastal zone either directly or indirectly. Direct pathways involve particulate and dissolved riverine loads (Rabalais et al. 2002) and wastewater outfalls, whereas indirect (diffuse) pathways include the effects of land clearing on particulate organic matter remineralization rates and consequent groundwater nutrient pools (Mackenzie et al. 2002; Lerman et al. 2004), nutrient-enriched fresh/saline groundwater discharge (D'Elia et al. 1981; Capone and Bautista 1985; Capone and Slater 1990; Taniguchi et al. 2002; Laws et al. 2004; Paytan et al. 2006), coastal erosion (Rooney and Fletcher 2005), dry and wet atmospheric deposition (Doney et al. 2007), and land-based wastewater disposal (Paul et al. 2000; Hunt 2006; Dailer et al. 2010).

Coastal zone nutrient dynamics are influenced by tidally regulated hydrostatic flows of submarine groundwater discharge (SGD) (D'Elia et al. 1981; Dollar and Andrews 1997; Laws et al. 1999; Taniguchi et al. 2002; Garrison et al. 2003; Burnett et al. 2003; Burnett and Dulaiova 2003; Herzfeld et al. 2006; Johnson et al. 2006; Paytan et al. 2006; Dulaiova and Burnett 2007), wave-enhanced sediment pore fluid transport (Riedl et al. 1972; Shum 1993; Webster 2003; Precht and Huettel 2004a; Hebert et al. 2007), and enhanced transport of shallow coastal brackish groundwater driven by water circulation cells forced by wave run-up (Li et al. 1999). Nutrient-rich SGD inputs flowing into nearshore coastal systems can potentially contribute significant proportions of the nutrient requirements of primary producers within the proximal coastal zone (Valiela et al. 1990; Valiela et al. 1992; Valiela et al. 1997). Therefore, it is of utmost importance

that we investigate the factors that regulate the spatiotemporal variability of nutrient fluxes if we are to understand the occurrence and distribution of macroalgal blooms along the proximal coastal zone.

Of all factors affecting land-ocean nutrient exchange, wave run-up has been identified as one of the principal mechanisms responsible for mass flux of sediment porefluids to the water column along regions with moderate to high wave activity (Li et al. 1999). For example, wave run-up-enhanced interactions between high ionic strength seawater and low ionic strength aquifer water can result in pulsed desorption of adsorbed nutrients (PO_4 and NH_4) to interstitial water within the vadose and saturated zones, subsequently resulting in PO_4 and NH_4 transport to the coastal zone (Li et al. 1999). Thus, factors that regulate the physical forces interacting with the shoreline may play a significant role in the spatiotemporal dynamics of dissolved nutrients within the proximal coastal zone, although limited work has been performed in this area.

The objective of this study was to explore the spatiotemporal variability of land-ocean dissolved nutrient fluxes in the proximal coastal zone. Because the interactions between physical oceanographic conditions (tides, wind, and waves) and coastal geomorphologic properties (e.g., degree of reef development, shelf slope) can regulate solute exchange between land and ocean, it is important that we attempt to isolate geomorphologic from physical effects. My study attempts to shed light on the factors affecting nutrient dynamics within the proximal coastal zone and their importance along a region characterized by a range of coastal geomorphologies.

In order to simplify the interpretation of observed nutrient dynamics along geomorphologically variable coastal regions I study all sites under the same tidal forcing

(i.e., simultaneous measurements). I combine observations of sea state, measurements of coastal water temperature, and multiple geochemical tracers to elucidate the effects of coastal geomorphology on the spatiotemporal variability of land-ocean fluid exchange along coastal Maui, a region currently experiencing a range of anthropogenic stressors (Smith et al. 2002; Hunt 2006; Herzfeld et al. 2006; Smith 2006; Herzfeld et al. 2008; Hunt and Rosa 2009).

3.3 SITE DESCRIPTIONS

Four distinct south-west facing regions were selected for our study based on (1) the level of anthropogenic impact to their surrounding watersheds, (2) the occurrence or absence of chronic macroalgal blooms along the coast, and (3) the degree of reef development: West Maui, North Kihei, South Kihei, and South Maui (Figure 3.1). Following are general descriptions of the selected study sites within each study region.

3.3.1 Olowalu (OLO) – West Maui

Olowalu (20.80842˚ N, 156.61155˚ W) has abundant (NOAA - NCCOS 2007) and stable (Jokiel et al. 2004) coral reefs. OLO lies within a high-wind zone generated by the intensification of Trade Winds as they travel through the isthmus and around the southeast region of the West Maui Mountains (Figure 3.1). Although this site was under sugar cane cultivation for >100 years, today it is only home to a small resident community, who enjoy good coastal water clarity, relatively low currents, predominantly low waves, abundant marine life, and major reef development. OLO experiences limited tourism due to its relatively distant location from major populated areas and a general lack of tourist facilities. The nearshore geomorphology at OLO is predominantly characterized by a shallow coral reef shelf that extends approximately 500 m from shore.

Mean rainfall within the OLO watershed ranges between <400 mm/yr near the coast to >9000 mm/yr at higher elevations (Giambelluca et al. 1986). Coastal erosion rates along this site are < 30 cm/year (Fletcher et al. 2001-2003).

3.3.2 Ukumehame Beach Park (UKU) – West Maui

Located a few kilometers south of OLO, Ukumehame (20.79435˚ N, 156.58202˚ W) also lies within the intensified Trade Wind region (Figure 3.1). Similarly, coral reef resources are fairly extensive at this site (i.e., shallow shelf to ~400 m offshore), with sparse coral-dominated pavement in the back reef region and 50-90% coral cover within 300-600 m from shore (NOAA - NCCOS 2007). The watershed draining into this site is fairly untouched by human activity and is steeply sloped for the most part. A narrow coastal plain dominated by wetlands separates the West Maui Mountains from shore. Coastal water resources at this site are mainly utilized by local fisherman and surfers. This site receives relatively frequent semi-direct surf from Trade Wind-generated waves and southern swells that funnel between the islands of Lanai and Kaho´olawe (Figure 3.1). Rainfall patterns are similar to the nearby OLO site. Coastal erosion rates along this portion of coastline range between <30 and ~120 cm/yr (Fletcher et al. 2001-2003).

3.3.3 North Waipuilani Beach Park (NWAI) – North Kihei

North Waipuilani (20.75958˚ N, 156.46007˚ W), along with Waipuilani and Kalama (see below), represent the northernmost extent of a region that has experienced extensive land cover change during the past 60 years, and where abundant chronic macroalgal blooms occur along the proximal coastal zone (Kobayashi 1970; Laws et al. 2004; Smith 2006). Remnants of traditional Hawaiian fishing practices (i.e., fish ponds) are evident along this stretch of coastline, but sub-areal rock enclosures typical of fish ponds are rare;

generally only submerged rock walls currently exist. The NWAI site lies inside of one of these submerged rock enclosures at the mouth of the Waipuilani gulch. Surface flows in the Waipuilani gulch occur only during periods of high rainfall. No rainfall occurred during our observation period. Remnant rocks enclose a portion of the shallow shelf where coral resources are minimal, and algal cover can reach 10 - 50 %. Further offshore (~300 m) a small band of high coral cover (50 - 90 % cover) emerges before the seafloor drops to un-colonized bare sand (NOAA - NCCOS 2007). Sugarcane fields to the north and east, and scrub forest to the south surround the northern portion of the city of Kihei. Coastal water resources in this region are minimally utilized for recreation or subsistence fisheries. In recent years (since ~1950) NWAI has experienced moderate sedimentation, and coastal erosion rates are ≤ 30 cm/yr (Fletcher et al. 2001-2003).

3.3.4 Waipuilani Beach Park (WAI) – North Kihei

Waipuilani (20.75598˚ N, 156.45978˚ W) is located less than 1 km south of NWAI, outside the remnant fish pond, and along a portion of coastline with thick accumulations of macroalgal biomass. This site is in the same watershed as NWAI and KAL. The coral resources, wind patterns, and land and sea use are similar to that previously described for NWAI. Coastal erosion rates along this region can reach >90 cm/yr (Fletcher et al. 2001-2003).

3.3.5 Kalama Beach Park (KAL) – North Kihei

Kalama (20.72838˚ N, 156.45115˚ W) represents the southernmost extent of chronic massive macroalgal accumulations. Coral resources at this site are minimal and limited to a small band along the reef slope (~ 400 – 500 m from shore). Wind patterns, watershed land use and slope, and level of tourism are similar to NWAI and WAI. From

a geomorphologic perspective, this site lies at the transition between a shallow coral shelf to the north and rapidly sloping seafloor to the south (Figure 3.1). Coastal erosion rates at this location can range from <30 cm/yr to as high as 120 cm/yr (Fletcher et al. 2001-2003).

Minimal potable groundwater resources are available along the Kihei region; thus, fresh water for this community is supplied from wells located >16 km away in the Iao aquifer of the West Maui Mountains. Wastewater from the Kihei community is treated at the Kihei Wastewater Reclamation Facility (KWWRF) (Figure 3.1). The KWWRF produces ~20 million liters per day of R-1 treated effluent (i.e., water that has been treated to produce significant reduction of viral and bacterial pathogens; highest grade wastewater according to Hawaii State Department of Health standards (HIDOH 2002), of which approximately ~8 million liters per day are reclaimed for irrigation of golf courses and agricultural seed corn fields. The remainder of the wastewater effluent (~12 million liters per day) is injected into the local aquifer a few kilometers inland from KAL (Hunt 2006; Fukunaga and Associates 2010).

3.3.6 Kamaole I (KAMI) and Kamaole III (KAMIII) Beach Parks – South Kihei

Both Kamaole I (20.71296˚ N, 156.44565˚ W) and Kamaole III (20.72059˚ N, 156.44773˚ W) lie in a geomorphic transition between well-developed reef flats to the north (KAL, WAI, and NWAI) and rocky shorelines to the south (AHI and LAP). The coastline along these sites is typified by sandy coves in between lava outcrops. These sites are a popular destination for tourists that visit the Kihei area because, contrary to the turbid water conditions in north Kihei, these sites are characterized by sandy beaches and good water clarity. Due to the lack of reef development at these sites, wave energy is able

to penetrate close to shore, dissipating at the beach. Beach slopes are steeper at these sites compared to all others. Wind patterns along this portion of coastline are similar to those of the northern Kihei sites, but are slightly more variable because north winds (i.e., intensified Trade Winds) are unable to maintain their intensity as they bend towards the south (personal observation). Coastal erosion rates at this location are mostly below 30 cm/yr, but can be >60 cm/yr at some locations (Fletcher et al. 2001-2003).

3.3.7 North Ahihi Kinau (AHI) and Laperouse Bay (LAP) – South Maui

North Ahihi Kinau (20.62317˚ N, 156.43973˚ W) and Laperouse (20.59878˚ N, 156.41987˚ W), the southern-most sites, are regions where recent (~1790) lava flows have entered the sea (Oostdam 1965). The AHI and LAP coral resources are limited to colonies growing sparsely along the lava-dominated hard bottom (personal observation). Water clarity is good, and this is a preferred dive/snorkeling destination for tourists. Due to its distance from Kihei and Wailea towns, these sites do not see nearly as much tourism as do KAMI and KAMIII; the tourism level is perhaps similar to that observed at OLO. Watersheds at these sites are fairly rugged, steeply sloping lava deserts with annual precipitation near 500 mm/yr at low elevations and 1000 mm/yr at higher elevation (Giambelluca et al. 1986). Harsh terrain has kept this area from any major development, with only low density family dwellings dotting a narrow band along the coastal zone boundary. Both AHI and LAP are exposed to southern swells, and LAP is a known location for large surf during summer months. Although currently undetermined, coastal erosion rates along this rocky shore appear to be extremely low and dependent on the physical weathering of lava rock at the coastline.

3.4 MATERIALS AND METHODS

3.4.1 Surface water temperature

Arrays of temperature sensors (Onset HOBO TidbiT, Bourne, Massachusetts, USA) were deployed along a shore-normal transect at UKU, WAI, and KAL in order to record the across-shelf spatiotemporal variability of surface water temperature at these sites (Figure 3.2) during the first discrete sample collection period (see below). Sensors recorded water temperature every five minutes, and were arrayed at 1.5 - 2 m intervals throughout the water column (Table 3.1). All sensors were calibrated prior to deployment at several temperatures using a mercury thermometer. Unfortunately, the sensor calibration file became corrupted, limiting our temperature analysis to comparisons of sensor variability about mean temperatures.

3.4.2 Tide height, visually observed wave height and wind speed

Tide height data (http://www.mobilegeographics.com:81/locations/3070.html) were obtained for Kihei, Maui and used to predict water heights at times of discrete sample collection using Matlab (Natick, Massachusetts, USA) shape-preserving curve-fitting interpolation tools. Wave heights just offshore of the beach breakers and wind speeds at the shoreline were visually estimated to the nearest half foot (~20 cm) and 5 knots (~0.5 m/s), respectively (Table 3.2).

3.4.3 Discrete surface water sampling and chemical analysis

Discrete water column samples were collected every 3 hours for 24 hours during June 8 - 9 and June 13 - 14, 2006 in a nearly synoptic fashion at five or six of our nine study sites, respectively (Figure 3.2). Seawater was sampled at the shoreline (~0.5 m water depth) using 150-mL plastic syringes pre-rinsed with site water. Water for dissolved nutrient analysis (60 mL) was filtered through pre-combusted glass fiber filters

(Whatman GF/F), and the filtrate stored in an acid-cleaned plastic bottle. All samples for dissolved nutrients were frozen immediately after sampling was concluded and kept frozen until analysis. Dissolved inorganic nutrients (PO_4, NO_3, NO_2, NH_4, and Si) were analyzed colorimetrically by the University of Washington Oceanography Technical Services according to standard methods (Gordon et al. 1993) using a segmented flow analyzer. Samples collected for salinity measurement were not filtered and were analyzed in the laboratory using a Seven Multi bench-top meter equipped with an InLab®731 conductivity probe (Metler Toledo, Columbus, Ohio, USA). Salinity probe response was calibrated against a dilution series of IAPSO salinity standard.

3.4.4 Radium isotopes sampling and analysis

Samples for naturally occurring radionuclides were collected simultaneously at three of the study sites (UKU, WAI, and KAL) using two different approaches. The first consisted of collecting 100 L of near-shore surface water every 3 hours for one day. Collected water was immediately filtered through a Mn-coated acrylic fiber (~1 L/min) in order to adsorb dissolved radium isotopes (Moore 1976). The second approach consisted of 24-hr near-bottom equilibrations of Mn-coated fibers deployed inside plastic mesh bags along a shore-normal transect (Figure 3.2). Immediately after the termination of the experiments, fibers were next-day shipped to Woods Hole Oceanographic Institution for measurement of short-lived radium isotope (^{223}Ra and ^{224}Ra) activity using delayed-coincidence counters (Moore and Arnold 1996; Rama and Moore 1996; Moore 2008). Data from our first approach were used to calculate groundwater outflow velocity, whereas data from the second approach were used to calculate radioisotopic ratios and thereby infer mechanisms affecting fluid exchange across the coastal zone.

3.4.5 Coastal water residence time

Various measurements of current speed have been made along Maui's coastal zone using diverse techniques (Table 3.3), and results indicate that typical speeds range over 0 - ~2 m/s, with an overall median of ~0.15 m/s. From our visual observations of wave height it is evident that a large wave event did not occur during our sample collection period (see section 3.2.5).

Results from Vitousek (2007) and Storlazzi and Jaffe (2003; 2008) indicate that cross-shore flows along similar coastlines off West Maui are dependent on wave height, whereas along-shore flows are mostly driven by tidal oscillations, Trade Wind intensification, and the occurrence of southern storms. Therefore, given that our observational periods did not appear to occur during anomalous conditions (i.e., no swell, no southern storm, and typical Trade Winds), we assume that along-shore currents at our sites during our observation period were similar to the median along-shore velocities reported in prior studies (Table 3.3).

On average, the width of the shelves along the Maui coastline approximate 500 m (personal observation). Water velocity data obtained from current meters at two of our sites (UKU and WAI) during different observational periods than those of this study show that mean current speeds approximate 0.15 ± 0.07 m/s, a value within the range of observations recorded by others along Maui coastal zones (Table 3.3). Because no detailed measurements of local currents at our sites were made during the observation periods of the present study, we estimate water residence time as the time it would take a parcel of water traveling at a mean speed of 0.15 m/s to traverse a 500-m long alongshore coastal distance. Under our simplified scenario, we calculate that it would take approximately 55 minutes for a water particle traveling at 0.15 m/s to traverse 500 m of

shelf. We, thus, assume a uniform water residence time (t) of 1 hour in our $Flux_i$ and V_{SGD} calculations at all sites (see below). Our assumed water residence time is within the range of values (1 - 6 hours) reported by Paytan et al. (2006), who conducted similar studies at nearby regions (Table 3.3). In a companion paper (Chapter 4) we report the time variability of dissolved nutrient fluxes at two of our sites (UKU and WAI), taking into account changing water residence times as calculated from in-situ current meter measurements and multiple conservative tracers. Higher assumed t will lead to lower calculated values of groundwater solute fluxes ($Flux_i$) and discharge velocities (V_{SGD}). Therefore, under the simplified water residence time estimates of the present study, $Flux_i$ and V_{SGD} (as calculated from EQs. 3.1 and 3.5) can be taken to represent mean solute transport to the coastal zone.

3.4.6 Land-ocean nutrient fluxes

Land-ocean nutrient fluxes were calculated by assuming that any surplus of nutrients ("excess" above oceanic concentrations) in the near-shore were the direct result of mixing between groundwater and offshore seawater (i.e., surface flow, advection, internal tides, and water-column remineralization processes are ignored). In other words, we consider localized land-ocean exchange along the proximal coastal zone to be the main process affecting dissolved nutrients, salt, and radium variability at our study sites. Therefore, we calculate land-ocean nutrient fluxes (mmol/m^2/day) as:

$$Flux_i = \frac{[(C_i - C_0) \cdot d_i]}{t} \qquad \text{(EQ. 3.1)}$$

where C_i denotes water column solute concentration at time i, C_o denotes mean open ocean solute concentration, d_i denotes water depth (in meters) at time i, and t is the water residence time (in days), which we assumed to be constant (1/24 day, or 1 hour). The

excess nutrient concentrations in the water column (C_i- C_o) are attributed to submarine groundwater discharge as defined by Burnett et al. (2003) (i.e., re-circulated saline sediment porefluids, fresh aquifer water discharge, or their mixture). In our flux calculations we ignore inputs from rivers (none were flowing during the study period), precipitation (no precipitation was observed during the study period), and losses due to evaporation (insignificant when compared to tidal volumetric flows occurring between measurements during the observational period) as possible contributions to dissolved nutrient concentrations in the proximal coastal zone during our study period. Furthermore, we focus on assessment of the spatiotemporal variability of land-ocean solute fluxes under the assumption that all of our study sites experience similar removal of non-conservative solutes via biological uptake and mixing with offshore waters. We recognize that such an assumption may not accurately represent local processes occurring at our sites, and in a companion paper (Chapter 4) we examine biological uptake and mixing corrections to land-ocean solute fluxes.

3.4.7 Groundwater outflow velocities (V_{SGD})

3.4.7.1 Nutrient and radium tracers

Although nutrients are not generally thought to be behave conservatively, previous studies along coastal zones of the Hawaiian islands have shown that nitrate and silicate can exhibit conservative mixing behavior (Dollar and Andrews 1997; Garrison et al. 2003; Laws and Ferentinos 2003; Laws et al. 2004; Johnson et al. 2008). Similarly, radium isotopes have been utilized to estimate land-ocean exchange (Burnett and Dulaiova 2003; Paytan et al. 2006). Following a similar approach, we estimated groundwater outflow velocities (V_{SGD}) from nutrients and radium tracers as:

$$V_{SGD} = \frac{Flux_i}{C_{GW}} \quad \text{(EQ. 3.2)}$$

where C_{GW} is the concentration (or activity, in the case of radium isotopes) of solute *i* in the shallow unconfined aquifer in close proximity to the coastal zone. Near-coast fresh/brackish groundwater measurements of radioisotopes and nutrients were not possible at all sites. In fact, groundwater dissolved nutrient and radioisotope data were only collected at WAI and UKU. For all of the other sites we therefore use the following approximations in order to calculate V_{SGD} for sites where actual measurements were unavailable. Radium, salt, and nutrient flux and V_{SGD} estimates for OLO, UKU, AHI, and LAP were made utilizing radium, salt, and nutrient data collected at a well located within the Ukumehame firing range (20.79892º N, 156.57653º W). Radium-based V_{SGD} estimates for NWAI, WAI, and KAL were made utilizing radioisotopic data collected from a ditch, located ~50 m inland from WAI, which intersects the shallow unconfined aquifer (i.e., it ponds water in the absence of prior rainfall). Groundwater data reported by Hunt (2006) from wells located "down-gradient" and "cross-gradient" from the Kihei Wastewater Reclamation Facility (KWWRF) were utilized to predict salt and nutrient-based V_{SGD} at KAL, and KAMI and KAMIII, respectively. Salt and nutrient data from a groundwater well located at WAI was utilized to predict salt- and nutrient-based V_{SGD} at NWAI and WAI.

3.4.7.2 Salt tracer

Fresh groundwater outflow velocities were also estimated using salt as a conservative tracer. Salt balance was calculated using a simple two end-member mixing model:

$$f_1 + f_2 = 1 \quad \text{(EQ. 3.3)}$$

$$C_{mix} = f_1 C_1 + f_2 C_2 \quad \text{(EQ. 3.4)}$$

where f_1 and f_2 represent the fraction of fresh groundwater and offshore water, respectively, that make the groundwater/offshore mixture, C_{mix} (Hunt and Rosa 2009). With two equations and two unknowns, we can solve for f_1 and f_2. Knowing f_1, the tidal depth (d, in meters), and the water residence time (t, in days), the fresh water outflow velocity (V_{SGD}, in m/day) can be calculated as:

$$V_{SGD} = f_1 \cdot \frac{d}{t} \quad \text{(EQ. 3.5)}$$

This method assumes groundwater discharge originates solely from fresh (i.e., aquifer) groundwater. Although we acknowledge that the discharge of brackish to salty groundwater is also present, we have no reasonable way of estimating such fluxes with the current dataset. Therefore, our groundwater outflow velocity should be considered a lower bound estimate of the true discharge of groundwater as defined by Burnett et al. (2003).

3.5 RESULTS AND DISCUSSION

Water-column surface water temperature, salinity, dissolved nutrient concentration, and radium isotope activity showed patterns of variability indicating that tides affect land-ocean exchange processes at our sites in different ways, both temporally and spatially. In this section, we first present data from temperature sensor arrays to illustrate apparent water mixing patterns during our observation period. We then present results showing the spatiotemporal variability of near-shore water-column chemical properties and their relationship to tides. We continue by presenting land-ocean solute flux and SGD estimates for our study sites. Lastly, we summarize the physico-chemical datasets,

identify land-ocean exchange patterns, and discuss the role of coastal geomorphology and anthropogenic impacts on the regulation of SGD nutrient flux variability.

3.5.1 Physical setting and temperature regime

3.5.1.1 Wind speed and wave height

Three observers visually estimated wind-speed and wave height during the observational periods. Although not a perfect means for the quantitative assessment of these properties, observations do indicate that light winds (2 – 6 m/s) and relatively calm seas (significant wave height between 5 – 51 cm) were predominant during our observation periods, resembling typical summer conditions along this shoreline. No statistically significant differences were found in wind predictions during distinct observation periods or across sites (Table 3.2), except for Laperouse, where highest wind speeds were observed (~15 m/s). Statistically significant differences were observed in wave conditions across sites (Table 3.2), but not between observed wave heights at Waipuilani (the site observed during both synchronous observation periods). Lack of significantly different wave height at Waipuilani suggests the wave regime was fairly similar during both observation periods (i.e., no swell events).

3.5.1.2 Cross-shelf temperature variability

Due to corruption of the sensor inter-calibration file, we solely report sensor deviations from their means over the observational period. Temperature variability patterns were quite different between sites, showing unique spatial patterns of water stratification (Figures 3.3 to 3.5). Water temperature variability at both UKU and WAI showed warmer temperatures nearshore and cooler temperatures offshore, whereas at

KAL temperature variability was stratified vertically in the water column. Following are brief descriptions of the temperature variability at our sampling locations.

3.5.1.2.a Ukumehame Beach Park (UKU) – West Maui

Temperature variability within the reef flat region at UKU is (to a first degree) dependent on solar insolation, with highest positive deviations (~2 ˚C) during peak solar insolation periods, and a maximum negative deviation (~1 ˚C) before sunrise (Figure 3.3A). However, temperature data for UKU is somewhat limited, as two of the sensor arrays (0 and 600 m) were lost during the observational period. Nevertheless, data showed water column temperature variability to follow a similar pattern to that observed at WAI (see below), with higher variability at the shallower, more inshore site, and lower variability at the further offshore site. From the pattern of water temperature variability at the reef crest (Figure 3.3B) it is evident that solar insolation, mixing, and advection of offshore waters affect the temperature regime at this site (i.e., temperature deviations seem to generally follow tidal oscillations).

3.5.1.2.b Waipuilani Beach Park (WAI) – North Kihei

Like UKU, temperature variability at WAI was also dependent on distance from shore (Figure 3.4). The reef flat here extends from the coast to ~ 300 meters offshore, and is dominated by a shallow (< 2 m depth) region overgrown by invasive algae (see sections 3.2.3 and 3.2.4). Between 300 – 400 m from shore the reef crest emerges, and it is occasionally exposed to the atmosphere during low tides, though this did not occur during our data collection period. The reef crest serves as a boundary that effectively hinders the exchange of inshore waters with offshore waters, regulating wave penetration closer to shore during low tides. The offshore boundary (i.e., reef slope) of the shallow

reef platform is approximately 500 m from shore (at ~10 m water depth). The seafloor slopes rapidly to depths greater than 100 m within a few hundred meters offshore from the reef slope. Our offshore temperature array was placed at this transition zone in approximately 20 m water depth.

The reef flat at WAI had the highest water column temperature variability of all geomorphic regions (i.e., reef flat, reef crest, offshore) across the shelf, and variability followed solar insolation (Figure 3.4A). The degree of variability within the water column decreased near the reef crest (Figure 3.4B), and was lowest offshore (Figure 3.4C). Temperature deviations co-varied positively with solar insolation at the reef flat and reef crest, whereas with tide height offshore, were negative temperature deviations (i.e., cooler water) were observed during receding/low tides, and positive deviations (i.e., warmer water) were observed during rising/high tides.

3.5.1.2.c Kalama Beach Park (KAL) – North Kihei

A different temperature regime was observed at KAL during the observation period, with markedly different patterns in the surface and bottom reef water (Figure 3.5). Surface sensors recorded water temperature variability following solar insolation (Figure 3.5A), whereas sub-surface (>1 m below the surface) temperature variability was predominantly dominated by tidal oscillations (Figure 3.5B). The maximum positive deviation of surface-layer water temperature approached 2˚C, and the maximum negative deviation approached ~1 ˚C. On the other hand, mean bottom water maximum positive and minimum negative variability was ca. 0.4 ˚C and -0.2 ˚C, respectively. The mean minimum temperature deviation at the surface was observed near lowest low tide, just prior to sunrise (5:44 am), whereas coldest near-bottom water was observed a few hours

before midnight. Constant, across-shelf vertical stratification of temperature variability at KAL suggests this coastal site either consistently receives higher temperature water from the shallower shelf to the north, has large discharge rates of colder groundwater through its seafloor, or both. Cold water intrusion could also possibly originate from the effects of internal tides, however, temperature anomalies due to possible internal tides events typically last between 1 – 2 hours (Leichter and Miller 1999; Storlazzi and Jaffe 2008). Consistent lower near-bottom water temperature deviations across the shelf suggest groundwater intrusion is predominantly responsible for the more stable temperatures observed below the sea-surface at this site.

3.5.1.2.d Interpreting temperature variability

Similarities and differences were observed in temperature variability at UKU, WAI, and KAL. Temperature variability changes linearly at WAI and UKU on the reef flats and reef crests; temperatures warm in the daytime hours, and cool at night. This pattern is suggestive of the effect of solar heating in these nearshore waters. While there is some evidence of daily heating at WAI in offshore waters, there is also a weak correspondence between the rising tide and warming temperatures. It is possible that warm waters are advected to the WAI offshore site; however, we would need a longer time record to determine if the tides affected WAI offshore waters over long time periods. KAL is the only site where there is distinct temperature variability between surface and bottom waters. Surface water variability at KAL followed a similar trend to WAI and UKU; temperatures warm in the daytime hours, and cool at night. This pattern is suggestive of the effect of solar heating in these nearshore waters. Near-bottom water at KAL does not vary linearly. There are numerous physical processes that could produce this type of

variability, for example internal tides or advection; however, given the short time record it is not possible to pinpoint specific physical forcing mechanisms producing this signal.

3.5.2 Spatiotemporal variability of surface water chemistry

3.5.2.1 Salinity and nutrient spatial variability

Water column inorganic nutrient data for both synoptic samplings are summarized in Table 3.4. During the first synoptic sampling (sampling 1) the mean salinity decreased from north to south (OLO to KAL). During the second synoptic sampling (sampling 2), salinity showed a depression compared to oceanic along Kihei's shallow shelf and minima along the southernmost sites (AHI and LAP). Mean salinities at the two Kihei sites (KAM I and KAM III) during sampling 2 were not significantly different than those observed at OLO and UKU during sampling 1, suggesting these sites experience a similar net salt balance (assuming physical conditions were similar during both sampling periods as suggested in section 3.5.1.1). Mean water-column dissolved nutrient concentrations followed a north-south pattern opposite to that of salinity (Table 3.4), except at AHI and LAP where low salinities and low nutrients were observed. Such patterns suggest that nutrients may originate from low salinity groundwater sources, though salinity minima and nutrient enrichment observed along the northern Kihei sites appears to be the result of complex interactions between natural and anthropogenic stressors.

Furthermore, it appears that KAMI and KAMIII represent a transition between the hydrologically altered northern Kihei area and the more hydrologically intact sites to the south, the latter showing clear evidence of relatively fresh SGD entering AHI and LAP, but with water column nutrient concentrations remaining low. The water chemistry transition from north to south (Kihei to LAP) parallels changes in the geomorphology of the coastal shelf that facilitates the retention of nutrients originating from anthropogenic

stressors (population center, and hydrologic alterations). In other words, higher nutrient inputs and reduced mixing with the open ocean observed at the north Kihei sites are consistent with the distinct water chemistry along this region.

Although little rain falls directly on the Kihei area, precipitation at higher elevations and along the Maui isthmus (Figure 3.2) infiltrates through the soils and recharges the local aquifer. Historically, groundwater flowing to Kihei would transport abundant nutrients to this coastal area and, to the first Hawaiian settlers, the Kihei region represented a place where ample food resources could be harvested (e.g., algae, fish), as evidenced by the abundant underwater remnants of fish pond structures (personal observation). The landscape along this region immediately prior to the 1970s was characterized by dirt roads that traversed diverse agricultural fields, open spaces, cattle grazing land, and homestead development (Maui County 2009).

During the 1970's the Kihei region experienced unprecedented anthropogenic changes to its hydrology and land cover as an effort to boost tourist visitation to the island (Kobayashi 1970). In order to facilitate the economic expansion, Maui residents chose to import fresh water to the region from the Iao aquifer located on the West Maui Mountains (Figure 3.1). Subsequent to the completion of the water line, Kihei experienced explosive population growth from a few hundred residents in the late 1970s to ~17,000 residents by the year 2000 (U.S. Census Bureau 2000). In addition, the region currently hosts approximately 19,000 visitors per day. Most of the water used in the area ultimately ends at the KWWRF (Fig 3.1). Approximately half of the KWWRF-treated effluent is re-used by golf courses and agricultural operations in the region, whereas the other half is injected into the local aquifer approximately a kilometer inland of the KAL

site. Wastewater injection at this site has led to massive hydrological and nutrient loads to the aquifer in this region (Dollar and Andrews 1997; Herzfeld et al. 2006; Hunt 2006; Smith 2006; Dailer et al. 2010). It is therefore no surprise to see lower salinities associated with higher nutrients along this coastal region.

3.5.2.2 Salinity and nutrient temporal variability

3.5.2.2.a Salinity

Salinity variability increased from OLO towards KAL during the first synoptic observations (Figure 3.6A). Of all sites, only KAL water-column salinity appeared to co-vary with tide height, but correlations were not significant (Table 3.5). The decreasing salinities observed at KAL during receding/low tides suggest that the hydrostatic pressure differential between the shallow unconfined aquifer and the coastal zone is likely responsible for the seepage of fresh water, as seen in other studies (Capone and Slater 1990; Taniguchi et al. 2002; Chanton et al. 2003; Taniguchi et al. 2003). The similar geomorphology and exposure to waves at the West Maui sites (OLO and UKU) and north Kihei sites (NWAI, WAI, and KAL) suggests the higher salt variability in north Kihei, relative to West Maui, is the result of higher hydrologic loading along this region.

During the second synoptic observations (Figure 3.6B), salinities at KAMIII were fairly constant and had near-oceanic values, whereas salinities at nearby KAMI were slightly lower, with the lowest (~30) occurring during the last observed receding tide. Salinities at both WAI and NWAI were lower than those observed at KAMI and KAMIII. Surface salinity at NWAI positively co-varied with tide height, but no such trend was observable at nearby WAI (Table 3.5). Salinities at AHI and LAP were generally the lowest recorded for all sites, and did not co-vary with tide height.

3.5.2.2.b Dissolved phosphate

During the first synoptic observations (Figure 3.7A), PO_4 concentrations at UKU, OLO, and WAI were fairly constant (~0.1 µM), whereas NWAI showed elevated concentrations (~0.5 µM) during the beginning of the observation period. Phosphate water column concentrations at NWAI co-varied weakly with tide height, suggesting either tidally driven PO_4 advection, or enhanced exchange between local submarine ground water PO_4 pools and coastal water via either enhanced diffusion of sediment pore fluids (Riedl et al. 1972; Webster and Taylor 1992; Shum 1993; Webster et al. 1996; Webster 2003), or wave run-up (Li et al. 1999). Water-column PO_4 concentrations at KAL reached the highest levels of all sites (0.7 µM). Significant negative correlations between PO_4 and tide height were only observed at KAL.

During the second synoptic observations (Figure 3.7B), PO_4 concentrations at all sites generally remained at or below 0.4 µM. Concentrations at WAI and NWAI varied inversely with tide height, and showed the largest variation in amplitude, but significant negative correlations were only observed at KAMI and KAMIII during this period (Table 3.5). The lowest mean PO_4 concentrations were observed at AHI and LAP, and were not significantly different from those observed at OLO and UKU (Table 3.4)

3.5.2.2.c Dissolved silicate

During the first synoptic observations (Figure 3.7C), water column dissolved silicate concentrations at UKU and OLO were lower than at other sites (Table 3.4). Silicate concentrations at KAL varied inversely with tide height and showed the greatest range (~5 – 50 µM). Although Si concentration variability followed a trend similar to that of salinity (Figure 3.6A), supporting the notion that hydrostatic pressure differential dominates fluid exchange across the land-ocean interface, no significant correlations

were found (Table 3.5). Concentrations at WAI co-varied with tide height, whereas NWAI silicate concentrations were variable and appeared to co-vary both positively and negatively with tide height. Highest mean Si concentrations were observed at the north Kihei sites during this period (Table 3.4)

During the second synoptic observations (Figure 3.7D), silicate enrichment was observed at NWAI and WAI during receding/low tides. Silicate concentrations at WAI were the highest observed (61.6 µM), and, for the most part, silicate varied positively with tide height, though a concentration peak was observed during low tide (6/14/06 11:00). Intermediate Si concentrations were observed at KAMI and KAMIII, with slight enrichments during receding tides. The lowest mean Si concentrations were observed at AHI and LAP (Table 3.4).

3.5.2.2.d Dissolved ammonium

Ammonium variability was low at OLO and UKU during the first synoptic observation period (Figure 3.7E). Water-column ammonium concentrations at NWAI decreased as tides receded, and were lowest at lowest low tide. Ammonium concentrations at KAL varied inversely with tide height, and peaked during lowest low tide (~5 µM).

During the second synoptic observations (Figure 3.7F), ammonium variability at KAMI, KAMIII, AHI, and LAP was generally low. However, a high ammonium concentration was recorded at LAP at the same time that PO_4 peaked, though this enrichment was not associated with a low salinity event (Figure 3.6B). Ammonium concentrations at WAI and NWAI varied inversely with tide height. Salinity data from WAI suggests that the observed NH_4 enrichment at this site during this observation period

originated from fresh/brackish groundwater inputs (i.e., lower salinities were observed in association with higher NH_4), whereas at NWAI NH_4 peaks may have originated from remineralization during low tide, low circulation periods (i.e., low-tide salinities increased as ammonium increased, suggesting particle entrapment followed by remineralization and upward diffusion to the water column) (Huettel et al. 1996; Reimers et al. 2004; Rusch et al. 2006).

3.5.2.2.e Dissolved inorganic nitrate plus nitrite (N+N)

During the first synoptic observations (Figure 3.7G), N+N levels at OLO and UKU were uniformly low and varied minimally, whereas N+N variability at NWAI and KAL was high. In contrast, different variability patterns were observed between NWAI and KAL. NWAI variability co-varied positively, whereas at KAL it varied inversely with tide height.

During the second synoptic observations (Figure 3.7H), N+N levels and variability at LAP and AHI were low. Concentrations of N+N at KAMI and KAMIII were slightly higher than at LAP and AHI, and generally varied inversely with tide height. Levels of N+N at WAI and NWAI co-varied with tide height.

3.5.2.3 Summary of nutrient and nutrient ratio spatiotemporal variability

Water-column salinity (Figure 3.6) and dissolved nutrient (Figure 3.7) temporal variability at the north Kihei sites (NWAI, WAI, and KAL) were higher than at any of the other sites. The variability of dissolved nutrients along these north Kihei sites described different trends. For example, during the first observation period, dissolved PO_4 and N+N concentrations at NWAI decreased with time, whereas the opposite was observed at the nearby KAL site despite similar tidal forcing. Interestingly, PO_4 and N+N

concentrations at WAI, a site located in-between NWAI and KAL, did not reach the high levels of either of the two adjacent sites, suggesting local processes are responsible for the observed distinct variability.

Significant positive correlations were observed between salinity and PO_4 at LAP and AHI (Table 3.5), suggesting that PO_4 inputs originate from either enhanced desorption of sedimentary PO_4 (Froelich et al. 1979) or, possibly, advection from deep oceanic sources (e.g., internal tides (Leichter et al. 1996; Storlazzi and Jaffe 2008); or the passage of eddies (Firing and Merrifield 2004, Rii et al. 2008)). However, if oceanic, deep-water PO_4 was being advected to this site, we would expect to see concurrent peaks of N+N with salinity increases, but such covariance was not observed (Figures 3.6 and 3.7). Instead, peak PO_4 at LAP was observed to co-occur with NH_4 peaks, supporting the hypothesis that PO_4 and NH_4 variability at this site is controlled by advective pore water exchange of saline groundwater enriched in nutrients by the remineralization of organic matter.

Comparisons of the mean DIN:DIP ratios at our sites to those for marine plankton (16:1, (Redfield 1934)) and marine macroalgae (30:1, (Atkinson and Smith 1983)) can help us discern the nutrient limitation state at each of our sampling locations. The DIN: DIP ratios across sites are variable and display a maximum along the Kihei region (Table 3.4). Lowest ratios were observed at OLO and UKU, suggesting that at these sites nitrogen may be limiting primary production of both plankton and macrophytes. High (above 30) mean DIN: DIP ratios along the northern Kihei region suggest these coastal waters are, on average, DIN replete, although high standard deviations indicate DIN may be limiting at times. Furthermore, mean DIN: DIP ratios along northern Kihei indicates

that these waters are capable of supporting the macroalgae overgrowth observed in the region (typical tissue molar N: P ≈ 30, Smith et al. 2006). Low coastal-water DIN: DIP ratios along KAMI and KAMIII suggest that, on average, these sites experience nitrogen limitation. Higher DIN:DIP ratio variability at KAMI than at KAMIII is the result of more variable DIN concentrations, indicating that nitrogen loading to KAMI is more variable, and potentially capable of sustaining macroalgae growth. Elevated DIN: DIP ratios were observed at AHI, but high ratios at this site are mainly an artifact of the very low (near-detection limit) DIP concentrations rather than any significant nitrogen enrichment. Similarly, high DIN: DIP ratios at LAP suggest that this site is, on average, nitrogen replete relative to largely depleted DIP concentrations.

Highest variability in DIN: PO_4 and Si: PO_4 (Figure 3.8) was observed at the north Kihei sites, with an apparent covariance opposite to tide height. Highest Si: DIN variability was observed at the two west Maui sites (OLO and UKU), where peak ratios occurred during lowest tide. The lack of salinity depression during low tides, and the fairly stable Si concentrations observed at these west Maui sites, indicate that Si: DIN variability is primarily controlled by DIN availability. At these west Maui sites, NH_4 is the dominant nitrogen species, suggesting that peaks in Si: DIN are the result of either advection of NH_4 from sediment pore fluids within this shallow shelf (Huettel et al. 1998; Precht and Huettel 2004b) or the accumulation of remineralization products from heterotrophs during periods of low water.

3.5.2.4 Diurnal patterns of radionuclide data

3.5.2.4.*a* Radionuclide time series measurements

Synoptic time series measurements of water-column radium isotope activities were made at UKU, KAL, and WAI (Figure 3.9). Excess water column ^{223}Ra and ^{224}Ra

activities (i.e., unsupported by decay of their radioactive parents ^{227}Ac and ^{228}Th) at UKU and KAL were significantly lower than those observed at WAI (Figure 3.9, and Table 3.6). Highest excess ^{223}Ra and ^{224}Ra were observed at WAI during the first observational high tide, but neither of these tracers correlated significantly with tide height (Table 3.5). Water column excess radium activities observed at KAL and UKU were higher at receding/low tides, but a significant negative correlation was only observed at KAL (Table 3.5), supporting the hypothesis that hydrostatic pressure differentials between the unconfined aquifer and the coast are responsible for SGD inputs at this site (Taniguchi et al. 2002; Burnett et al. 2003; Burnett and Dulaiova 2003; Dulaiova and Burnett 2007). Elevated excess ^{223}Ra and ^{224}Ra activity observed at WAI during high tide suggests that radium is either being transported from radium accumulating within coastal sediments as a result of the radioactive decay of parent isotopes, or from the brackish recirculation zone along the beach face due to wave run-up (Li et al. 1999; Slomp and Van Cappellen 2004; Herzfeld et al. 2006). The high variability of our excess radium measurements at WAI during the short period between observations favors active transport of porefluids (as opposed to tidal-induced hydrostatic exchange) as an explanation for our surface water enrichments at this site.

3.5.2.4.*b* Mn-fiber in-situ equilibrations

Radium isotopes are released from aquifer material only in brackish to salty conditions (Moore 1999); therefore, enrichment of radium isotopes in coastal waters indicates that seawater has come into contact with the shallow unconfined aquifer. Near-bottom Mn fiber equilibrations were used to measure radium isotopic activity and activity ratios of parent (^{228}Th and ^{227}Ac) and daughter (^{224}Ra and ^{223}Ra) radionuclides over the

duration of the first observation period (Figure 3.10 A-F, Table 3.7). Our in-situ equilibration observations at WAI show excess ^{223}Ra and ^{224}Ra activities reached ~2 and 20 dpm, respectively, ~150 m from shore, whereas UKU and KAL showed enrichments of ~1 dpm for ^{223}Ra and 14 – 25 dpm for ^{224}Ra closest to shore, with a decrease offshore (Figure 3.10A and C, Table 3.7). Patterns of the ratios of excess ^{223}Ra to excess ^{224}Ra (or excess ratios) were distinct at KAL compared to both UKU and WAI, with the latter two sites showing highest ratios close to shore, and rapidly decreasing within 150 m from shore (Figure 3.10E). Fluctuations in excess ^{224}Ra : ^{223}Ra ratios varied about the overall mean of ~15, with KAL having more invariant excess ratios compared to UKU and WAI. A rise in excess ratio (~17) was also observed at the WAI 300 m site.

Groundwater samples collected from a ditch approximately 50 m inland at WAI contained 41.2 dpm/m^3 excess ^{223}Ra, 810.4 dpm/m^3 excess ^{224}Ra, and an excess ^{224}Ra : ^{223}Ra ratio of ~19.7. The similarity between the groundwater excess ^{224}Ra : ^{223}Ra ratio and the ratios observed along the coastal margin at WAI indicate that a shallow aquifer is actively interacting with coastal waters. Moreover, significant negative correlations between ^{227}Ac and salinity at KAL (Table 3.5) suggest that ^{223}Ra originates from fresh groundwater inputs, whereas an inverse correlation is observed at WAI, suggesting ^{227}Ac inputs originate from the advection of brackish/salty porefluids.

3.5.3 Nutrient and radium fluxes

Means, standard deviations, and ranges of calculated solute fluxes are summarized in Tables 3.8 and 3.9. From our estimates, it is clear that higher Si and DIN fluxes were observed at NWAI, WAI, KAL, KAMI, and KAMIII, whereas PO_4 fluxes were low across sites. Highest Si, DIN, and PO_4 flux ranges were observed along NWAI to KAL,

the stretch of coastline currently experiencing chronic macroalgal blooms (Table 3.9). However, the data show that nutrient fluxes can alternate between net source (positive flux) and net sink (negative flux) at most sites. This alternating sink/source behavior is observed even within sites along the relatively eutrophic Kihei region (NWAI to KAL) (Table 3.9). Mean negative Si and PO_4 fluxes occurred at AHI and LAP, and mean negative DIN fluxes occurred at UKU, indicating that on average these sites either serve as a net sink for these solutes, or that our assumed mean open ocean water column Si, PO_4, and DIN concentrations (Table 3.4) are slightly elevated compared to the offshore oceanic water present during our sampling. Open ocean water samples reported in Table 3.4 were collected at a maximum offshore distance of 1 km (see Herzfeld 2011), and are therefore perhaps not representative of true oceanic concentrations. If they are not, our negative nutrient fluxes (i.e., depletion) within the coastal zone can be an artifact of our assumed oceanic end-member. Nevertheless, flux deviations from zero are small, suggesting these sites are not experiencing enhanced land-based nutrient enrichments.

3.5.4 Groundwater flow rates (V_{SGD})

Groundwater flow rates calculated using various tracers are summarized in Tables 3.8 and 3.9, and Figure 3.11 and 3.12. All V_{SGD} estimates are below Magnitude 6 on the USGS Spring Discharge Magnitude Scale (a measure of spring flow rates) or <3.78 L/min, with mean flow rates closer to magnitude 8, or <0.5 L/min (Rosenau et al. 1977). Our calculated groundwater discharge velocities are within the range of porefluid velocities observed by other investigators during flume experiments or field measurements (Table 3.10). V_{SGD} calculated using Si and DIN (Fig 3.11 A, B, D, E) show somewhat similar patterns to those calculated via the salinity mixing model (Fig.

3.11 C and F), but are lower by a factor of two. Such discrepancies may result from rapid Si or DIN uptake by phytoplankton and macrophytic algae in the water column, and/or by phototrophs within sediments (Jahnke et al. 2000), or may be due to significant dissimilatory nitrate reduction during the transit of groundwater through the sediment column before release to the water column (Slater and Capone 1987; Slomp and Van Cappellen 2004). From our $V_{SGD\ Si}$ and $V_{SGD\ DIN}$ data it is apparent that tidal oscillations can affect exchange differently at NWAI, WAI, and KAL (i.e., via wave run-up during high tides or hydrostatic pressure differential during low tides). The different exchange responses to similar oscillations further support the hypothesis that local processes were controlling nutrient exchange during the observation period.

Radium-based V_{SGD} estimates at KAL and WAI are two orders of magnitude lower than estimates based on salinity, and are of similar magnitude to silicate-based estimates (Tables 3.8 and 3.9). Discrepancies between salt and radium-based V_{SGD} estimates suggest that fresh groundwater discharging at KAL and WAI have not reached full equilibrium with radium in the source rock (i.e., slower water transit through the unconfined aquifer would allow for secular equilibrium to be established). The lack of equilibrium and the close proximity of these sites to the KWWRF further suggest elevated groundwater outflows at these sites are not part of the base flow. Elevated groundwater discharge is most likely the result of the increased hydrologic loading imposed on the area by water imports and wastewater disposal practices (Hunt 2006; Smith 2006; Dailer et al. 2010).

3.5.5 Land-ocean exchange patterns

Results from principal components (PC) analysis of all dissolved nutrient and salinity data show that the first two PCs can account for 73.5 % of the total variance (see inset table in Figure 3.13). Figure 3.13 shows the plot of PC1 versus PC2; the high positive eigenvectors in the first two principal components can be used to interpret the plot as nutrient enrichment (x-axis) versus salinity (y-axis). Cluster analysis of these data (Figure 3.14) indicates that sites with statistically distinct water column dissolved nutrient variability fall into three distinct groups: (1) high nutrient mixed salinities (HNMS), (2) low nutrient high salinity (LNHS), and (3) low nutrient low salinity (LNLS) (Figure 3.13). Data clusters identify coastal regions with similar types of geochemical variability.

Results indicate that the coastal region along northern Kihei (NWAI to KAL) experiences higher variability in nutrient loading (i.e., at HNMS sites). Radium isotopes, salinity, and dissolved nutrient data suggests the variability of nutrient fluxes along this region result from a combination of altered watershed hydrology (i.e., wastewater and agricultural inputs), and amplified pulses of nutrient-rich groundwater entering the coastal waters during periods of higher physical forcing (i.e., tides, wind, and waves). Thus, the high variability in nutrient fluxes poses a great challenge for the establishment of baseline and future evaluation of changing nutrient fluxes along this region. However, our results show that the probability of encountering higher nutrient flux events is greater along the north Kihei region than at any of the other three regions.

Cluster analysis indicates that the nutrient variability along the south Kihei and West Maui sites (i.e., LNHS regions) is significantly different from the other two site types (Figure 3.14). Such nutrient variability occurs within coastal waters with fairly stable,

near-oceanic salinities (Table 3.4, Figure 3.6). We therefore interpret these sites within the LNHS region as representative of a region with either rapid water circulation, lower eutrophication, or both. Near-oceanic salinities were predominant at KAMI, KAMIII, OLO, and UKU, therefore it may prove to be challenging to estimate nutrient fluxes based on conservative tracers such as salinity given the evidently rapid exchange of water between the coastal zone and the ocean. Lastly, the LNLS group represents regions in an apparent pristine state where fresh SGD enters the coastal zone after its passage through mostly unaltered watersheds. Establishing baseline flux data at LNLS sites will require low analytical detection limits (i.e., lower than 0.04 μM PO_4 obtained in this study).

To summarize, results from our data analysis suggest that, in order to best estimate nutrient fluxes, it is critically important that we note the physical and geomorphologic setting during sample collection given that these factors can drastically affect nutrient flux variability on timescales of hours (if not minutes). In other words, monitoring programs must incorporate measurements of the physical factors regulating land-ocean interaction (i.e., tidal elevation, sea state, and currents) concurrently with geochemical data collection.

It is also critically important that water monitoring programs establish an understanding of the variability of the ocean circulation and its effects on land-ocean nutrient fluxes before long-term datasets are collected. Neglecting to establish an initial understanding of the nutrient flux variability at a specific coastal site can lead to significant measurement bias, affecting one's ability to draw conclusions from the analysis of long term datasets. We argue that if monitoring programs were to utilize a stratified approach (i.e., with different regions executing region-specific monitoring

approaches) to monitor surface waters, instead of using uniform periodic sampling schemes, our capacity to interpret results would be improved and changes to land ocean nutrient flux be better quantified. Based on our results, heavily populated regions where watershed nutrient loads and hydrologic alterations are greatest show significant flux variability between tides, therefore periodic, high frequency sampling (sub-tidal) is the best advisable monitoring approach within this region. On the other hand, use of less frequent (e.g., weekly or monthly) sampling strategies may prove to be an appropriate effort for the detection of change in water quality within undeveloped or developing coastal regions, such as OLO, UKU, AHI, and LAP, where the variability of nutrient flux was minimal over the observation periods.

3.5.6 Physical and geomorphologic controls on nutrient flux variability

The coastal zone geomorphology and wave regime varied widely along our study region (see site descriptions, Figure 3.2), and such site-specific features lead to distinct land-ocean exchange dynamics for different chemical species. For example, silicate, DIN and PO_4 fluxes at NWAI followed temporal trends opposite to those observed at KAL, and at NWAI the fluxes generally decreased as the tidal elevation dropped, whereas at KAL fluxes generally increased.

The KAL site is located at the southern edge of the shallow shelf characteristic of the north Kihei sites where temperature data suggests shallow shelf water exits toward the open ocean (see section 3.5.1.2.d). Elevated hydrologic loading near KAL (i.e., KWWRF effluent injections) appears to result in elevated groundwater flows from the unconfined aquifer towards the coastal zone (Hunt 2006). In addition, the gradual disappearance of the shallow shelf near KAL can further facilitate the flow of

groundwater to the coastal zone. Correlations between salinity, nutrient, and radio-isotopic data support the hypothesis that nutrient exchange at KAL is dominated by high hydrologic loads of nutrient-rich fresh water on land. Lastly, from distinct surface and bottom water temperature variability data obtained at KAL we conclude that these waters are influenced by the transport of shallow shelf water from the north, local groundwater inputs, and active (i.e., sub-tidal) water exchange with the open ocean.

On the other hand, patterns of high nutrients during higher tidal elevation observed at NWAI suggest the shallow shelf impedes hydrostatic land-ocean exchange during low tides. During high tidal elevation, waves are capable of penetrating deeper into the coastal zone, leading to enhanced fluid exchange with near-shore sediments (Huettel et al. 1998; Huettel and Webster 2001; Webster 2003) and the shallow unconfined aquifer via wave run-up at the beach-face (Li et al. 1999). Our observations suggest that periodic water circulation at the beach face is driven by wave run-up events that are, in turn, controlled by factors that regulate wave penetration (i.e., emergence of barriers such as reef crests during low tide). The interplay between net fresh groundwater flow and the wave- and tide-enhanced circulation of saline water at the beach face determines the flux magnitude and periodicity of those chemical species most subject to surface adsorptive processes (Li et al. 1999; Charette and Sholkovitz 2002; Charette and Sholkovitz 2006). Thus, a knowledge of the interplay between coastal aquifers and geomorphological regulators of tidal and wave energy are crucial to understanding the periodicity of land-ocean solute fluxes in the proximal coastal zone.

3.6 CONCLUSIONS

We present simultaneous observations of coastal zone nutrient dynamics along multiple sites in Maui, Hawaii. Our results illustrate that land-ocean exchange along our study sites is highly variable and dependent on factors that regulate the synergistic interaction between tides, waves, and groundwater reservoirs (e.g., shallow unconfined aquifer and sediment pore fluids). Water column stratification, nutrient and radionuclide concentrations, and their heterogeneous spatiotemporal relationships, indicate that multiple, simultaneous processes enhance the land-ocean water exchange in the coastal zone.

Specific surface water stratification at our sites was utilized to deduce water circulation patterns and, ultimately, nutrient residence times. Given that non-extraordinary waves (5 – 51 cm) and wind (2 – 6 m/s) conditions predominated during our study period, we conclude that the distinct water column temperature stratification observed at KAL was the result of apparently usual oceanographic conditions interacting with inputs of cold water across the bottom and warm surface water advection from regions to the north (predominant wind direction was from the north during the observation periods, with consequent wind-induced currents towards the south; see Chapter 4 for example of surface water currents response to wind forcing in this region). On the other hand, temperature variability at WAI and UKU showed that cross-shore variability was dependent on solar insolation and tidal forcing. From our temperature data it is apparent that the periodicity with which UKU and WAI coastal waters mix with offshore waters is similar. Therefore, differences in macroalgal growth observed between these two sites must be a function of the nutrient loads.

Our results show that the evident nitrogen enrichments along north Kihei correspond to higher SGD inputs along this region. Lower salinity water was observed entering along the coast near Kihei with greater frequency than at most of the other regions. Large mass flux of freshwater was also observed along the south Maui region, though nutrient loads appear to be small at these sites. Given that perennial rivers are absent along all of our study regions, freshwater and nutrient inputs to the coastal zone must originate from submarine groundwater discharge; radium isotope ratios support the conclusion that the shallow unconfined aquifer is readily interacting with coastal waters.

Nutrient variability observed along north Kihei (NWAI, WAI, and KAL) also showed variable response to tide height despite the close proximity of these sites and identical tidal forcing. It is apparent that heterotrophic waste generation (ammonification) or active porefluid transport is responsible for fluctuating DIN inputs along West and South Maui sites, whereas NO_3+NO_2 enriched groundwater is the predominant nitrogen source for DIN fluctuations in the coastal waters of the Kihei region. Both submarine groundwater discharge (calculated using different geochemical tracers) and nutrient fluxes show higher rates along WAI and NWAI, and highest rates at KAL. Peak nutrient delivery to the coastal zone at KAL is most likely a result of the high hydrologic and nutrient loading by KWWRF a few kilometers inland of this site (Hunt 2006; Fukunaga & Associates 2010; Figure 3.2).

Obvious nutrient loads observed along Kihei raises the question of whether N or P (or a micronutrient) is limiting macroalgal growth within this region. Analysis of dissolved nutrient ratios suggests the north Kihei region is, on average, N-replete and P-poor, though temporal variability observed during our observation periods indicates that shifts

between N and P limitation may occur over short periods of time (hours). Dissolved nutrient ratios observed at West Maui and South Maui sites also suggest these sites are P-poor.

The interaction between hydrostatic forces (i.e., tide height) along the diverse geomorphology of our study regions resulted in variable land-ocean exchange dynamics for water and nutrients. Furthermore, coastal geomorphology appears to play a significant role in the regulation of wave penetration to the shoreline. It is likely that the distinct nutrient flux responses to tidal forcing along the north Kihei region are the result of 1) coastal geomorphologic effects (i.e., the extent of shallow reef shelf) on hydrostatic flows from the shallow unconfined aquifer to the coast, and 2) wave penetration to the coast.

It seems that, given the heterogeneity in coastal geomorphology along our study region, the role of physical forces on nutrient flux dynamics may be highly heterogeneous, suggesting that care must be exercised when extrapolating single-point flux measurements to an entire coastline. However, our analysis of within-site dissolved nutrient variability (PCA analysis) indicates that similar behavior in dissolved nutrient variability can be observed along different coastal regions. Similarities in the variability of dissolved nutrient concentrations (and associated fluxes) across different regions suggests distinct coastal types can be identified. Coastal typology appears to be the result of the combined effects of land alteration by humans, altered land hydrology, and local interactions between tides and the coastal geomorphology.

This study illustrates the importance of understanding how coastal geomorphology and tides affect coastal water chemistry. Our results appear to be of great relevance to

resource managers who attempt to understand changes in coastal water chemistry using synoptic water sampling schemes. Significant spatiotemporal variability observed in our study show how significant bias can be introduced to data analysis if ignored. Thus, understanding local factors (i.e., geomorphology, wave modulation by tides) that can bias long term datasets (e.g., seasonal effects) may prove invaluable to the early detection of changing water chemistry and its associated ecological ramifications.

3.7 ACKNOWLEDGEMENTS

I would like to extend my gratitude to Meghan Dailer and Mark Vermeij for their assistance in the field, and to Christopher Colgrove for laboratory assistance. This project was partially supported by NOAA ECOHAB Program, and NSF award OCE-0327332. Finally we would like to thank James Krest and Christopher D'Elia for providing logistical support during manuscript preparation at USFSP.

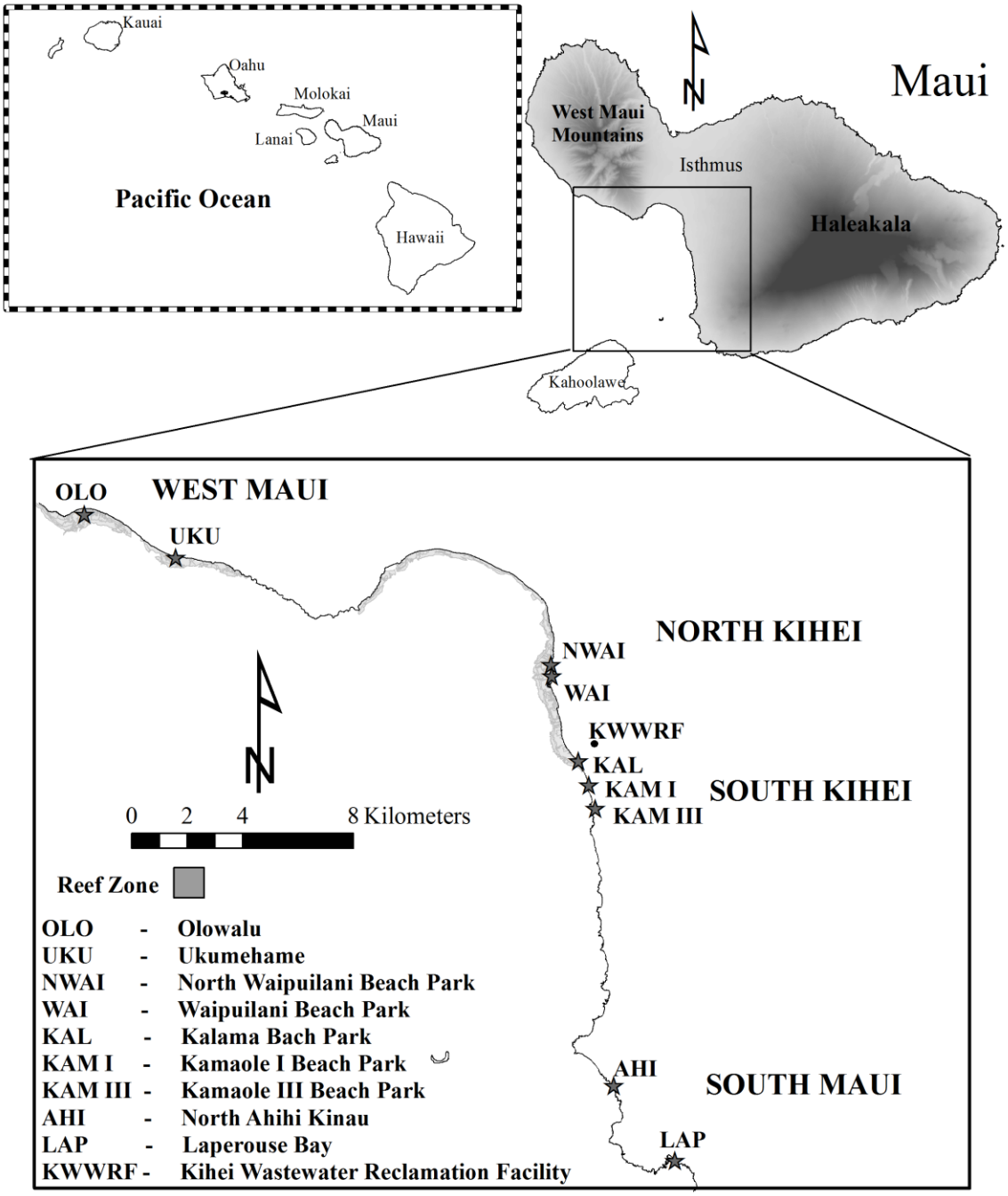

Figure 3.1 – Location of sites sampled synchronously during this study.

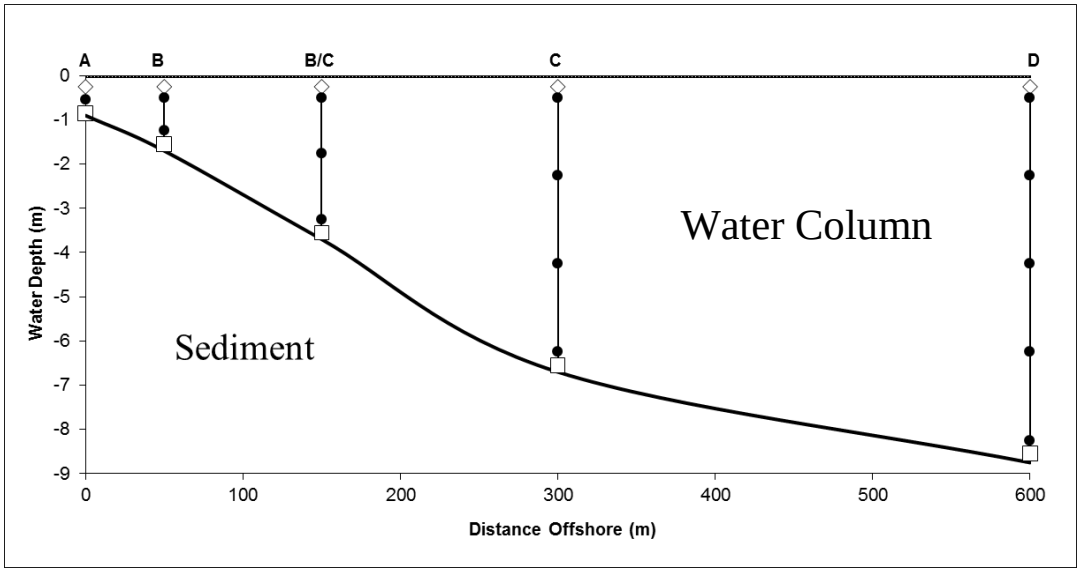

Figure 3.2 – Generalized depiction of temperature sensor array and 24-hour Mn-fiber deployment scheme at all sites. Squares denote anchor and 24-hr equilibrated Mn-fiber location, diamonds denote subsurface buoys, dots denote temperature sensors, and lines connecting dots denote polypropylene rope.

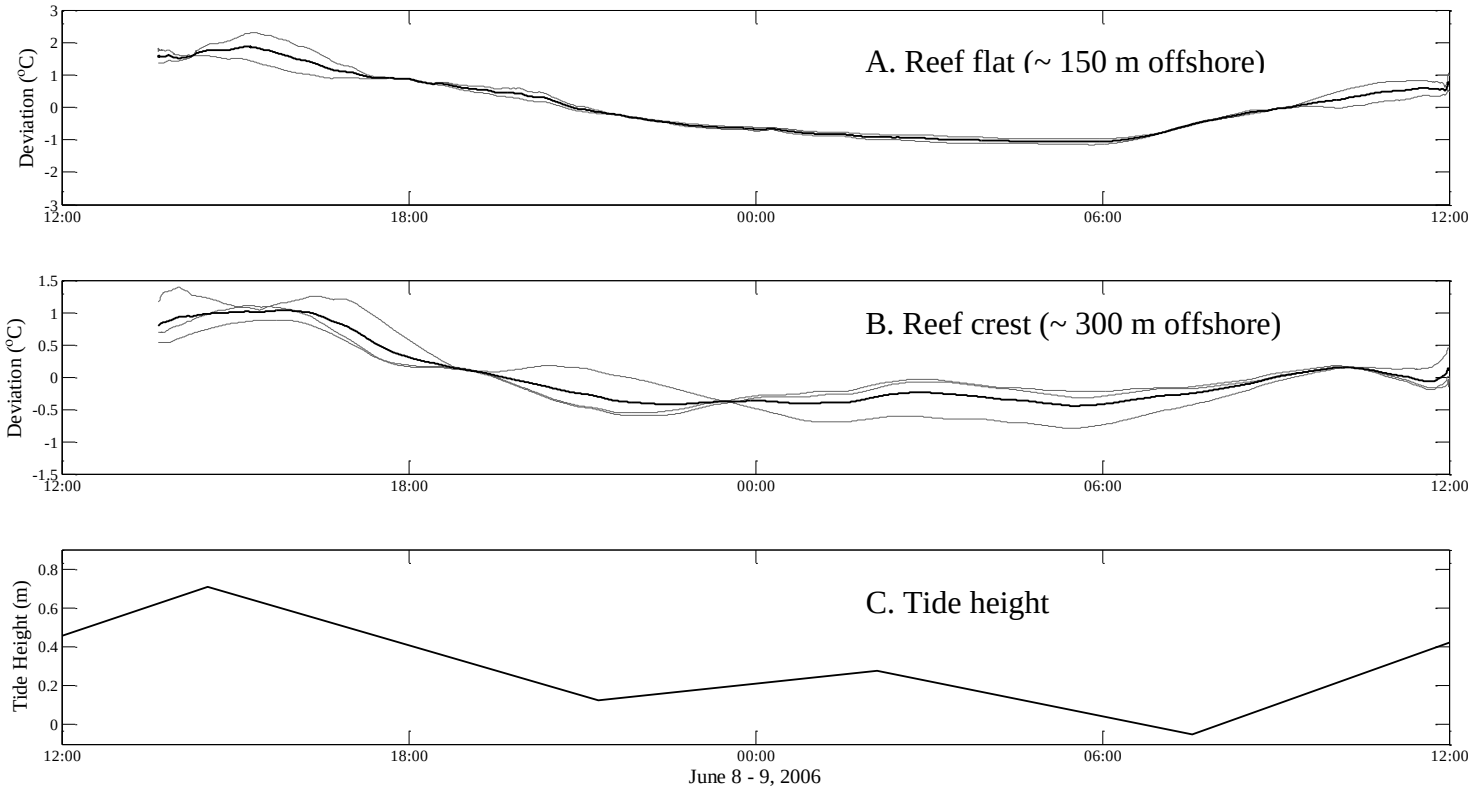

Figure 3.3 –Sensor temperature deviation from its mean (A and B) and tide height (C) at the Ukumehame (UKU) array during the observation period. Data are reported for sensor arrays 150 m (A) and 300 m (B) offshore. Light gray lines in panels A and B denote single sensor time series of the temperature deviations measured at the specific locations, and solid black lines denotes mean of all deviations (i.e., mean from all gray lines).

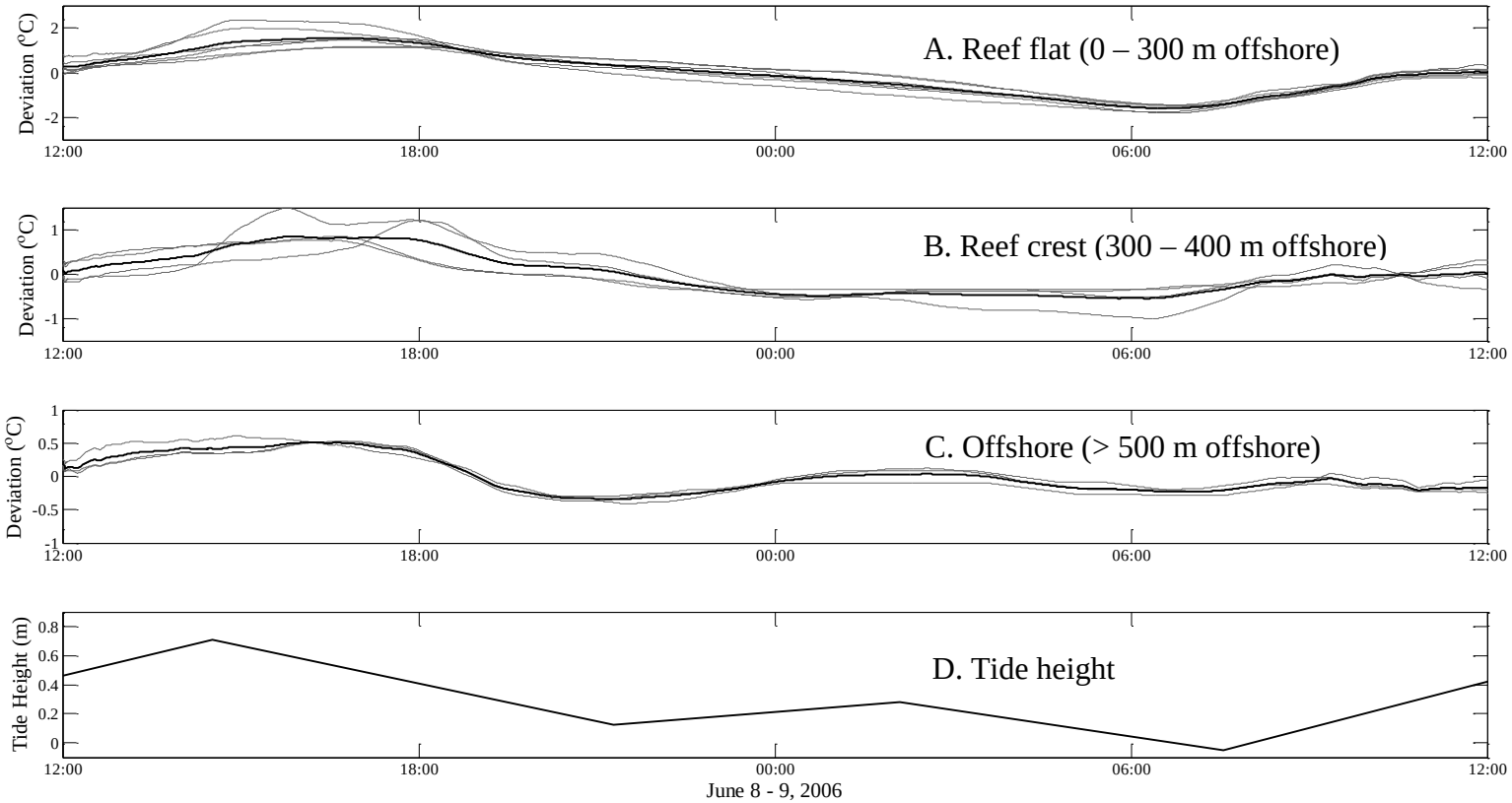

Figure 3.4 - Sensor temperature deviation from its mean (A-C), and tide height (D) at the Waipuilani (WAI) array during the observation period. Data are reported for sensor arrays located 0-300 m (A), 300-400 m (B), and >500 m (C) offshore. Light gray lines in panels A, B, and C denote single sensor time series of the temperature deviations measured at the specific locations, and solid black lines denotes mean of all deviations (i.e., mean from all gray lines). Solid black line denotes mean of all deviations.

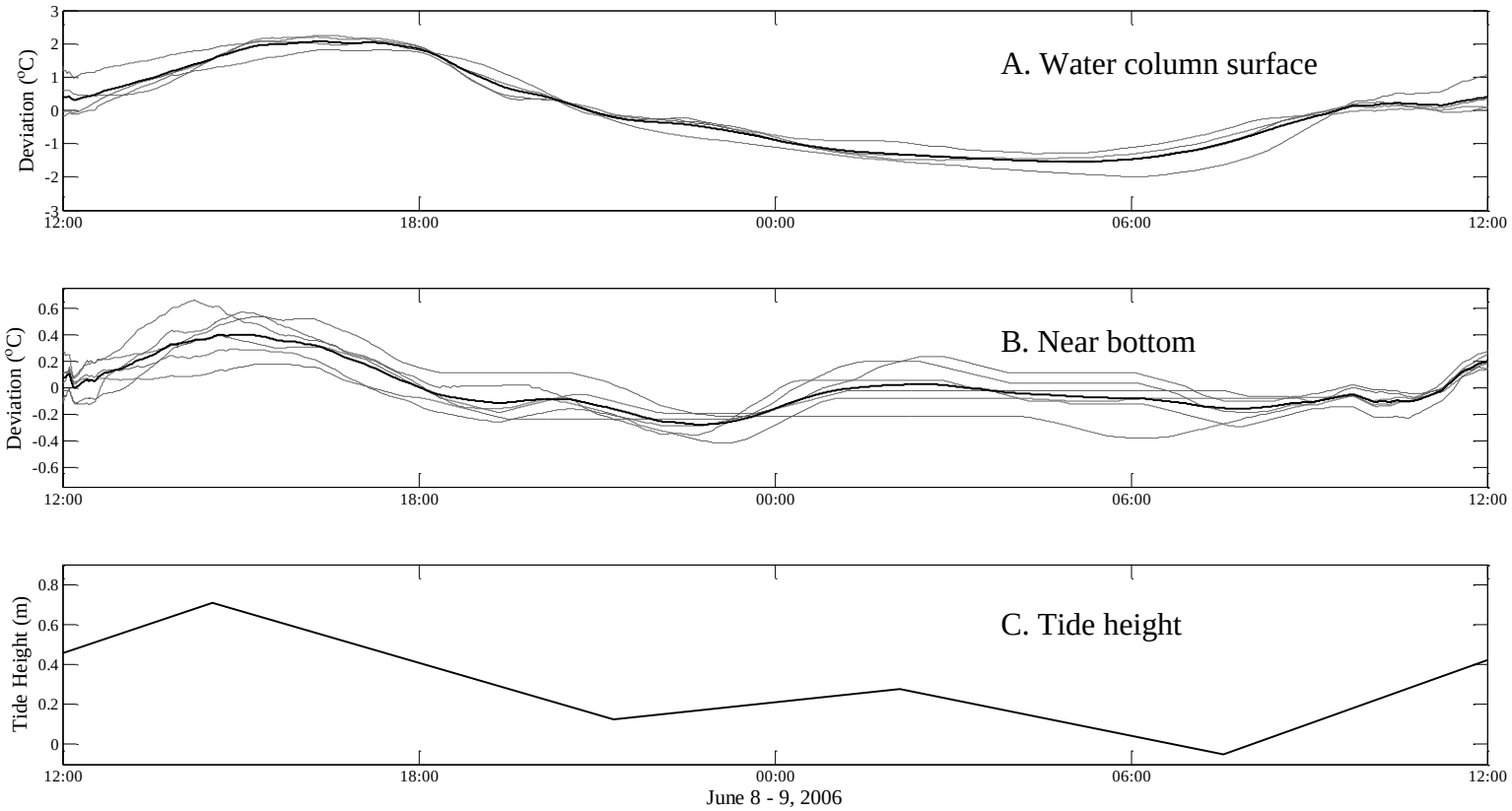

Figure 3.5 –Sensor temperature deviation from its mean (A and B) and tide height (C) at the Kalama (KAL) array during the observation period. Data are reported for sensors at the surface of the water column (A) and sensors immediately below the surface/near-bottom (B). Light gray lines in panels A and B denote single sensor time series of the temperature deviations measured at the specific locations, and solid black lines denotes mean of all deviations (i.e., mean from all gray lines).

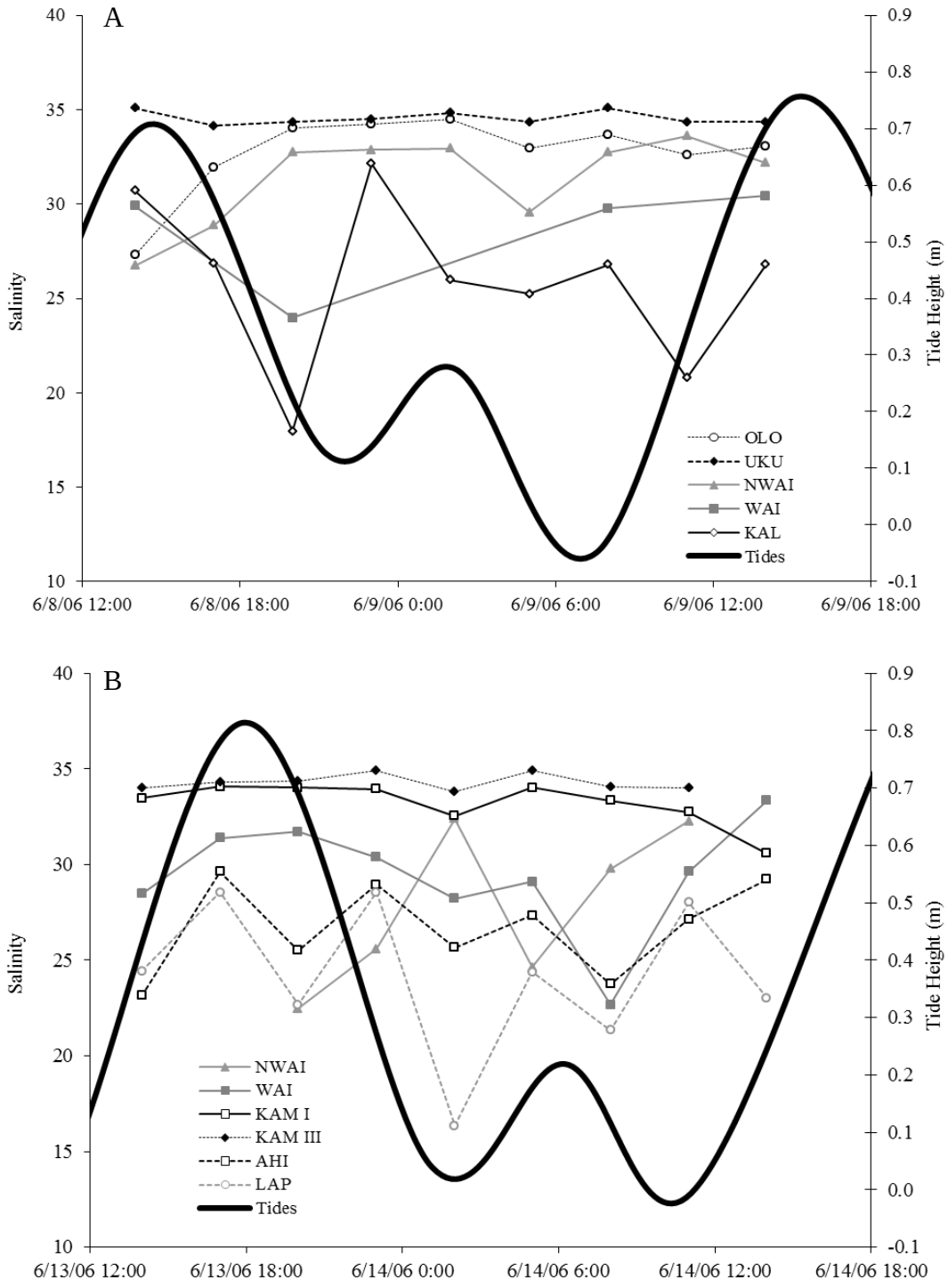

Figure 3.6 – Synoptic salinity time-series data during (A) first sampling and (B) second sampling.

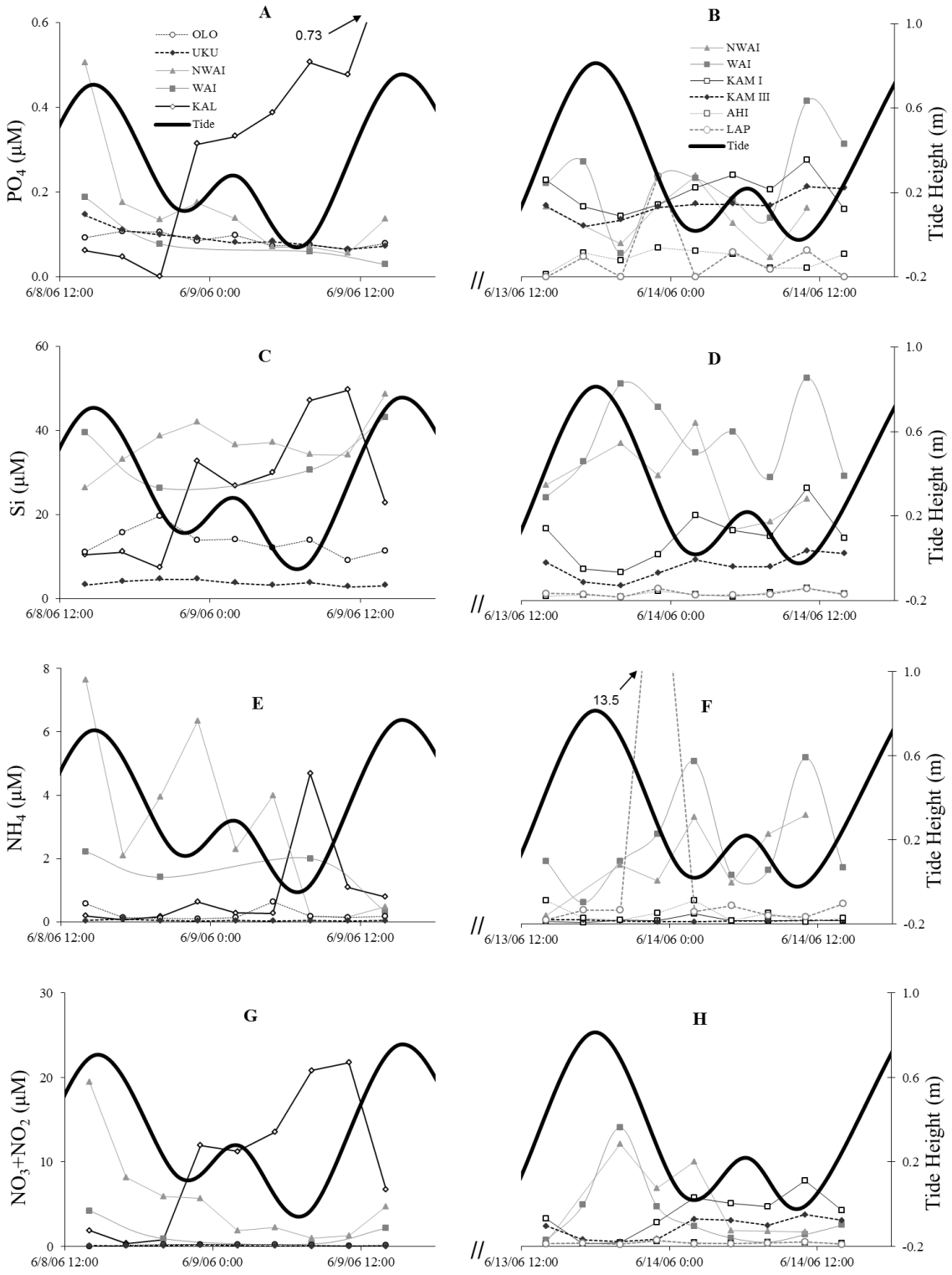

Figure 3.7 – Synoptic time-series of water column dissolved nutrient data during (A, C, E, and G) first sampling, and (B, D, F, and H) second sampling (N+N = NO_3+NO_2).

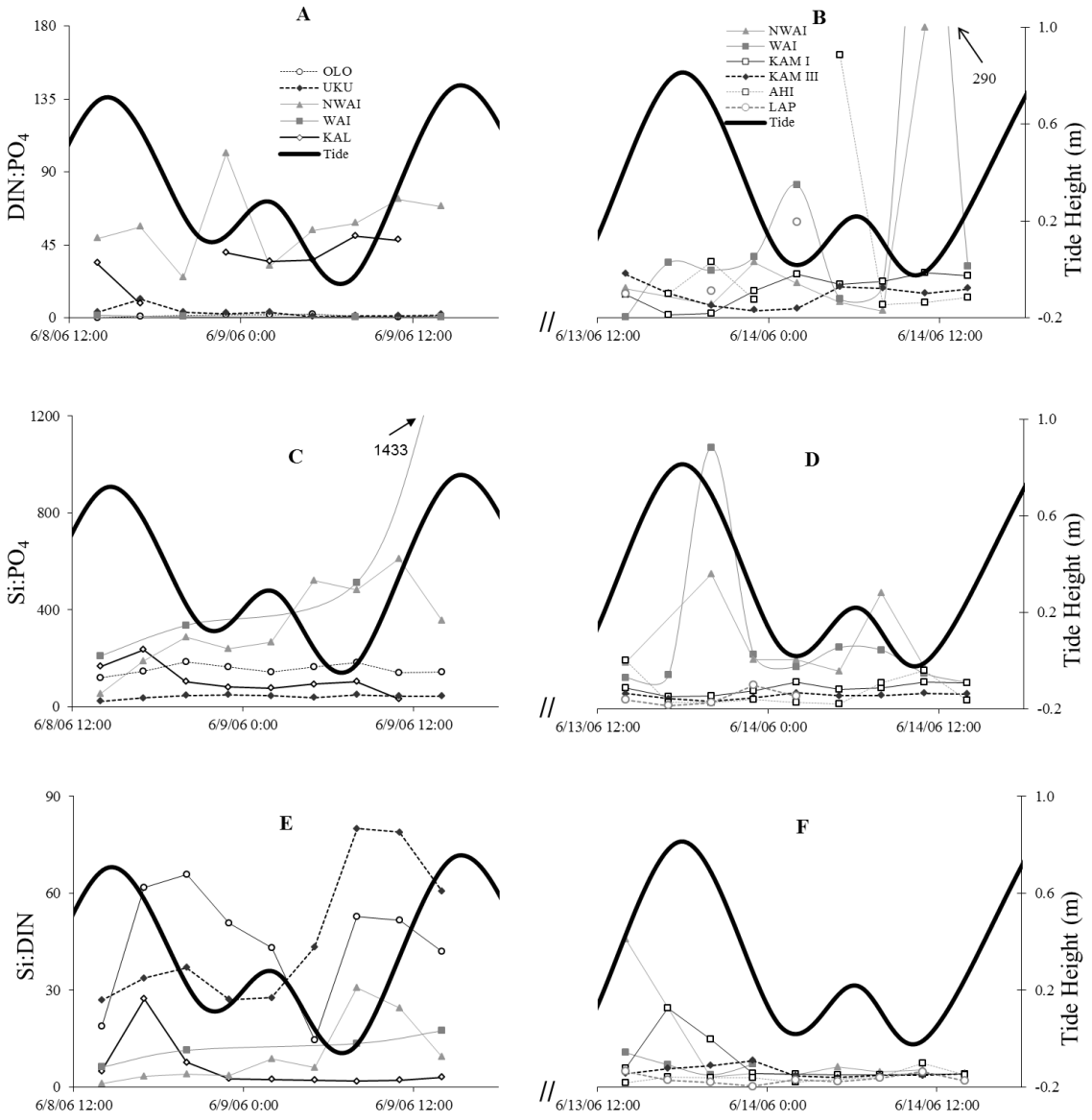

Figure 3.8 – Synoptic time-series of water column dissolved nutrient ratios data during (A, C, and E) first sampling, and (B, D, and F) second sampling (DIN = NO_3+NO_2+NH_4).

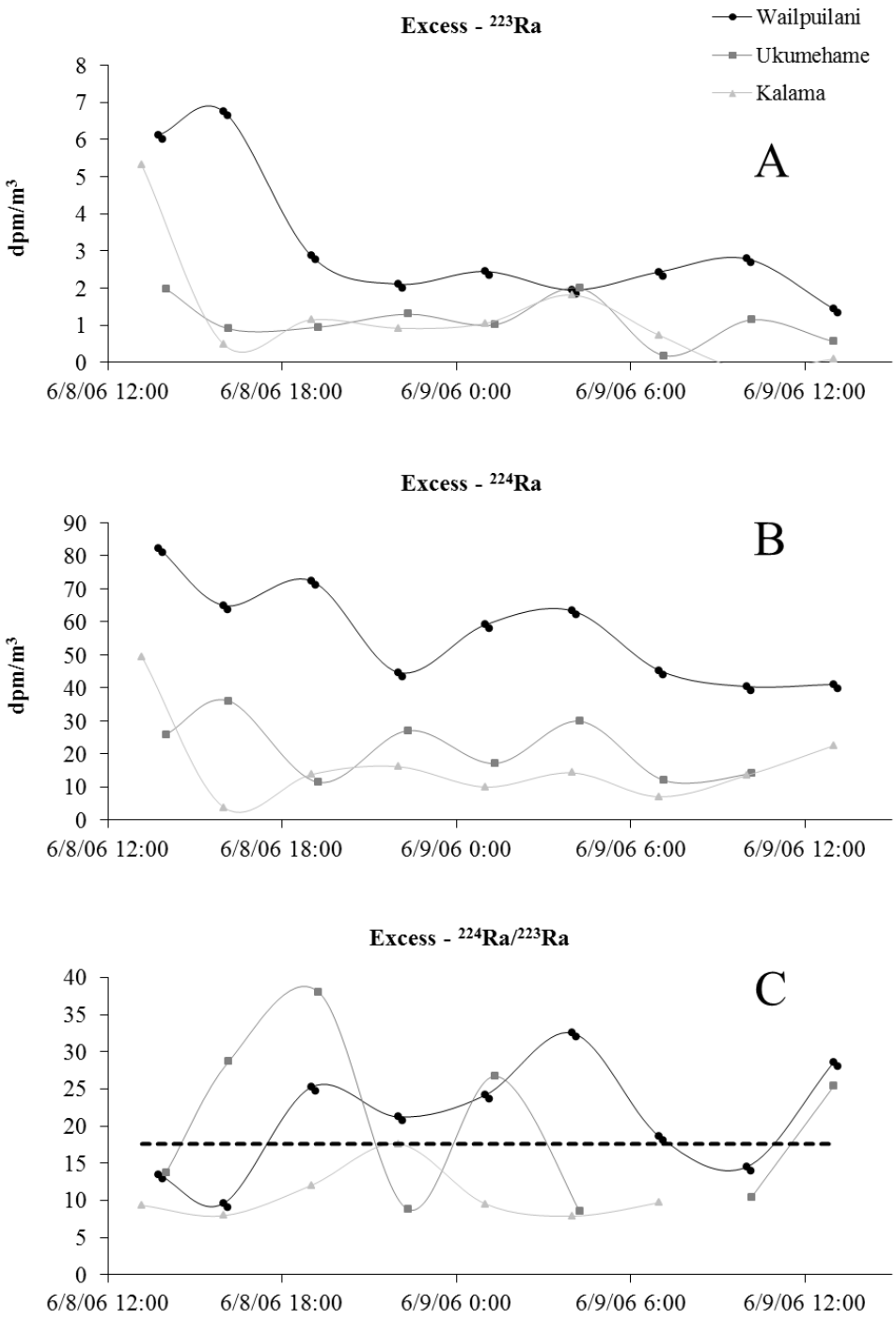

Figure 3.9 – Synoptic time-series of excess (daughter – parent) radionuclide activity and their ratios in surface waters. Thick horizontal dashed line represents the mean excess ^{224}Ra/ excess ^{223}Ra for all sites during the first observation period (the samples collected from KAL after 6/9/2006 7:00 are excluded from the mean ratio calculation because of too much uncertainty in the measurement).

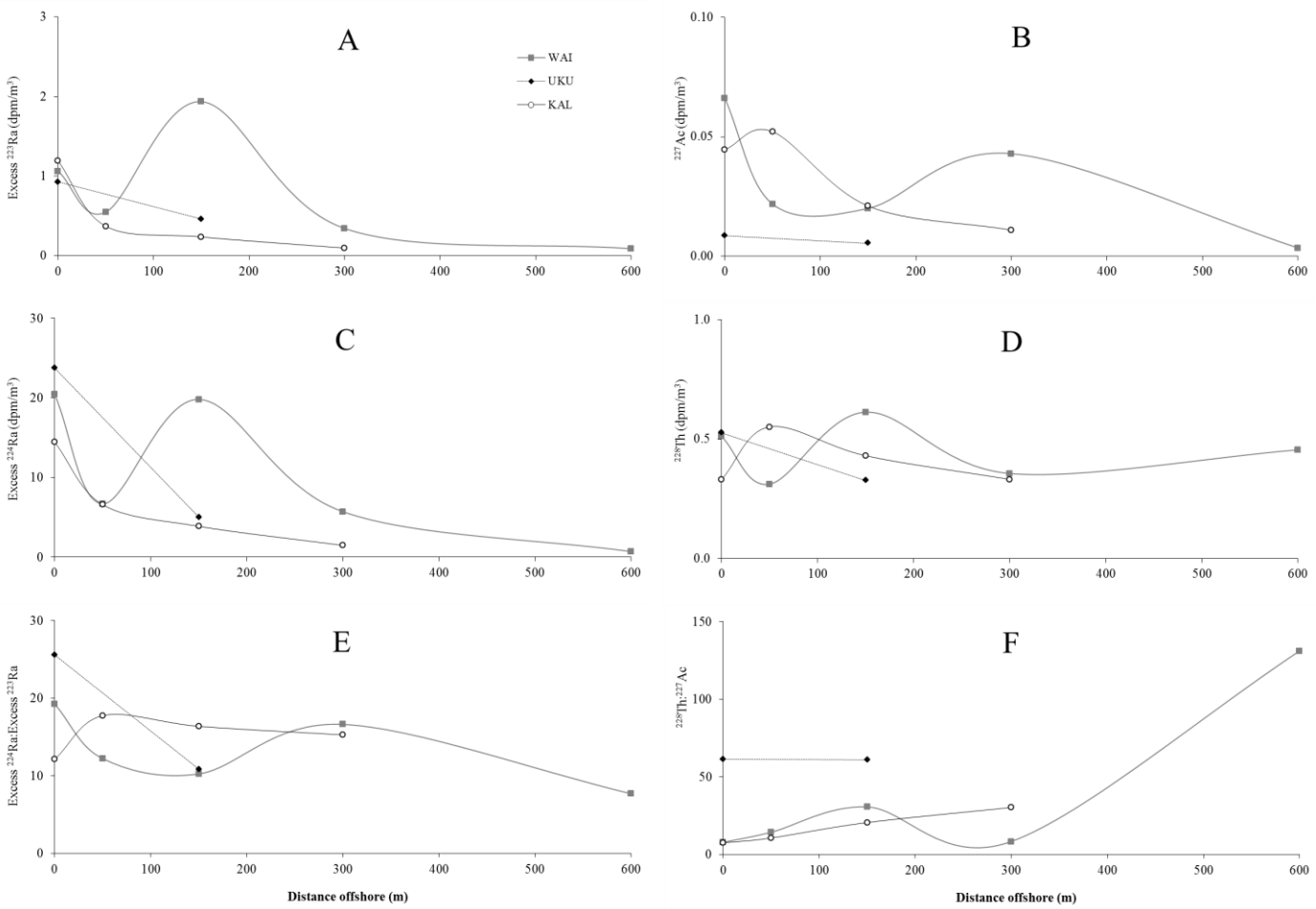

Figure 3.10 – Excess daughter (Ra and ^{224}Ra, panels A and C) and parent (^{227}Ac and ^{228}Th, panels B and D) radionuclide activity and their respective activity ratios (panels E and F) from 24-hour in-situ equilibrations of Mn fibers.

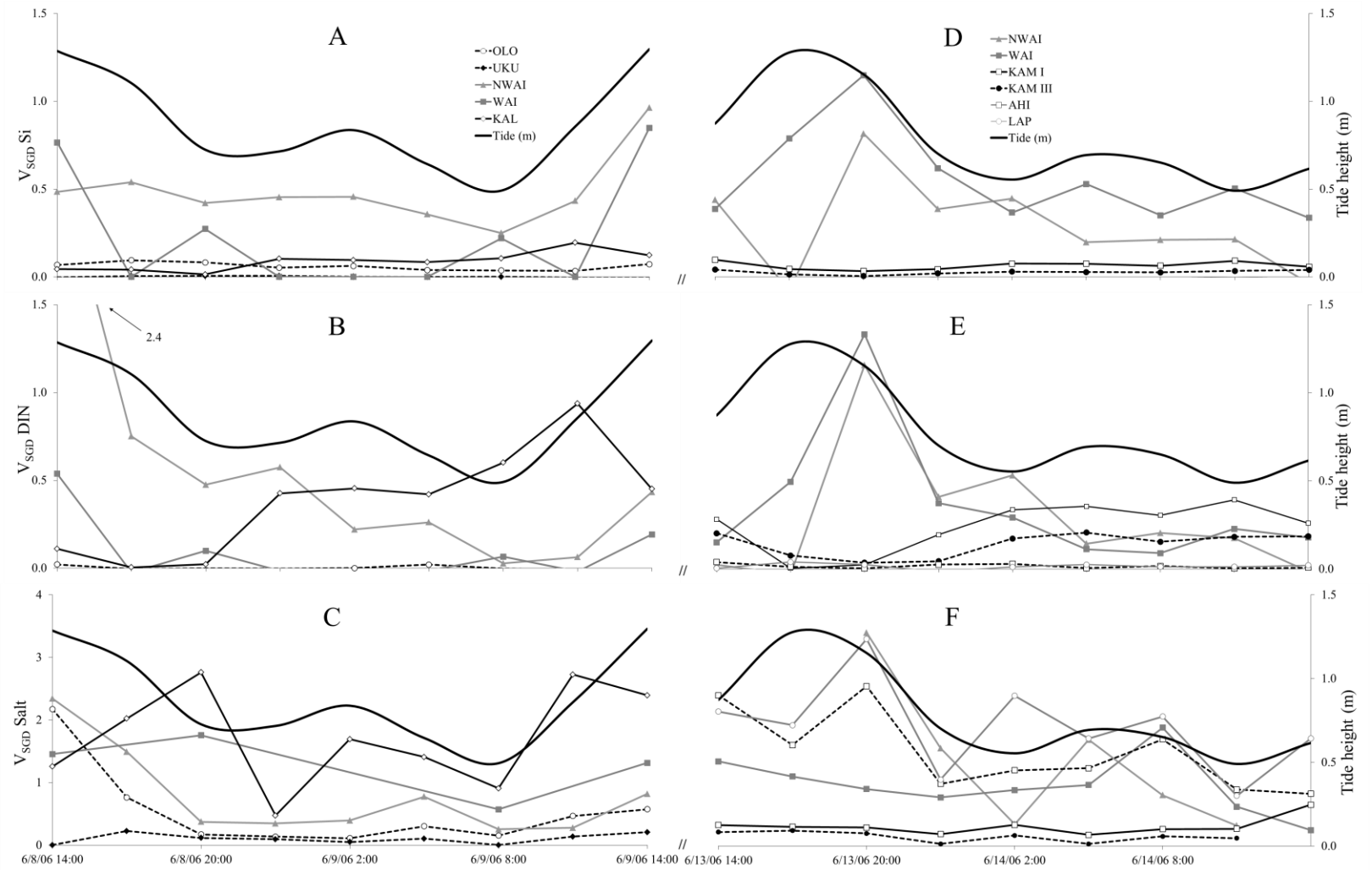

Figure 3.11 - Submarine groundwater discharge velocity (m day^{-1}) at different sites calculated using multiple tracers during first (A-C) and second (D-F) synoptic observation period. Estimates at AHI and LAP using Si as a tracer resulted in negative V_{SGD}, and are not shown.

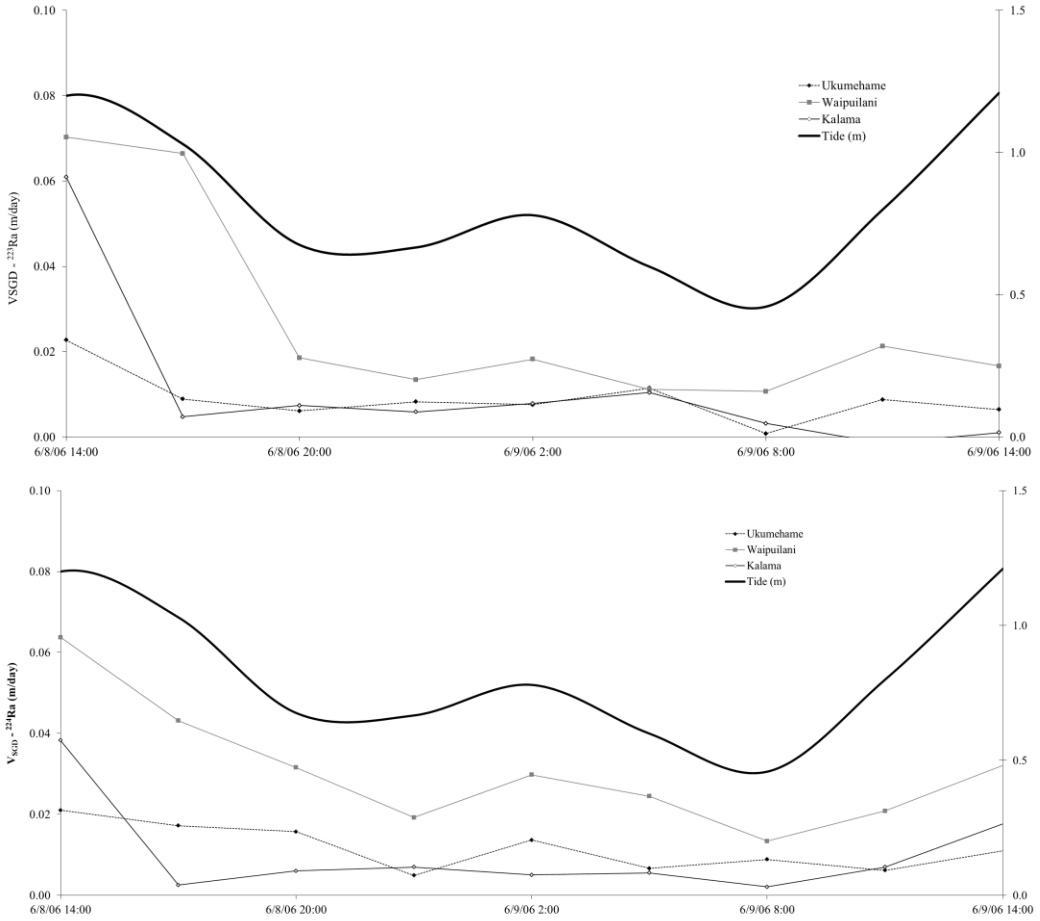

Figure 3.12 - Submarine groundwater discharge velocity (m day^{-1}) at different sites calculated using radium tracers during the first sampling.

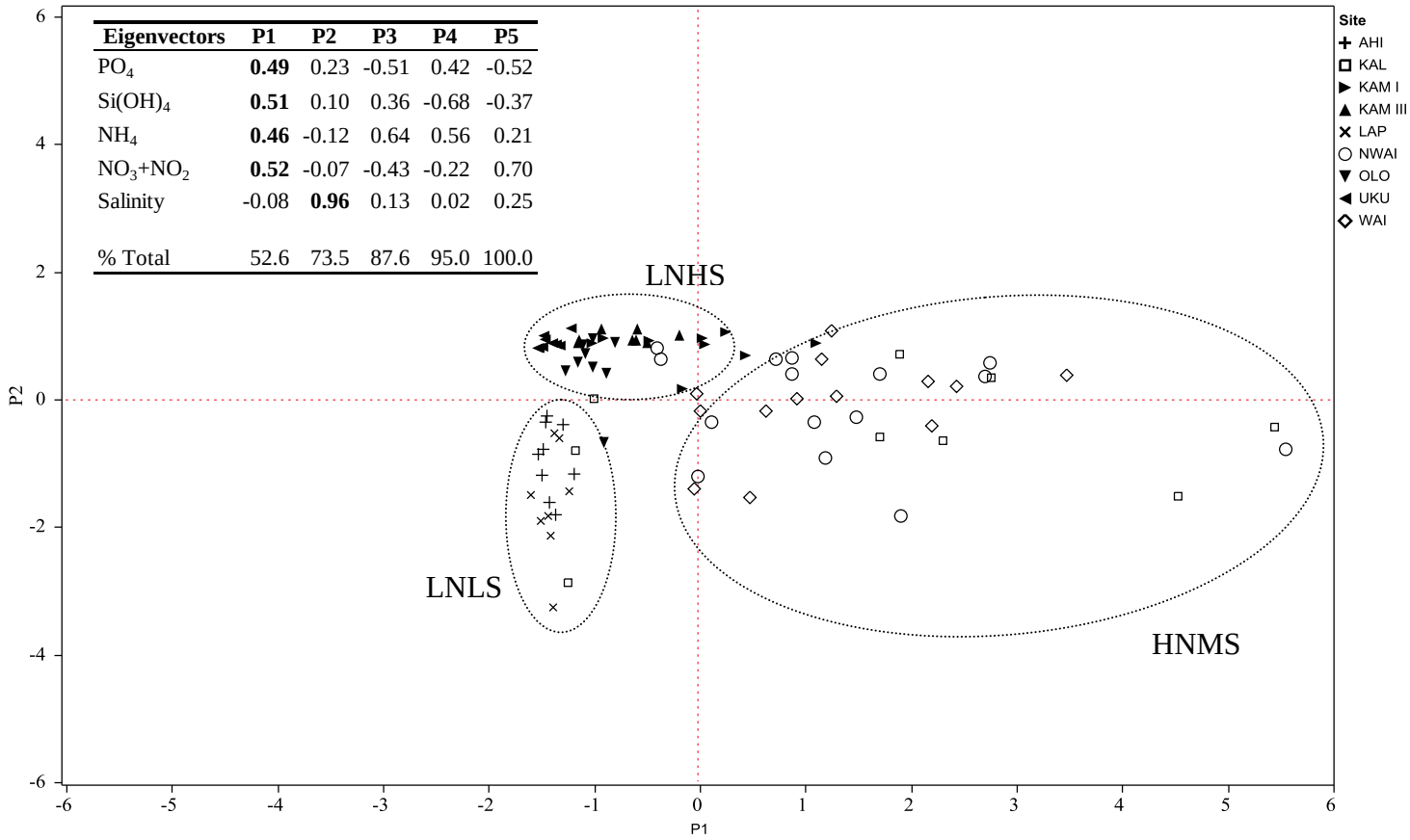

Figure 3.13 - Correlation-based principal components analysis of all dissolved nutrient and salinity data. Inset table shows the eigenvectors for all principal components and the percent of total variance explained by each component. The LNLS (low nutrient low salinity), LNHS (low nutrient high salinity), and HNMS (high nutrient mixed salinity) denominations reflect classifications as per cluster analysis (see Chapter 3 appendix Figure A3.1).

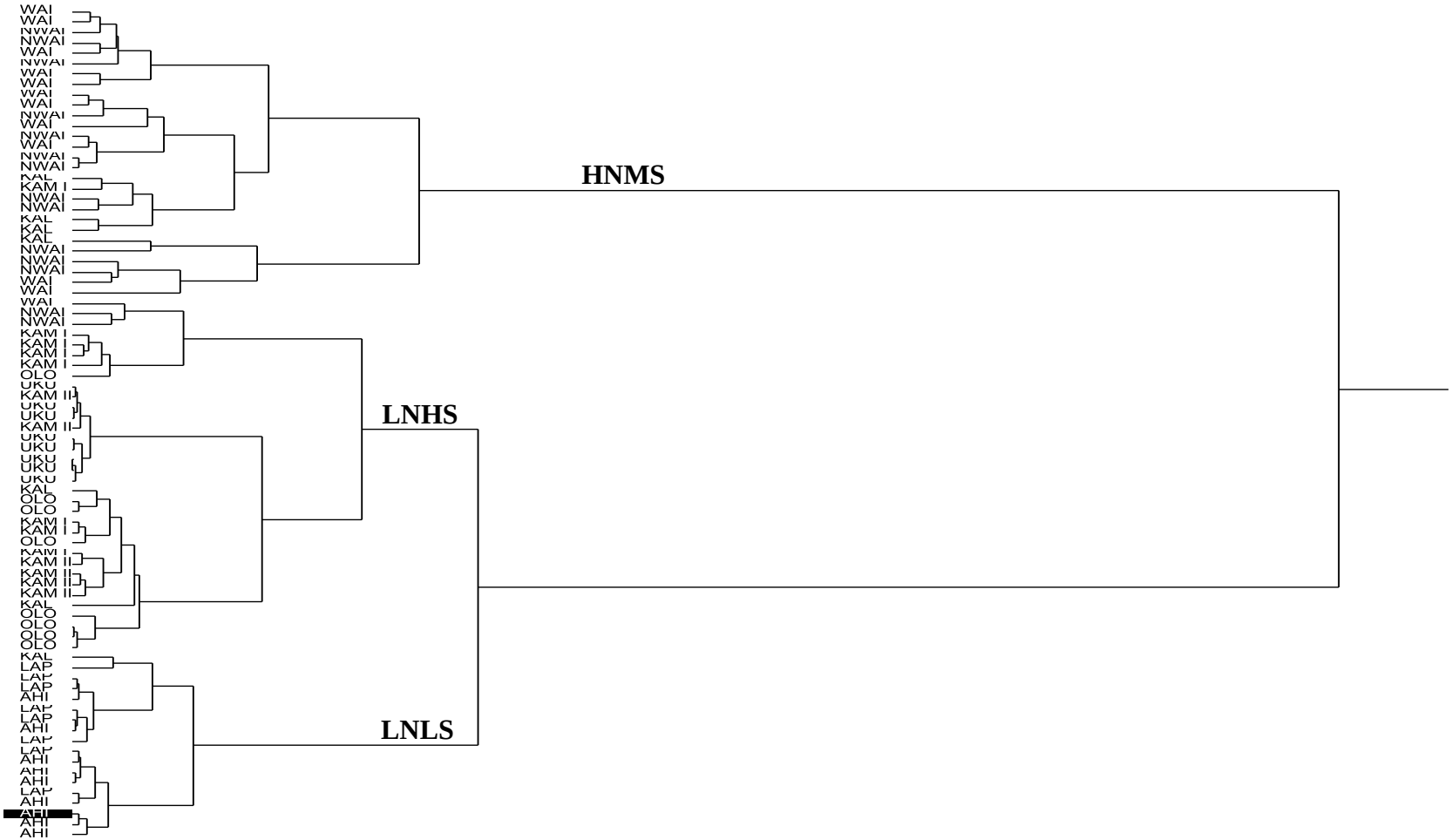

Figure 3.14 - Cluster analysis of all data using Ward's minimum variance method and showing distance scale. High nutrient mixed salinity (HNMS), low nutrient high salinity (LNHS), and low nutrient low salinity (LNLS) denominations as per groups observed in principal components analysis.

Table 3.1 –Distance from shore of water sampling sites, approximate water depth at each location, and depth (above sediment-water interface) of temperature loggers.

Site ID	Distance from Shore (m)	Approx. Water Depth (m)	Temperature Sensor Depth (m)
OLO	0	1	
UKU	0	1	0
	50	1.5	0, 0.9
	150	1.5	0, 0.9
	300	5	0, 0.9, 3
	500	10	0, 3, 6, 9
NWAI	0	1	
WAI	0	1	0
	50	1.5	0, 0.9
	150	5	0, 0.9, 3
	300	7	0, 3, 6
	600	10	0, 3, 6, 9
KAL	0	1	0
	50	1.5	0, 0.9
	150	7	0, 3, 6
	300	10	0, 3, 6, 9
KAMI	0	1	
KAMIII	0	1	
AHI	0	1	
LAP	0	1	

Table 3.2 – Mean of visually observed wind speed and wave height at sites sampled; standard deviation and number of observations (n) are given in parentheses. Superscripts denote results of Student's t-test multiple comparisons; identical letters denote sample means not significantly different from each other at the 0.05 significance level.

	Observed Wind speed (m/s)	Observed Wave Height (cm)	Observer ID
First synchronous observations			
Olowalu	-	-	1
Ukumehame	1 (1, n = 9)^{b}	19 (16, n = 9)^{cd}	1
North Waipuilani	-	-	2
Waipuilani	2 (3, n = 8)^{b}	5 (15, n = 9)^{d}	2
Kalama	2 (2, n = 9)^{b}	36 (12, n = 9)^{ab}	3
Second synchronous observations			
North Waipuilani	4 (4, n = 8)^{b}	19 (13, n = 9)^{d}	3
Waipuilani	5 (5, n = 9)^{b}	24 (13, n = 9)^{d}	3
Kamaole I	2 (2, n = 9)^{b}	15 (12, n = 9)^{cd}	1
Kamaole III	2 (2, n = 9)^{b}	31 (23, n = 9)^{bc}	1
N. Ahihi Kinau	2 (2, n = 9)^{b}	51 (26, n = 9)^{a}	2
Laperouse	6 (6, n = 9)^{a}	51 (21, n = 9)^{a}	2

Table 3.3 - Water currents along the proximal coastal zone. Negative current denotes either south or west flows depending on the site orientation along the coast. AS= along-shore current velocity, XS= cross-shore current velocity.

Location	Approx. Distance from Shore (m)	Water Depth (m)	Geo - morphology	Date	Method	Observation period	Current Speed (m/s)		Current Velocity (m/s)				Water Residence Time* (days)
							Mean (stdev)	Range	AS		XS		
									Mean	Range	Mean	Range	
West Maui[a]	1 - 2000	20 m	various	June/July - 03	VM-ADCP transects	5 days	0.24 (0.23)	0.01 - 1.96					0.02
West Maui[a]	1 - 2000	5 m	various	June/July - 03	VM-ADCP transects	5 days	0.10						0.06
Kahana, Maui[b]	300	2 m	open bay	July 02 - Feb 03	moored ADCP meter	6 months				-0.05 - 0.05		-0.05 - 0.05	0.12
Kahana, Maui[b]	750	10 m	open bay	Nov 01 - Feb 03	moored ADCP meter	15 months				-0.10 - 0.10		-0.05 - 0.05	0.06 - 0.12
Honolua, Maui[c]	0 - 1250	surface	semi-enclosed bay	July 03	Ra isotopes	few hours							3
Kahana, Maui[c]	0 - 350	surface	open bay	July 03	Currents and Ra isotopes	few hours							0.10 - 1.56
Mahinahina, Maui[c]	0 - 350	surface	exposed shore	July 03	Ra isotopes	few hours							1.56
Honokowai, Maui[c]	0 - 400	surface	exposed shore	July 03	Ra isotopes	few hours							1.56
Kaanapali, Maui[d]	various	surface	point		SWAN model			0.00 - 0.7					0.01
UKU (Site B)[e]	50	< 2 m	point (backreef)	Mar-07	moored Aquadopp meter	3 days	0.11 (0.06)	0.002 - 0.55	-0.01	-0.24 - 0.23	-0.02	-0.53 - 0.51	0.05
UKU (Site C)[e]	300	3 m	point (backreef)	Mar-07	moored Aquadopp meter	3 days	0.12 (0.06)	0.005 - 0.53	-0.009	-0.187 - 0.167	0.0015	-0.412 - 0.532	0.05
UKU (Site D)[e]	500	5 m	point (forereef)	Mar-07	moored Aquadopp meter	3 days	0.09 (0.05)	0.003 - 0.715	-0.019	-0.63 - 0.25	0.008	-0.49 - 0.34	0.06
NWAI[e]	300	< 2 m	inside fish pond (backreef)	Jun-05	moored Aquadopp meter	2.5 days	0.09 (0.05)	0.00 - 0.42	-0.03	-0.31 - 0.22	-0.01	-0.36 - 0.33	0.06
WAI (Site B)[e]	50	< 2 m	margin (backreef)	Jan/Feb-06	moored Aquadopp meter	9 days	0.10 (0.06)	0.003 - 0.714	-0.02	-0.25 - 0.29	-0.01	-0.64 - 0.71	0.06
WAI (Site B)[e]	50	< 2 m	margin (backreef)	Mar-07	moored Aquadopp meter	2.5 days	0.16 (0.07)	0.003 - 0.72	0.006	-0.30 - 0.29	-0.04	-0.54 - 0.71	0.04
WAI (Site C)[e]	300	< 2 m	margin (backreef)	Jun-05	moored Aquadopp meter	2.5 days	0.13 (0.08)	0.001 - 0.56	-0.04	-0.41 - 0.30	-0.03	-0.56 - 0.36	0.04
WAI (Site C)[e]	300	< 2 m	margin (backreef)	Jan/Feb-06	moored Aquadopp meter	9 days	0.14 (0.08)	0.004 - 0.70	-0.005	-0.36 -0.37	-0.009	-0.645 -0.673	0.04
WAI (Site C)[e]	300	< 2 m	margin (backreef)	Mar-07	moored Aquadopp meter	2.5 days	0.18 (0.09)	0.009 - 1.019	0.004	-1.00 - 0.36	-0.04	-0.72 - 0.70	0.03
WAI (Site D)[e]	500	5 m	margin (forereef)	Mar-07	moored Aquadopp meter	2.5 days	0.12 (0.07)	0.005 - 0.53	0.02	-0.33 - 0.42	-0.002	-0.36 - 0.43	0.05

Data sources: a= Storlazzi et al. (2006); b= Storlazzi and Jaffe (2008), Figure 7; c= Street et al. (2008); d=Vitousek (2007), Figure 16; e =Herzfeld et al., 2011. *Water residence times (if not reported in referenced study) are calculated as the time it would take water flowing at the mean current speed to transit across a linear coastal distance of 500 m.

Table 3.4 –Mean (stdev) of dissolved nutrient (in μM) and salinity data from synoptic diurnal observations. Superscripts denote results of Student's t-test multiple comparisons: entries with the same letter have sample means not significantly different from each other at the 0.05 significance level. †Data from Herzfeld (2011), * Data from Hunt (2006).

	Collection Date	Salinity (PSU)	PO_4	Si	NO_3	NO_2	NH_4	DIN	DIN:DIP
OLO	6/8-9/2006	32.70 (2.17, n = 9)^{a}	0.09 (0.02, n = 9)^{cd}	13.45 (3.05, n = 9)^{de}	0.10 (0.06, n = 9)^{c}	0.02 (0.01, n = 9)^{c}	0.24 (0.21, n = 9)^{cd}	0.37 (0.21, n = 9)^{d}	4.33 (2.87, n = 9)^{c}
UKU	6/8-9/2006	34.57 (0.35, n = 9)^{a}	0.09 (0.02, n = 9)^{cd}	3.66 (0.64, n = 9)^{fg}	0.04 (0.05, n = 9)^{c}	0.01 (0.01, n = 9)^{c}	0.04 (0.02, n = 9)^{d}	0.10 (0.05, n = 9)^{d}	1.04 (0.46, n = 9)^{c}
NWAI	6/8-9/2006	31.37 (2.37, n = 9)^{b}	0.16 (0.14, n = 9)^{bc}	36.73 (6.17, n = 9)^{b}	5.15 (5.37, n = 9)^{b}	0.44 (0.41, n = 9)^{a}	3.01 (2.71, n = 9)^{a}	8.60 (7.94, n = 9)^{ab}	50.05 (24.31, n = 9)^{a}
WAI	6/8-9/2006	28.52 (3.05, n = 4)^{bc}	0.09 (0.07, n = 4)^{b}	34.90 (7.78, n = 4)^{a}	1.68 (1.55, n = 4)^{bc}	0.20 (0.21, n = 4)^{b}	1.49 (0.84, n = 4)^{ab}	1.50 (2.17, n = 9)^{bc}	46.00 (24.45, n = 4)^{ab}
KAL	6/8-9/2006	25.93 (4.39, n = 9)^{d}	0.32 (0.24, n = 9)^{a}	26.35 (15.35, n = 9)^{c}	9.68 (8.03, n = 9)^{a}	0.21 (0.10, n = 9)^{ab}	0.91 (1.46, n = 9)^{bcd}	10.79 (9.13, n = 9)^{a}	32.67 (15.57, n = 8)^{abc}
NWAI	6/13-14/2006	27.86 (4.20, n = 6)^{b}	0.14 (0.06, n = 7)^{bc}	32.65 (10.82, n = 7)^{b}	4.80 (4.63, n = 7)^{b}	0.17 (0.07, n = 7)^{a}	2.07 (1.20, n = 7)^{a}	5.47 (5.38, n = 9)^{ab}	63.78 (59.31, n = 7)^{a}
WAI	6/13-14/2006	29.44 (3.03, n = 9)^{bc}	0.23 (0.10, n = 9)^{b}	44.16 (11.87, n = 9)^{a}	3.36 (4.14, n = 9)^{bc}	0.21 (0.12, n = 9)^{b}	2.54 (1.61, n = 9)^{ab}	6.11 (4.27, n = 9)^{bc}	49.45 (90.38, n = 9)^{ab}
KAMI	6/13-14/2006	33.19 (1.14, n = 9)^{a}	0.20 (0.04, n = 9)^{b}	17.56 (7.30, n = 9)^{d}	3.80 (2.43, n = 9)^{b}	0.02 (0.01, n = 9)^{c}	0.12 (0.08, n = 9)^{d}	3.94 (2.46, n = 9)^{cd}	18.46 (10.04, n = 9)^{bc}
KAMIII	6/13-14/2006	35.89 (4.78, n = 9)^{a}	0.17 (0.03, n = 9)^{bc}	9.35 (3.30, n = 9)^{ef}	2.19 (1.19, n = 9)^{bc}	0.05 (0.02, n = 9)^{c}	0.09 (0.02, n = 9)^{d}	2.33 (1.21, n = 9)^{cd}	13.16 (5.69, n = 9)^{c}
AHI	6/13-14/2006	26.71 (2.35, n = 9)^{cd}	0.04 (0.02, n = 9)^{d}	1.86 (0.77, n = 9)^{g}	0.36 (0.09, n = 9)^{c}	0.00 (0.00, n = 9)^{c}	0.31 (0.26, n = 9)^{cd}	0.67 (0.28, n = 9)^{d}	31.67 (50.00, n = 9)^{bc}
LAP	6/13-14/2006	24.15 (3.97, n = 9)^{d}	0.05 (0.08, n = 9)^{d}	1.99 (0.83, n = 9)^{g}	0.37 (0.15, n = 9)^{c}	0.00 (0.01, n = 9)^{c}	1.83 (4.37, n = 9)^{abc}	2.20 (4.50, n = 9)^{cd}	27.57 (20.07, n = 5)^{abc}
Open Ocean†	various	34.21 (0.53, n=158)	0.09 (0.03, n=164)	3.5 (2.84, n=164)	0.15 (0.2, n=164)	0.02 (0.01, n=164)	0.15 (0.27, n=164)	0.32 (0.35, n=164)	3.86 (3.21, n=164)
UKU well	Mar-07	0.37 (0.01)	0.92 (0.17)	1064.15 (19.35)	181.76 (1.08)	0.00 (0.00)	0.54 (0.08)	182.30 (1.16)	202.73 (36.80)
WAI well	Jan-06	0.83 (0.18)	3.70 (0.43)	452.51 (18.65)	163.12 (5.58)	0.05 (0.03)	0.04 (0.11)	163.21 (5.58)	44.91 (4.08)
KAL "cross-gradient"*	see source	1.16	1.65	1182.08	110.00	0.57	2.86	112.86	68.54
KAL "down-gradient"*	see source	1.58	6.01	1513.21	234.43	0.57	6.43	241.43	40.20

Table 3.5 – Summary of sites with significant correlation coefficients (r) between measured variables at alpha = 0.05. An underlined site denotes a significant negative correlation coefficient.

	PO_4	Si	NO_3	NO_2	NH_4	DIN	Salinity	Tide Height	Obs. Wind	Obs. Wave	^{223}Ra	^{224}Ra	^{228}Th
Si	OLO, UKU, KAL, KAMI, KAMIII												
NO_3	KAL, KAMI, KAMIII, LAP	UKU, NWAI, KAL, KAMI, KAMIII, AHI, LAP											
NO_2	UKU, KAL, KAMIII, AHI	OLO, UKU, KAL, KAMI, LAP	OLO, WAI, KAL, KAMIII, AHI, LAP										
NH_4	UKU, KAL	KAL	KAL	NWAI, KAL									
DIN	UKU, WAI, KAL, KAMI, KAMIII	UKU, WAI, KAL, KAMI, KAMIII	OLO, UKU, NWAI, WAI, KAL, KAMI, KAMIII	UKU, NWAI, WAI, KAL, KAMIII, AHI	OLO, NWAI, WAI, KAL, AHI, LAP								
Salinity	KAMIII, AHI, LAP	KAMIII	KAMIII	KAMIII		KAMIII							
Tide Height	KAL, KAMI, KAMIII	KAMI, KAMIII, AHI	KAL, KAMI, KAMIII	KAL, KAMIII		KAL, KAMI, KAMIII	KAMIII						
Obs. Wind	KAL, KAMIII	KAMIII, LAP	KAL	KAL	KAMIII	KAL		KAL					
Obs. Wave			UKU		KAL, KAMIII	UKU			UKU, NWAI, WAI, KAMI, AHI				
^{223}Ra	WAI		WAI	WAI	WAI, KAL	WAI		KAL	WAI	KAL			
^{224}Ra	WAI			WAI	KAL	WAI					WAI		
^{228}Th	WAI		WAI	WAI		WAI		WAI	WAI	WAI	WAI	UKU, WAI	
^{227}Ac	UKU, WAI	UKU	WAI	WAI		WAI	KAL			KAL	UKU	WAI	WAI

Table 3.6 – Radionuclide data for the 24-hr near-shore surface water time-series. Mean of diurnal radio-isotopic data are shown in boldface with standard deviation, and number of observations (n) in parentheses. Superscripts denote results of Student's t-test multiple comparisons: entries with the same letters have sample means not significantly different from each other at the 0.05 significance level. AR = Activity ratio.

Location	Date/Time	Volume Filtered (L)	^{223}Ra (dpm/m^3)	^{224}Ra (dpm/m^3)	^{228}Th (dpm/m^3)	^{227}Ac (dpm/m^3)	Excess-^{223}Ra (dpm/m^3)	Excess-^{224}Ra (dpm/m^3)	^{224}Ra/^{223}Ra AR	Excess ^{224}Ra/^{223}Ra AR
Ukumehame	6/8/06 14:00	32	2.14	30.70	3.56	0.16	1.98	27.14	14.38	13.73
	6/8/06 16:10	72	0.97	27.34	1.43	0.07	0.90	25.91	28.22	28.74
	6/8/06 19:15	70	0.95	37.18	1.13	0.00	0.95	36.05	39.33	38.06
	6/8/06 22:20	80	1.37	13.32	1.93	0.08	1.30	11.39	9.70	8.79
	6/9/06 1:20	90	1.13	27.76	0.66	0.11	1.01	27.10	24.62	26.72
	6/9/06 4:15	82	2.16	18.46	1.33	0.16	2.00	17.13	8.54	8.57
	6/9/06 7:10	85	0.22	31.25	1.35	0.04	0.18	29.89		
	6/9/06 10:10	80	1.30	13.56	1.62	0.16	1.14	11.94	10.42	10.44
	6/9/06 13:00	70	0.67	15.63	1.56	0.12	0.55	14.07	23.18	25.38
	Mean (stdev, count)		**1.21 (0.63, n= 9)^b**	**23.91 (8.80, n= 9)^b**	**1.62 (0.81, n= 9)^b**	**0.10 (0.06, n= 9)^a**	**1.11 (0.59, n= 9)^b**	**22.29 (8.85, n= 9)^b**	**19.80 (10.91, n= 8)^a**	**20.05 (11.11, n= 8)^a**
Waipuliani	6/8/06 13:45	25	6.70	88.80	6.44	0.58	6.12	82.36	13.24	13.45
	6/8/06 16:00	40	6.85	68.36	3.40	0.10	6.74	64.96	9.98	9.64
	6/8/06 19:00	78	3.06	75.28	2.84	0.19	2.87	72.44	24.57	25.23
	6/8/06 22:00	82	2.19	46.61	1.90	0.08	2.11	44.71	21.33	21.23
	6/9/06 1:00	60	2.71	62.48	3.34	0.27	2.45	59.14	23.01	24.18
	6/9/06 4:00	60	1.96	65.61	2.28	0.02	1.95	63.33	33.41	32.52
	6/9/06 7:00	80	2.53	46.64	1.37	0.09	2.44	45.27	18.43	18.58
	6/9/06 10:00	70	2.85	42.79	2.36	0.06	2.79	40.43	15.04	14.50
	6/9/06 13:00	80	1.57	43.68	2.59	0.13	1.44	41.09	27.88	28.59
	Mean (stdev, count)		**3.38 (1.98, n= 9)^a**	**60.03 (16.17, n= 9)^a**	**2.95 (1.46, n= 9)^a**	**0.17 (0.17, n= 9)^a**	**3.21 (1.88, n= 9)^a**	**57.08 (15.02, n= 9)^a**	**20.77 (7.43, n= 9)^a**	**20.88 (7.52, n= 9)^a**
Kalama	6/8/06 13:10	40	5.38	52.30	2.80	0.07	5.31	49.50	9.72	9.33
	6/8/06 16:00	100	0.53	4.72	0.92	0.06	0.48	3.80	8.83	7.95
	6/8/06 19:00	100	1.25	15.04	1.29	0.11	1.15	13.76	12.00	12.01
	6/8/06 22:00	100	0.92	16.99	0.83	0.00	0.92	16.16	18.56	17.61
	6/9/06 1:00	100	1.05	11.24	1.25	0.00	1.05	9.99	10.72	9.53
	6/9/06 4:00	100	1.87	14.95	0.66	0.06	1.81	14.29	7.97	7.89
	6/9/06 7:00	100	0.81	8.78	1.76	0.09	0.72	7.02	10.80	9.70
	6/9/06 10:00	100	0.00	14.52	1.04	0.19	-0.19	13.48		
	6/9/06 13:00	100	0.15	23.23	0.69	0.07	0.09	22.54	150.40	257.93
	Mean (stdev, count)		**1.33 (1.62, n= 9)^b**	**17.97 (13.88, n= 9)^b**	**1.25 (0.68, n= 9)^b**	**0.07 (0.06, n= 9)^a**	**1.26 (1.63, n= 9)^b**	**16.73 (13.42, n= 9)^b**	**28.62 (49.31, n= 8)^a**	**41.49 (87.51, n= 8)^a**

Table 3.7 – Radionuclide data for 24-hr Mn-fiber equilibration deployments. AR = Activity ratio

Location	Distance Offshore (m)	Site ID	^{223}Ra (dpm)	^{224}Ra (dpm)	^{226}Ra (dpm)	^{228}Ra (dpm)	^{228}Th (dpm)	^{227}Ac (dpm)	^{224}Ra/^{226}Ra AR	^{224}Ra/^{223}Ra AR
UKU	0	A	0.94	24.26	50.40	5.23	0.53	0.01	0.48	25.89
	50	B			24.85	1.45	0.41	0.04		
	150	B-C	0.47	5.34	14.60	b.d.	0.33	0.01	0.37	11.44
	300	C								
	600	D								
WAI	0	A	1.13	20.95	15.29	5.74	0.51	0.07	1.37	18.58
	50	B	0.57	7.00	5.62	1.97	0.31	0.02	1.25	12.29
	150	B-C	1.96	20.42	16.23	5.24	0.61	0.02	1.26	10.44
	300	C	0.39	6.05	33.47	4.77	0.36	0.04	0.18	15.70
	600	D	0.09	1.13	12.40	b.d.	0.46	0.00	0.09	12.35
KAL	0	A	1.24	14.77	34.49	2.77	0.33	0.04	0.43	11.94
	50	B	0.42	7.13	26.21	4.58	0.55	0.05	0.27	16.86
	150	B-C	0.26	4.28	16.14	1.46	0.43	0.02	0.27	16.71
	300	C	0.11	1.79	8.00	b.d.	0.33	0.01	0.22	16.81
	600	D								

Table 3.8 - Mean solute fluxes and calculated groundwater outflow velocities (V_{SGD}) using different tracers; standard deviations are given in parentheses. Superscripts denote results of Student's t-test multiple comparisons: entries with the same letters have sample means not significantly different from each other at the 0.05 significance level. We exempt V_{SGD} calculations using PO_4 due to significant bias introduced by adsorptive processes during transition across the land-ocean interface (Charette and Sholkovitz 2006).

	Flux					**Vsgd (m/day)**				
	dpm/m^2/day		**mmol/m^2/day**							
Site ID	**^{223}Ra**	**^{224}Ra**	**Si**	**DIN**	**PO_4**	**^{223}Ra**	**^{224}Ra**	**Salinity**	**Si**	**DIN**
OLO			2.66 (0.95)^{de}	0.02 (0.08)^{c}	0.00 (0.03)^{bcd}			0.54 (0.65)^{cd}	0.06 (0.02)^{b}	0.00 (0.01)^{c}
UKU	0.37 (0.24)^{b}	9.46 (4.52)^{b}	0.03 (0.17)^{ef}	-0.09 (0.04)^{c}	0.00 (0.01)^{bcd}	0.01 (0.01)^{b}	0.01 (0.01)^{b}	0.10 (0.08)^{d}	0.00 (0.00)^{b}	-0.01 (0.00)^{c}
NWAI			7.27 (4.76)^{b}	2.94 (3.89)^{ab}	0.01 (0.04)^{bc}			1.01 (0.92)^{bc}	0.39 (0.25)^{a}	0.43 (0.57)^{a}
WAI	1.13 (0.97)^{a}	25.05 (12.21)^{a}	10.34 (5.13)^{a}	1.53 (2.21)^{bc}	0.01 (0.03)^{bc}	0.03 (0.02)^{a}	0.03 (0.02)^{a}	1.07 (0.47)^{bc}	0.40 (0.27)^{a}	0.23 (0.39)^{bc}
KAL	0.46 (0.78)^{ab}	8.19 (9.31)^{b}	5.62 (3.37)^{bc}	3.66 (2.87)^{a}	0.06 (0.08)^{a}	0.01 (0.02)^{b}	0.01 (0.01)^{b}	1.74 (0.80)^{a}	0.09 (0.05)^{b}	0.38 (0.30)^{ab}
KAMI			3.17 (1.08)^{cd}	1.13 (0.66)^{c}	0.03 (0.01)^{b}			0.32 (0.14)^{d}	0.06 (0.02)^{b}	0.24 (0.14)^{bc}
KAMIII			1.29 (0.59)^{def}	0.67 (0.32)^{c}	0.02 (0.02)^{bc}			0.15 (0.08)^{d}	0.03 (0.01)^{b}	0.14 (0.07)^{c}
AHI			-0.46 (0.31)^{f}	0.13 (0.10)^{c}	-0.01 (0.02)^{cd}			1.49 (0.63)^{ab}	-0.01 (0.01)^{b}	0.02 (0.01)^{c}
LAP			-0.42 (0.30)^{f}	0.12 (0.12)^{c}	-0.02 (0.01)^{d}			1.90 (0.73)^{a}	-0.01 (0.01)^{b}	0.02 (0.02)^{c}

Table 3.9 - Ranges of solute fluxes and calculated groundwater outflow velocity (V_{SGD}) using different tracers

	Flux					**Vsgd (m/day)**					
	dpm/m^2/day		**mmol/m^2/day**								
Site ID	**^{223}Ra**	**^{224}Ra**	**Si**	**DIN**	**PO_4**	**^{223}Ra**	**^{224}Ra**	**Salinity**	**Si**	**DIN**	**Overall Range**
OLO			1.50 - 4.19	-0.06 - 0.16	-0.01 - 0.01			0.11 - 2.17	0.03 - 0.09	-0.01 - 0.02	-0.01 - 2.17
UKU	0.03 - 0.93	3.97 - 17.02	-0.18 - 0.25	-0.16 - -0.05	-0.01 - 0.02	0.00 - 0.02	0.00 - 0.02	0.00 - 0.22	0.00 - 0.01	-0.02 - -0.01	-0.02 - 0.22
NWAI			-1.49 - 18.16	-0.2 - 16.10	-0.04 - 0.17			0.25 - 3.40	-0.08 - 0.96	-0.03 - 2.37	-0.08 - 3.40
WAI	0.44 - 2.89	10.84 - 51.65	4.14 - 21.65	-0.16 - 9.06	-0.03 - 0.08	0.01 - 0.07	0.01 - 0.06	0.25 - 1.89	0.00 - 1.15	-0.02 - 1.33	-0.02 - 1.89
KAL	-0.06 - 2.51	1.68 - 31.04	0.85 - 12.26	0.04 - 9.00	-0.02 - 0.26	0.00 - 0.06	0.00 - 0.04	0.47 - 2.76	0.01 - 0.19	0.00 - 0.94	0.01 - 2.76
KAMI			1.64 - 4.76	0.02 - 1.86	0.01 - 0.04			0.18 - 0.66	0.03 - 0.10	0.00 - 0.39	0.00 - 0.66
KAMIII			0.23 - 2.04	0.17 - 0.98	0.01 - 0.02			0.03 - 0.24	0.00 - 0.04	0.04 - 0.21	0.00 - 0.24
AHI			-0.94 - -0.02	0.03 - 0.30	-0.02 - 0.00			0.83 - 2.54	-0.02 - 0.00	0.00 - 0.04	-0.02 - 2.54
LAP			-0.97 - -0.02	-0.11 - 0.31	-0.03 - 0.00			0.80 - 3.30	-0.02 - 0.00	-0.01 - 0.04	-0.01 - 3.30

Table 3.10 – Literature estimates of groundwater discharge rate induced by waves, density gradients, and total submarine groundwater discharge. For comparison purposes, original units have been converted to discharge volume assuming discharge rate across a 1 m^2 of seafloor.

Units (L/min)	Origin and type of sediment	Measurement type	Tracer	Reference
Wave-driven porefluid transport				
0.00 - 0.06	wave amplitude 10 cm, water depth 20 cm, k=2.9 x 10^{-11} m^2, wavelength 120 cm, median grain = 250 µm	various	various	Huettel, et al., 2003
0.41	Rhodamine tracer, wave amplitude 6-8 cm, water depth ~20 cm, k=1.32 - 2.02 x 10^{-11} m^2, wavelength ~80 cm, median grain = 100-300 µm	wave tank, oscillating flow-topography interaction	Rhodamine WT	Precht and Huettel, 2003
0.03	Rhodamine tracer, wave amplitude 6-8 cm, water depth ~20 cm, k=1.32 - 2.02 x 10^{-11} m^2, wavelength ~80 cm, median grain = 100-300 µm	wave tank, wave pumping	Rhodamine WT	Precht and Huettel, 2003
0.00 - 0.02	Lotic beaches at Onslow Bay, North Carolina (USA)	in-field thermistors	Temperature	Riedl, 1972
0.36 - 3.18	Mid-Atlantic Bight (USA), continental shelf sand deposit	iodide breaktrhough	Iodide	Reimers, etal., 2004
0.20 - 0.93	Mid-Atlantic Bight (USA), continental shelf sand deposit	shipboard sediment columns		Reimers, etal., 2004
0.09 - 0.21	amphioxus coarse sands, LeRacou (Roussillon), France	in- field, flourescein	Fluorescein	Webb and Theodor, 1968
0.22	advection, waves	field	Fluorescein	Precht and Huettel, 2004
1.58	advection, unidirectional flow	field	Fluorescein	Precht and Huettel, 2004
0.01	wave pumping	field	Fluorescein	Precht and Huettel, 2004
0.02	advection, unidirectional flow with mounds	particle tracer on flume	particles	Huettel, et al, 1996
1.23 - 2.40	coastal sandy sediments, Campese Bay, Giglio Island, Italy	in-field optical sensors detecting neutrally bouyant flourescein	Fluorescein	Precht and Huettel, 2004
0.24 - 3.72	Mid-Atlantic Bight shelf sandy sediments	lab, intact core, induced flow	O_2	Rusch, 2006
0.01 - 0.03	coastal sandy sediments, Campese Bay, Giglio Island, Italy	in-field optical sensors detecting neutrally bouyant flourescein	Fluorescein	Precht and Huettel, 2004
0.50 - 0.83	coastal sandy sediments, south shore of Oahu, Hawaii (Kilo Nalu observatory)	in-situ fluorescein dye dispersal	Fluorescein	Hebert et al., 2007
0.02 - 3.78	Kahekili, Maui sediments. Permeability 2.93 x 10^{-10} - 9.2 x 10^{-11} m^2	Modeled sediments from Kahekili, Maui	modeled water molecules	Herzfeld et al., 2010b
Density driven transport				
0.10	salt water aquarium filled with sediment saturated with a solution of dye in freshwater	laboratory	O_2	Webster, et al., 1996
0.06	convection, thermal	field	O_2	Precht and Huettel, 2004
Submarine groundwater discharge (SGD)				
0.87 - 2.60	Gulf of Aqaba, Israel	mixing model	Radium	Paytan et al., 2006
34.72 - 76.02	Hawaii, Kona	mixing model	Radium	Paytan et al., 2006
24.00 - 78.87	West Maui, Kahana	mixing model	Radium	Paytan et al., 2006
9.77 - 10.42	Florida, Key Largo	mixing model	Radium	Paytan et al., 2006
57.87 - 60.67	Mauritius, West Coast	mixing model	Radium	Paytan et al., 2006
0.03 - 0.50	Pocasset, West Fallmouth	chambers and seepage meter	Water and salt	Valiela, etal 1990
0.21 - 128.47	various locations Hawaii, Hawaii	mixing model	Radium	Street et al., 2008
0.01 - 0.02	Barbados, West Indies coral reefs	piezometers, seepage meters	Salinity, nitrate	Lewis, 1987
0.00 - 0.05	Various sites along south and west shores of Maui, Hawaii, proximal coastal zone	mixing model	Radium	This study
0.00 - 2.36	Various sites along south and west shores of Maui, Hawaii, proximal coastal zone	mixing model	Salt	This study
-0.06 - 0.80	Various sites along south and west shores of Maui, Hawaii, proximal coastal zone	mixing model	Silicates	This study
-0.02 - 1.64	Various sites along south and west shores of Maui, Hawaii, proximal coastal zone	mixing model	DIN	This study

3.8 LITERATURE CITED

Atkinson, M.J. and S.V. Smith. 1983. C:N:P ratios of benthic marine plants. Limnology and Oceanography, 28(3): 568-574.

Burnett, W.C. et al. 2003. Groundwater and pore water inputs to the coastal zone. Biogeochemistry, 66: 3-33.

Burnett, W.C. and H. Dulaiova. 2003. Estimating the dynamics of groundwater input into the coastal zone via continuous radon-222 measurements. Journal of Environmental Radioactivity, 69: 21-35.

Capone, D. and J. Slater. 1990. Inter-annual patterns of water table height and groundwater derived nitrate in nearshore sediments. Biogeochemistry, 10(3, Groundwater Inputs to Coastal Waters): 277-288.

Capone, D.G. and M.F. Bautista. 1985. A groundwater source of nitrate in nearshore marine sediments. Nature, 313: 214-216.

Chanton, J.P. et al. 2003. Seepage rate variability in Florida Bay driven by Atlantic tidal height. Biogeochemistry, 66(1/2): 187-202.

Charette, M.A. and E.R. Sholkovitz. 2002. Oxidative precipitation of groundwater-derived ferrous iron in the subterranean estuary of a coastal bay. Geophysical Research Letters, 29(10): 85.1 - 85.4.

Charette, M.A. and E.R. Sholkovitz. 2006. Trace element cycling in a subterranean estuary: Part 2. Geochemistry of the pore water. Geochimica et Cosmochimica Acta, 70(4): 811-826.

D'Elia, C.F., K.L. Webb, and J.W. Porter. 1981. Nitrate-rich groundwater inputs to Discovery Bay, Jamaica: A significant source of N to local coral reefs? Bulletin of Marine Science, 31: 903-910.

Dailer, M., R.S. Knox, J.E. Smith, M. Napier, and C.M. Smith. 2010. Using $\delta^{15}N$ values in algal tissue to map locations and potential sources of anthropogenic nutrient inputs on the island of Maui, Hawai‘i, USA. Marine Pollution Bulletin, 60(5): 655-671.

Dollar, S.J. and C. Andrews. 1997. Algal blooms off West Maui: Assessing causal linkages between land and the coast ocean, National Oceanic and Atmospheric Administration Coastal Ocean Program Office, Honolulu, Honolulu.

Doney, S.C. et al. 2007. Impact of anthropogenic atmospheric nitrogen and sulfur deposition on ocean acidification and the inorganic carbon system. PNAS, 104: 14580-14585.

Dulaiova, H. and W.C. Burnett. 2007. Evaluation of the flushing rates of Apalachicola Bay, Florida via natural geochemical tracers. Marine Chemistry, doi:10.1016/j.marchem.2007.09.001.

Erisman, J.W. et al. 2008. How a century of ammonia synthesis changed the world. Nature Geoscience, 1(October): 636-639.

Firing, Y.L. and M.A. Merrifield. 2004. Extreme sea level events at Hawaii: Influence of mesoscale eddies. Geophysical Research Letters, 31(L24306): 1-4.

Fletcher, C.H. et al. 2001-2003. Erosion hazard maps of the Kihei, Maui coastline, http://www.co.maui.hi.us/departments/Planning/erosion.htm, 1:3000.

Froelich, P.N. et al. 1979. Early oxidation of organic matter in pelagic sediments of the eastern equatorial Atlantic: suboxic diagenesis. Geochimica et Cosmochimica Acta, 43(7): 1075-1090.

Fukunaga & Associates. 2010. http://fukunagaengineers.com/projects/kihei/kihei01.htm. Accessed August 2010.

Galloway, J.N. and E.B. Cowling. 2002. Reactive nitrogen and the world: 200 years of change. Ambio, 31(2): 64-71.

Garrison, G.H., C.R. Glenn, and G.M. McMurtry. 2003. Measurement of submarine groundwater discharge in Kahana Bay, O'ahu, Hawai'i. Limnology and Oceanography, 48(2): 920-928.

Giambelluca, T.W., M.A. Nullet, and T.A. Schoroeder. 1986. Rainfall Atlas of Hawai'i. Report R76.

Gordon, L.I., Joe C. Jennings, J., Ross, A.A. and Krest, J.M. 1993. A Suggested protocol for continuous flow automated analysis of seawater nutrients (phosphate, nitrate, nitrite and silicic Acid) in the WOCE Hydrographic Program and the Joint Global Ocean Fluxes Study, College of Oceanic and Atmospheric Sciences, Oregon State University.

Hawaii State Department of Health (HIDOH). 2002. Guidelines for the treatment and use of recycled water. Wastewater Branch. pp. 239

Hebert, A.B., F.J. Sansone, and G. Pawlak. 2007. Tracer dispersal in sandy sediment porewater under enhanced physical forcing. Continental Shelf Research, 27: 2278-2287.

Herzfeld, I. et al. 2006. Diurnal nutrient dynamics associated with a nuisance algal bloom on south Maui, Hawaii, Ocean Sciences Meeting - TOS AGU ASLO, Honolulu, Hawaii.

Herzfeld, I. et al. 2008. Diurnal dissolved inorganic C, N, P, and Fe dynamics in permeable back-reef sediments of the south shore of Maui, Hawaii, Ocean Sciences Meeting, Orlando, Florida.

Huettel, M. and I.T. Webster. 2001. Porewater flow in permeable sediments. In: B.P. Boudreau and B.B. Jorgensen (Editors), The benthic boundary layer. Oxford University Press, pp. 144-179.

Huettel, M., H. Røy, E. Precht, and S. Ehrenhauss. 2003. Hydrodynamical impact on biogeochemical processes in aquatic sediments. Hydrobiologia, 494: 231-236.

Huettel, M., W. Ziebis, and S. Forster. 1996. Flow-induced uptake of particulate matter in permeable sediments. Limnology and Oceanography, 41(2): 309-322.

Huettel, M. et al. 1998. Advective transport affecting metal and nutrient distributions and interfacial fluxes in permeable sediments. Geochimica et Cosmochimica Acta, 62(4): 613-631.

Hunt, C.D.J. 2006. Ground-water nutrient flux to coastal waters and numerical simulation of wastewater injection at Kihei, Maui, Hawaii. U.S. Geological Survey Scientific Investigations Report 2006–5283, pp. 69.

Hunt, C.D.J. and S.N. Rosa. 2009. A multitracer approach to detecting wastewater plumes from municipal injection wells in nearshore marine waters at Kihei and Lahaina, Hawaii. US Geological Survey Scientific Investigations Report 2009-5253. 182pp

Jahnke, R.A. et al. 2000. Benthic flux of biogenic elements on the Southeastern US continental shelf: influence of pore water advective transport and benthic microalgae. Continental Shelf Research 20 109 -127.

Johnson, A. et al. 2006. Thermal infrared surveys and nutrients reveal substantial submarine groundwater discharge systems emanating from the Kona Coast of Hawaii, Ocean Sciences Meeting - TOS AGU ASLO, Honolulu, Hawaii.

Johnson, A.G. et al. 2008. Aerial infrared imaging reveals large nutrient-rich groundwater inputs to the ocean. Geophysical Research Letters, 35: L15606, doi:10.1029/2008GL034574.

Jokiel, P.L. et al. 2004. Hawai'i coral reef assessment and monitoring program: Spatial patterns and temporal dynamics in reef coral communities. Pacific Science, 58(2): 159-174.

Kobayashi, Noboru. 1970. Kihei Civic Development Plan. Prepared for Maui County Planning Commission. Wailuku, Maui. February.

Laws, E.A., D. Brown, and C. Peace. 2004. Coastal water quality in the Kihei and Lahaina districts of the island of Maui, Hawaiian Islands: Impacts from physical habitat and groundwater

seepage: Implications for water quality standards. International Journal of Environment and Pollution, 22(5): 531-546.

Laws, E.A. and L. Ferentinos. 2003. Human impacts on fluxes of nutrients and sediment in Waimanalo Stream, O'ahu, Hawaiian Islands. Pacific Science, 57(2): 119-140.

Laws, E.A., D. Ziemann, and D. Schulman. 1999. Coastal water quality in Hawaii: the importance of buffer zones and dilution. Marine Environmental Research, 48: 1 - 21.

Leichter, J.J. et al. 1996. Pulsed delivery of subthermocline water to Conch Reef (Florida Keys) by internal tidal bores Limnology and Oceanography, 41(7): 1490-1501

Lerman, A., F.T. Mackenzie, and L.M. Ver. 2004. Coupling of the perturbed C-N-P cycles in industrial time. Aquatic Geochemistry, 10: 3-32.

Lewis, J.B. 1987. Measurements of groundwater seepage flux onto a coral reef: Spatial and temporal variations. Limnology and Oceanography, 32(5): 1165-1169.

Li, L., Barry, D.A., F. Stagnitti, and J.-Y. Parlange. 1999. Submarine groundwater discharge and associated chemical input to a coastal sea. Water Resources Research, 35(11): 3253-3259.

Mackenzie, F.T., L.M. Ver, and A. Lerman. 2002. Century-scale nitrogen and phosphorus controls of the carbon cycle. Chemical Geology, 190: 13-32.

Maui County. 2009. Maui Island Plan. General Plan 2030 DRAFT.

Moore, W.S. 1976. Sampling 228Ra in the deep ocean. Deep Sea Research, 23: 647-651.

Moore, W.S. 1999. The subterranean estuary: A reaction zone of ground water and sea water. Marine Chemistry, 65(1-2): 111-125.

Moore, W.S. 2008. Fifteen years experience in measuring 224Ra and 223Ra by delayed-coincidence counting. Marine Chemistry, 109: 188-197.

Moore, W.S. and R. Arnold. 1996. Measurement of 223Ra and 224Ra in coastal waters using a delayed coincidence counter. Journal of Geophysical Research, 101(C1): 1321-1329.

NOAA - National Centers for Coastal Ocean Science (NCCOS). 2007. Atlas of the shallow-water benthic habitats of the main Hawaiian Islands. NOAA Technical memorandum NOS NCCOS 61, Biogeography Team. Silver Spring, MD. 331 pp.

Oostdam, B.L. 1965. Age of lava flows on Haleakala, Maui, Hawaii. Geological Society of America Bulletin, 76: 393-394.

Paul, J.H. et al. 2000. Rapid movement of wastewater from on-site disposal systems into surface waters in the lower Florida Keys. Estuaries, 23(5): 662-668.

Paytan, A. et al. 2006. Submarine groundwater discharge: An important source of new inorganic nitrogen to coral reef ecosystems. Limnology and Oceanography, 51(1): 343-348.

Precht, E. and M. Huettel. 2003. Advective pore-water exchange driven by surface gravity waves and its ecological implications. Limnology and Oceanography, 48(4): 1674-1684.

Precht, E. and M. Huettel. 2004a. Rapid wave-driven advective pore water exchange in a permeable coastal sediment. Journal of Sea Research, 51(2): 93-107.

Precht, E. and M. Huettel. 2004b. Rapid wave-driven advective pore water exchange in a permeable coastal sediment. Journal of Sea Research, 51: 93-107.

Rabalais, N.N., E.R. Turner, and W.J. Wiseman Jr. 2002. Gulf of Mexico hypoxia, a.k.a. "The Dead Zone". Annu. Rev. Ecol. Syst., 33: 235-263.

Rama and W.S. Moore. 1996. Using the radium quartet for evaluating groundwater input and water exchange in salt marshes. Geochimica et Cosmochimica Acta, 60(23): 4645-4652.

Redfield, A.C. 1934. On the proportions of organic derivates in seawater and their relation to the composition of plankton. Woods Hole Oceanographic Institution. Contribution No. 30.

Reimers, C.E. et al. 2004. In situ measurements of advective solute transport in permeable shelf sands. Continental Shelf Research, 24: 183-201.

Riedl, R.J., N. Huang, and R. Machan. 1972. The subtidal pump: a mechanism of interstitial water exchange by wave action. Marine Biology, 13: 210-221.

Rii, Y.M. et al. 2008. The transient oasis: Nutrient-phytoplankton dynamics and particle export in Hawaiian lee cyclones. Deep Sea Research Part II: Topical Studies in Oceanography, 55(10-13): 1275-1290.

Rooney, J.J.B. and C.H. Fletcher. 2005. Shoreline change and Pacific climatic oscillations in Kihei, Maui, Hawaii. Journal of Coastal Research, 21(3): 535-547.

Rosenau, J.C. et al. 1977. Springs of Florida. Bulletin No. 31. USGS. Tallahassee, Florida. 466 pp.

Rusch, A. et al. 2006. Benthic oxygen consumption and organic matter turnover in organic-poor, permeable shelf sands. Aquatic Geochemistry, 12: 1-19.

Shum, K.T. 1993. The effects of wave-induced pore water circulation on the transport of reactive solutes below the rippled sediment bed. Journal of Geophysical Research, 98(C6): 10,289-10,301.

Slater, J. and D. Capone. 1987. Denitrification in aquifer soil and nearshore marine sediments influenced by groundwater nitrate. Applied and Environmental Microbiology, 53(6): 1292-1297.

Slomp, C.P. and F. Van Cappellen. 2004. Nutrient inputs to the coastal ocean through submarine groundwater discharge: controls and potential impact. Journal of Hydrology, 295: 64-86.

Smith, J.E. 2006. Algal blooms on Maui. A final report to the City and County of Maui and the Environmental Protection Agency. 75 pp.

Smith, J.E., C.L. Hunter, and C. Smith. 2002. Distribution and reproductive characteristics of nonindigenous and invasive marine algae in the Hawaiian Islands. Pacific Science, 56(3): 299 - 315.

Storlazzi, C.D. and B.E. Jaffe. 2003. Coastal circulation and sediment dynamics along West Maui, Hawaii. Part I: Long-term measurements of currents, temperature, salinity and turbidity off Kahana, West Maui: 2001-2003, USGS Open File Report 03-482.

Storlazzi, C.D. and B.E. Jaffe. 2008. The relative contribution of processes driving variability in flow, shear, and turbidity over a fringing coral reef: West Maui, Hawaii. Estuarine, Coastal and Shelf Science, 77: 549-564.

Street, J.H. et al. 2008. Submarine groundwater discharge and nutrient addition to the coastal zone and coral reefs of leeward Hawaii. Marine Chemistry, 109: 355-376.

Taniguchi, M. et al. 2002. Investigation of submarine groundwater discharge. Hydrological Processes, 16(11): 2115-2129.

Taniguchi, M. et al. 2003. Spatial and temporal distributions of submarine groundwater discharge rates obtained from various types of seepage meters at a site in the Northeastern Gulf of Mexico. Biogeochemistry, 66(35-53).

U.S. Census Bureau. 2000. http://www.census.gov/main/www/cen2000.html. Accessed April 2009.

Valiela, I. et al. 1990. Transport of groundwater-borne nutrients from watersheds and their effects on coastal waters. Biogeochemistry, 10: 177-197.

Valiela, I. et al. 1992. Couplings of watersheds and coastal waters: sources and consequences of nutrient enrichment in Waquoit Bay, Massachusetts. Estuaries, 15(4): 443-457.

Valiela, I. et al. 1997. Macroalgal blooms in shallow estuaries: Controls and ecophisiological and ecosystem consequences. Limnology and Oceanography, 42(5, part 2): 1105-1118.

Vitousek, S. 2007. Nearshore hydrodynamics at Kaanapali, Maui & Hawaii extreme wave statistics. Master's Thesis, University of Hawaii at Manoa, Honolulu, 60 pp.

Webster, I.T. 2003. Wave enhancement of diffusivities within surficial sediment. Environmental Fluid Dynamics, 3: 269-288.

Webster, I.T. et al. 1996. Solute exchange by convection within estuarine sediments. Estuarine, Coastal and Shelf Science, 42: 171-183.

Webster, I.T. and J.H. Taylor. 1992. Rotational dispersion in porous media due to fluctuating flows. Water Resources Research, 28(1): 109-119.

CHAPTER IV - PHYSICAL REGULATION OF LAND-OCEAN CNP FLUXES AND COASTAL ZONE METABOLISM

4.1 ABSTRACT

Land-ocean nutrient exchange along proximal coastal regions is highly dynamic and dependent on physical forces (e.g., wind, waves, tides) impinging on the coast. This study focuses on intensive physical and biogeochemical observations at two coastal sites in Maui, Hawaii with similar geomorphology, and wind and wave exposure. Time series data indicate wind speed imparts the greatest control on near-bottom water currents, whereas tide height actively modulates wave energy penetrating towards the shoreline. However, no significant correlations between wind speed and water currents were observable mainly due to the temporal variability of their interaction. Highest near-bottom water velocities were observed during periods of high wind and lowest tidal elevation. Analysis of spatiotemporal time-series data within our study basins suggest enhanced transport of nutrients from the shallow unconfined aquifer and porewater (via wave run-up at the beach face and the wind-induced currents along the rippled bottom) are responsible for observed nutrient enrichments in the coastal zone. We utilize a modified version of the LOICZ modeling approach to predict land-ocean conservative and non-conservative CNP fluxes and evaluate the net metabolic state of the coastal zone during various times of the year. Coastal water residence times predicted from salt, current meters, and isotopes of radium and radon show remarkable agreement and indicate that water residence times within our study basins range between 1 – 6 hours (on average), but can be highly variable throughout the day. Net ecosystem metabolism estimates from our modeling indicate that high temporal variability (i.e., on scale of hours) is evident within our study basins, and (on average) our coastal sites can shift between net autotrophic and net heterotrophic states during different periods of the year. Similarly, net calcification and net nitrogen cycling *(N_{fix} – N_{den})* can shift polarity on hourly to monthly timescales. We conclude that long, high frequency biogeochemical and physical oceanographic time-series measurements are needed in order to accurately describe the metabolic state and the seemingly chaotic natural complexity of land-ocean solute exchange within the proximal coastal zone.

Key words: coastal zone, net ecosystem metabolism, biogeochemistry, residence time, physics

4.2 INTRODUCTION

Two of the most fundamental properties of coral reefs are their diverse nutrition, and the fact that they thrive in well-lit warm, turbulent water (Bilger and Atkinson 1992; Atkinson and Bilger 1992; Hearn et al. 2001; Falter 2002; Atkinson and Falter 2003). The nutrition of coral reefs is tightly coupled to autochthonous sources, however, closer to land the origin of nutrients diversify, although closer to land the origin of nutrients diversifies. Close to land, nutrient sources for these nearshore coastal systems include both autochthonous and allochthonous (e.g. terrestrial sediment inputs, submarine groundwater discharge, dry deposition) materials, all of which help subsidize the metabolic requirements of these systems.

Physical energy impinging upon coral reefs (tides, waves, currents) generates water movement, enhancing the dynamic transport of essential nutrients (dissolved and particulate) across the benthic boundary layer (Atkinson and Bilger 1992), and between water column and other nutrient reservoirs such as sediments (Huettel et al. 1998; Falter and Sansone 2000a; Rusch and Huettel 2000; Huettel et al. 2003; Precht and Huettel 2004; Reimers et al. 2004; Wild et al. 2004b), reef framework cavities (Tribble et al. 1992; De Goeij et al. 2008), aquifers (Valiela et al 1980; Capone and Bautista 1985; Slater and Capone 1987; Pigott and Laughlin 1988; Capone and Slater 1990; Valiela et al. 1990; Valiela et al. 1997), and eroding coastlines (Rooney and Fletcher 2005). Moreover, the interaction between coastal geomorphology and tides (see Chapter 3), regional upwelling (Leichter and Miller 1999; Menge et al. 2003), and large-scale eddies (Firing and Merrifield 2004; Rii et al. 2008), all can exert significant effects on nutrient dynamics within the coastal zone.

The exchange of fluids between sediment and water column has been linked to physical forces such as wave activity (Webb and Theodor 1968; Li 1999; Falter and Sansone 2000a; Webster 2003), turbulence induced by diurnal wind patterns (Oldham and Lavery 1999), bottom currents

(Huettel and Gust 1992; Huettel et al. 2003; Precht and Huettel 2004), and aquifer recharge rates (Capone and Slater 1990). In theory (Webster et al. 1996; Boudreau 2000; Webster 2003) and in laboratory and flume experiments (Huettel et al. 1996; Huettel et al.1998; Huettel and Webster 2001; Huettel et al. 2003) it has been shown that physical forces acting on permeable sediments (typical of coral reefs) can significantly affect solute exchange rates and sedimentary catabolic processes (Rusch et al. 2006). For example, waves propagating through these systems can induce pressure gradients at the sediment surface, generating flow of fluids through the sediment pores (Webster and Taylor 1992; Precht and Huettel 2003; Webster 2003; Precht and Huettel 2004). Also, waves and diurnal fluctuations in wind stress can generate oscillating currents that interact with rippled sand beds or an otherwise rough bottom, resulting in an active flow of water-column fluids through the bed (Huettel et al. 1998; Huettel et al. 2003), re-suspension of bottom sediments (Storlazzi et al. 2004), and translocation of pore fluids (Herzfeld et al. 2006). Therefore, highly energetic conditions (e.g., high waves/wind) are expected to enhance flushing of sub-oxic sediment porefluids into the water column.

Although the processes that enhance exchange within permeable coastal margins have been studied extensively in the recent past (Van Der Loeff 1981; Van Der Loeff et al. 1981; Moore 2000a; Moore 2000b; Huettel and Webster 2001; Precht and Huettel 2003; Webster 2003; Precht and Huettel 2004; Reimers et al. 2004; Wild et al. 2004a; Wild et al. 2004b; Hebert et al. 2007), gaps exist in our knowledge of the synergistic interaction between physics on land-ocean solute exchange and coastal zone metabolism over short time scales. Especially lacking are studies that evaluate the short-term variability of nutrient concentrations and the sources and forces that shape their distribution within coastal margins with permeable sediments. In this study we explore land-ocean carbon, nitrogen, and phosphorus (CNP) exchange and net metabolism under variable

physical forcing. Given that the role of physical forces on coastal zone circulation and biogeochemistry is still imperfectly understood (Crossland et al. 2005), we couple a modified version of the Land-Ocean Interactions in the Coastal Zone (LOICZ) modeling approach (Gordon et al. 1996) with multiple concurrent estimates of water residence time to more accurately account for the effects of physical forces on land-ocean CNP exchange and net metabolism over different time scales ranging from a few (3) hours to months.

4.3 STUDY SITE BACKGROUND

Studies were performed at Waipuilani Beach Park (WAI), Kihei, Maui, USA (20° 45′ 21.24″ N, 156° 27′ 34.40″ W), between Koieie fishpond and Kawililipoa an area experiencing year-round chronic macroalgal blooms (Smith and Smith 2006), and at Ukumehame Beach Park (UKU), West Maui, Maui (20° 40’ 13” N, 156° 35’ 17” W), an area generally devoid of chronic blooms (Figure 4.1). Detailed descriptions for these sites are provided in Chapter 3.. Briefly, Kihei is a community of approximately 17,000 people (U.S. Census Bureau 2000) whose livelihood depends on the tourism industry. Most of the land within the city limits is urbanized with several golf courses and beach parks as open spaces. Local wind and rainfall are greatly affected by Haleakala volcano and the West Maui Mountains (Giambelluca et al. 1986). At Kihei, the Haleakala volcano impedes the transfer of humidity from the trade winds to the area (median rainfall = 38 cm/yr) and significant rainfall only occurs when the region experiences southern storms (Laws et al. 2004; Hunt 2006). Similarly, UKU is located within a low precipitation (median rainfall = 37.6 cm/yr) region in the lee of the West Maui Mountains. At both sites, streams (gulches) are dry for most of the year and only flow during storm events. Stream-flow during storms is high and tends to carry large quantities of particulate matter to the coastal zone.

Land use within the UKU and WAI watersheds is drastically different. Watersheds surrounding UKU were under sugar cane cultivation for several decades, but since the mid 1990's they have remained uncultivated and undeveloped. On the other hand, since the 1970's the land cover and hydrology of watersheds surrounding WAI have been largely developed since the introduction of a pipe carrying water from West Maui, across Kihei, to the town of Wailea (Figure 4.1) (Kobayashi et al. 1970).

From 1900 to 1997 the coastline in the Kihei study region has either receded or prograded almost 100 m (Rooney and Fletcher 2005). Current erosion rates along the WAI study site are estimated to average 39.6 cm/yr ("moderately rapid"), and between 30.5 – 122 cm/yr at UKU (Fletcher et al. 2001-2003). Changes in the shoreline are believed to be caused by a combination of factors including sea-level rise, direct anthropogenic changes to the coastal margins (i.e. construction of seawalls), and modulation of Kona storms by the Pacific Decadal Oscillations (Rooney and Fletcher 2005).

The shallow marine environment of the North Kihei region has been known to local communities and ancient Hawaiians for its elevated macroalgal and fish abundance (personal communication with local residents). However, hydrologic alterations, land change, intense agriculture, poor wastewater disposal practices, and increased coastal erosion have led to the nutrient enrichment of groundwater and coastal waters along the Kihei region (Dollar and Andrews 1997; Fletcher et al. 2001-2003; Laws et al. 2004; Hunt 2006; Smith 2006; Dailer et al. 2010; Chapter 3), resulting in the chronic occurrence of high biomass build-up of red (*Hypnea musciformis*) and green (*Ulva fasciata*) nuisance macroalgae along its shores. Potential economic benefits to this community have been estimated to reach $30 million per year if nutrient loads were to be reduced (Cesar et al. 2002; Van Beukering and Cesar 2004).

4.4 MATERIALS AND METHODS

The coastal regions along WAI and UKU were selected for this study because of their similar coastal geomorphology (i.e., a shallow shelf extends from shore to approximately 500 m offshore) (Figure 4.1), but different population densities along the coastal zone. This enables an examination of anthropogenic effects on coastal zone nutrient fluxes and net metabolic state. Description of the experimental design, sample collection, and chemical, physical, and statistical data analyses follow.

4.4.1 Experimental design

Four sampling stations were established along shore-normal transects at both WAI and UKU (Figure 4.1). One station was located at the mean lowest low tide line (station A), the second station (station B) was located ~50 m offshore from station A, and the other two stations were located 300 m and 500 m (stations C and D, respectively) offshore from station A. Sediment interstitial water sampling wells were only installed at stations A and B using a modified version of Falter and Sansone's (2000b) design. Briefly, two wells were constructed of ¼ " SCH80 PVC pipes with small openings drilled at either 7 or 25 cm depth, respectively. Wells were fitted with barbed connectors that connected to narrow bore Tygon® tubing. Tubing ended with a three-way stopcock for easy of sampling with a Luer-lock sampling syringe. Sampling volume (including dead volume and syringe pre-rinsing volume) did not exceed 250 mL. Assuming mean sediment porosity of 0.45 (Chapters 2 and 3), the extracted sediment interstitial water originated from a sphere 5 cm in radius around each sampling depth.

4.4.2 Sample collection and analysis

4.4.2.1 Dissolved nutrients, carbonate chemistry, and salinity

Discrete water samples were collected across the WAI shelf every 3-h during June 2005, January 2006, February 2006, and March 2007, and at UKU during March 2007 only. Discrete water column and porewater samples were collected and split in the following manner: 50 mL for

dissolved nutrient analysis (PO_4, Si, NO_3, NO_2, and NH_4), 20 mL for dissolved inorganic carbon (DIC) and total alkalinity (TA) analysis, and 20 mL for salinity analysis. Approximately 20 mL was used to triple rinse sample bottles prior to sample collection. Water samples for nutrient analysis and DIC/TA were filtered through pre-combusted GF/F glass fiber filters into HCl-cleaned 60-mL plastic bottles and pre-combusted 20-mL glass scintillation vials, respectively. Salinity samples were stored unfiltered in 30-mL plastic bottles until analysis. Dissolved nutrients were kept frozen until analysis (Dore et al. 1996). Fifty microliters (50 μL) of saturated $HgCl_2$ was added to each DIC/TA sample. Samples for DIC/TA were kept stored in the dark at room temperature until analysis.

Dissolved inorganic nutrients (PO_4, Si, NO_3, NO_2, and NH_4) were analyzed colorimetrically using standard methods (Gordon et al. 1993) at the University of Washington Oceanography Technical Services (K.A. Krogslund). Dissolved inorganic carbon (DIC) and total alkalinity (TA) were analyzed via carbon coulometry (UIC Coulometrics) with an average accuracy of 0.73 μmol/kg, and via potentiometric Gran titration (Almgren et al. 1983) with an average accuracy of 0.62 μmol/kg. Both DIC and TA samples were checked for accuracy against certified reference material (CRM) obtained from Andrew Dickson at Scripps Institution of Oceanography (Dickson 2001). Other carbonate system parameters (pCO_2 , and calcite and aragonite saturation state (Ω)) were calculated using CO2SYS for Matlab (Lewis and Wallace 1998) and DIC and TA data. We used the constants of Mehrbach et al. (1973) as refit by Dickson and Millero (1987), K_{SO4} from Dickson (1990), and pH on the NBS scale to parameterize the CO2SYS code.

4.4.2.2 Radium isotopes

Samples for radium isotope analysis were collected at our study sites using two different approaches. The first approach consisted of collecting 100 L of near-shore (station A) surface water

every 3 h for 1 day. Collected water was immediately filtered through a Mn-coated acrylic fiber (~1 L/min) in order to adsorb dissolved radium isotopes (Moore 1976). After filtration, Mn-fibers were hand-squeezed firmly and placed inside individual plastic bags. The second approach consisted of 24-hour near-bottom equilibrations of Mn-coated fibers deployed across our sampling stations (Figure 4.1). Immediately after the termination of the experiments, fibers were next-day air-shipped to Woods Hole Oceanographic Institution, Massachusetts, USA for analysis of short- (^{223}Ra and ^{224}Ra) and long-lived (^{226}Ra and ^{228}Ra) radium isotopes using delayed-coincidence counters (Rama and Moore 1996; Moore and Arnold 1996; Moore 2008) and gamma spectroscopy.

4.4.2.3 Continuous radon measurements

Surface-water dissolved radon (^{222}Rn) concentrations were monitored during March 2007 observational periods at both WAI and UKU using a method identical to that described by Burnett and Dulaiova (2003). Briefly, surface water from station A was transferred to the beach (via a submersible pump) and the water stream run through an air-water exchanger that distributed radon from the running flow of water to a closed air loop. The air stream was then fed to a commercially available radon-in-air monitoring system (RAD7, Durridge Co. Inc., Billerica, and Massachusetts, USA) that determines the concentration of ^{222}Rn by collection and measurement of the α-emitting daughters, ^{214}Po and ^{218}Po. Since the distribution of radon at equilibrium between the air and water phases is governed by well-known temperature dependence, the radon concentration in the water is easily calculated. The ^{218}Po window in the RAD7 was utilized for Rn assessment, resulting in data collection every 30 minutes. Surface water dissolved ^{222}Rn concentrations were utilized to estimate total groundwater discharge (V_G) after appropriate corrections for tidal and wind-induced gas losses were applied (see section 4.4.3.2).

4.4.2.4 Physical oceanographic measurements

Near-continuous physico-chemical data were collected during most observational periods. Table AC1 summarizes specific locations of data collection during all observation periods. Salinity, temperature, dissolved oxygen (DO), pH, and chlorophyll a (fluorescence) data were collected using an YSI multi-parameter data sonde (YSI Incorporated, Ohio, USA) logging data at 10-minute intervals deployed 0.25 m above the seafloor at stations B and C.

Oceanic and atmospheric physical conditions during our sampling periods were monitored by a cross-shore array of Nortek Aquadopp (Nortek AS, Norway) current meters collecting near-bottom (0.58 m above the sediment-water interface) water velocity data every 5 seconds, and a wind meter station (vane and anemometer) located on top of the Sugar Beach Resort Maui (20º 47' 05.80" N, 156º 28' 02.20" W) maintained by Weather Flow Inc. that collects wind data every 5 minutes. Current meters were also utilized to collect data for calculation of hourly surface wave conditions. Hourly wave height and wave period data were calculated using the zero-crossing technique coded using Matlab (MathWorks, Natick, Massachusetts, USA), and the mean-detrended Aquadopp pressure measurements collected at 1Hz for 20 min every hour.

4.4.2.5 Photosynthetically active radiation (PAR)

Near-bottom PAR data were collected in situ during all sampling periods at 5-min intervals using a LiCOR® LI-193 Spherical Quantum Sensor (LiCOR Environmental, Lincoln, Nebraska USA) capable of measuring the photon flux from all directions (i.e., quantum scalar irradiance). PAR sensors were connected to a LiCOR® Li-1400 Data Logger housed inside water-proof pressure housing that was anchored to the seafloor. We report the quantum scalar irradiance measured by our sensors as µmol quanta m^{-2} s^{-1}.

4.4.2.6 In-situ algal nutrient uptake data

In-situ macroalgal growth experiments were performed during the June 2005, January 2006, and March 2007 observational periods at WAI and during March 2007 at UKU. These experiments provided an estimate of cross-shelf nutrient uptake rates by the two dominant algal species in the region: *Hypnea musciformis* (HYP) and *Ulva fasciata* (ULV). Dominance of HYP and ULV suggest these two algal species have a clear ability to out-compete other algae for resources (i.e., they exhibit the highest expected nutrient uptake rates).

The growth rates were determined by measuring the wet weight gain of field-incubated, caged, algal fragments after a known period of time (usually between 48 and 72 h). Algal cages consisted of ~500 cm^3 wire cubes covered with moderately coarse green nylon mesh (Figure 4.2). Replicate caged algal fragments were deployed along shore-normal transect at each site (Smith and Smith 2006).

Fresh-to-dry algal mass ratios obtained during March 2007 experiments were used to predict dry mass production from the fresh mass data for the other two observational periods (June 2005 and January 2006). Dry algal sub-samples from June 2005 and January 2006 experiments were pulverized and analyzed for tissue carbon and nitrogen content (%) and stable isotope composition (^{15}N and ^{13}C) using a Carlo Erba NC2500 Elemental Analyzer (CE Elantech, Inc., Lakewood, New Jersey , USA) and a Finnigan MAT ConFloII (Finnigan MAT, Bremen, Germany) system at the Stable Isotope Laboratory, University of Hawaii Manoa. Tissue phosphorus content was determined colorimetrically from digestates (Aspila et al. 1976) using a Perkin-Elmer (Waltham, Massachusetts, USA) 6500 ICP spectrophotometer (University of Hawaii Analytical Services). Tissue molar C: N: P ratios in combination with growth rates were utilized to predict algal molar C, N, and P uptake rates. Results from the June 2005, and January 2006 algal growth measurements have been reported elsewhere (Smith and Smith 2006; Umezawa et al. 2008). In this paper we

summarize the results from the previously published studies, and report for the first time the results from the March 2007 measurements made at Waipuilani and Ukumehame.

4.4.2.7 Ocean-atmosphere CO_2 fluxes

The time-variant carbon dioxide flux across the air-sea interface can be determined as:

$$F = k \times s \times \rho \times (pCO_{2w} - pCO_{2a}) \qquad \text{(EQ. 4.1)}$$

where the flux (F, mol C $m^{-2}yr^{-1}$) is a function of the gas transfer velocity (k, m/yr), the gas solubility (s, mol kg^{-1} atm^{-1}), the water density (ρ, kg m^{-3}), and the difference between atmospheric and ocean gas partial pressure (pCO_2, atm) (Millero and Sohn 1992). Surface water pCO_2 (pCO_{2w}) during each time step was calculated from TA and DIC data as previously described (see section 4.3.2.1). Atmospheric CO_2 mole fractions (in dry air) during the individual observational periods obtained from the monthly record at Mauna Loa Observatory (www.esrl.noaa.gov/gmd/ccgg/trends/co2_data_mlo.html, accessed 1/15/2008) were utilized for pCO_{2a} in the flux calculations (June 2005: 379.5 µatm ; January and February 2006: 381.5 µatm ; March 2007: 382.9 µatm).

It has been widely noted that k is a function of wind speed; in our flux calculations we estimate k from wind speed as described by Liss and Merlivat (1986), Wanninkhof (1992), Wanninkhof and McGillis (1999), Nightingale, et al. (2000a), and Nightingale, et al. (2000b). Although it has been shown that the effects of temperature on gas solubility and the Schmidt number (and therefore k) nearly balance each other, we use the exact approximations as recommended by Wanninkhof (1992, his Tables A1 and A2). We estimate CO_2 fluxes using all five k parameterizations and report the mean flux at both stations A and B. Furthermore, we report the mean ocean-atmosphere gas flux for the innermost 50 m of the coastal zone during each observational period as the mean of the gas flux estimates for stations A and B. Positive fluxes denote net ocean-to-air gas transport.

4.4.3 Budgeting approach

Budgetary calculations followed a similar approach to that described by the LOICZ program (Gordon et al. 1996), utilizing water, salt, and non-conservative (nutrient) fluxes to understand net metabolic processes (i.e., carbon, phosphorus, and nitrogen cycling) within the coastal zone. The LOICZ modeling approach was originally designed for use in hydrodynamically simple settings over relatively long timescales (week to months). We utilize a modified version of the LOICZ approach to describe land-ocean exchange variability over short timescales (hours) in a complex hydrodynamic setting. In this study we evaluate the accuracy of LOICZ salt-based water residence time estimates by comparing them to various other field-based estimates of water residence time. We utilize shelf-wide averages of dissolved constituents within the water column and time-variant mean water residence times to correct for non-conservative nutrient fluxes under changing coastal water circulation conditions. A detailed description of our time-variant budgeting approach follows.

4.4.3.1 Model boundaries

Determination of a suitable model boundary for the open systems observed in this study is a difficult task given that water reaching the center of the modeled basin can originate from seemingly open boundaries (Figure 4.1), and that water residence times are dependent on physical factors that affect current speeds within the basin. Although current speeds can be highly variable, if we consider previous physical oceanographic studies along the Maui coastal zone (Table 3.3), it is apparent that typical current speeds are, on average, 0.15 m/s. Using this mean current speed, and under our 3-hr sampling scheme, we expect the water chemistry measured at our stations to originate from an area approximately 750 m in radius (i.e., half the mean travel distance of coastal water during a 3-h period). We note that a previous study by Storlazzi et al. (2006) indicated that a turbidity front located near the reef slope/crest transition separates less saline, more turbid inshore

water from saltier, less turbid offshore water. Such fronts appear to result from increased turbulence and sediment re-suspension induced by wind, wave, and tidal energy focusing along the inner shelf (Storlazzi et al 2006). We then, using the mean current speed and evidence from distinct water chemistry fronts estimates, choose the least of the two (i.e., 500 m) to set the boundaries of our budgetary approach as the area bounded by a box 100 m alongshore and 500 m across-shore, believing it to be appropriate for determining coastal processes at our study sites.

4.4.3.2 Water and salt budgets

The LOICZ approach (Gordon et al. 1996) makes use of mass conservation to account for the transfer of solutes from one compartment (land or ocean) to the coastal zone. A general schematic of the approach is shown in Figure 4.3. Briefly, the coastal zone can be represented as a system (box) that receives/delivers inputs/outputs to the surroundings. The approach first establishes a water budget and then a salt budget (Figure 4.3). Thus, utilizing the continuity equation for our coastal basin, time-variant changes in the water budget for our coastal basin can be described by the summation of inputs minus outputs during a specified period of time as

$$\Delta V_{SYST} = \sum inputs - \sum outputs \quad \text{(EQ. 4.2)}$$

where ΔV_{SYST} represents the change in water volume within the basin over a specific period of time. The right-hand-side (RHS) of equation 4.2 can be further expanded as

$$\Delta V_{SYST} = (V_P + V_G + V_Q + V_{OTHER}) - (V_E + V_R) \quad \text{(EQ. 4.3)}$$

Given that there was no precipitation (V_P), stream discharge (V_Q), or any other direct discharge (V_{OTHER}) (e.g., wastewater discharge) to our basin, we assume these to be zero in our water budget. Moreover, due to the short time interval between observations, and the rapid fluctuation of tides within the basin, we assume evaporation (V_E) to be a negligible component of our water budget. Therefore, the water inventory within our basin is the direct result of residual oceanic (V_R) and fresh

groundwater (V_G) inputs. We estimate water depth at every time interval (h_i) using pressure sensors in our current meters and quantify the change in total basin water volume between any two time intervals ($\Delta V_{SYST\,i}$) by multiplying the basin area (Area = A_{SYST} = 100 m x 500 m) by the change in water depth. Furthermore, if we assume that the gain or loss of water from our basin is predominantly due to oceanic tidal flows, we can temporarily ignore the effects of V_G on ΔV_{SYST}, allowing us to calculate V_R.

The next step in the LOICZ budgeting approach is to generate a salt budget (Figure 4.3). Using our salt concentrations measured during the observation periods, we calculate the fractional contribution (i.e., the fractions of fresh and salt water in the mixture assuming conservative mixing) of oceanic and fresh water (f_o and f_f) to the surface waters in our study basins at each time step (i) as

$$f_{f\,i} = (S_{SYST\,i} - S_O)/(S_G - S_O) \quad \text{(EQ. 4.4)}$$

$$f_{o\,i} = 1 - f_{f\,i} \quad \text{(EQ. 4.5)}$$

where $S_{SYST\,i}$ is the mean basin surface water salinity at time i, S_O is the mean ocean salinity, and S_G is the mean fresh groundwater salinity. We then predict the respective fresh (V_G) and oceanic (V_O) water volumes as

$$V_{G\,i} = (A \times h_i) \times f_{f\,i} = V_{SYST\,i} \quad \text{(EQ. 4.6)}$$

$$V_{O\,i} = V_{SYST\,i} \times f_{o\,i} \quad \text{(EQ. 4.7)}$$

where $V_{G\,i}$ and $V_{O\,i}$ are the fresh and oceanic water volumes, respectively, at time i; A is the basin area; and h_i is the average water depth within the basin at time i. It follows then that the change in salt within the basin between any two sampling periods can be estimated from the balance between residual flows, groundwater inputs, and mixing (Vx) as,

$$\Delta V_{SYST} S_{SYST} = V_R(S_O + S_{SYST})/2 + V_G S_G + V_X(S_{SYST} - S_O) \quad \text{(EQ. 4.8)}$$

Given that V_R can be calculated from the water budget as the water lost or gained between time steps, and all other terms in EQ 4.8 are known, it is then algebraically simple to solve for V_X. We use our estimates of residual flow (V_R) and mixing (V_X) to estimate the apparent water residence time (aRT_{salt}) within our basin (Gordon et al. 1996) as

$$aRT_{salt} = (V_{SYST})_i / (V_R + V_X) \quad \text{(EQ. 4.9)}$$

where V_R and V_X are in units of volume/time.

4.4.3.3 Stoichiometricaly linked non-conservative CNP fluxes

Nutrient fluxes entering the coastal zone can mix both conservatively and non-conservatively. In order to understand the time-variant non-conservative (i.e., excess) CNP mass flux to the coastal zone, we first estimate the expected mass contribution of any solute *X* from fresh groundwater and oceanic sources using linear models

$$X_{Gi} = V_{G\,i} \; x \; X_G \quad \text{(EQ. 4.10)}$$

$$X_{O\,i} = V_{O\,i} \; x \; X_O \quad \text{(EQ. 4.11)}$$

where $X_{G\,i}$ and $X_{O\,i}$ are the molar masses of solute *X* originating from fresh groundwater and oceanic sources, respectively. X_G and X_O are the mean solute *X* concentrations (mol/L) in groundwater in the shallow unconfined aquifer and ocean, respectively. Multiplying the mean basin concentrations ($[X_{basin}]_i$) by the basin volume yields the molar mass within the basin (X_{basin}) at time *i*. We can then predict the excess of solute X (difference from observed) inventories at time *i* as

$$X_{basin} = [X_{basin}]_i \; x \; V_{SYST\,i} \quad \text{(EQ. 4.12)}$$

$$X_{excess} = X_{basin} - (X_{Gi} + X_{Oi}) \quad \text{(EQ. 4.13)}$$

Changes in excess inventories of X between observations can be predicted from (1) non-conservative processes affecting this solute within our study basin, and (2) the average water residence time between time-steps

$$\Delta X = ((X_{excess\ i+3} - X_{excess\ i}) \times 3)/[(aRT_i + aRT_{i+3})/2] \quad \text{(EQ. 4.14)}$$

where X can represent moles of DIC, DIN (NO_3+NO_2+NH_4), or PO_4, and aRT (in *hours*) represents the mean apparent water residence time as estimated from salt or other tracers (see below). Normalizing the time elapsed between measurements (3 h) by the average aRT between measurements serves to scale the mass transfer. For example, if we know the water residence time is 0.5 hours, then during the 3 hour period between measurements there was 6 times (i.e., 3/0.5) as much material transfer.

4.4.5 Current- and radioisotope-based apparent water residence time (aRT) estimates

Salt-based estimates of the apparent water residence time within our study basin were calculated following the LOICZ approach as discussed above (see section 4.3.3.2). However, multiple tracers can help us to better constrain water residence times. In this section we elaborate on the utilization of current measurements, and radium and radon radioisotopic data to estimate water residence times within our study basin.

4.4.5.1 Current-based apparent water residence time estimates (aRT_{curr})

Current meter data from multiple deployments across the study basins were utilized to estimate water residence time. We estimate water residence time as the time it would take a parcel of water traveling at mean $speed_i$ to travel through our study boundaries

$$aRT_{curr} = 500/(average\ speed_i) \quad \text{(EQ. 4.15)}$$

where $speed_i$ is the 3-hr average water velocity observed prior to each discrete water sample collection.

4.4.5.2 Radium-based apparent water residence time estimates (aRT_{Ra})

Naturally occuring radium isotopes can be used as tracers of coastal flushing rates (Moore 2000b; Dulaiova and Burnett 2007; Paytan et al. 2006). These flushing rates can be used to

estimate the residence time of other groundwater derived components, such as nutrients, in the near-shore region. Saline SGD is a source of radium isotopes and once the radium isotopes enter the surface water and their activities are no longer supported by their parent nuclides residing in the sediments, they decay according to their specific decay constants. Apparent radium ages (i.e., the age of a water mass based on the radium isotopic ratio) may be calculated using the ratio of the activity of a short-lived radium isotope (e.g., ^{224}Ra half-life = 3.6 days) to that of a longer-lived one (e.g., ^{226}Ra half-life = 1600 years) given that, as the water mass moves away from its source and ages, ^{224}Ra decays faster than ^{226}Ra, resulting in changing ratios. Uniform ratios across a shelf can be interpreted as reflecting rapid water transport (i.e., transport is faster than decay), whereas rapidly changing ratios across a shelf can be interpreted as slower advection. We can calculate the apparent water age (after Dulaiova and Burnett 2007) as

$$aRT_{Ra} = \ln \frac{\left[\frac{^{224}Ra}{^{226}Ra}\right]_s}{\left[\frac{^{224}Ra}{^{226}Ra}\right]_{obs}} * \frac{1}{\lambda_{224} - \lambda_{226}} \quad , \qquad \text{(EQ. 4.16)}$$

where λ_{224} (0.1893 day^{-1}) and λ_{226} (1.19 x 10^{-6} day^{-1}) are the decay rate constants for ^{224}Ra and ^{226}Ra, respectively.

4.4.5.3 ^{222}Radon-based apparent water residence time estimates (aRT_{Rn})

Groundwater advection rates (V_G) calculated using continuous Rn measurements (see section 4.4.2.3) were used to solve the continuity equation and to calculate V_R. We use V_X as previously determined in the salt balance and the Rn-based V_R estimates to calculate the apparent water residence times within the basin using EQ. 4.9.

4.4.6 Land-ocean CNP fluxes

Calculated excess solute mass within the basin (see section 4.4.3.3) is not only a function of inputs and outputs, but also a result of biogeochemical transformations occurring within the system. Therefore, we must modify EQ. 4.3 accordingly in order to account for any losses or gains within the system due to non-conservative processes. We estimate all major carbon sinks and sources within our basin using geochemical data collected or modeled from our observations, and then stoichiometrically link these estimates to N and P flux estimates for each of the observational periods.

Various processes are considered to control dissolved inorganic carbon in a water body. Non-conservative fluxes for carbon that are considered to contribute to deviations (i.e., excess) from that expected from simple mixing between two water masses can be summarized as

$$\Delta DIC_{excess} = \Delta DIC_{org} + \Delta DIC_{calc} + \Delta DIC_{gas} + \Delta DIC_{sed} \quad \text{(EQ. 4.17)}$$

where *org*, *calc*, *gas*, and *sed* subscripts denote DIC release/removal originating from production of organic matter by primary producers (i.e., macroalgae), calcification, air-sea gas exchange, and sediment porewater, respectively. We directly estimate the *excess (i.e., excess from expected from conservative mixing)*, *org*, *calc*, and *gas* contributions and compute the ΔDIC_{sed} contribution by difference. We calculate ΔDIC_{org} as

$$\Delta DIC_{org} = \Delta DIP_{excess} \; x \; (C:P)_{macroalgae} \quad \text{(EQ. 4.18)}$$

where $(C:P)_{macroalgae}$ is the weighted average C:P molar nutrient uptake ratio of macroalgae as observed during June 2005 and January 2006 observation periods (assuming 1:1 contributions of both algal species sampled, see below).

Carbonate shelves dominate along our study sites; therefore calcification is considered a potentially important process affecting non-conservative excess DIC. We estimate the change in DIC_{calc} via the alkalinity anomaly technique, which exploits the fact that surface water alkalinity is

the net result of calcification and dissolution processes acting within a basin (Smith and Key 1975; Kinsey 1978; Chisholm and Gatusso 1991). This technique is based upon the stoichiometry of calcium carbonate precipitation.

$$Ca^{2+} + 2HCO_3^- \rightarrow CaCO_3 + H_2O + CO_2 \quad \text{(EQ. 4.19)}$$

Defining carbonate alkalinity (*TA*) and total dissolved inorganic carbon (*TDIC*) as (DOE 1994)

$$TA = HCO_3^- + 2CO_3^{2-} \quad \text{(EQ. 4.20)}$$

$$TDIC = CO_2^* + HCO_3^- + CO_3^{2-} \quad \text{(EQ. 4.21)}$$

it follows that for every molecule of $CaCO_3$ precipitated, two moles of *TA* and one mole of *DIC* are removed. Therefore, changes in DIC due to calcification can be estimated as half the change in *TA* between time steps (corrected for water residence time) as

$$\Delta DIC_{calc} = ((ExcessTA_{i+3} - ExcessTA_i) \times 3/((aRT_i + aRT_{i+3})/2) \quad \text{(EQ. 4.22)}$$

Uptake and release of CO_2 gas by the coastal ocean can also impact DIC within the basin. Inputs/outputs of CO_2 to the basin during time *i* (ΔDIC_{gas}) were estimated using CO_2 flux results from our wind-induced gas transfer coefficient parameterizations (see above). We calculate ΔDIC_{gas} as

$$\Delta DIC_{gas} = -A \times t \times (CO_{2\ flux\ i} + CO_{2\ flux\ i+3})/2 \quad \text{(EQ. 4.23)}$$

where *A* is the basin area (m^2), *t* is the time interval between measurements (in years), and the negative sign is a sign adjustment so that a positive ΔDIC_{gas} flux indicates a net CO_2 flux into the basin.

4.5 RESULTS AND DISCUSSION

Multiple field expeditions to WAI and UKU resulted in ample records of the physical and geochemical conditions within our study basins during the observation periods. Data gathered from the atmosphere, unconfined aquifers, the nearshore water column, and sediment interstices are

summarized in Tables 4.1 to 4.9. We present detailed descriptions of the physical, chemical, and biological parameters measured during all of the observation periods in order to provide insight into the processes that control land-ocean CNP fluxes and coastal zone net metabolism.

4.5.1 General water current regime during the observation periods

Mean near-bottom current speed, direction, and principal axes of variability during all of our observation periods are shown in Figure 4.4. Average current speeds remained near or below 5 cm/s during all observation periods and mean flow was across-shore. Water current variability at WAI was greatest at station C (~ 300 m offshore). The large variability in water current observed at station D during January 2006 is thought to be the result of the placement of the current meter on a sand bed at the end of a reef groove, with the meter recording an intensified flow within the groove, advecting back and forth with incoming waves and tides, with negligible net water movement. Variability of water current at UKU was of similar magnitude as observed at WAI, but lower mean flow (3.5 cm/s) was observed across the shelf (Tables 4.1 and 4.8).

From the observed water current velocities it is possible to estimate the apparent distance traveled by a water particle between discrete water column chemical measurements (Table 4.10). From such results it is apparent that within 3 hours water masses travel ~500 m in a south-southwest direction across the shelf at WAI, and ~400 m in a south-southwest direction across the shelf at UKU. The apparent travel distance of water parcels approximates the spatial scales of our water budget model boundaries, suggesting that independent samples were obtained by our discrete, 3-hr sampling intervals.

4.5.2 Spatiotemporal variability of physico-chemical parameters

Figures 4.5 to 4.24 show the continuous and discrete time-series data obtained during all observation periods. It is readily apparent from these time-series plots that physical forcing and

surface water geochemistry were variable (i.e., min (max) wind speed (0.0 (15.6) m/s), surface currents (3.5 (17) cm/s), dissolved nutrient concentrations (DIP: 0.04 (0.38); DIN: 0.00 (24.13); Si: 0.54 (79.72) µM) during most observation periods. In order to understand the interaction between wind and tides and their effect on water chemistry, we planned sampling expeditions during distinct tidal phases hoping to capture their interaction, given that early afternoon wind intensifications are typical in this region (see site descriptions). We, in fact, we were able to couple (June 2005) and decouple (January 2006) the wind and tidal forces as initially planned (Figures 4.5 and 4.9). However, the passage of a high pressure system during our February 2006 observation period (Figure 4.9) resulted in an unanticipated wind shift, which resulted in an unanticipated opportunity to observe physical interactions between tide height and wind speed within the coastal zone. During our fourth observation period (March 2007) tidal forces, again, fluctuated, but the wind remained fairly constant from the south as a result of the passage of a low pressure weather system, resulting (again) in unanticipated observation of physical interactions in the coastal zone at WAI. We were also able to perform measurements at UKU during March 2007 under what seemed to be typical (i.e., winds between 0 – 10 m/s; significant wave height between 0 – 50 cm; personal observation) conditions at this site. We used this unique set of nearshore time-series observations to gain a better understanding of the physical context in which the coastal zone geochemical measurements were made, and to parameterize gas transfer coefficients and flux calculations used to calculate water residence times.

4.5.2.1 Waipuilani Beach Park (WAI)

4.5.2.1.a June 2005

Peak tidal and wind forcing during June 2005 coincided, and surface water currents responded to northeasterly wind-forcing by flowing towards the southwest (Figures 4.5 to 4.7). Positive modulation of wave height by tidal elevation observed during this period (i.e., observed covariance

between tide height and wave height in Figure 4.5) indicates that the reef crest may actively regulate the penetration of wave energy into the shallow shelf region during mid-to-low tide.

Surprisingly, large water-column salinity depressions co-varied with wind, tide, current velocity, and wave height (Figure 4.5), suggesting that either active freshwater advection occurs opposite to any expected hydraulic gradient, or physical factors (e.g., wave run-up, tidal pumping, oscillatory flows acting on the seabed) are enhancing the discharge of fresh/brackish submarine groundwater to the coastal zone (Webb and Theodor 1968; Shum 1993; Huettel et al. 1998; Li et al. 1999; Falter and Sansone 2000a; Huettel and Webster 2001; Webster 2003). However, there is also temporal variability in the salinity data that seems to be unrelated to any observed physical forcing (Figure 4.5).

Surface water salinity depressions (Figure 4.5) observed during rising/highest high tides were associated with high nutrient concentrations (Figure 4.6) during this observation period. Analysis of dissolved nutrient ratios within the water column indicates that nutrient dynamics result from the transport of different nutrient pools (i.e., groundwater, sediment porewater, the offshore ocean). For example, surface water dissolved inorganic nitrogen (DIN) to dissolved inorganic phosphorus (DIP) ratios (DIN:DIP) fluctuated from ca. mean WAI well groundwater values (~45, Table 4.9) during high tide, to near-oceanic values (~16, Redfield 1934) during low tide (Figure 4.6). Although, in general, temperature, pH, and DO all followed diel patterns (Figure 4.5), pH and DO experienced rapid decreases during surface water salinity depression events. Anomalous observations and their co-occurrence with nutrient pulses suggest fresh/brackish, suboxic, lower pH groundwater is entering the coastal zone at this site.

Nearshore surface water DIC and TA were higher than typical offshore values during most of the observation period (Figure 4.7, Table 4.3). Slight depressions in DIC, TA, and pCO_2 were

observed during peak solar insolation (Figure 4.7), presumably due to uptake by primary producers and light-enhanced calcification (Chalker and Taylor 1978; Moya et al. 2006), whereas lowest $\Omega_{aragonite}$, and $\Omega_{calcite}$ were observed during night/early morning, reflecting higher respired CO_2 (CO_2* in EQ. 4.21) accumulations in surface waters during periods of no/low solar insolation. Likewise, greatest ocean-to-atmosphere pCO_2 flux was observed during the night (Figure 4.8A), with highest degassing (i.e., positive flux) occurring before sunrise, whereas pCO_2 flux minima occurred soon after the period of highest solar insolation (noon). Light-rich primary production within the WAI shelf appears to control CO_2 flux drawdowns, whereas intense remineralization during the first hours of the night resulted in flux releases to the atmosphere during this observation period. Rapid positive and negative changes in pCO_2 flux indicate this site can change between CO_2 source or sink within hours.

Although the specific role of physical forces on nutrient dynamics is impossible to de-convolve from this dataset due to the co-occurrence of peak tide, peak waves, and peak wind, our observations of the co-occurrence of coastal zone water chemistry with elevated physical forcing strongly suggest that physical processes were responsible for the enhanced transport of sediment porefluids to the proximal coastal zone. However, in order to be more conclusive, observations of coastal zone water chemistry under de-coupled physical forcing are needed. We successfully performed such de-coupled observations during our second WAI observation period, as described below.

4.5.2.1.b De-coupling of physical forces: January-February 2006 observation period

Physical, chemical, dissolved nutrients, and carbonate chemistry data collected during the January-February 2006 observation period are shown in Figures 4.9 to 4.15. Winds showed clear diurnal periodicity during this observation period, with highest (north) wind speeds between middle

to late afternoon, effectively de-coupling them from peak tide height which occurred near midnight (Figures 4.9 to 4.11). The effects of tide-wind interactions on surface water current speed at sites B and C (Figures 4.9 and 4.10) seem to change as the amplitude of the tidal oscillation diminished. During the higher tidal oscillation period (January 2006), the effect of wind speed on surface water currents was greatest during low/receding tides and appeared to be brought to a halt during peak tide height; thus, wind and tides appeared to have opposite effects on shelf water velocity (i.e., higher wind velocity induced higher water currents, whereas higher tide height induced lower water currents). Tide-wind modulation of shelf water velocity during the first day in February 2006 appeared to be similar to observations of January. However, strong (southerly) surface water currents during the second half of the February 2006 observation period seemed to be mainly dependent on strong (northerly) wind forcing acting on the shelf under diminished tidal oscillations.

During previous observations (June 2005) the role of wind and tides on shelf water flow could not be de-convolved. From our January-February 2006 data, however, we can conclude that water currents along the WAI shelf are mainly forced by wind. The extent of wind effects on currents is further regulated by the amplitude of the tidal oscillations; the most effective wind-induced forcing occurred during periods with lower tidal amplitude (e.g., February 2006), and the forcing was greatest closer to shore (i.e., station B) where it is shallower. Although flows at the mid-shelf station (station C) were much lower than those close to shore, a similar forcing pattern can be discerned.

Wave penetration during the Jan-Feb time period followed tidal periodicity similar to the observations of June 2005. Wave heights were greater closer to shore, presumably due to wave shoaling in the upward sloping shelf. Wave height increases during the February 2006 period reflect intensification of wind-generated waves upon arrival of a high atmospheric pressure system.

Although salinities remained fairly constant during the January 2006 observation period, water column dissolved nutrient concentrations (again) peaked during rising/high tides (Figure 4.12). Highest DIN:DIP ratios (~40) were observed during rising/high tides, suggesting that local groundwater from the unconfined aquifer is reaching the coastal zone (Figure 4.12). Although nearshore current speeds appear to respond to intensified winds, dissolved nutrient concentrations do not appear to co-vary with wind speed during this observation period, suggesting that nutrient enrichments within the basin are not the result of advection from off-site sources. Instead, nutrient dynamics within the basin appear to be the result of local land-ocean interactions. Specifically, results from this observation period indicate tidal forcing is mainly responsible for nutrient variability across the shelf. The co-variance between tide height and wave penetration, and the presence of elevated nutrient concentrations closest to shore, suggest that enhanced solute transport between the shallow unconfined aquifer (Li 1999), sediment interstitial fluids (Reimers et al. 2004; Herbert et al. 2007), and surface waters is an important mechanism responsible for dissolved nutrient variability on this shelf.

Dissolved nutrient variability during the February 2006 observation period was distinct from the other two periods (Figure 4.13). For approximately half of the observation period, wind patterns were similar to those previously observed at this site (i.e., there was daily early afternoon wind intensification). The passage of a high pressure front during the latter portion of the observation period produced steady southerly winds (Figure 4.9). Continuous data obtained from our instruments located near the seabed recorded higher currents, higher wave heights, and lower salinities almost immediately following the shift in wind speed and direction. Discrete surface water salinity samples collected across-shore during this period indicates that lower surface salinity was more likely to occur closer to shore, suggesting that local processes (rather than advection)

were responsible for the freshwater inputs (Figure 4.13). The presence of fresh water inputs within the shelf during periods of higher currents and elevated waves indicates that surface water salinity depression during this period is likely either the result of enhanced fresh or brackish submarine groundwater discharge due to wave run-up (Li 1999), or to the effects of oscillatory and unidirectional water-column flow interacting with the rippled/rough shelf surface (Precht and Huettel 2003; Hebert et al. 2007).

Carbon dioxide flux during the January 2006 and February 2006 observation periods (Figure 4.8B and C, respectively) showed negative (atmospheric-to-ocean) fluxes from noon to ~15:00, even under strong wind forcing. This gas invasion corresponded to periods of high solar insolation and receding tides, suggesting rapid depletion of water column DIC by primary producers under a reduced areal DIC inventory (i.e., due to lower water volume). Higher surface water $\Omega_{aragonite}$ and $\Omega_{calcite}$ values, resulting from higher concentrations of CO_3^{2-} ions under reduced HCO_3^- due to uptake by primary producers (Lee 2008) during the day, and diminished during the night (Figures 4.14 and 4.15). Lowest $\Omega_{aragonite}$ (3.29) and $\Omega_{calcite}$ (5.03) were observed during the early morning hours and were well above saturation with respect to their mineral phases (i.e., no dissolution is expected), and similar to observations during June 2005 (Figure 4.7).

4.5.2.1.c March 2007

Wind forcing during the March 2007 observation period at WAI was distinct from that during all prior observation periods (Figures 4.16 to 4.20). Nearly constant south winds appear to induce cross-shore flows at station B and C, and alongshore currents at station D (Figure 4.4). Modulation of current speeds by tidal stage and wind speed can be discerned, similarly to February 2006 observations, and slight tidal modulation on incident wave height was observed on the shelf (stations B and C), but not offshore (station D).

Although relatively few surface water chemical data were obtained during this observation period, a few patterns are discernible from the available data. Mean surface water salinity showed negative co-variation with tide height close to shore (within the first 50 m). Moreover, temperature followed diurnal oscillations during the early observation period, and varied minimally during the latter portion due to reduced solar insolation under cloudy atmospheric conditions. The effects of reduced quantum flux on primary production during the latter portion of the observation period are observable in the DO % saturation plot (Figure 4.16). Interestingly, although peak DO decreased during periods with low quantum flux, DO minima (~75 % saturation) remained relatively unchanged, suggesting water circulation remained fairly unchanged throughout the observation period. Previous observation periods along this shelf indicated that higher water currents occur mainly during receding tides as wind effects on the shallow shelf intensify (see section 4.5.2.1.b). The fact that water column DO was stable under high (nighttime) demand under low water column oxygen inventories (due to less water volume on the shelf) suggests active surface water advection, or wave induced turbulence, may have buffered DO levels within the shelf. Relatively low significant wave heights observed during this period suggest this may not be the predominant DO buffering mechanism. It is, therefore, concluded that surface water DO minima were buffered by advection of offshore water.

DIN, Si, PO_4, and DIN:DIP ratios all negatively co-varied with salinity during the observation period. However, although highest PO_4 concentrations were observed close to shore, an opposite gradient was observed towards the furthest offshore sites for the other parameters. The presence of such gradients and the fact that they corresponds to similar gradients in salinity (i.e., lower levels further offshore) suggests that either (1) brackish water from the south (where nutrient-enriched groundwater has been repeatedly observed entering the coastal zone (Hunt 2006; Smith et al. 2006;

Dailer et al. 2010; Hunt and Rosas 2010; Herzfeld unpublished data)) was being advected to our site, or (2) cross-shore flows transported inner waters offshore. Low DIN and high PO_4 in surface waters resulted in lower than oceanic DIN:DIP ratios (1-16) across the shelf.

It is highly improbable that denitrification and/or desorption of PO_4 are the mechanisms dominating DIN:DIP ratios given that both of these necessitate suboxic or anoxic water conditions (Patrick and Khalid 1974; Froelich et al. 1979; Ingall and Jahnke 1994; Ingall and Jahnke 1997), neither of which were observed within surface waters at any of the sites (Figure 4.16). Alternatively, it is plausible for nutrients originating from southern sites to have been transported to our site via the northerly water transport present during this observation period (Figures 4.16 – 4.18). However, for DIN:DIP ratios to diminish from 38 (the approximate DIN:DIP ratio of groundwater down-gradient from the Kihei Wastewater Reclamation Facility located approximately 2 miles south of our study site, Hunt 2006) to the minimum of approximately 1 observed during this observation period (Table 4.2), large pools of N must have been lost during transit. A prime candidate for this accelerated N loss may be nutrient uptake by high N:P-tissue macroalgae (~45:1; Atkinson and Smith 1983). For algae to achieve the reduction in the observed dissolved nutrient ratios (assuming the mean uptake rates recorded by our experiments, see below) would have required approximately 25 hours (in order to reduce the ratios from 33 to 1), or 10 hours (if reducing the ratio from 16 to 1). It seems more likely that low DIN:DIP ratios observed within the study basin are the result of nutrient uptake from offshore oceanic sources which have lower mean DIN:DIP ratios (Table 4.9). However, the reason for the co-occurrence of these low DIN:DIP ratios with lower salinity water remains unknown.

Surface water carbonate geochemistry data collected during this observation period are fairly limited (Figure 4.20, Table 4.3), and patterns in their variability are difficult to discern. General

decreases in surface water DIC, TA, pCO_2, $\Omega_{aragonite}$ and $\Omega_{calcite}$ could be observed close to shore. Carbon dioxide flux (Figure 4.8D) calculated from TA and DIC data show positive (ocean-to- air) and negative (air-to-ocean) fluctuations during the observation period, indicating the dynamic nature of the CO_2 system in the nearshore environment.

4.5.2.2 Ukumehame (UKU): March 2007

Time-series of physical and chemical data collected at UKU during March 2007 are summarized in Figures 4.21 - 4.25, and Table 4.8. Moderately strong winds (mean ~ 7 m/s) from the southeast were fairly steady throughout the entire study period. Water flow inside the shelf (stations B and C) showed slight tidal modulation (Figures 4.21 and 4.22), with higher water currents occurring during lowest tide whereas further offshore (station D) near bottom currents were lower and no tidal modulation of water currents was evident (Figure 4.23). Significant wave height decreased in size further inshore, and did not show any modulation by tide height, as was observed at WAI. Decreasing wave heights further inshore, and a lack of tidal modulation of waves across the shelf, suggests that the reef crest continuously functions as a physical barrier to incoming wave energy.

Slight depressions in the salinity record spanning a few hours were present at station B during low tide, and salinity depressions at station C appear random throughout the entire record. Temperature followed typical diel cycles at all sites. Solar insolation reaching the seafloor was highest at station B, but was not drastically different from that at stations C or D. DO and pH at station B showed typical diel cycles driven by primary production within the shelf. Oxygen saturation remained close to 100% and pH near typical oceanic values (~ 8.1) throughout the night.

Dissolved nutrients at UKU, although variable, were, on average, lower than those observed at WAI during all observation periods. DIN and PO_4 concentrations decreased further inshore, whereas dissolved silicate enrichments were observed closer to shore. The occurrence of episodes

with lower offshore salinity suggests dissolved nutrients are being advected from a nearby site to the south (possibly Maalaea Bay where fresh groundwater discharge has been observed to be high possibly due to fractures to the country rock (i.e., basalt) during harbor construction (H. Dulaiova personal observations); however, no significant correlations were observed between salinity and DIN or PO_4 (data not shown). Dissolved silicate enrichments, on the other hand, were observed closer to shore with episodes of relatively higher concentrations during high tides. DIN:DIP ratios were generally lower closer to shore mainly as a result of changes in the surface water DIN concentrations (mostly ammonium, Table 4.8), and did not show any discernible diurnal or tidal periodicity.

Variability of surface water carbonate chemistry at UKU followed diel cycles (i.e., solar insolation) similar to those observed at WAI. Lower DIC, TA, and pCO_2 and highest $\Omega_{aragonite}$ and $\Omega_{calcite}$ were observed around noon. pCO_2 showed strong atmosphere-to-ocean fluxes during our observation period show strong influxes (atmosphere to ocean) during early/midafternoon and near neutral fluxes during the rest of the day (Figure 4.8E).

4.5.3 Algal growth experiments

Algal growth experiments were performed during June 2005, January 2006, and March 2007, but algal tissue analyses were not performed on samples collected during March 2007. A summary of all algal growth experiment results are shown in Table 4.11. Average algal growth rates were positive (i.e., there were net mass gains) during most study periods, except for *Hypnea musciformis* at WAI during March 2007. During the latter observation period, strong wind forcing interacting with waves may have resulted in higher cage agitation than during other growth periods, and it is possible that greater cage agitation lead to loss of *H. musciformis* fragments, resulting in an apparent mass loss (Table 4.11). No such losses were observed in *Ulva fasciata*, due perhaps to its

higher tensile strength. Mass gains and tissue carbon, nitrogen, and phosphorus concentrations were used to estimate molar uptake rates. These rates for different observation periods at WAI were fairly similar (Table 4.11). However, C:P uptake ratios at WAI were approximately half of those observed at UKU, indicating higher P availability (i.e., lower P limitation to algal growth) occurs at WAI. The mean of the *H. musciformis* molar N:P uptake rates observed at WAI during June 2005 and January 2006 (~44) were similar to the DIN:DIP ratio of groundwater at this site (~45; Table 4.9). Note that the DIN:DIP uptake ratios listed for WAI and UKU during March 2007 are the mean uptake ratios from previous observations.

4.5.4 Apparent water residence time estimates from multiple tracers

Estimates of apparent water residence time within the study sites were performed for each time interval using salinity, current speed, and radium and radon isotopic data (Table 4.12). There is general agreement between the salinity, current meter, and radon estimates, whereas slightly elevated residence times are predicted using radium isotopes. Best agreement was found between salt and radon estimates, suggesting that these two tracers integrate processes occurring across similar spatial scales. In contrast, current meter data is only able to capture advective water movement, yet solutes dissolved in water are subject to both advective and diffusive transport. The higher, more variable apparent residence times predicted from the current meter data suggest that diffusive processes responsible for mixing between coastal water and the ocean may be non-negligible.

Highest estimates of apparent water residence time were obtained from radium isotopes. The basic assumptions of the radium-based apparent water residence time approach are (after Dulaiova and Burnett 2007) that: (1) there is a single major source of ^{224}Ra and ^{223}Ra for the basin; (2) the source supplies a constant $^{224}Ra/^{223}Ra$ activity ratio (AR) on the time scale of the water residence

time; (3) the losses of radium after leaving the source are only by dilution by waters with no excess ^{223}Ra or ^{224}Ra (which does not affect the ratio) and radioactive decay; and (4) the offshore coastal water contains negligible amounts of excess ^{224}Ra and ^{223}Ra. Multiple lines of evidence indicate that the surface water chemistry within our basins are the result of inputs from various sources (e.g., fresh groundwater, and brackish and salty porewater); hence our initial assumptions of having a single major radium source ((1) and (2) above) may not be valid. A better understanding of all sources of radium isotopes within our basin (groundwater, sediment particles, porewater), and how their exchange with surface waters may vary over time may prove invaluable to our understanding of radium-based water residence times estimates within these basins.

4.5.5 Analysis of net ecosystem metabolism (NEM) from stoichiometrically-linked non-conservative fluxes

Fresh groundwater dissolved inorganic CNP fluxes estimated from our water and salt balances are summarized in Table 4.13. Although the DIC:DIP ratios of all groundwater estimates for both sites vary considerably, the DIN:DIP ratios are remarkably constant (43:1) and are consistent with the hypothesis that shallow unconfined aquifer water, enriched in DIN, is actively entering the coastal zone at these sites. Fresh groundwater DIC fluxes were stoichiometrically linked to groundwater DIC:DIN and DIC:DIP ratios in order to estimate DIN and DIP mass fluxes to the coastal zone via fresh groundwater discharge.

High variability in the CO_2 flux was observed during all of our observation periods. Average physico-chemical and wind parameterizations required for the estimation of gaseous losses of CO_2 are shown in Table 4.14. Wind parameterizations resulted in mean gas transfer coefficient values ranging between 2.8 to 16.2 m/day; values well within the range reported by other authors (Liss and Merlivat 1986; Wanninkhof 1992; Wanninkhof and McGillis 1999; Nightingale et al. 2000a; Nightingale et al. 2000b; Ho et al. 2006). High CO_2 evasion rates occurred during the night,

whereas highest drawdown rates occurred during periods of highest solar insolation (i.e., during periods of highest primary production), indicating that CO_2 flux in or out of the coastal zone is mainly controlled by biogeochemical processes rather than solely by wind speed.

Estimates of NEM (calcification, production, and nitrogen cycling) are shown in Table 4.13. From our estimates it is apparent that net calcification, net production *(p-r)*, and net nitrogen cycling *(N_{fix}-N_{den})* at WAI during June 2005 were significantly different from all other observation periods. The highest rates of carbonate dissolution, net primary production, and denitrification were all observed during June 2005. Moreover, our results demonstrate that the shelf at WAI can alternate (on average) from net carbonate dissolution to slight net calcification. Net autotrophy (i.e., positive *(p-r)*) was observed during all observation periods at WAI, whereas net heterotrophy was observed at UKU. Primary production estimates at WAI estimated from our budgetary approach fall within the upper range of observations performed at other locations worldwide (Table 4.15) and are not surprising given the massive accumulation of macroalgae at this site. Mean net heterotrophy observed at UKU falls within the range observed at other reef flats and shallow lagoons (Table 4.15). Estimates of net nitrogen metabolism at WAI suggest that this site can alternate between net nitrogen losses (i.e., denitrification) to net nitrogen gains (i.e., N-fixation). Net nitrogen metabolism at UKU suggests this site, despite high diurnal variability, loses nitrogen to denitrification.

Based on our budgetary approach, negative net calcification (i.e., dissolution) occurred at WAI during June 2005, and January 2006, and at UKU during March 2007 (Table 4.13). Net calcification observed at WAI during February 2006 and at UKU, although variable, was not significantly different from zero ($Z = 0.03$, $p = 0.5$). Highest dissolution rates calculated for WAI during June 2005 suggest that this site was actively losing its reef structure during this period.

Although questions remain about the effect of sulfide additions to water column TA (and consequently calculated calcification rates), the close match between CO_2 flux and *(p-r)* estimates and those reported by others (Table 4.15) suggests that sulfide effects on carbonate geochemistry were minimal during our observation periods.

4.6 CONCLUSIONS

Assessment of the water quality within coastal systems with complex hydrodynamics is a difficult task. Our results demonstrate that the coastal zones along southern Maui are dynamic regions where groundwater is actively mixing with surface coastal waters. Transport and biogeochemical transformations in these coastal waters can be observed to lead to distinct changes in water column chemistry on timescales of hours and spatial scales of meters. The lack of a tidal modulation of currents during periods of constant wind further indicates that wind is the most important physical force controlling water flow within our study sites. Tidal height, on the other hand, seems to modulate wave penetration into these shallow shelves.

Higher significant wave heights were observed to penetrate onto shallower zones of the WAI shelf during periods of high tidal elevation, and often coincided with high dissolved nutrients concentrations in the water column. Water column dissolved oxygen, sediment porewater nutrients, salinity, and DIN:DIP ratios in surface water, porewater, shallow unconfined groundwater, and algal tissue analyses corroborate the hypothesis (Chapters 2 and 3) that nutrient inputs to the coastal zone during periods of high wave activity originate from the sediment and the shallow unconfined aquifer. We conclude that chronic nuisance macroalgal growth along WAI is the result of enhanced transport of groundwater nutrients to the coastal zone via wave run-up and wave-induced oscillatory flows along the shelf.

Apparent water residence times calculated using four distinct methods show remarkable agreement during the individual study periods. Of all these estimates, salt and radon tracers showed the closest agreement, followed by estimates computed from currents and radium isotopes. The close agreement between salt- and current-based estimates, and the ease and inexpensive nature of their measurement, encourages the further exploration of the utility of salt as a tracer in coastal areas with complex hydrodynamics.

The observed variability in NEM, as calculated from our budgeting approach, indicates that the biogeochemical functioning of the WAI shelf can be drastically different over hours and at different times of the year. Highest nutrient fluxes were also observed during the June 2005 observation period. Metabolic responses observed during June 2005, a period with the highest tidal amplitude (summer solstice) and high winds, appear to be the result of enhanced groundwater (fresh and brackish) nutrient transport to the study area.

Lastly, our data demonstrate that the water quality and metabolic functionality of a coastal region with complex hydrodynamics can be quite variable. We argue that monitoring programs that are designed to capture changes in water chemistry over months-to-seasons (but not much shorter periods) fail to capture a mechanistic understanding of land-ocean nutrient exchange. We further suggest that, in order to comprehend biogeochemical processes within the proximal coastal zone, continuous long-term observations of water chemistry and physical oceanography are needed. Knowledge of the interactions between physical forces and the distinct nutrient reservoirs within the proximal coastal zone is indispensable for the success of any monitoring program designed to detect biogeochemical (or metabolic) change in physically active coastal zones, particularly if the latter contain permeable sediments or are subject to significant groundwater inputs.

4.7 ACKNOWLEDGEMENTS

The authors would like to extend their gratitude to Christopher Colgrove, Matthew Ross, Megan Ross, Heather Spalding, Megan O'Brian, Mark Vermeij, and Rebecca Briggs for field and laboratory assistance; Craig Glenn for access to the carbon coulometer; and Chris D'Elia and James Krest for logistical support at USFSP during the preparation of this manuscript. We extend a special mahalo to Marion Chavane, Jeff Sevadjian, and Curt Storlazzi for assistance with Matlab coding. This work was supported by NOAA-ECOHAB Program, and the National Science Foundation award #652179.

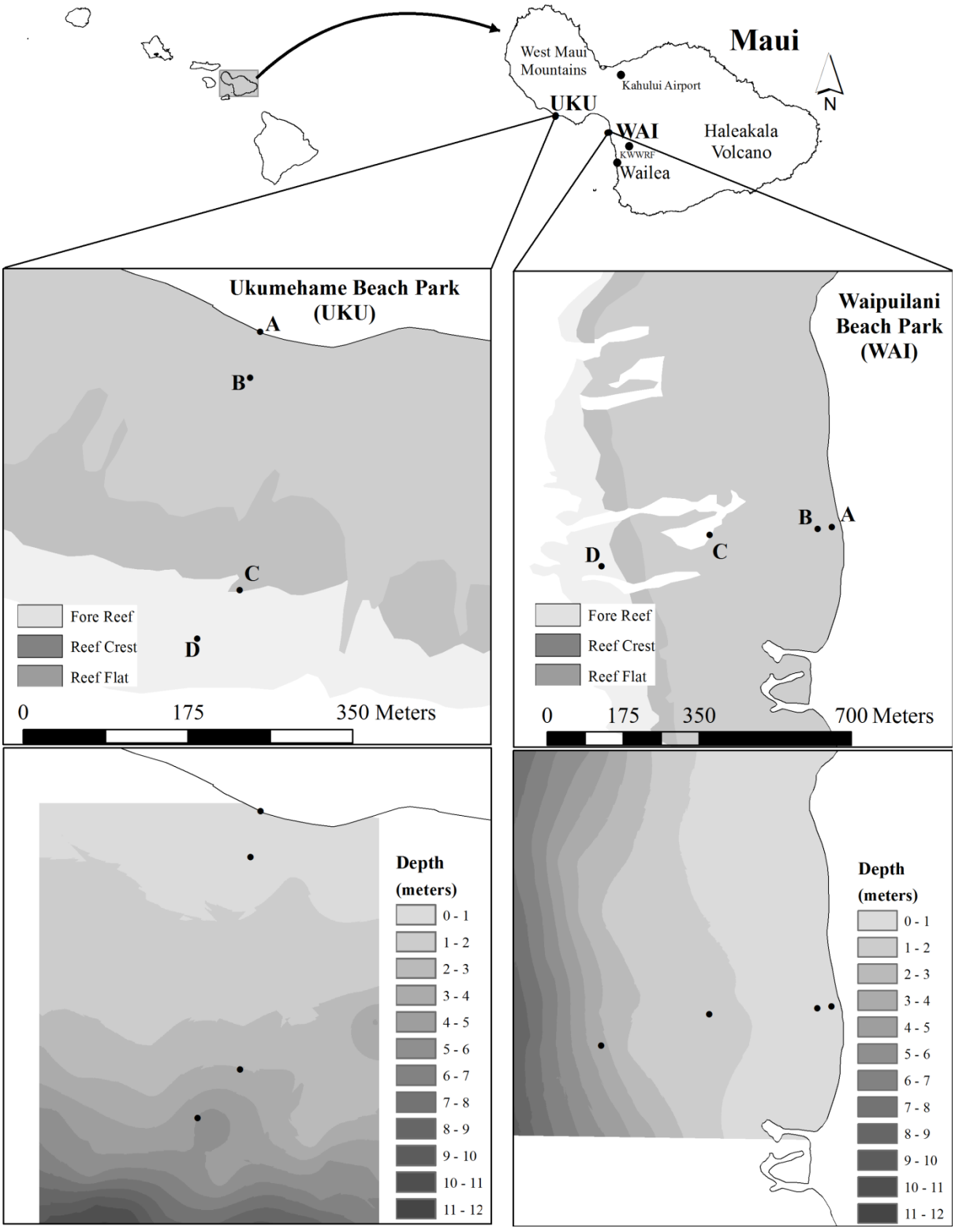

Figure 4.1 – Field site and sampling station locations, general schematics of reef zones, and offshore depth contours. KWWRF = Kihei Wastewater Reclamation Facility.

Figure 4.2 – Experimental cages used to measure in-situ macroalgae growth.

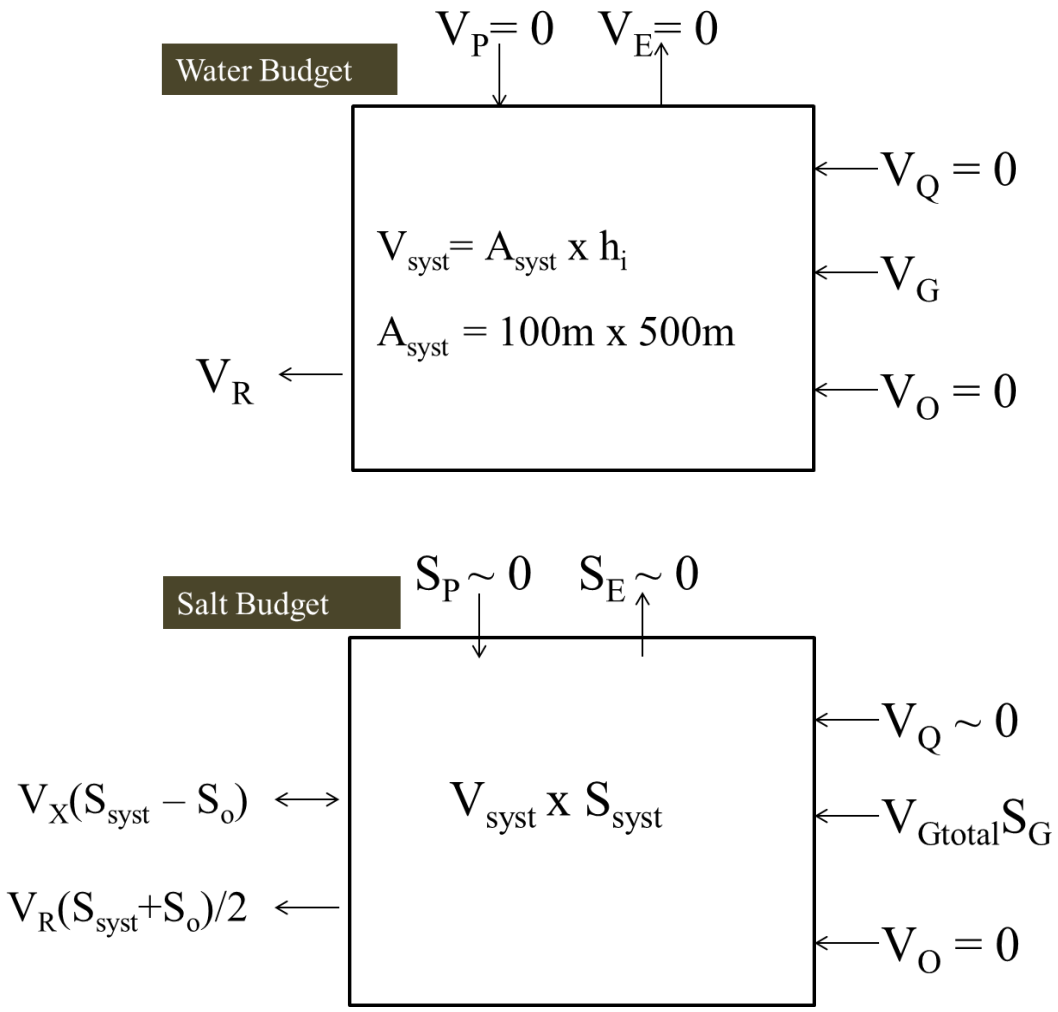

Figure 4.3 - Schematics of water and salt budgets (after Gordon et al., 1996). See text for explanation of abbreviations.

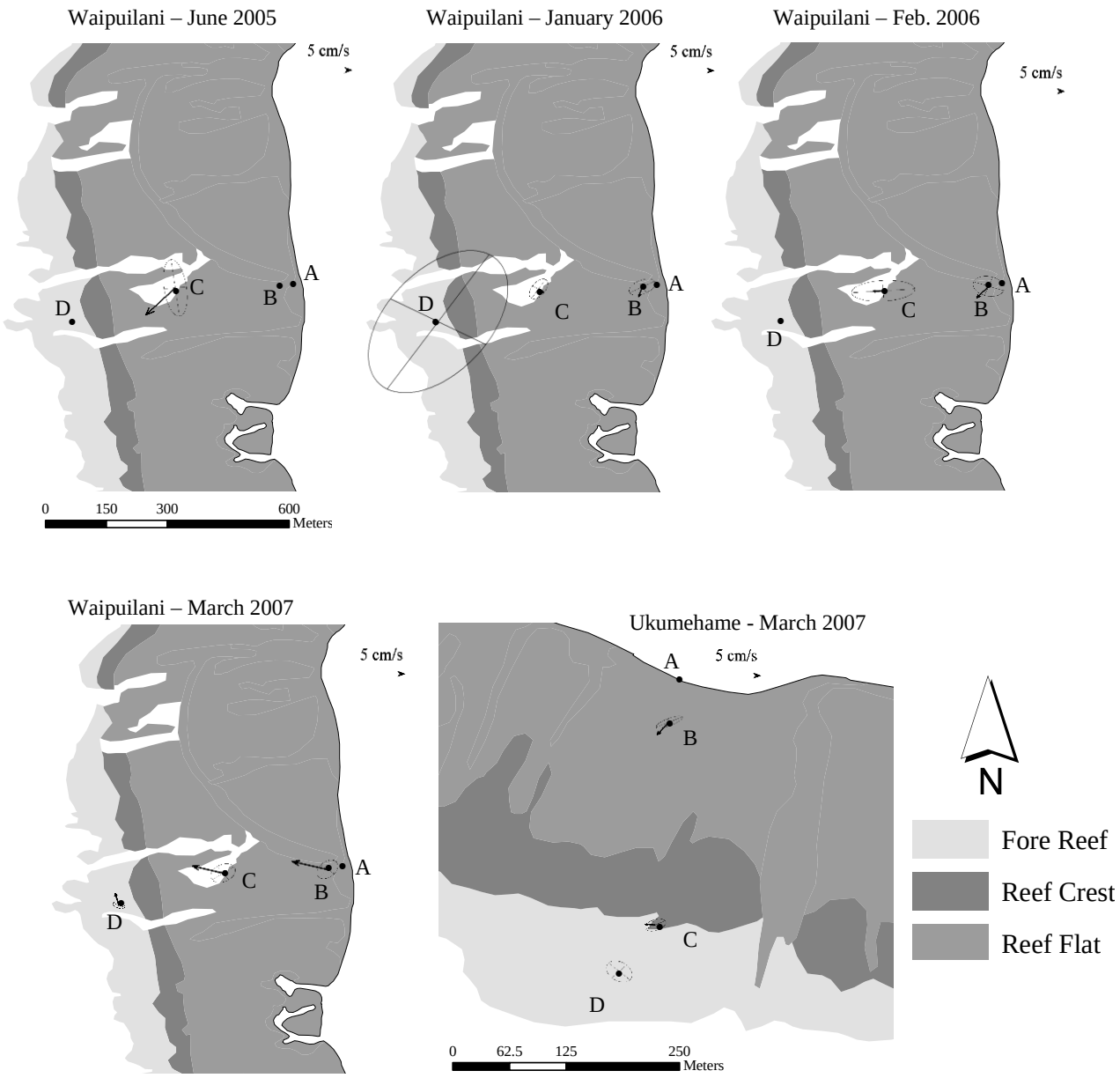

Figure 4.4 – Mean near-bottom current speed and ellipses showing principal axes of surface current variability.

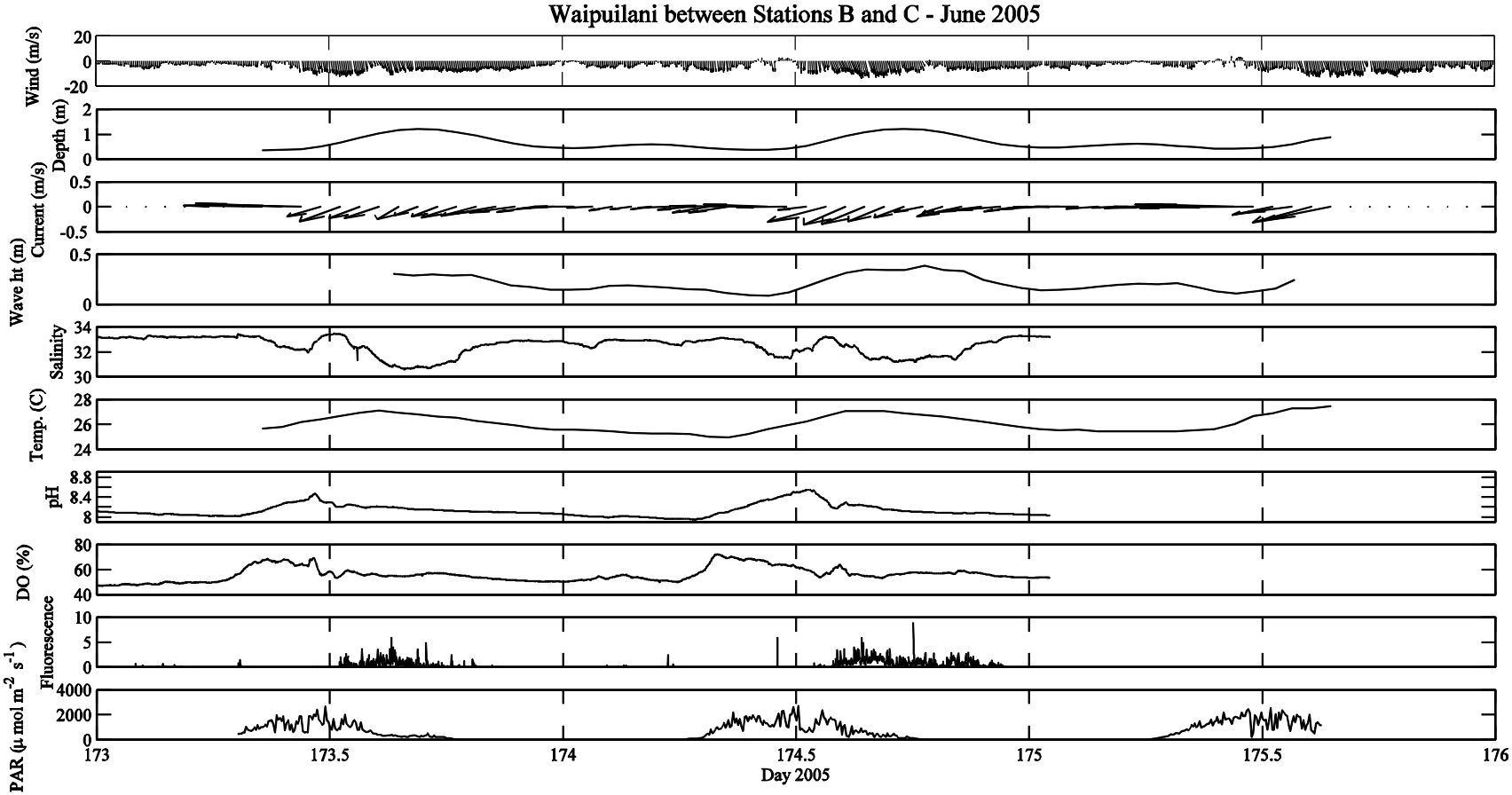

Figure 4.5- Summary of all time-series data collected at Waipuilani between stations B and C during June 2005.

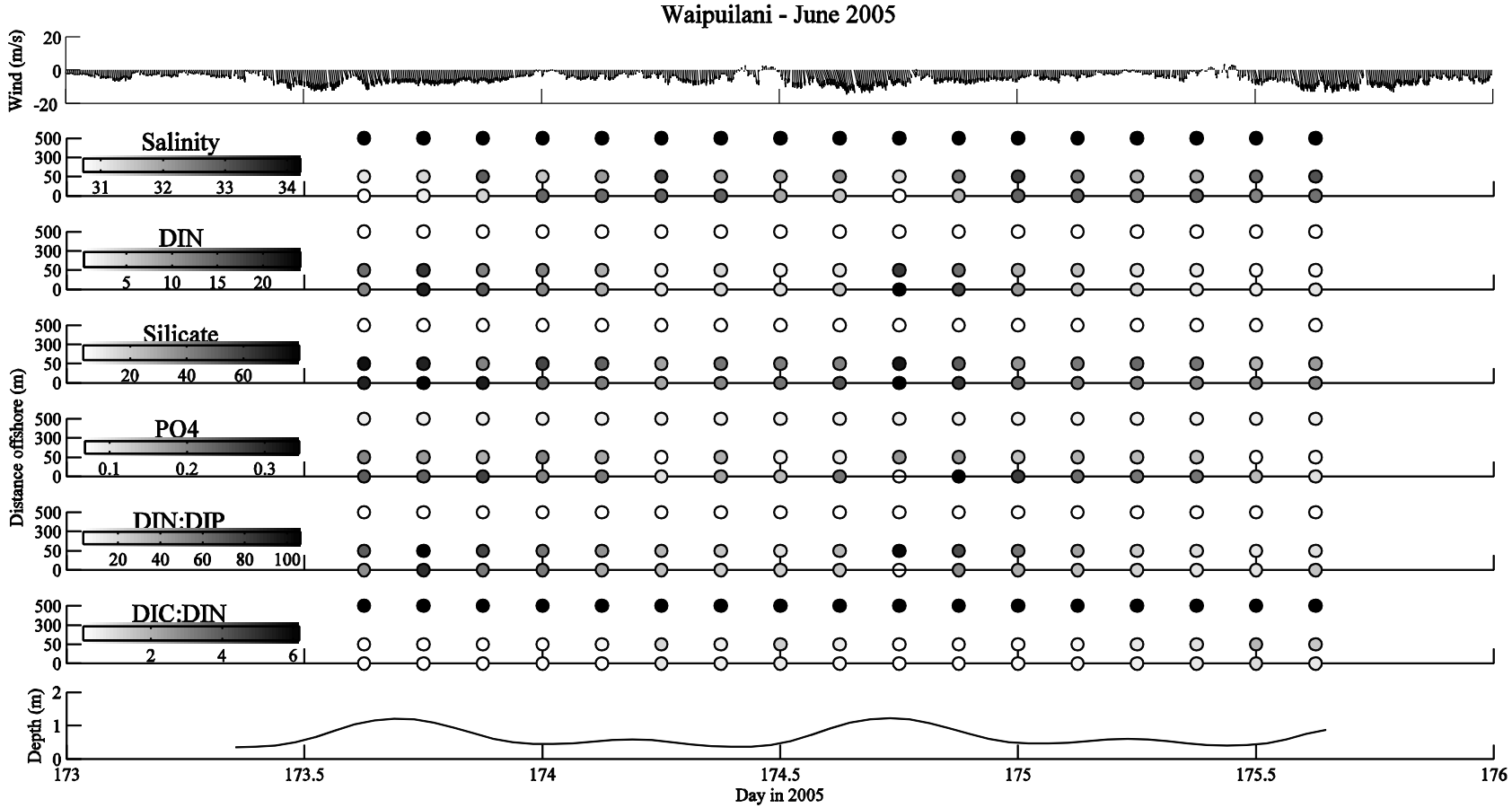

Figure 4.6 - Discrete cross-shore dissolved nutrient concentrations and tide height time-series data collected at Waipuilani during June 2005, along with wind speed data collected from WeatherFlow Kihei wind station (see text for details). Offshore (500 m) dissolved nutrient data are the mean surface water concentration offshore of coastal Maui (see Table 4.9).

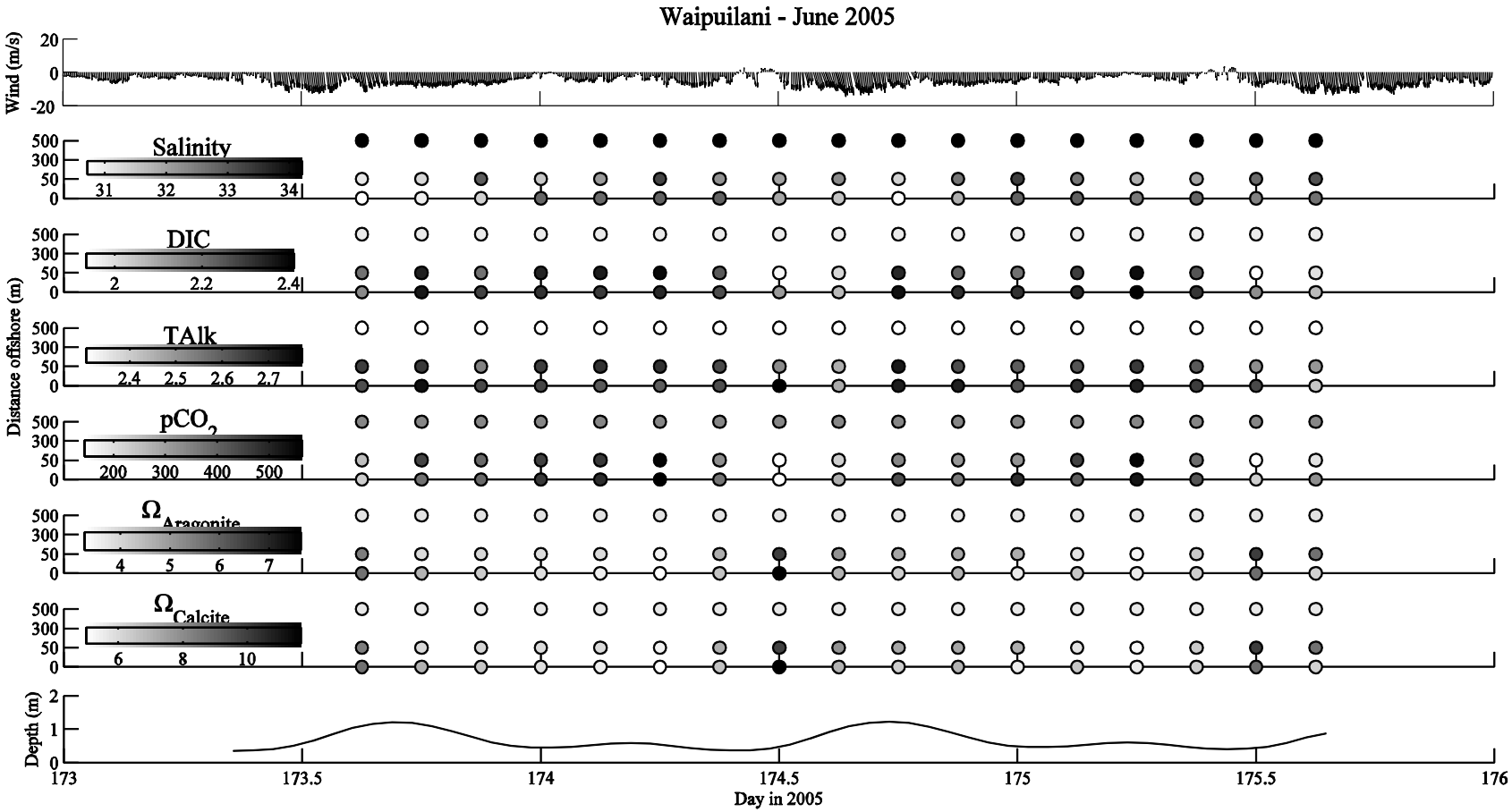

Figure 4.7 - Discrete cross-shore carbonate chemistry and tide height time-series data collected at Waipuilani during June 2005, along with wind speed data collected from WeatherFlow Kihei wind station (see text for details). Offshore (500 m) DIC, Talk, and pCO_2 data are the long-term average surface water chemistry at station ALOHA (Keeling et al. 2004); offshore (500 m) $\Omega_{calcite}$ and $\Omega_{aragonite}$ were calculated using CO2SYS software and DIC and TA; carbonate dissociation constants are from Mehrbach, refit by Dickson and Millero; and K_{SO4} is from Dickson (seawater scale) at 25º C.

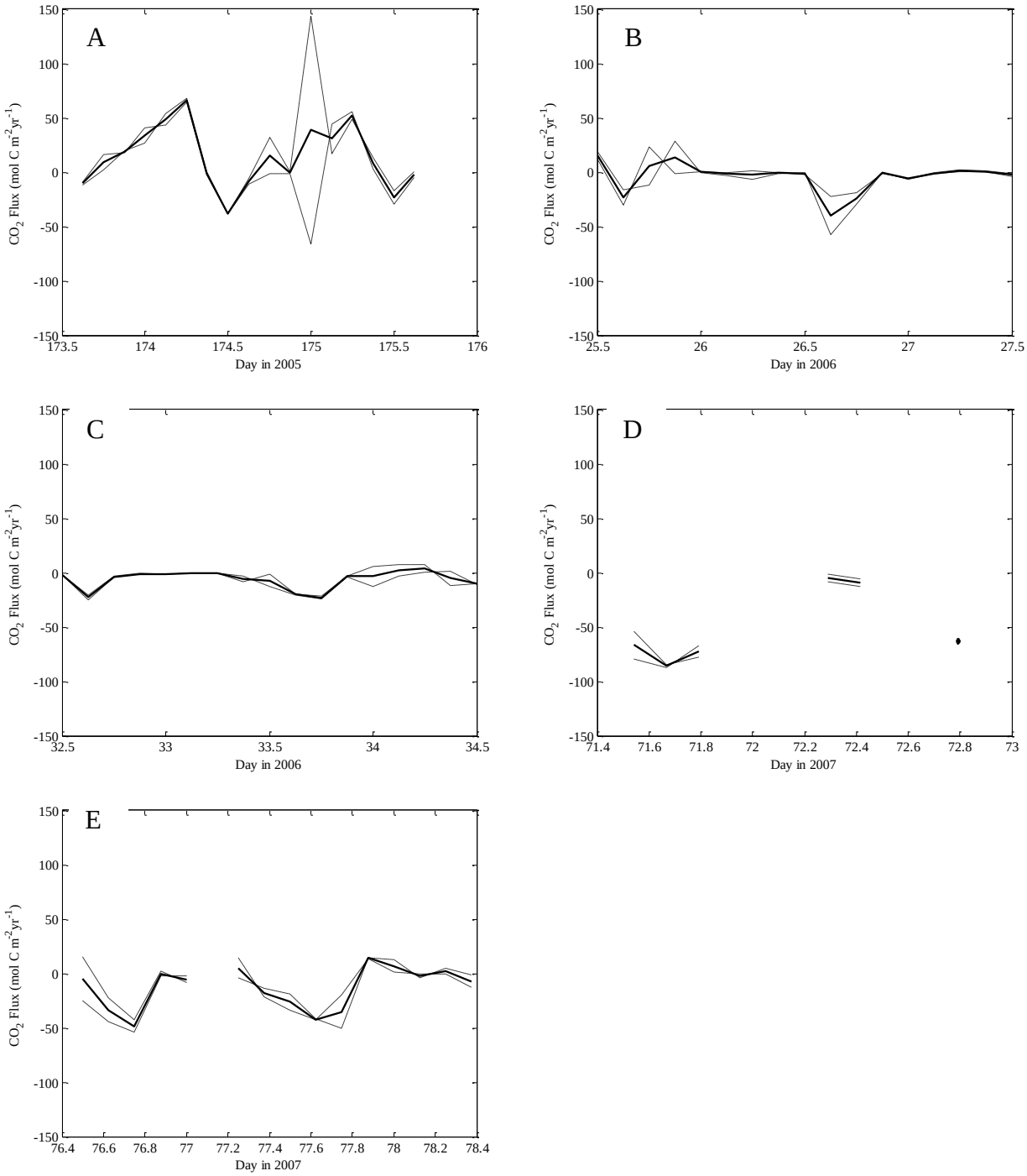

Figure 4.8 - Carbon dioxide flux at Waipuilani during June 2005 (A), January 2006 (B), February 2006 (C), and March 2007 (D), and at Ukumehame during March 2007 (E) . Dashed lines denote flux calculations at sites A and B. Solid lines denote the mean flux ($F_{CO2\ (0\text{-}50)}$). Positive values denote net ocean-to-atmosphere gas fluxes.

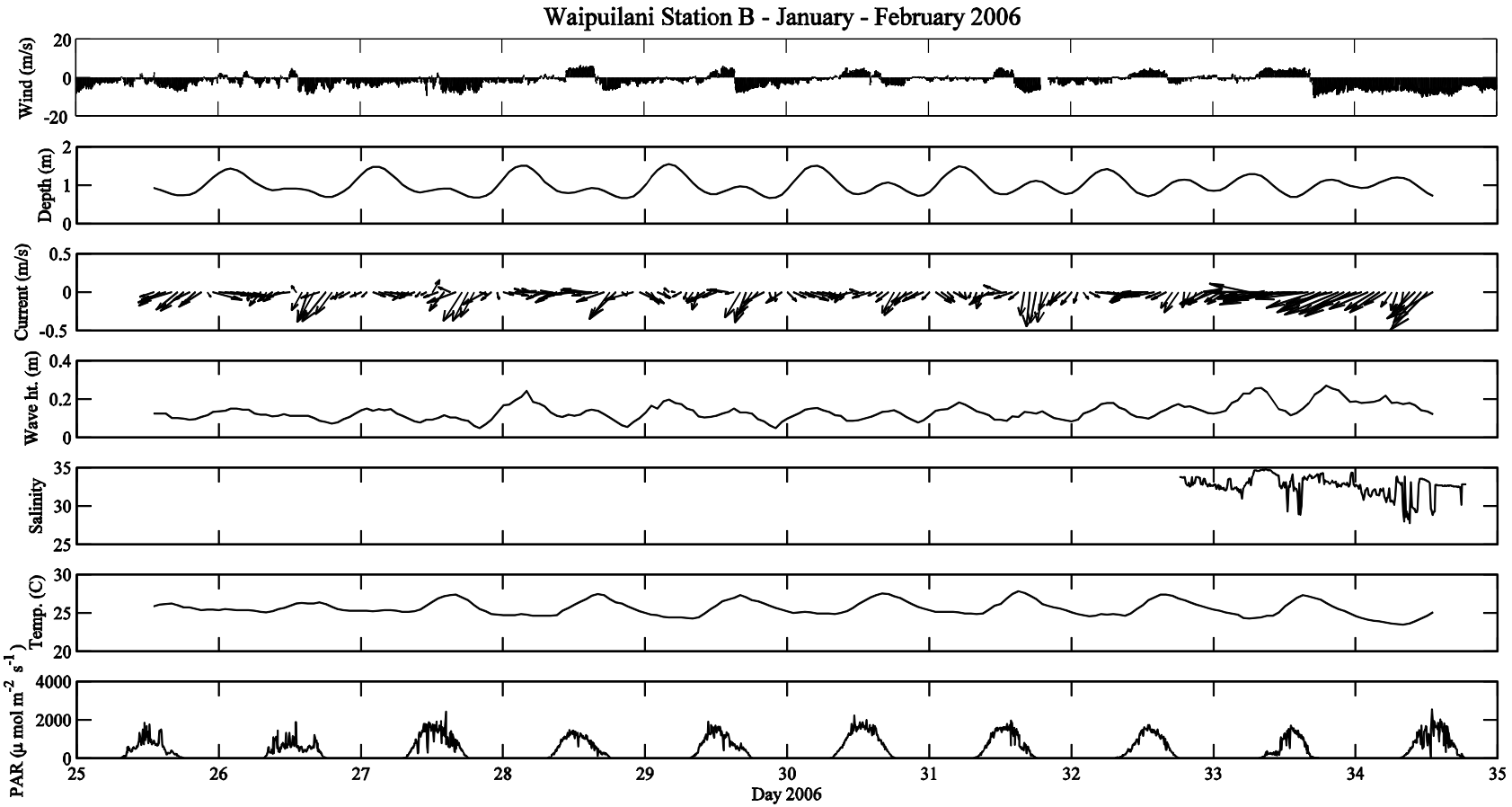

Figure 4.9 - Summary of all time-series data collected at Waipuilani station B during January-February 2006.

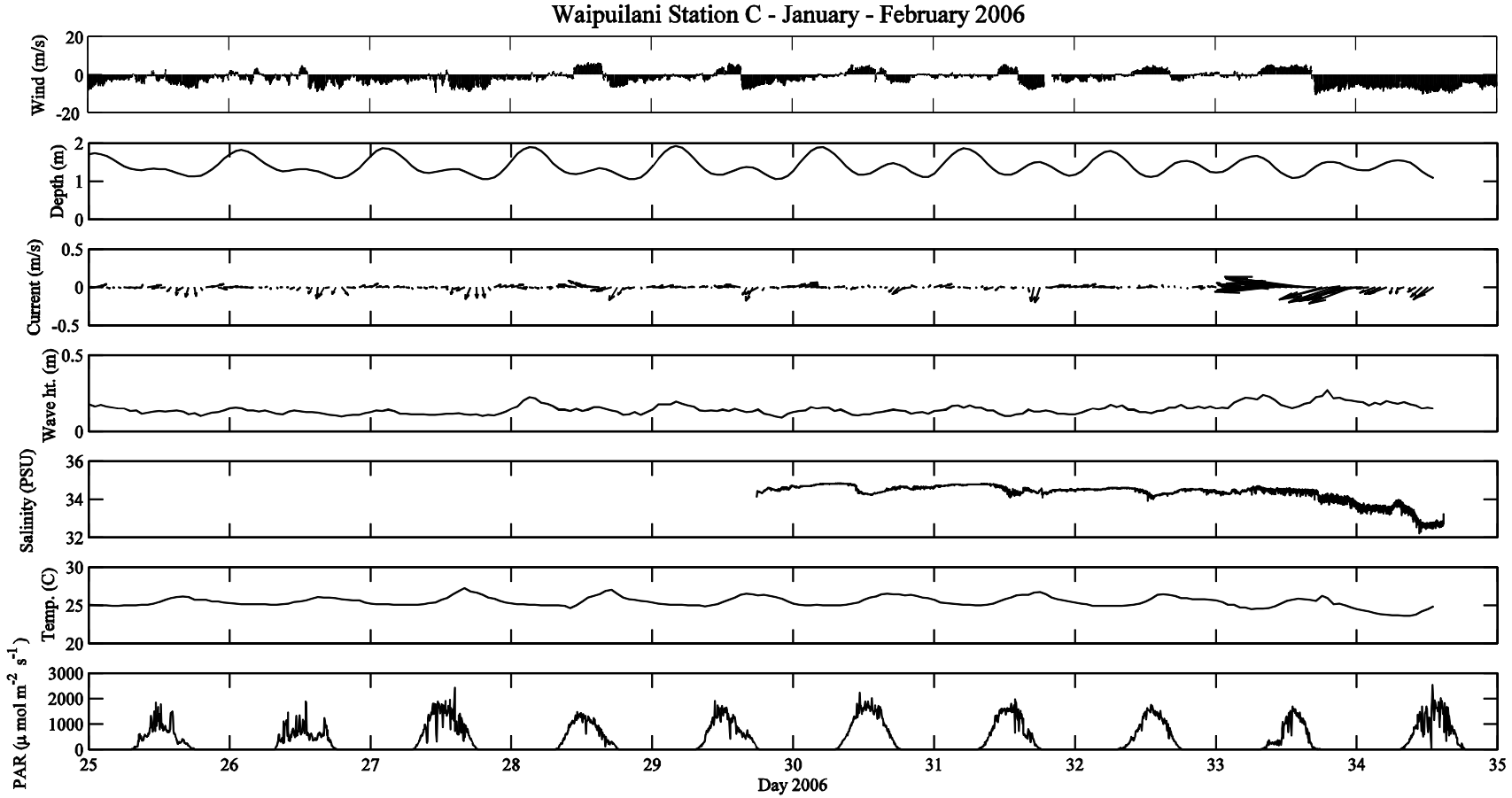

Figure 4.10 - Summary of all time-series data collected at Waipuilani station C during January-February 2006.

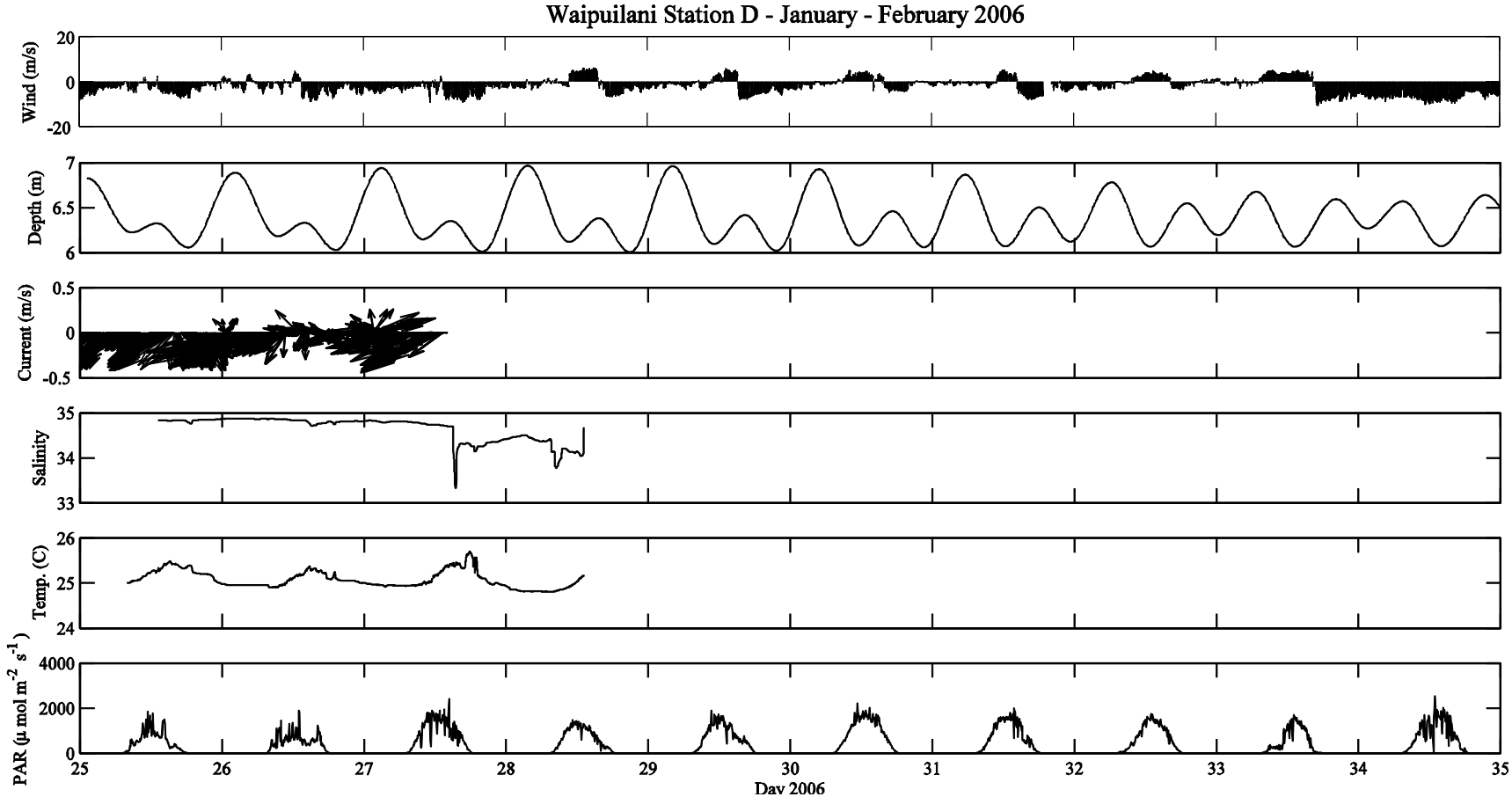

Figure 4.11 - Summary of all time-series data collected at Waipuilani station D during January-February 2006.

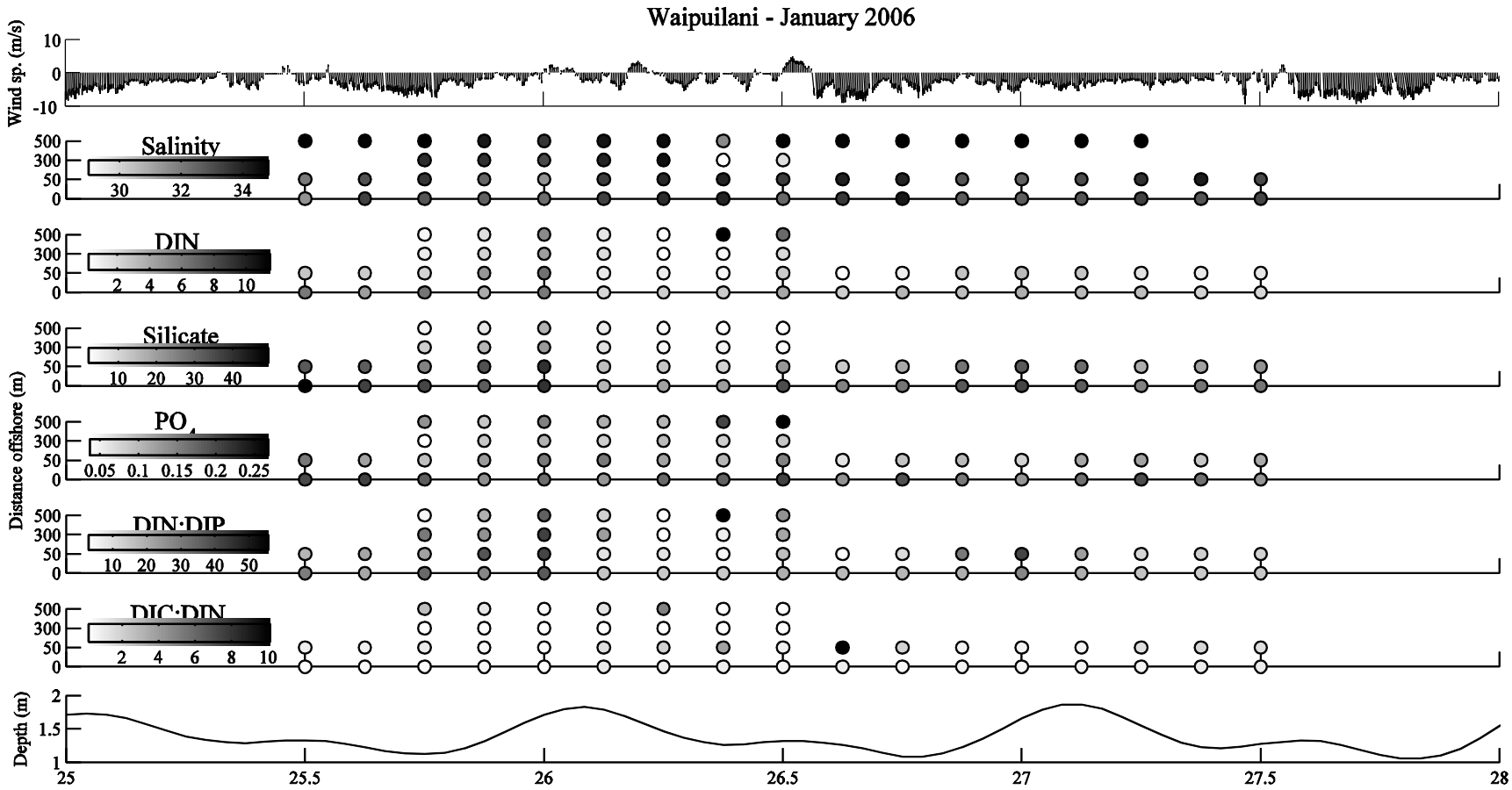

Figure 4.12 – Discrete cross-shore dissolved nutrients and tide height time-series data collected at Waipuilani during January 2006, along with wind speed data collected from WeatherFlow Kihei wind station (see text for details).

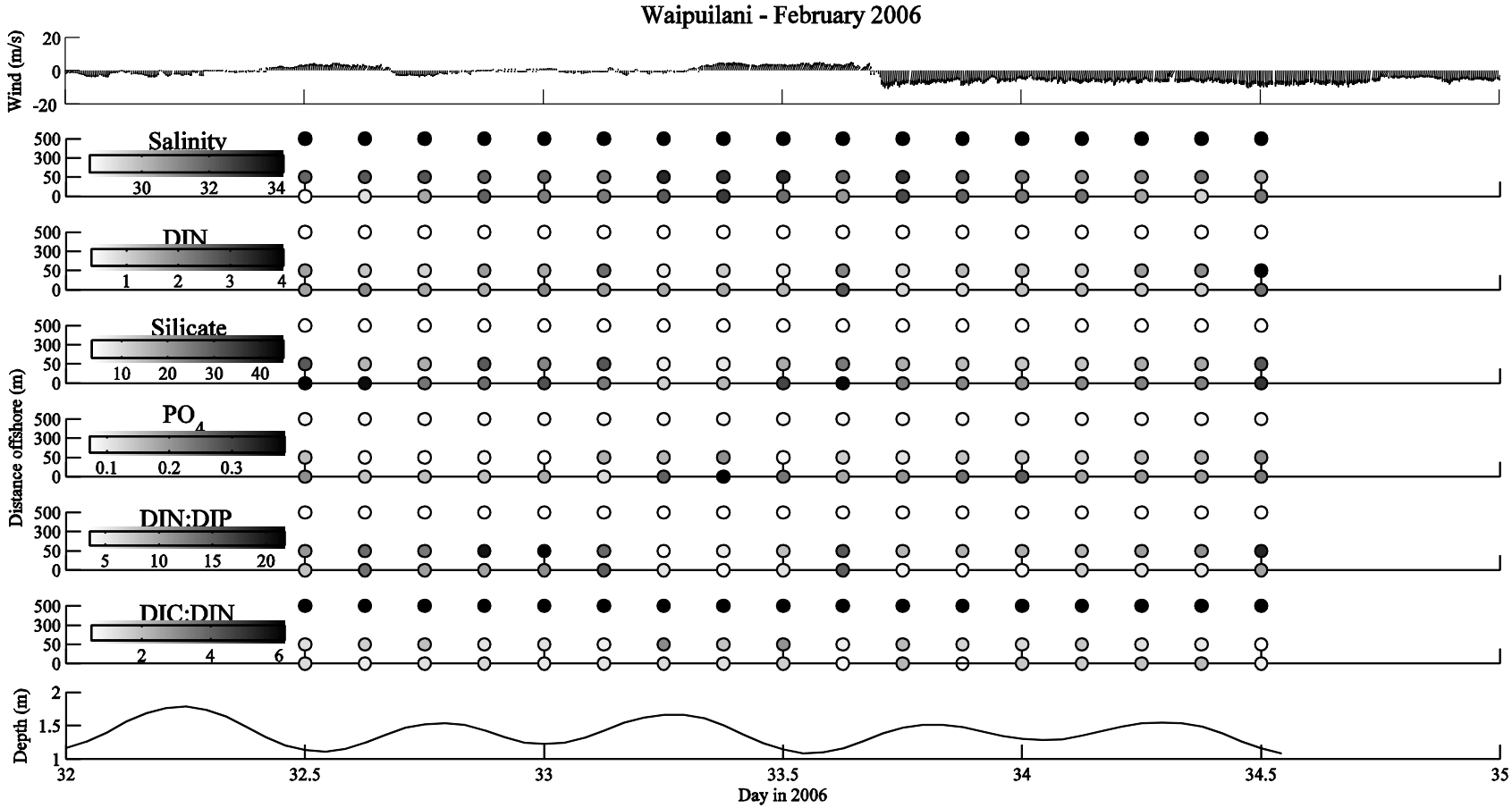

Figure 4.13 - Discrete cross-shore dissolved nutrients and tide height time-series data collected at Waipuilani during February 2006, along with wind speed data collected from WeatherFlow Kihei wind station (see text for details). Offshore (500 m) dissolved nutrient data are the mean surface water concentration offshore of coastal Maui (see Table 4.9).

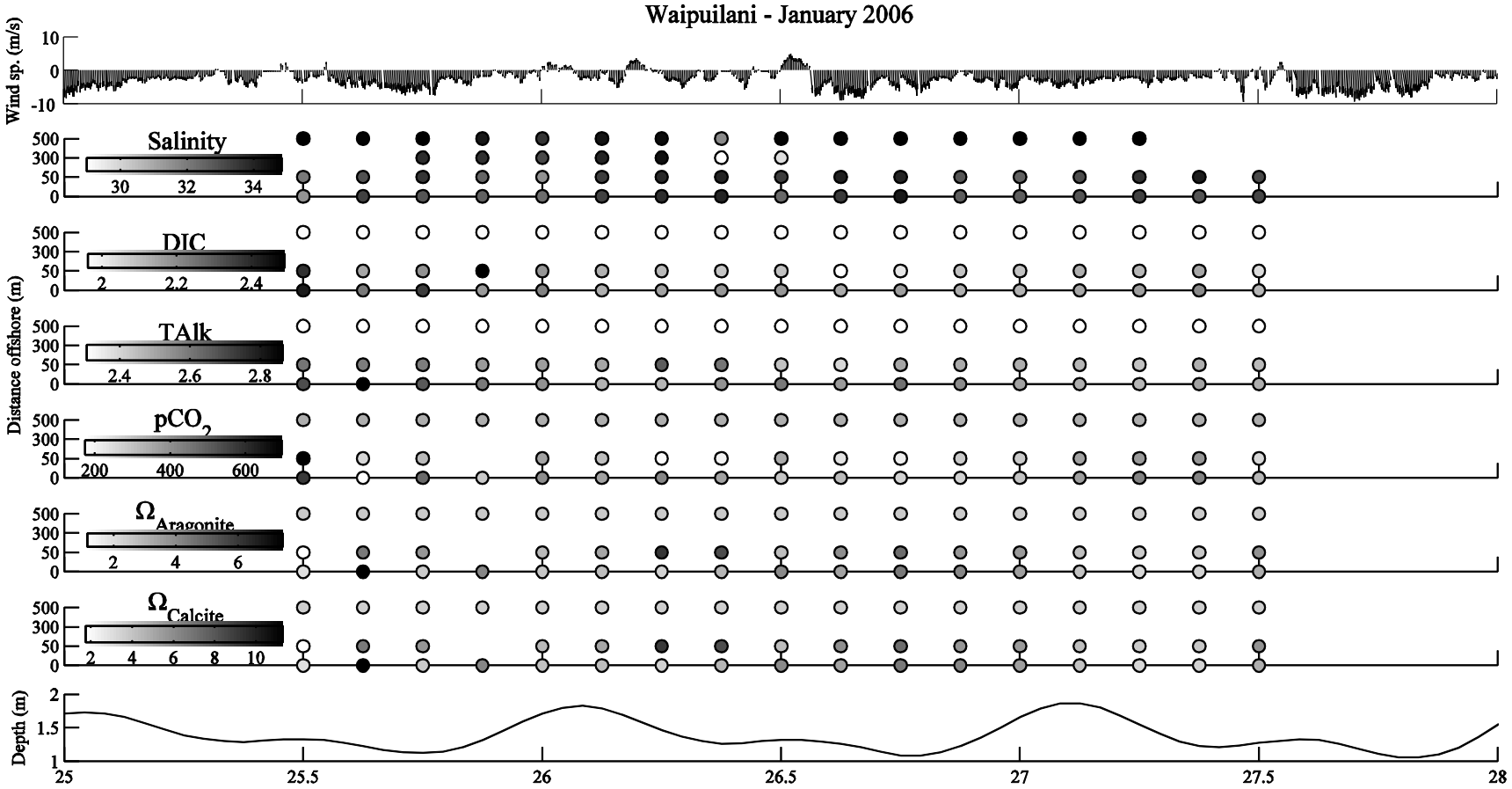

Figure 4.14 - Discrete cross-shore carbonate chemistry and tide height time-series data collected at Waipuilani during January 2006, along with wind speed data collected from WeatherFlow Kihei wind station (see text for details). Offshore (500 m) DIC, Talk, and pCO_2 data are the long-term average surface water chemistry at station ALOHA (Keeling et al. 2004); offshore (500 m) $\Omega_{calcite}$ and $\Omega_{aragonite}$ were calculated using CO2SYS software and DIC and TA; carbonate dissociation constants are from Mehrbach, refit by Dickson and Millero; and K_{SO4} is from Dickson (seawater scale) at 25º C.

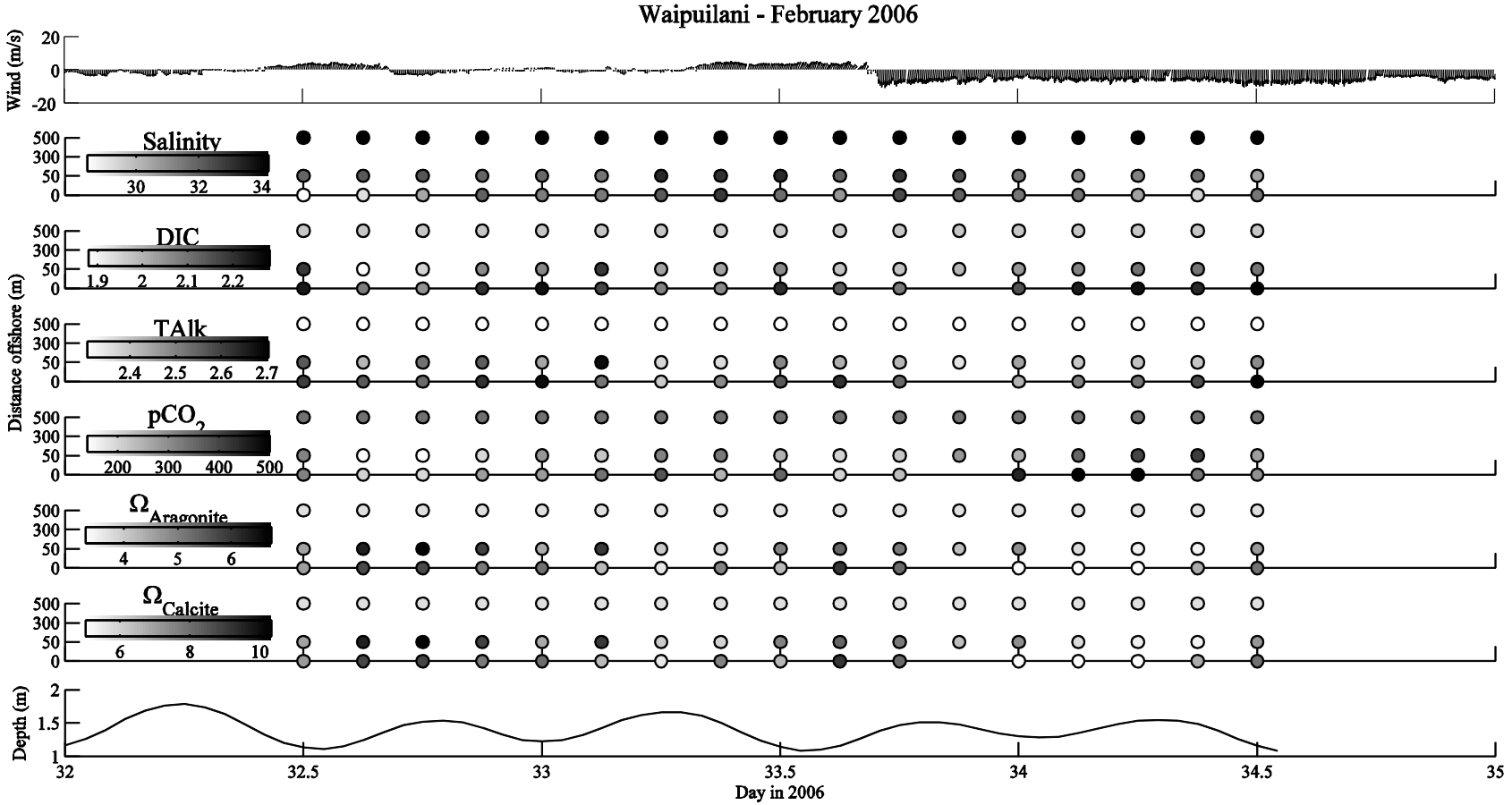

Figure 4.15 - Discrete cross-shore carbonate chemistry and tide height time-series data collected at Waipuilani during February 2006, along with wind speed data collected from WeatherFlow Kihei wind station (see text for details). Offshore (500 m) DIC, Talk, and pCO_2 data are the long-term average surface water chemistry at station ALOHA (Keeling et al. 2004); offshore (500 m) $\Omega_{calcite}$ and $\Omega_{aragonite}$ were calculated using CO2SYS software and DIC and TA; carbonate dissociation constants are from Mehrbach, refit by Dickson and Millero; and K_{SO4} is from Dickson (seawater scale) at 25º C.

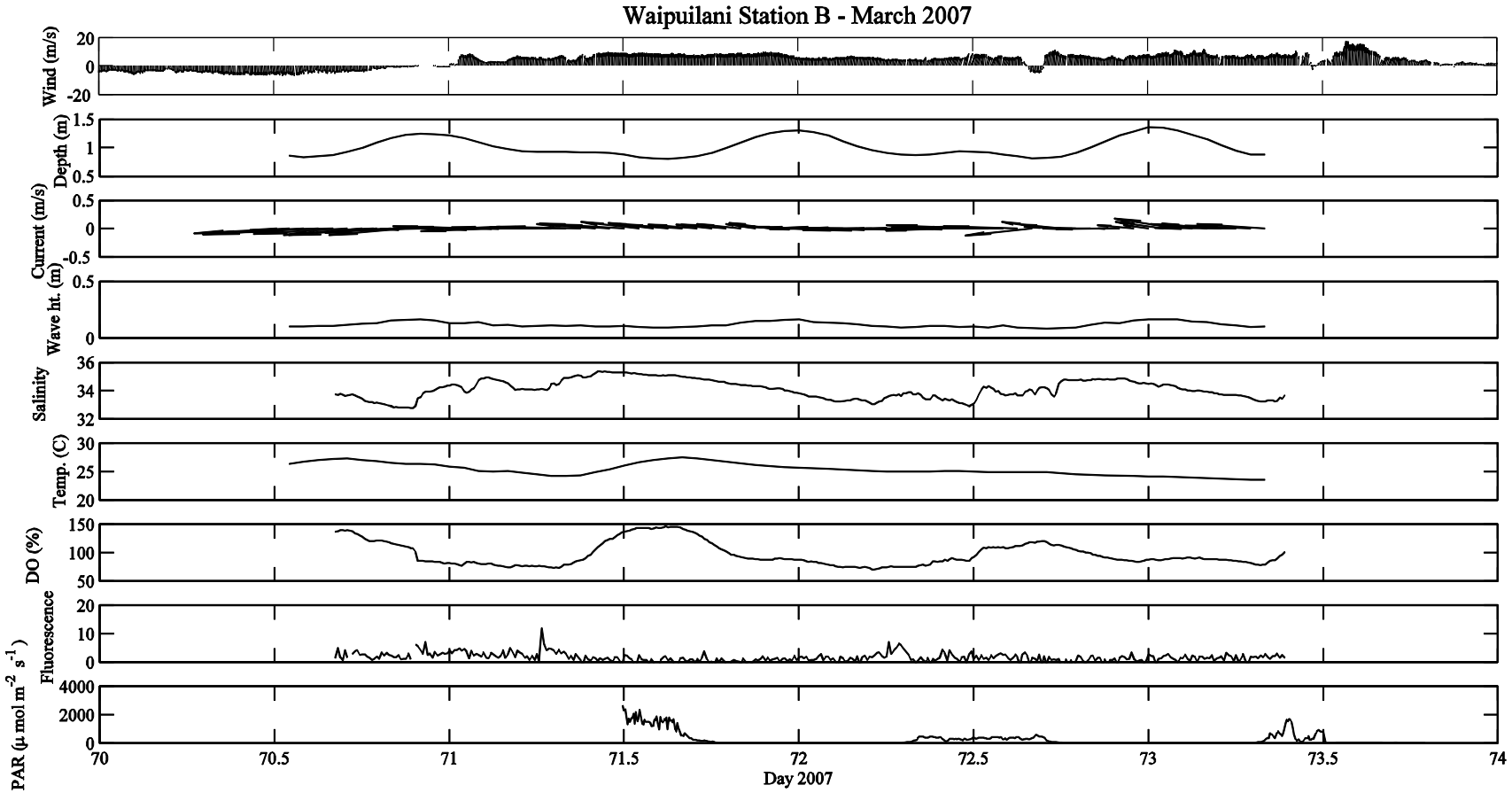

Figure 4.16 - Summary of all time-series data collected at Waipuilani station B during March 2007.

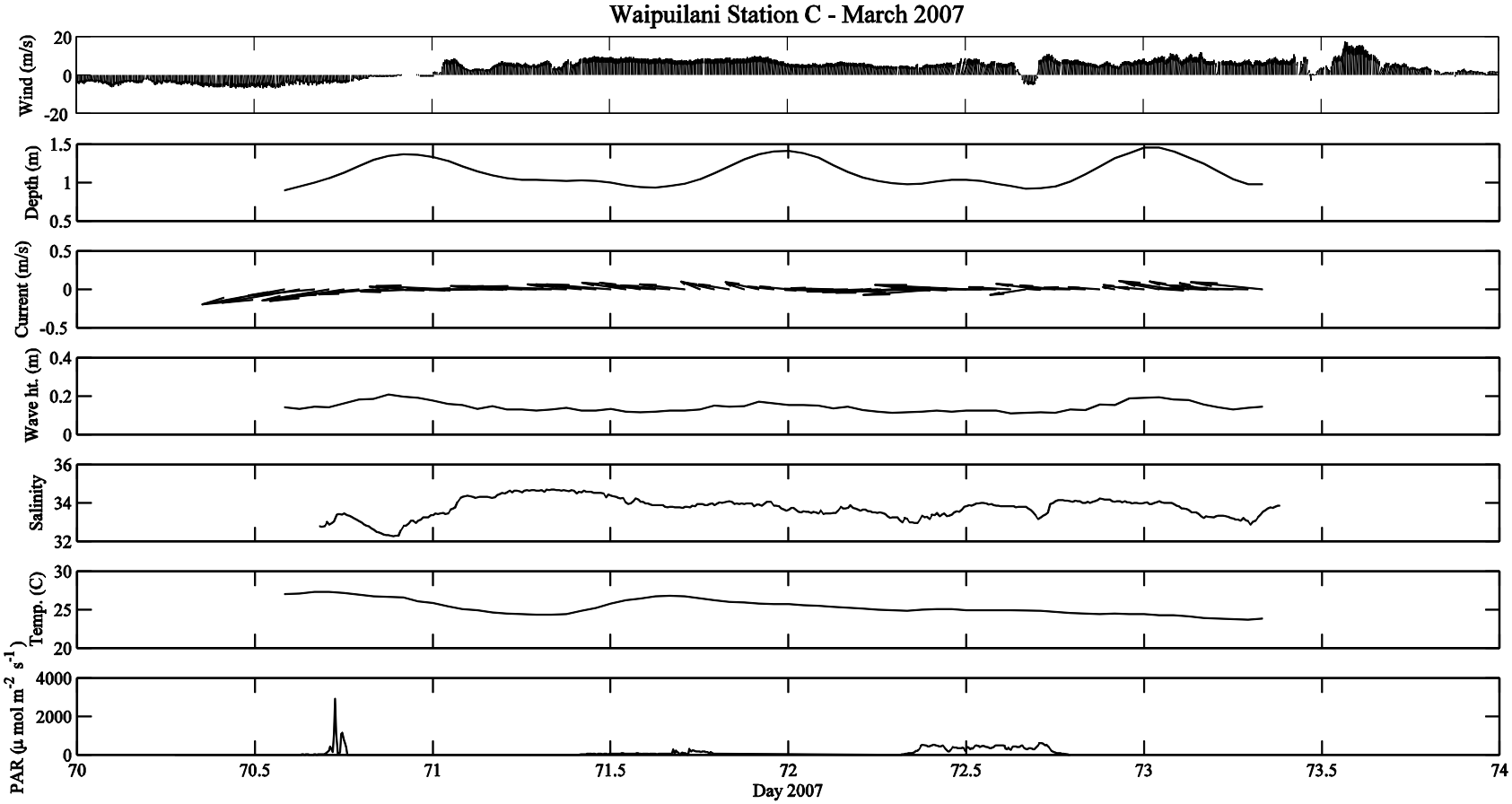

Figure 4.17 - Summary of all time-series data collected at Waipuilani station C during March 2007.

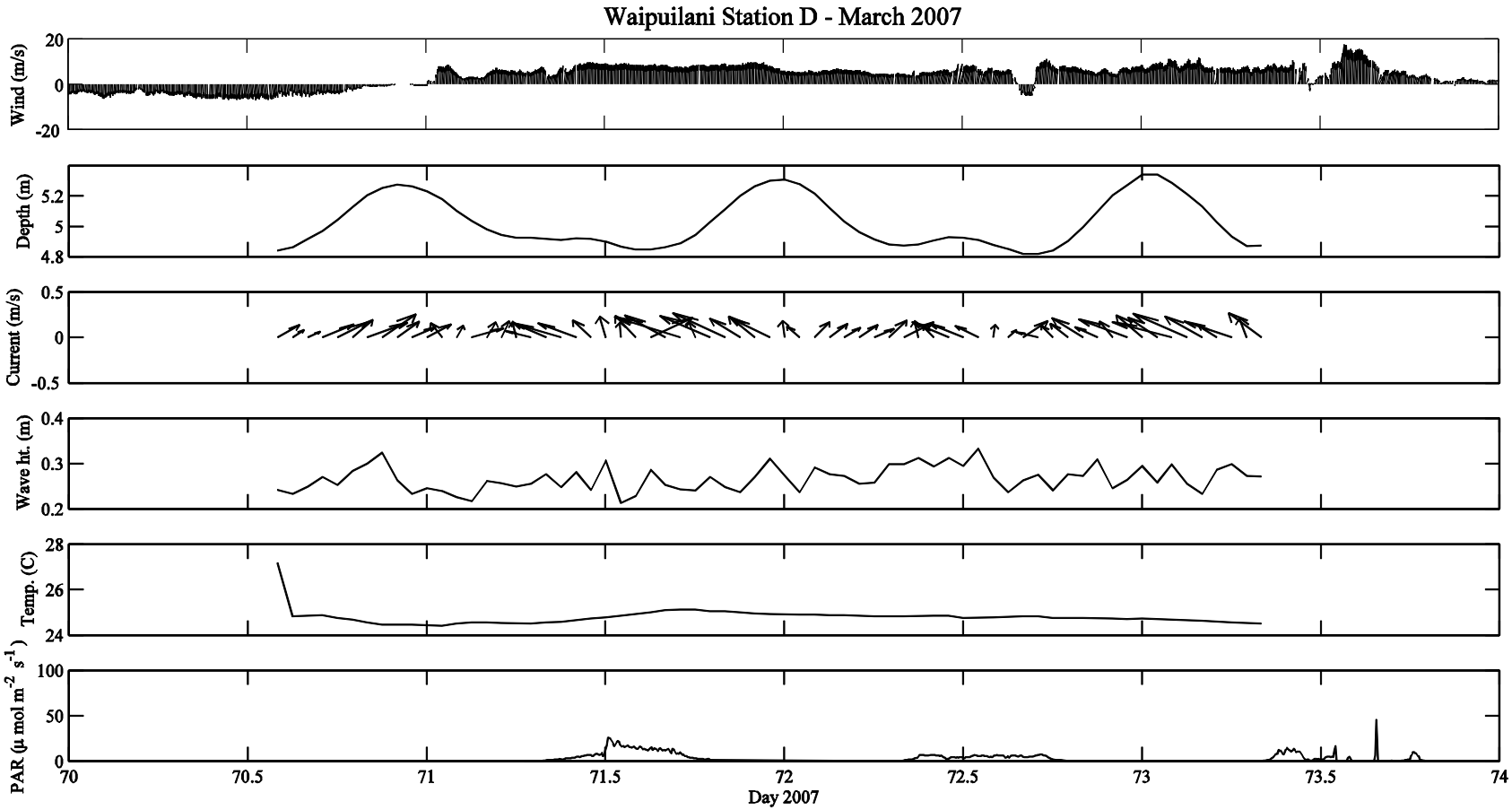

Figure 4.18 - Summary of all time-series data collected at Waipuilani station D during March 2007.

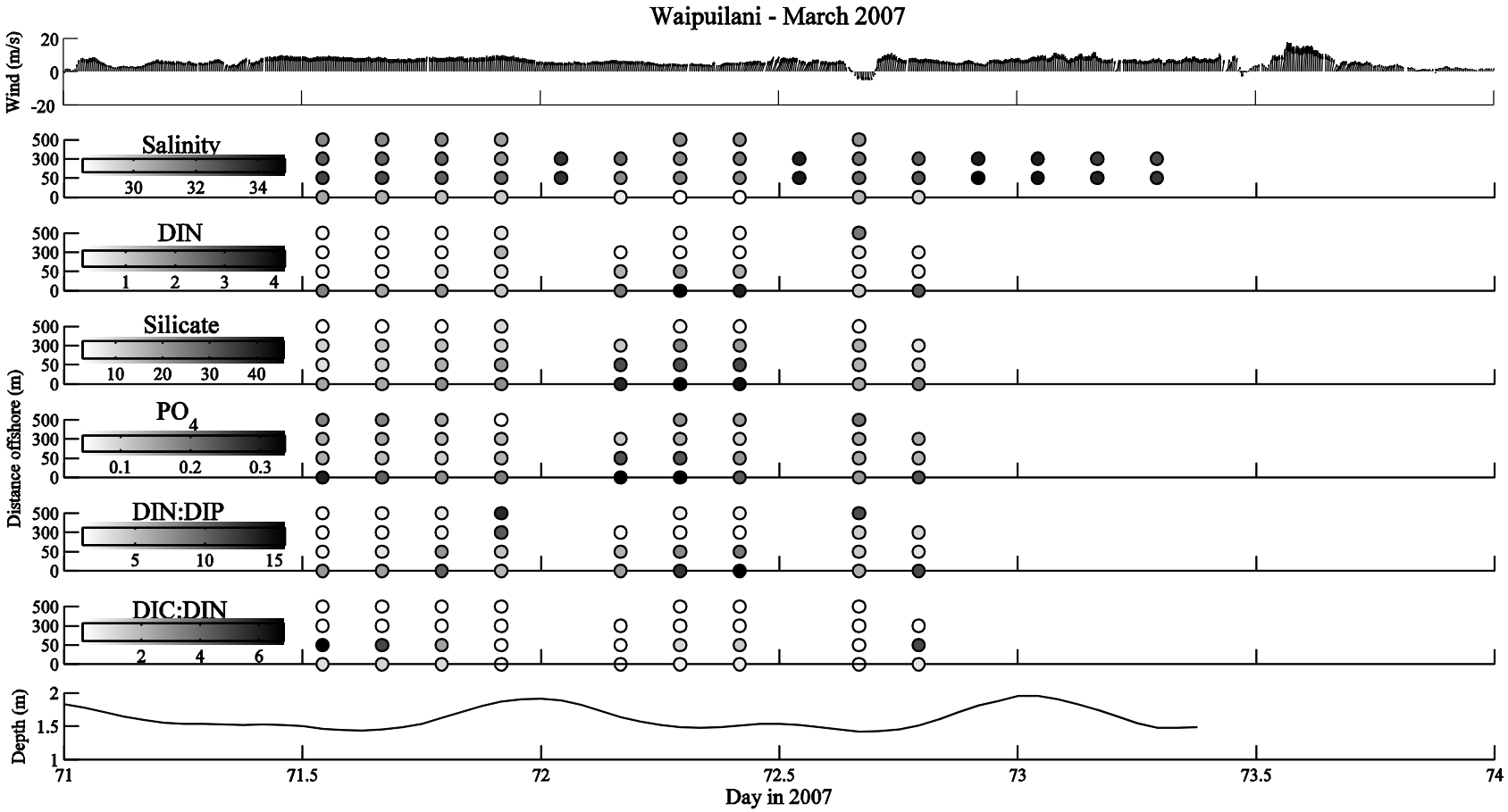

Figure 4.19 - Discrete cross-shore dissolved nutrient and tide height time-series data collected at Waipuilani during March 2007, along with wind speed data collected from WeatherFlow Kihei wind station (see text for details).

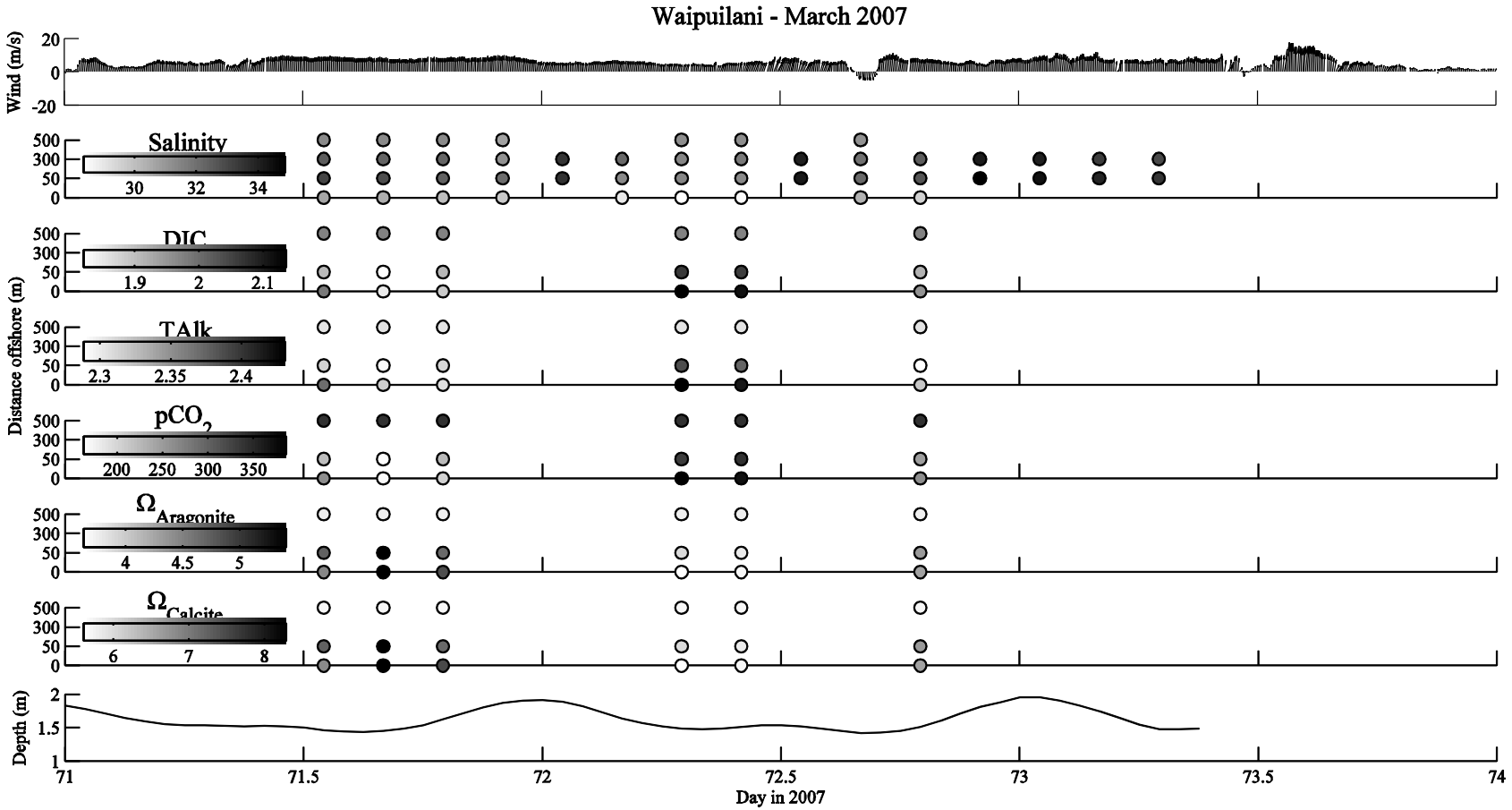

Figure 4.20 - Discrete cross-shore carbonate chemistry and tide height time-series data collected at Waipuilani during March 2007, along with wind speed data collected from WeatherFlow Kihei wind station (see text for details). Offshore (500 m) DIC, Talk, and pCO_2 data are the long-term average surface water chemistry at station ALOHA (Keeling et al. 2004); offshore (500 m) $\Omega_{calcite}$ and $\Omega_{aragonite}$ were calculated using CO2SYS software and DIC and TA; carbonate dissociation constants are from Mehrbach, refit by Dickson and Millero; and K_{SO4} is from Dickson (seawater scale) at 25º C.

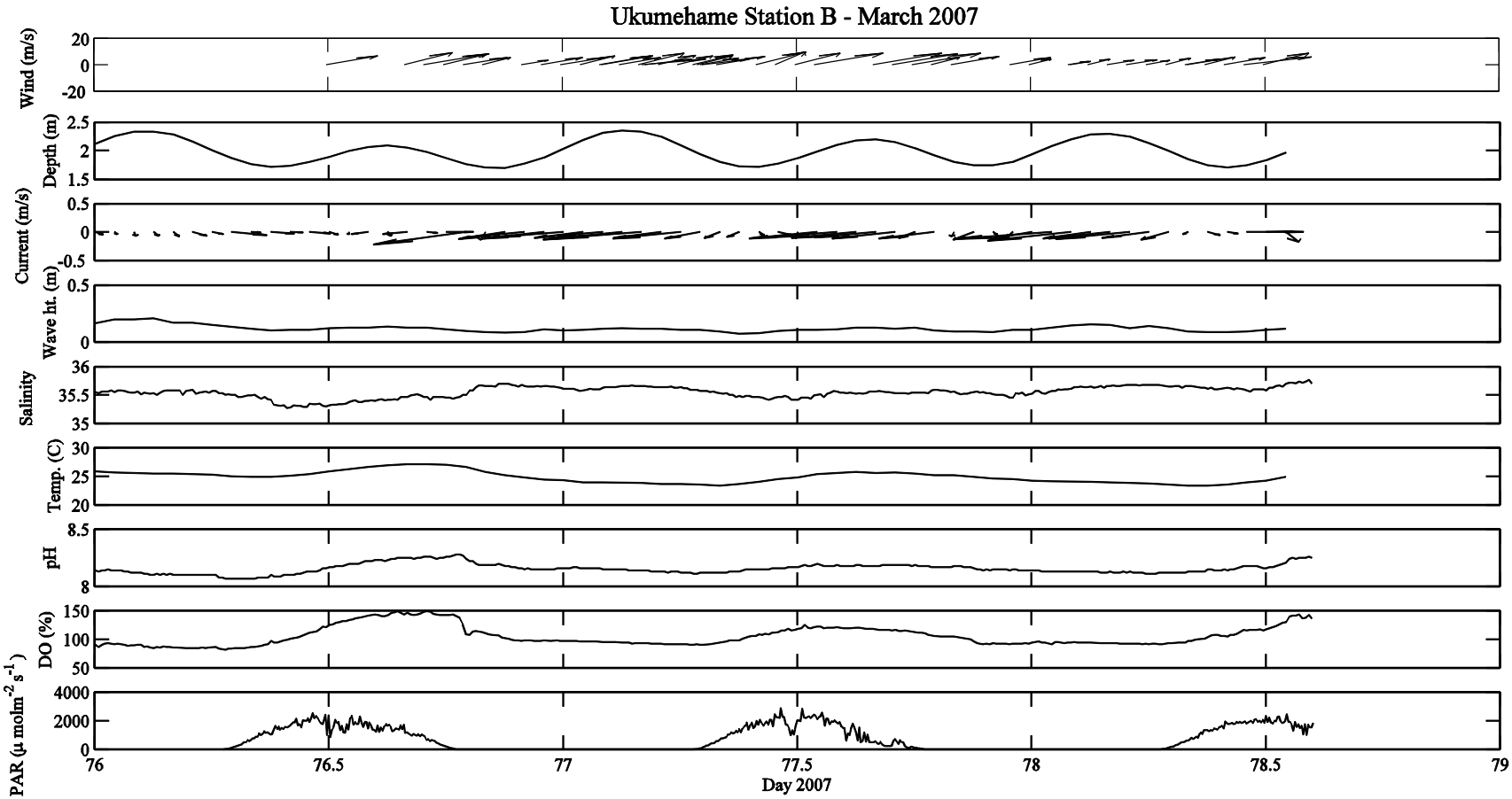

Figure 4.21 - Summary of all time-series data collected at Ukumehame station B during March 2007.

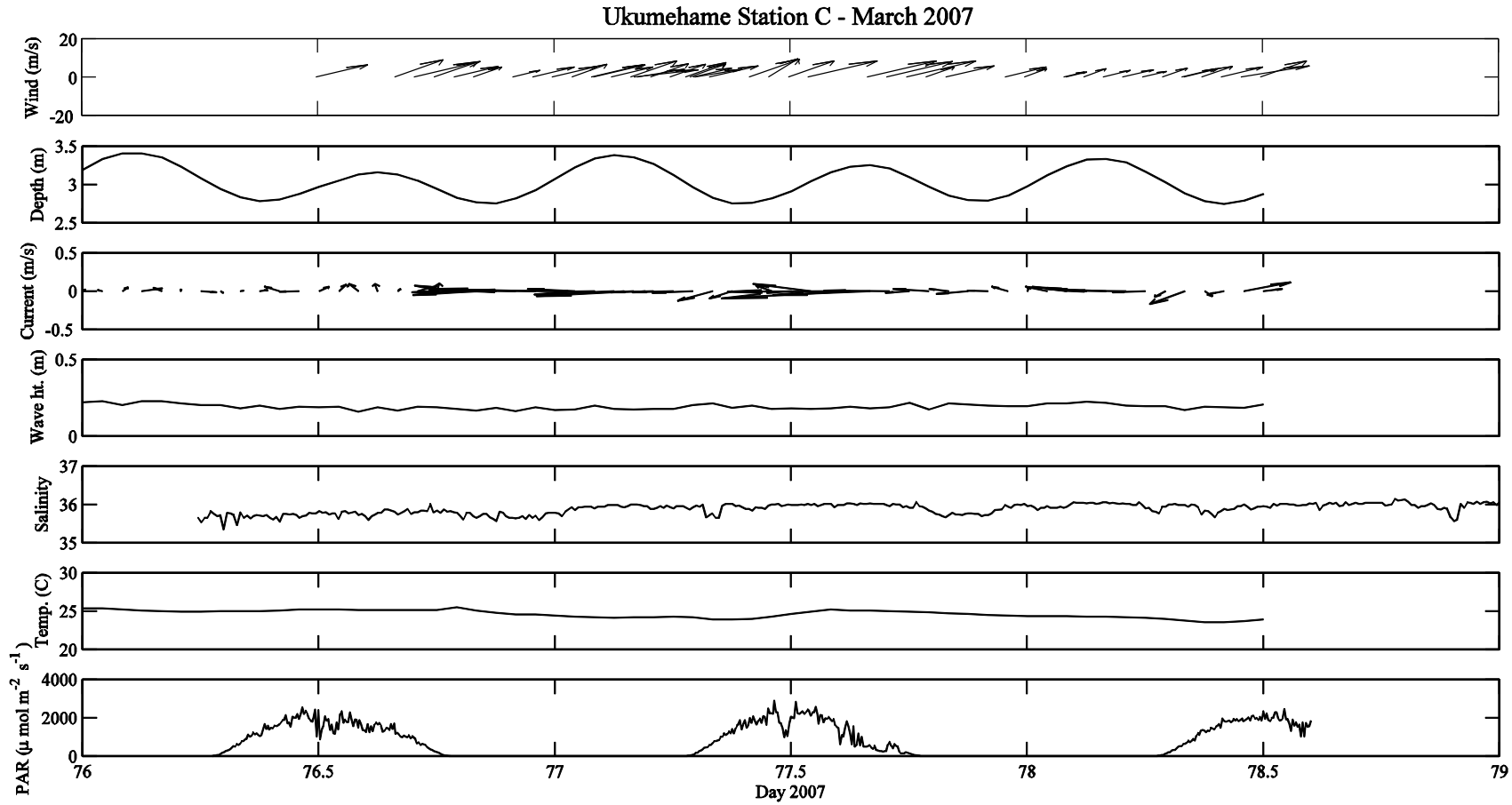

Figure 4.22 - Summary of all time-series data collected at Ukumehame station C during March 2007.

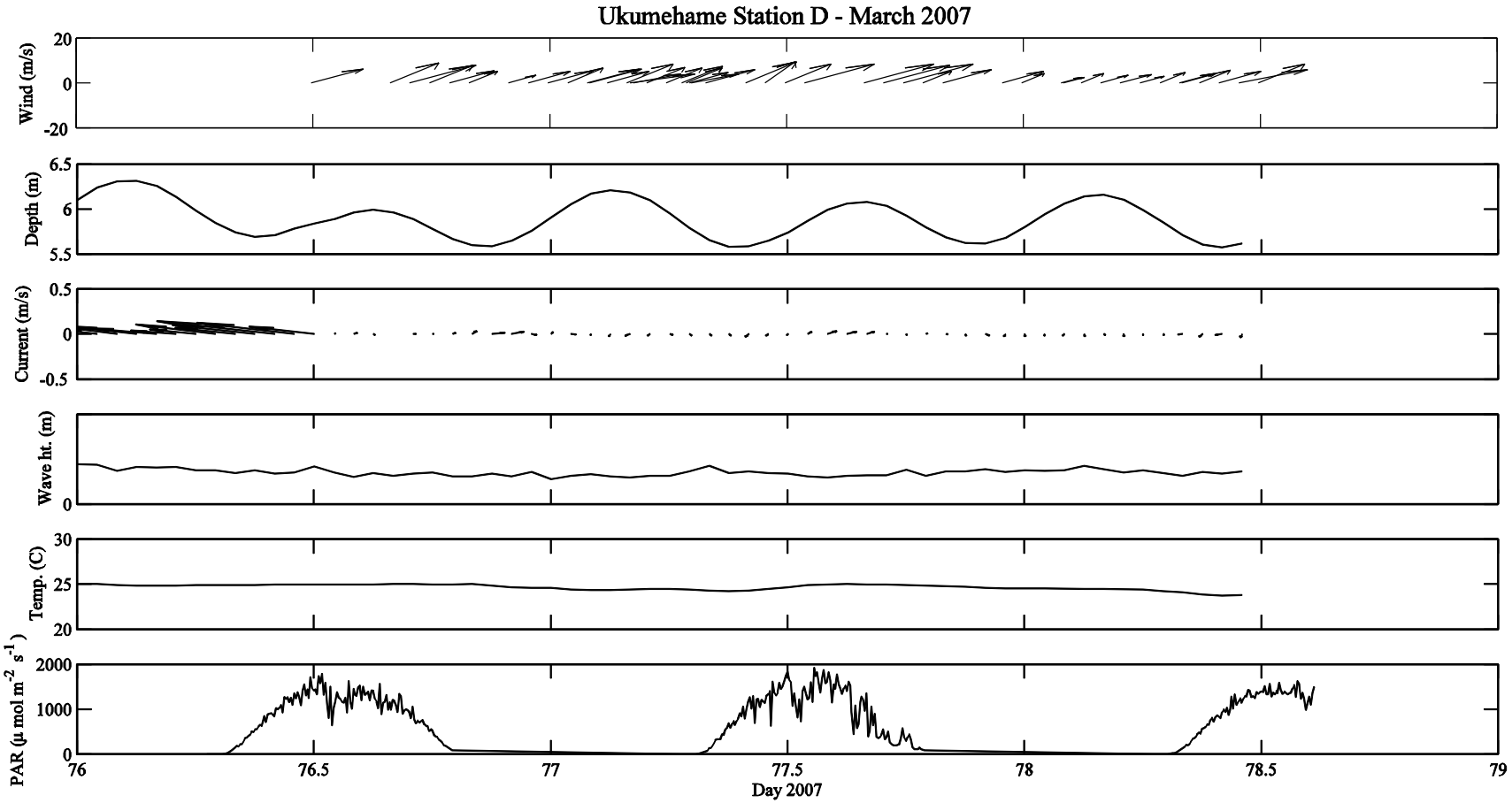

Figure 4.23 - Summary of all time-series data collected at Ukumehame station D during March 2007.

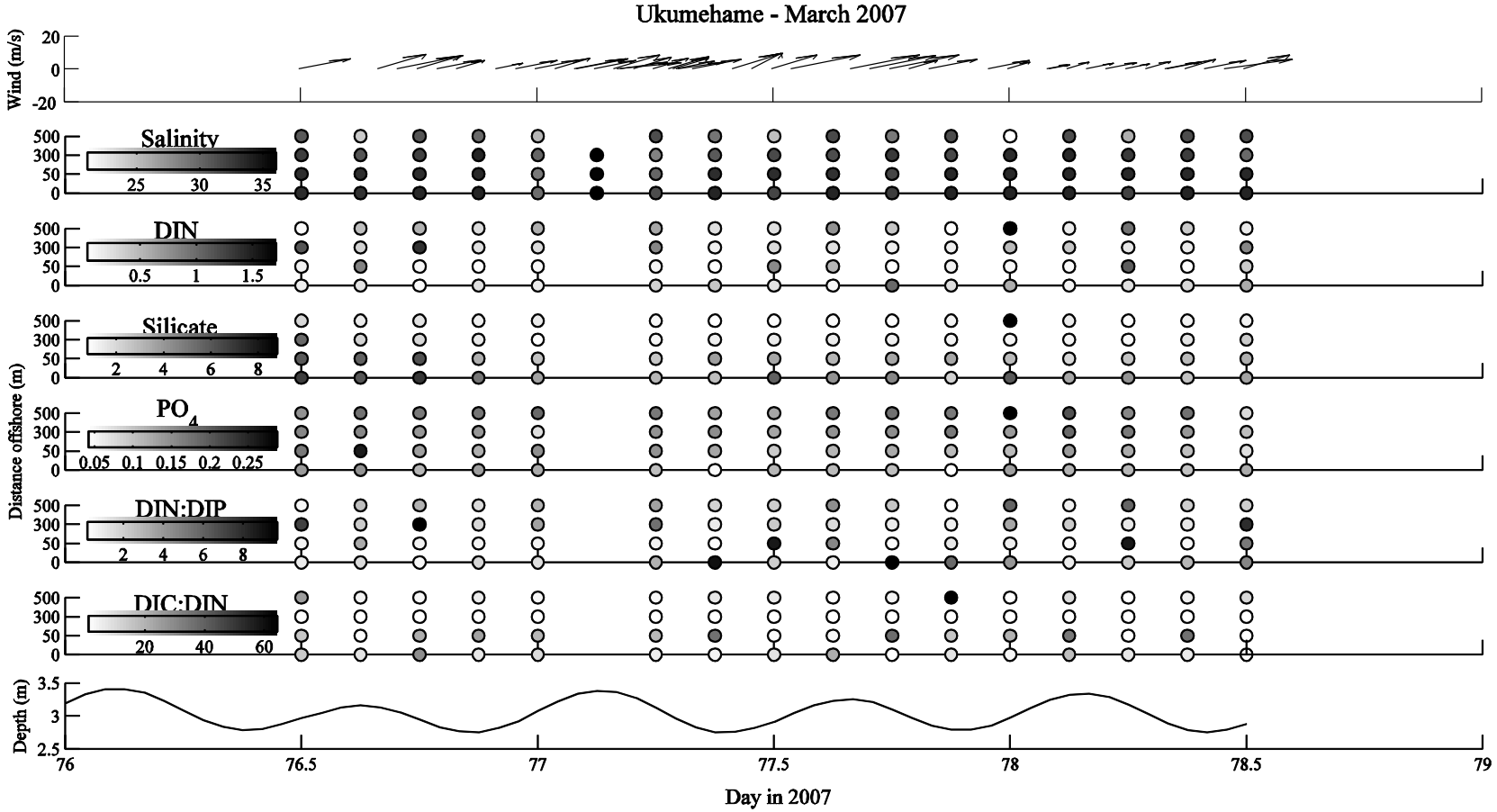

Figure 4.24 - Discrete cross-shore dissolved nutrients and tide height time-series data collected at Ukumehame during March 2007, along with wind speed data collected from the Kahului Airport, Maui (see text for details).

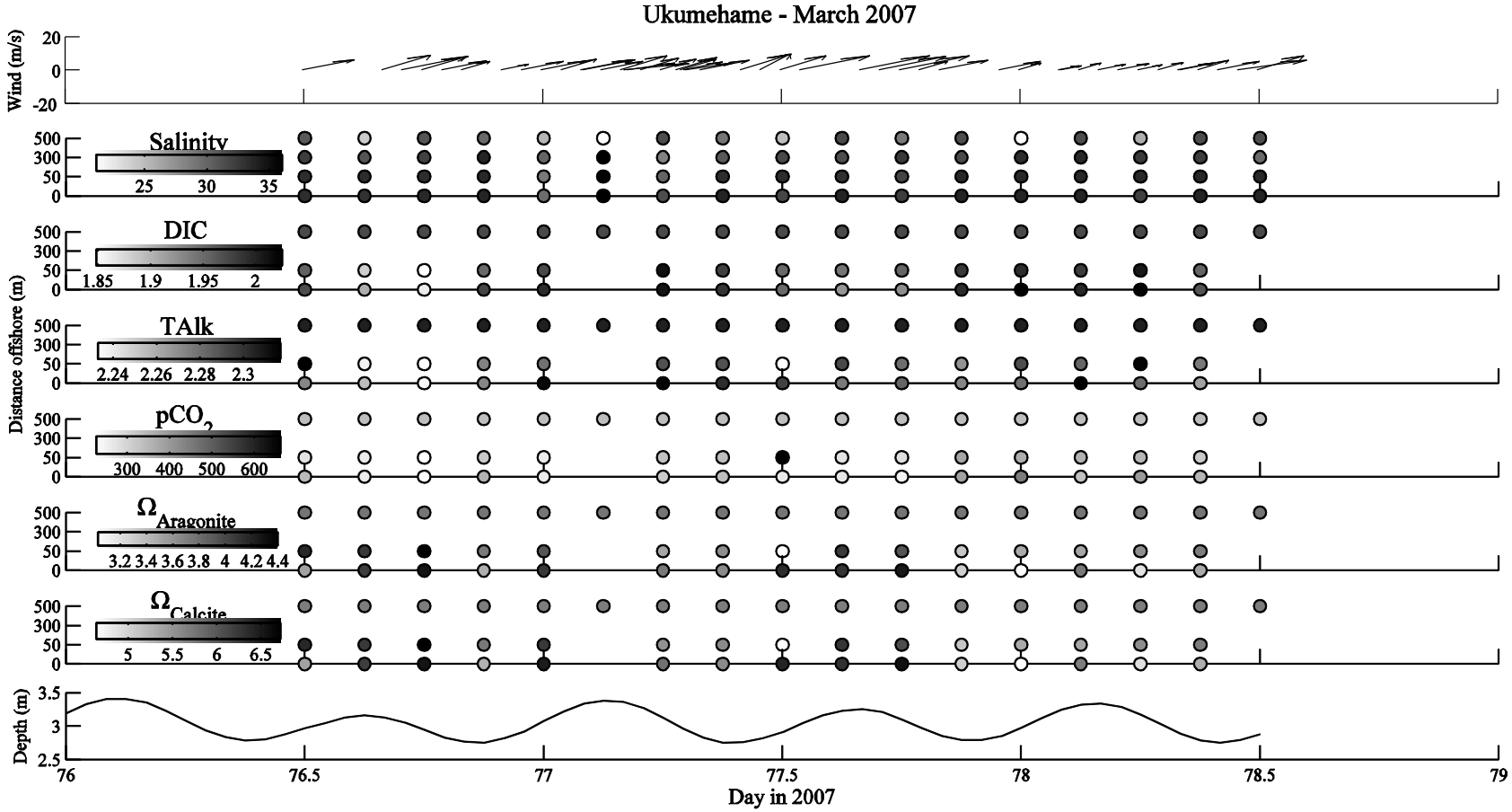

Figure 4.25 - Discrete cross-shore carbonate chemistry and tide height time-series data collected at Ukumehame during March 2007, along with wind speed data collected from the Kahului Airport, Maui (see text for details). Offshore (500 m) DIC, Talk, and pCO_2 data are the long-term average surface water chemistry at station ALOHA (Keeling et al. 2004); offshore (500 m) $\Omega_{calcite}$ and $\Omega_{aragonite}$ were calculated using CO2SYS software and DIC and TA; carbonate dissociation constants are from Mehrbach, refit by Dickson and Millero; and K_{SO4} is from Dickson (seawater scale) at 25º C.

Table 4.1 – Summary of physical data collected at Waipuilani during all observation periods. N = sample count; Q1 = 25% quartile; Q3 =75% quartile.

	Month	Year	N	Mean	StDev	Minimum	Q1	Median	Q3	Maximum
Temperature (ºC)	June	2005	44	26.12	1.00	24.00	25.40	26.01	26.96	28.40
	January	2006	35	25.42	0.38	24.91	25.15	25.33	25.55	26.35
	February	2006	31	25.10	1.19	23.12	24.25	24.90	25.97	27.26
	March	2007	66	24.76	1.11	21.38	24.13	24.84	25.17	27.62
Sigma-t	June	2005	27	20.97	0.75	19.51	20.31	21.02	21.71	21.89
	January	2006	14	21.75	1.22	19.23	20.72	22.14	22.81	23.12
	February	2006	31	20.92	0.60	19.51	20.63	20.79	21.21	22.24
	March	2007	39	20.43	1.38	16.98	19.49	20.41	20.94	23.49
Water Depth (cm)	June	2005	34562	116.9	27.5	81.5	95.9	106.0	134.7	203.1
	January	2006	58800	139.7	23.4	108.6	122.9	131.6	158.1	186.1
	February	2006	58800	137.5	15.8	108.5	124.7	138.3	150.8	166.3
	March	2007	54000	162.6	17.5	92.2	98.3	104.0	130.3	145.6
Wave Height (cm)	June	2005	49	20.8	7.9	8.7	14.6	18.5	28.1	38.6
	January	2006	49	12.4	1.4	9.8	11.2	12.6	13.5	15.6
	February	2006	49	18.2	3.2	12.0	15.5	17.9	20.6	27.3
	March	2007	49	14.4	2.5	10.9	12.5	13.8	15.7	20.8
Water Velocity (cm/s)	June	2005	71280	12.9	1.8	10.6	11.7	12.7	13.5	17.9
	January	2006	58800	11.9	1.1	10.2	11.0	11.7	12.9	14.0
	February	2006	58800	19.1	4.0	13.5	16.2	18.7	22.4	27.1
	March	2007	58800	18.2	1.5	15.5	17.0	18.1	19.2	22.0
Wind Velocity (m/s)	June	2005	566	6.4	3.5	0.0	3.6	6.3	8.5	15.6
	January	2006	568	3.5	1.9	0.0	2.4	3.1	4.7	10.1
	February	2006	571	4.9	2.8	0.0	2.2	5.6	7.2	11.0
	March	2007	65	7.4	1.7	4.0	5.7	7.8	8.5	11.8

Table 4.2 – Summary of surface water salinity and dissolved nutrient data collected at Waipuilani during all observation periods. N = sample count; Q1 = 25% quartile; Q3 =75% quartile.

	Month	Year	N	Mean	StDev	Minimum	Q1	Median	Q3	Maximum
Salinity	June	2005	33	32.19	0.75	30.72	31.52	32.31	32.83	33.39
	January	2006	48	33.09	1.04	29.75	32.60	33.29	33.87	34.85
	February	2006	34	30.77	0.88	28.45	30.41	30.60	31.32	32.80
	March	2007	33	30.14	1.03	26.62	29.50	30.36	30.86	31.41
DIN (µM)	June	2005	34	8.47	6.38	1.03	3.21	6.54	12.51	24.13
	January	2006	46	3.27	3.41	0.19	1.35	2.59	3.79	21.91
	February	2006	34	1.58	0.66	0.65	1.14	1.55	1.86	4.03
	March	2007	32	1.08	1.02	0.18	0.38	0.61	1.52	4.22
DIP (µM)	June	2005	33	0.17	0.06	0.07	0.14	0.17	0.22	0.34
	January	2006	46	0.13	0.05	0.05	0.09	0.13	0.16	0.25
	February	2006	34	0.17	0.07	0.07	0.13	0.17	0.21	0.38
	March	2007	32	0.18	0.06	0.04	0.14	0.17	0.22	0.34
NO_3 (µM)	June	2005	34	7.48	6.27	0.50	2.04	5.37	11.61	21.63
	January	2006	46	1.63	1.62	0.00	0.38	0.98	2.40	6.63
	February	2006	34	0.84	0.55	0.41	0.50	0.68	1.03	3.48
	March	2007	32	0.66	0.68	0.00	0.18	0.33	1.12	2.59
Si (µM)	June	2005	34	49.64	14.42	26.51	41.10	44.54	60.01	79.72
	January	2006	46	23.50	11.55	1.57	13.08	25.34	32.68	49.40
	February	2006	34	23.71	9.69	6.11	16.37	23.50	30.68	45.00
	March	2007	32	18.67	11.21	3.24	10.24	16.88	24.80	45.68
DIN:DIP	June	2005	33	43.0	25.4	14.4	23.5	32.9	58.2	106.3
	January	2006	60	21.7	19.0	2.5	8.8	17.3	27.3	86.8
	February	2006	34	10.2	4.8	3.9	5.8	9.8	13.8	21.8
	March	2007	46	5.3	5.8	0.5	1.9	2.8	6.9	30.4
DIC:DIP	June	2005	33	14820	6147	6769	10763	13201	16447	35086
	January	2006	34	16333	4716	10390	12934	15521	18356	29950
	February	2006	33	14040	5403	5370	10284	12780	15285	28541
	March	2007	12	10903	3680	6377	8152	9877	14014	18192

Table 4.3 – Summary of collected (pH, DIC, and TA) and computed (pCO_2 and Ω) surface water carbonate chemistry at Waipuilani during all observation periods. N = sample count; Q1 = 25% quartile; Q3 =75% quartile. pH sensor failed during January 2006 field deployment.

	Month	Year	N	Mean	StDev	Minimum	Q1	Median	Q3	Maximum
pH	June	2005	26	8.162	0.139	7.961	8.053	8.145	8.214	8.518
	January	2006	0	*	*	*	*	*	*	*
	February	2006	31	8.111	0.140	7.853	8.010	8.110	8.200	8.467
	March	2007	15	8.165	0.097	8.020	8.090	8.167	8.230	8.357
DIC (mmol/kg)	June	2005	34	2.2414	0.1335	1.9342	2.1539	2.2944	2.3340	2.4120
	January	2006	34	2.1650	0.1081	1.9629	2.1126	2.1447	2.1849	2.4879
	February	2006	33	2.1082	0.0985	1.8808	2.0487	2.0884	2.1983	2.2815
	March	2007	12	1.9678	0.1046	1.8206	1.8929	1.9363	2.0650	2.1359
TA (mmol/kg)	June	2005	34	2.6246	0.0842	2.4145	2.6011	2.6383	2.6781	2.7721
	January	2006	34	2.5416	0.0914	2.3982	2.4799	2.5180	2.5971	2.8647
	February	2006	33	2.5043	0.0977	2.3546	2.4208	2.5013	2.5635	2.7032
	March	2007	12	2.3444	0.0491	2.2886	2.3093	2.3192	2.3850	2.4307
pCO_2 (µatm)	June	2005	34	368.1	120.5	144.6	270.9	379.6	457.5	563.7
	January	2006	34	387.8	303.7	174.9	268.3	319.8	393.2	1997.5
	February	2006	34	286.4	102.8	0.0	215.2	285.0	343.6	500.2
	March	2007	12	265.3	76.0	163.6	208.1	254.5	341.0	386.0
Ω Aragonite	June	2005	34	4.57	1.00	3.28	3.88	4.24	4.88	7.64
	January	2006	34	4.43	1.08	1.15	3.88	4.41	4.97	7.44
	February	2006	33	4.73	0.93	3.29	3.97	4.69	5.33	6.74
	March	2007	12	4.43	0.62	3.63	3.81	4.41	4.85	5.41
Ω Calcite	June	2005	34	6.97	1.53	5.00	5.92	6.48	7.46	11.67
	January	2006	34	6.74	1.63	1.75	5.90	6.71	7.57	11.32
	February	2006	33	7.25	1.43	5.03	6.06	7.19	8.15	10.32
	March	2007	12	6.81	0.93	5.61	5.86	6.76	7.44	8.29

Table 4.4 - Summary of 7 cm well porewater salinity and dissolved nutrient data collected at Waipuilani during all observation periods. N = sample count; Q1 = 25% quartile; Q3 =75% quartile.

	Month	Year	N	Mean	StDev	Minimum	Q1	Median	Q3	Maximum
Salinity	June	2005	32	32.36	0.94	30.84	31.90	32.23	32.62	35.49
	January	2006	33	33.49	0.99	32.09	32.78	33.50	33.97	36.69
	February	2006	28	30.86	1.12	29.64	30.07	30.64	31.43	35.32
	March	2007	10	30.04	0.65	28.74	29.57	30.30	30.51	30.78
DIN (µM)	June	2005	33	31.91	23.79	3.38	7.37	31.88	53.89	80.35
	January	2006	33	52.20	58.00	2.40	11.50	19.50	110.20	173.50
	February	2006	28	6.58	5.08	1.13	2.40	4.53	11.26	18.88
	March	2007	10	5.91	7.04	0.48	1.10	4.71	6.84	23.87
DIP (µM)	June	2005	33	0.49	0.19	0.18	0.29	0.57	0.64	0.74
	January	2006	33	0.60	0.31	0.14	0.37	0.54	0.89	1.17
	February	2006	28	0.29	0.12	0.13	0.18	0.25	0.35	0.52
	March	2007	10	0.28	0.13	0.12	0.18	0.26	0.37	0.51
NO_3 (µM)	June	2005	33	6.28	6.05	0.04	1.50	3.75	10.04	18.51
	January	2006	33	2.88	2.52	0.09	0.87	1.73	4.60	8.51
	February	2006	28	1.74	1.18	0.47	0.85	1.50	2.17	5.57
	March	2007	10	2.31	1.66	0.31	0.58	2.30	3.83	4.73
Si (µM)	June	2005	33	58.97	13.18	36.16	46.42	63.61	69.50	78.78
	January	2006	33	37.99	14.86	17.98	27.37	33.63	53.15	66.72
	February	2006	28	30.79	10.44	13.67	22.90	29.86	41.85	46.03
	March	2007	10	27.06	5.29	19.76	23.75	26.23	29.15	39.70
DIN:DIP	June	2005	33	58.53	34.24	10.59	117.91	59.63	23.18	86.00
	January	2006	33	66.03	51.40	14.53	210.78	40.86	27.44	104.18
	February	2006	28	20.92	10.61	4.90	41.45	21.73	12.76	29.91
	March	2007	10	20.18	23.07	2.16	80.31	12.96	5.38	27.37
DIC:DIP	June	2005	33	5996	2658	3244	12612	4768	3984	7899
	January	2006	32	4947	2183	2492	10906	4276	3293	5998
	February	2006	28	8781	3151	4534	15129	8367	6136	11834
	March	2007	10	8917	4399	4081	17917	7927	5453	11799

Table 4.5 - Summary of collected (DIC and TA) and computed (pCO_2 and Ω) 7 cm porewater carbonate chemistry data collected at Waipuilani during all observation periods. N = sample count; Q1 = 25% quartile; Q3 =75% quartile.

	Month	Year	N	Mean	StDev	Minimum	Q1	Median	Q3	Maximum
DIC (mmol/kg)	June	2005	33	2.4626	0.2151	1.9714	2.3047	2.4575	2.6662	2.8014
	January	2006	32	2.4923	0.3907	2.0477	2.2178	2.3235	2.8592	3.4204
	February	2006	29	2.1873	0.1567	1.9392	2.0604	2.1398	2.3382	2.4475
	March	2007	10	2.0508	0.0459	1.9797	2.0145	2.0517	2.0948	2.1145
TA (mmol/kg)	June	2005	32	2.5913	0.1015	2.3406	2.5574	2.5910	2.6567	2.8167
	January	2006	32	2.8026	0.3777	2.3693	2.5167	2.6498	3.2087	3.7936
	February	2006	29	2.5407	0.1263	2.3612	2.4513	2.5235	2.6274	2.7732
	March	2007	10	2.3305	0.0411	2.2603	2.2900	2.3406	2.3562	2.3942
pCO_2 (µatm)	June	2005	32	1926.0	1984.0	283.0	623.0	1000.0	2464.0	7084.0
	January	2006	34	585.9	312.3	0.0	424.9	537.2	796.4	1279.5
	February	2006	29	380.1	153.3	173.2	259.2	354.1	474.5	824.0
	March	2007	10	401.2	56.2	330.0	365.6	384.7	441.7	507.6
Ω Aragonite	June	2005	32	2.09	1.16	0.36	1.04	2.14	3.02	4.22
	January	2006	32	3.82	1.57	2.27	3.15	3.46	4.00	11.57
	February	2006	29	4.26	0.97	2.38	3.71	4.16	4.89	6.79
	March	2007	10	3.36	0.29	2.85	3.08	3.48	3.59	3.68
Ω Calcite	June	2005	32	3.19	1.76	0.56	1.59	3.26	4.61	6.44
	January	2006	32	5.82	2.39	3.47	4.78	5.28	6.10	17.60
	February	2006	29	6.52	1.49	3.66	5.67	6.39	7.47	10.42
	March	2007	10	5.16	0.45	4.36	4.73	5.35	5.52	5.65

Table 4.6 - Summary of 25 cm porewater salinity and dissolved nutrient data collected at Waipuilani during all observation periods. N = sample count; Q1 = 25% quartile; Q3 =75% quartile.

	Month	Year	N	Mean	StDev	Minimum	Q1	Median	Q3	Maximum
Salinity	June	2005	32	32.32	0.65	30.71	32.10	32.43	32.64	33.95
	January	2006	34	33.16	0.80	31.71	32.63	33.15	33.91	34.49
	February	2006	33	30.52	0.84	29.26	29.81	30.61	31.06	32.62
	March	2007	9	29.04	3.25	20.74	28.76	30.25	30.67	30.85
DIN (µM)	June	2005	34	10.93	5.94	2.95	6.35	9.55	15.90	22.36
	January	2006	34	22.44	22.56	0.97	5.29	16.45	25.35	74.68
	February	2006	33	40.41	43.82	1.09	3.06	19.59	76.54	124.44
	March	2007	7	5.61	3.61	1.15	3.24	5.33	6.33	12.79
DIP (µM)	June	2005	34	0.30	0.10	0.12	0.21	0.29	0.41	0.49
	January	2006	34	0.51	0.29	0.09	0.30	0.42	0.59	1.21
	February	2006	33	0.61	0.44	0.13	0.24	0.36	0.97	1.52
	March	2007	7	0.34	0.07	0.21	0.33	0.33	0.40	0.43
NO_3 (µM)	June	2005	34	7.88	6.34	1.58	3.16	4.40	12.61	21.56
	January	2006	34	4.22	3.82	0.14	1.37	3.07	6.77	15.14
	February	2006	33	2.12	3.04	0.03	0.18	1.07	2.90	14.98
	March	2007	7	3.28	1.54	0.55	2.78	2.90	4.43	5.26
Si (µM)	June	2005	34	52.44	8.12	39.11	46.59	51.26	56.69	72.80
	January	2006	34	38.19	13.60	9.94	27.61	39.61	49.91	58.08
	February	2006	33	38.70	16.43	14.12	22.72	44.96	53.33	58.83
	March	2007	7	25.68	2.97	21.34	23.40	24.83	28.75	29.24
DIN:DIP	June	2005	34	36.69	19.94	7.31	71.62	36.89	17.97	51.12
	January	2006	33	51.31	53.44	8.52	273.59	38.48	12.33	81.70
	February	2006	7	15.32	7.58	5.54	29.52	14.78	9.78	18.99
	March	2007	34	38.59	22.35	11.56	112.64	35.25	18.06	51.65
DIC:DIP	June	2005	32	6754	5102	2222	23724	5432	3841	7206
	January	2006	33	6364	4179	1797	16224	5919	2738	8563
	February	2006	6	6214	1915	4629	9988	5807	5013	6930
	March	2007	33	8771	3393	4584	18140	8280	5875	11625

Table 4.7 - Summary of collected (DIC and TA) and computed (pCO_2 and Ω) 25 cm porewater carbonate chemistry data collected at Waipuilani during all observation periods. N = sample count; Q1 = 25% quartile; Q3 =75% quartile.

	Month	Year	N	Mean	StDev	Minimum	Q1	Median	Q3	Maximum
DIC (mmol/kg)	June	2005	33	2.3427	0.1253	2.0881	2.2502	2.3954	2.4294	2.5188
	January	2006	32	2.3746	0.2213	2.0404	2.1860	2.3528	2.5240	2.9458
	February	2006	33	2.3444	0.2862	1.9073	2.0872	2.3240	2.6244	2.7678
	March	2007	6	2.0185	0.0602	1.9339	1.9616	2.0216	2.0754	2.0933
TA (mmol/kg)	June	2005	33	2.6843	0.1536	2.4156	2.5643	2.7010	2.7661	2.9678
	January	2006	32	2.6169	0.1797	2.1638	2.4675	2.6244	2.7488	2.9659
	February	2006	33	2.6796	0.2674	2.3245	2.4029	2.6660	2.9643	3.1681
	March	2007	5	2.3040	0.0282	2.2801	2.2821	2.2864	2.3348	2.3351
pCO_2 (µatm)	June	2005	32	468.4	175.3	142.6	332.1	453	585.8	820.1
	January	2006	34	789	1356	0	356	547	732	8256
	February	2006	33	459.4	180.9	101.9	317.9	425.7	590	797.8
	March	2007	5	408.5	84.7	274.8	330.2	424.9	478.7	487.2
Ω Aragonite	June	2005	32	4.21	1.37	2.51	3.20	3.71	5.25	7.65
	January	2006	32	3.26	1.26	0.12	2.85	3.41	3.73	6.74
	February	2006	33	4.14	1.23	2.92	3.35	3.97	4.32	9.85
	March	2007	5	3.30	0.47	2.91	2.93	3.22	3.71	4.08
Ω Calcite	June	2005	32	6.42	2.09	3.83	4.88	5.65	8.00	11.66
	January	2006	32	4.97	1.91	0.18	4.32	5.19	5.69	10.24
	February	2006	33	6.35	1.89	4.49	5.13	6.08	6.61	15.09
	March	2007	5	5.06	0.73	4.46	4.49	4.94	5.68	6.26

Table 4.8 - Summary of all data collected at Ukumehame during the March 07 observation period. pH (calc) is the pH calculated from CO2SYS model using TA and DIC data. N = sample count; Q1 = 25% quartile; Q3 =75% quartile.

	Month	Year	N	Mean	StDev	Minimum	Maximum	Median	Q1	Q3
WC										
Temperature (ºC)	March	2007	102	24.6	1.0	22.9	27.8	24.4	23.8	25.1
Salinity	March	2007	86	29.65	2.88	19.60	31.84	31.30	28.29	31.54
Sigma-t	March	2007	94	20.8	2.4	11.7	24.6	21.1	20.1	22.4
Water Depth (cm)	March	2007	102	366.3	171.2	149.0	630.0	306.3	210.0	577.8
Wave Height (cm)	March	2007	50	0.2	0.0	0.1	0.2	0.2	0.1	0.2
Water Velocity (cm/s)	March	2007	51	3.5	2.6	0.4	16.9	3.0	1.9	4.3
Wind Velocity (m/s)	March	2007	47	6.96	2.07	3.10	10.30	6.70	5.70	8.45
pH	March	2007	17	8.164	0.038	8.110	8.260	8.160	8.135	8.180
DIC (mmol/kg)	March	2007	30	1962.7	44.2	1848.7	2024.9	1972.9	1948.7	1992.7
TA (mmol/kg)	March	2007	30	2205.6	417.2	0.0	2317.0	2280.2	2272.1	2293.8
pCO_2 (µatm)	March	2007	30	329.1	82.4	227.2	662.0	326.1	266.4	358.1
Ω Aragonite	March	2007	30	3.6	0.8	0.0	4.4	3.7	3.5	4.1
Ω Calcite	March	2007	30	5.6	1.2	0.0	6.7	5.7	5.3	6.3
pH (calc)	March	2007	30	8.155	0.720	4.360	8.390	8.270	8.230	8.333
DIN (µM)	March	2007	86	0.41	0.41	0.00	1.96	0.29	0.13	0.51
DIP (µM)	March	2007	86	0.14	0.04	0.04	0.29	0.14	0.12	0.17
NO_3 (µM)	March	2007	86	0.14	0.26	0.00	1.80	0.06	0.00	0.17
$Si(OH)_4$ (µM)	March	2007	86	2.56	1.82	0.54	8.82	1.89	1.21	3.55
DIN:DIP	March	2007	86	3.02	2.79	0.00	11.56	2.11	0.88	4.22
DIC:DIP	March	2007	30	17810	7991	7239	49796	16453	14115	18299
PW7										
Salinity	March	2007	29	29.78	3.40	21.72	31.98	31.45	29.84	31.57
DIC (mmol/kg)	March	2007	27	2331.3	164.0	1960.1	2557.9	2272.5	2216.7	2490.9
TA (mmol/kg)	March	2007	27	2504.1	135.2	2227.3	2707.8	2458.7	2395.9	2635.7
pCO_2 (µatm)	March	2007	27	851.1	249.8	393.2	1263.3	915.5	646.2	1048.1
Ω Aragonite	March	2007	27	3.6	0.7	2.7	6.1	3.3	3.1	3.8
Ω Calcite	March	2007	27	2.3	0.5	1.8	4.0	2.2	2.0	2.5
pH (calc)	March	2007	27	7.971	0.115	7.820	8.240	7.930	7.870	8.040
DIN (µM)	March	2007	29	6.16	5.09	0.17	19.48	5.47	2.15	8.59
DIP (µM)	March	2007	29	0.72	0.42	0.14	1.46	0.55	0.38	1.07
NO_3 (µM)	March	2007	29	0.66	0.53	0.02	1.78	0.53	0.25	1.10
$Si(OH)_4$ (µM)	March	2007	29	35.88	27.52	6.71	79.11	17.96	13.05	65.63
DIN:DIP	March	2007	29	8.20	3.99	0.43	18.90	7.56	5.14	10.56
DIC:DIP	March	2007	27	4109	2338	1690	11231	3655	1961	4900
PW25										
Salinity	March	2007	31	30.73	1.54	25.46	31.94	31.35	31.06	31.48
DIC (mmol/kg)	March	2007	29	2481.2	201.9	2256.5	2868.0	2437.4	2299.8	2600.1
TA (mmol/kg)	March	2007	29	2667.1	243.5	2401.5	3185.5	2614.9	2462.4	2821.0
pCO_2 (µatm)	March	2007	29	883.6	169.8	512.6	1190.5	877.0	765.3	1008.2
Ω Aragonite	March	2007	29	3.9	1.0	2.5	6.7	3.6	3.1	4.6
Ω Calcite	March	2007	29	2.5	0.7	1.6	4.4	2.3	2.0	3.0
pH (calc)	March	2007	29	7.966	0.095	7.800	8.170	7.940	7.900	8.040
DIN (µM)	March	2007	31	51.34	55.26	4.37	180.65	18.15	11.02	85.71
DIP (µM)	March	2007	31	0.64	0.37	0.01	1.85	0.64	0.45	0.74
NO_3 (µM)	March	2007	31	0.36	0.38	0.00	1.27	0.24	0.10	0.38
$Si(OH)_4$ (µM)	March	2007	31	25.88	4.60	16.01	32.89	24.53	23.01	30.86
DIN:DIP	March	2007	31	594.7	2710.2	10.4	15166.0	24.2	15.3	139.6
DIC:DIP	March	2007	29	15258	52303	1339	284908	3693	3139	5187

Table 4.9 - Summary of inland groundwater well data for WAI and UKU, and mean coastal water chemistry. Salinity and nutrient data were obtained from Herzfeld (unpublished data). Offshore DIC, TA, and pCO_2 data are the long-term average surface water chemistry at station ALOHA (Keeling et al. 2004); pH at Waipuilani, and offshore $\Omega_{calcite}$ and $\Omega_{aragonite}$ were calculated using CO2SYS software and DIC and TA with carbonate dissociation constants from Mehrbach (1973), refit by Dickson and Millero (1987), and K_{SO4} from Dickson (1990) (seawater scale) at 25º C. Asterisks denote missing data.

	Land Well		
	Waipuilani	**Ukumehame**	**Offshore**
Salinity	0.83 (0.18) n=31	0.37 (0.01) n=3	34.21 (0.53), n=158
PO_4 (µM)	3.70 (0.43, n= 32)	0.92 (0.17) n=3	0.09 (0.03), n=164
Si (µM)	452.5 (18.65, n= 32)	1064 (19.35) n=3	3.50 (2.84), n=164
NO_3 (µM)	163.1 (5.58, n= 32)	181.8 (1.08) n=3	0.15 (0.20), n=164
NO_2 (µM)	0.05 (0.03, n= 32)	0.00 (0.00) n=3	0.02 (0.01), n=164
NH_4 (µM)	0.04 (0.11, n= 32)	0.54 (0.08) n=3	0.15 (0.27), n=164
DIN (µM)	163.2 (5.58, n= 32)	182.3 (1.16) n=3	0.32 (0.35), n=164
DIC (mmol/kg)	3546 (204.0, n= 32)	*	1.974
TA (mmol/kg)	3677 (258.7, n= 32)	*	2.306
$p\,CO_2$ (µatm)	1184 (410.8, n= 32)	*	341.8
pH	8.20 (0.21, n= 32)	*	8.2
Ω calcite	3.31 (2.23, n= 32)	*	5.71
Ω aragonite	1.98 (1.32, n= 32)	*	3.76
DIN:DIP	44.54 (4.25, n= 32)	202.7 (36.8, n = 3)	3.90 (3.20, n = 164)
DIC:DIP	966.4 (131.72, n= 31)	*	*

Table 4.10 - Mean and standard deviation of the theoretical particle travel distance per 3-hour observational period.

Site/Month	Year	Distance Offshore (m)	Stn.	Current Speed (m/s)	Current Direction (degrees)	Particle Travel per 3-h Period (m)
Waipuilani						
January	2006	50	B	0.04 (0.02)	210 (71)	430 (217)
February	2006	50	B	0.04 (0.03)	203 (62)	481 (331)
March	2007	50	B	0.05 (0.03)	207 (118)	552 (360)
January	2006	300	C	0.03 (0.02)	161 (88)	377 (198)
February	2006	300	C	0.06 (0.05)	240 (77)	647 (531)
March	2007	300	C	0.05 (0.02)	223 (97)	521 (256)
January	2006	500	D	0.07 (0.04)	148 (99)	733 (464)
March	2007	500	D	0.03 (0.01)	249 (115)	294 (125)
Ukumehame						
March	2007	50	B	0.03 (0.02)	195 (40)	325 (187)
March	2007	250	C	0.03 (0.02)	185 (113)	342 (238)
March	2007	500	D	0.04 (0.03)	183 (85)	459 (377)

Table 4.11 - Summary of mean (standard deviation) macroalgae growth, uptake rate, tissue composition and uptake molar ratios during June 2005, January 2006, and March 2007 experiments performed at WAI and UKU. No tissue analyses were performed for samples collected during March 2007. Asterisk (*) denotes data from Smith and Smith, 2006. Italicized data were calculated from average tissue composition from June 2005 and January 2006 sampling periods.

			Uptake rate				Tissue composition					Uptake molar ratio			
Month-Yr	**Site**	**Algae**	**mg dry/hr**	**µmol C/hr**	**µmol N/hr**	**µmol P/hr**	**%C**	**%N**	**%P**	**del 15N**	**del 13C**	**C:P**	**N:P**	**C:N**	**C:N:P**
JUNE 05*	WAI	Hypnea	0.61 (0.19)	11.97 (3.79)	1.22 (0.42)	0.03 (0.01)	23.70 (1.33)	2.79 (0.25)	0.15 (0.03)	6.23 (0.62)	-17.12 (1.49)	392.6 (41.8)	39.6 (3.2)	9.9 (0.8)	393:40:1
JAN 06*	WAI	Hypnea	0.97 (0.23)	19.01 (4.55)	2.12 (0.57)	0.04 (0.01)	23.66 (1.10)	3.05 (0.22)	0.14 (0.02)	5.74 (0.72)	-20.81 (1.06)	442.8 (59.2)	48.7 (4.7)	9.1 (0.7)	443:49:1
MARCH 07	WAI	Hypnea	-0.10 (1.17)	*-1.97*	*-0.21*	*0.00*									
MARCH 07	UKU	Hypnea	1.23 (0.64)	*24.26*	*2.57*	*0.06*						*421.7*	*44.6*	*9.5*	*421:45:1*
JUNE 05*	WAI	Ulva	0.86 (0.40)	16.38 (7.46)	1.09 (0.49)	0.02 (0.01)	22.77 (1.74)	1.74 (0.27)	0.08 (0.01)	5.76 (0.58)	-16.97 (0.75)	758.7 (129.2)	50.2 (10.4)	15.2 (1.2)	759:50:1
JAN 06*	WAI	Ulva	1.05 (0.28)	20.92 (5.86)	1.81 (0.58)	0.03 (0.01)	24.57 (2.71)	2.46 (0.38)	0.07 (0.02)	5.58 (0.63)	-19.22 (1.64)	950.0 (326.5)	79.8 (23.5)	11.8 (1.0)	950:80:1
MARCH 07	WAI	Ulva	0.98 (1.11)	*19.33*	*1.47*	*0.02*						*815.3*	*62.0*	*13.2*	*815:62:1*
MARCH 07	UKU	Ulva	2.99 (1.31)	*58.98*	*4.49*	*0.07*						*815.3*	*62.0*	*13.2*	*815:62:1*
Weighed Average												*655.1*	*54.2*	*11.0*	*655:54:1*

Table 4.12 - Mean (standard deviation) apparent water residence time estimated using various tracers

		Apparent Residence Time (h)			
Site/Month	Year	Salt	Current Meter	Radium	Radon
Waipuilani					
June	2005	2.5 (0.6, n=16)	1.1 (0.2, n=17)		
January	2006	2.7 (0.4, n=16)	4.4 (2.6, n=17)	5.6 (0.9, n=8)	
February	2006	2.8 (0.5, n=16)	3.7 (2.3, n=17)		
March	2007	2.7 (0.3, n=14)	3.7 (2.2, n=15)	5.9 (0.3, n=12)	2.8 (0.3, n=10)
Ukumehame					
March	2007	2.8 (0.3, n=16)	5.4 (2.6, n=17)	5.9 (0.5, n=12)	2.3 (1.3, n=11)

Table 4.13 - Summary of fresh groundwater flux estimates and net metabolic state of WAI and UKU during the different observation periods (l.d. = limited dataset). See text for description of terms.

		WAI				UKU
Parameter	Units	June 05	January 06	February 06	March 07	March 07
Fluxes						
SGD_{fresh} DIC Flux	$mol/m^2/day$	2.8 (2.4)	3.4 (1)	1 (0.4)	l.d.	2.3 (1.6)
SGD_{fresh} DIN Flux	$mol/m^2/day$	0.13 (0.11)	0.1 (0.04)	0.09 (0.02)	l.d.	0.12 (0.07)
SGD_{fresh} DIP Flux	$mol/m^2/day$	0.003 (0.003)	0.002 (0.001)	0.002 (0)	l.d.	0.003 (0.002)
SGD_{fresh} nutrient ratio	unitless	933:43:1	1485:43:1	481:43:1	l.d.	839:43:1
Air-Sea CO_2 Flux	$mmol/m^2/day$	38.4 (105.3, n= 34)	-10.8 (42.2, n= 34)	-16.7 (24.3, n= 34)	-137.8 (91.3, n= 12)	-35.4 (57.5, n= 30)
Metabolism						
Net Calcification	$mol/m^2/day$	-0.459 (1.733)	-0.051 (0.278)	0.002 (0.343)	l.d.	-0.007 (2.492)
(p-r)	$mol/m^2/day$	0.531 (2.338)	0.101 (0.896)	0.005 (0.042)	l.d.	-0.153 (1.24)
(Nfix-Nden)	$mol/m^2/day$	-0.048 (0.271)	-0.001 (0.026)	0.005 (0.042)	l.d.	-0.021 (0.188)

Table 4.14 - Mean (with standard deviation and number of samples in parentheses) of parameters used to estimate the gas transfer coefficient (k) used in CO_2 flux calculations and budgeting.

		WAI				UKU
Parameter	Units	June 05	January 06	February 06	March 07	March 07
Temperature	ºC	26.1 (1.2, n= 34)	25.6 (0.4, n= 34)	25.1 (1.1, n= 34)	24.9 (1.3, n= 32)	24.8 (1.4, n= 34)
Salinity	psu	32.2 (0.8, n= 34)	33.1 (0.7, n= 34)	30.8 (0.9, n= 34)	29.8 (0.8, n= 18)	35.7 (0.2, n= 34)
Wind speed	m/s	6.4 (3, n= 34)	3.2 (1.8, n= 34)	3.2 (1.6, n= 34)	7.6 (1.3, n= 34)	7.4 (2.3, n= 34)
Solubility (s)	mol/kg/atm	0.028 (0.001, n= 34)	0.028 (0, n= 34)	0.029 (0.001, n= 34)	0.029 (0.001, n= 16)	0.029 (0.001, n= 32)
Density (rho)	kg/m^3	1020.9 (0.7, n= 34)	1021.8 (0.5, n= 34)	1020.1 (0.8, n= 34)	1019.3 (0.5, n= 18)	1024 (0.5, n= 34)
Gas transfer coeff. (k)	m/day	13.4 (13.1, n= 34)	3.4 (4.2, n= 34)	2.8 (2.1, n= 34)	15.6 (5.3, n= 32)	16.2 (9.5, n= 34)

Table 4.15 - Net community primary production estimates from the literature for shallow tropical coastal systems.

Site	Net Community Production ($mol/m^2/day$)	Reference
Reef Flat	-0.22 - 0.31	Atkinson and Falter, 2003
Algal Pavement	0.00 - 0.13	Atkinson and Falter, 2003
High Coverage	-0.83 - 0.25	Atkinson and Falter, 2003
Sandy Areas	-0.04 - 0.03	Atkinson and Falter, 2003
Shallow Lagoon	-0.20 - 0.28	Atkinson and Falter, 2003
Entire Reef systems	0.00 - 0.07	Atkinson and Falter, 2003
Moorea, Tiahura Barrier Reef, French Polynesia	0.09 - 0.22	Gattuso et al., 1996
Yonge Reef, Great Barrier Reef	0.04 - 0.49	Gattuso et al., 1996
Moorea, Tiahura Barrier Reef, French Polynesia	-0.22 - 0.07	Sournia etal 1981
Moorea, Tiahura Barrier Reef, French Polynesia	0.08	Pichon 1985
Moorea, Tiahura Barrier Reef, French Polynesia	-0.15 - 0.10	Payri 1987
Moorea, Tiahura Barrier Reef, French Polynesia	0.002	Gattuso etal 1993
Discovery Bay, Jamaica	3.00	Pigott, Jefferson, Laughlin, 1988
Kavaratti Atoll reef flat	0.30	Qasim and Sankarana-rayanan 1970
Eniwetok Atoll algal flat	0.47	Smith and Marsh 1973
Kauai - coral-algal flat	0.06	Kohn & Helfrich 1957
Rongelap Atoll - coral-algal flat	0.03	Sargent & Austin 1949, 1954
One Tree Island lagoon reef	0.02	Kinsey 1972
Coconut Island, Hawaii coral-algal flat	-1.00	Gordon and Kelly 1962
Waipuilani, Maui, Hawaii	0.005 - 0.531	This study
Ukumehame, Maui, Hawaii	-0.153	This study

Table 4.16 - Net calcification estimates from the literature for shallow tropical coastal systems.

Location	Calcification (mol C /m^2/day)	Reference
Shiraho coral reef, Ishigaki Island, Ryukyus of Japan	0.100	Kayannne, et al., 1995
Moorea, Tiahura Barrier Reef, French Polynesia	0.186	Gattuso, et al., 1996
Yonge Reef, Great Barrier Reef	0.253	Gattuso, et al., 1996
Patch reef, HI	0.043 - -0.034	Yates and Halley, 2003
Patch reef, FL	0.011 - -0.013	Yates and Halley, 2003
Dense seagrass, FL	0.017 - -0.015	Yates and Halley, 2003
Coral rubble, HI	0.007 - -0.027	Yates and Halley, 2003
Sand bottom, HI	0.000 - -0.006	Yates and Halley, 2003
Sand bottom, FL	0.007 - -0.007	Yates and Halley, 2003
Moorea, Tiahura Barrier Reef, French Polynesia	0.000 - 0.016	Sournia etal 1981
Moorea, Tiahura Barrier Reef, French Polynesia	0.074	Pichon 1985
Moorea, Tiahura Barrier Reef, French Polynesia	-0.007 - 0.330	Payri 1987
Moorea, Tiahura Barrier Reef, French Polynesia	0.005 - 0.052	Le Campion-Alsumard et al 1993
Moorea, Tiahura Barrier Reef, French Polynesia	0.243	Gattuso etal 1993
Gulf of Aqaba	0.163	Barnes and Lazar 1993
Fanning Is. (complete reef system)	0.027	Smith and Pesret 1974
Canton Is. (complete reef system)	0.014	Smith and Jokiel 1975
One Tree Is. (complete reef system)	0.041	Kinsey 1977
Lizard Is. (complete reef system)	0.049	Kinsey and Davies 1979a
Christmas Is. (complete reef system)	0.003	Smith et al. 1985
Enewatak, Marshall Is. - outer reef slope	0.111	Smith and Harrison 1977
Discovery Bay, Jamaica (outer reef slope)	0.219	Kinsey 1982
Lizard Is. Patch reef	0.110	Kinsey 1979
Lizard Is. Laggon reef edge	0.139	Kinsey 1979
Kaneohe Bay fringe reef edge	0.246	Kinsey 1979
Kaneohe Bay, Hawaii Patch reefs	0.274 - 0.329	Kinsey 1979
Johnstone Is. Back-reef	0.274	Kinsey 1979
Rib Reef back-reef	0.274	Kinsey 1983b
Abrolhos coral shoal	0.320	Smith 1981
One tree Is (algal pavement)	0.110	Kinsey 1977
Lizard I. (algal pavevement)	0.066	Kinsey 1979
One Tree Is.	0.126	Kinsey 1972
Enewatak, Marshall Is. - Reef flat coral/algal zones	0.110	Smith 1973
Lizard Is.	0.110	LIMER Team 1976
One Tree Is. - Reef flat coral/algal zones	0.126	Kinsey 1977
Lizard Is - Reef flat coral/algal zones	0.126	Kinsey 1979
Lizard Is. - Reef flat coral/algal zones	0.085	Kinsey 1979
Moorea - Reef flat coral/algal zones	0.014	Sournia 1981
French Frigate Shoals - Reef flat coral/algal zones	~0.178	Atkinson & Grigg 1984
Rib Reef - Reef flat coral/algal zones	0.100	Barnes & Devereux 1984
Tulear (Madagascar) - Reef flat coral/algal zones	0.052	Pichon and Morrisey 1985
One Tree Is. - Shallow lagoonal environments	0.055	Kinsey & Domm 1974
One Tree Is. - Shallow lagoonal environments	0.041	Kinsey 1979
French Frigate Shoals- Shallow lagoonal environments	0.038	Atkinson & Grigg 1984
Enewatok, Marshal Is. (complete reef system)	0.110	Smith, SV 1974
Fanning Is. (complete reef system)	0.030	Smith, SV 1974
One Tree Is. , Great Barrier Reef	0.130	Kinsey 1973
Bahamas Bank	0.014	Broecker and Takahashi, 1966
Various	<0.274	Chave et al. 1972
Discovery Bay, Jamaica	0.096-0.219	Kinsey, 1981
Kaneohe Bay, Hawaii	0.033-0.274	Kinsey, 1981
Caribbean reefs (various sources)	0.274-0.329	Kinsey, 1981
Pacific reefs (various sources)	0.014-0.274	Kinsey, 1981
Ukumehame, Maui, Hawaii	-0.007	This study
Waipuilani, Maui, Hawaii	-0.459 - 0.002	This study

Table 4.17 - Air-sea CO_2 flux estimates from the literature for tropical and temperate estuaries and shallow tropical coastal systems. Negative fluxes denote gas transfer from water to the air.

Site	CO_2 Flux ($mmol/m^2/day$)	Reference
coral reef, Hog Reef, Bermuda	-3.3	Bates et al., 2001
coral reef,Okinawa Reef	-4.9	Ohde and Van Woesik, 1999
coral reef,Yonge Reef, Great Barrier Reef	-4.1	Frankignoulle et al., 1996
coral reef,Moorea, French Polynesia	-0.3	Frankignoulle et al., 1996, Gatuso et al., 1997, 1993)
Inner estuaries, Randers Fjord	-12.1	Gazeau et al., 2005
Inner estuaries, Lorie	-177.0	Abril et al., 2003, Abril et al., 2004
Inner estuaries, Elbe	-145.2	Frankignoulle et al., 1998
Inner estuaries, Rhine	-184.4	Frankignoulle et al., 1998
Inner estuaries, Thames	-108.8	Frankignoulle et al., 1998
Inner estuaries, Scheldt	-201.6	Frankignoulle et al., 1998
Inner estuaries, Tamar	-172.6	Frankignoulle et al., 1998
Inner estuaries, Gironde	-204.9	Frankignoulle et al., 1998
Inner estuaries, Douro	-84.4	Frankignoulle et al., 1998
Inner estuaries, Sado	-208.2	Frankignoulle et al., 1998
Inner estuaries, York River	-85.8	Raymond et al., 2000
Inner estuaries, Satilla River	-17.0	Cai and Wang, 1998
Inner estuaries, Hooghly	-116.4	Mukhopadhyay et al., 2002
Godavari	-14.0	Bouillon et al., 2003
Mandovi-Zuari	-38.9	Sarma et al.,, 2001
Outer estuaries, Scheldt	-5.2	Borges and Frankignoulle, 2002a
Outer estuaries, Amazon	1.4	Kortzinger, 2003
Outer estuaries, Kaneohe Bay, Hawaii	-4.1	Fagan and Mackenzie, 2007
Moorea, Tiahura Barrier Reef, French Polynesia	2.1 - -1.5	Frankignoulle, et al., 1996
Yonge Reef, Great Barrier Reef Australia	-2.7 - -6.5	Frankignoulle, et al., 1996
Moorea, Tiahura Barrier Reef, French Polynesia	0 - -114	Gattuso, et al., 1996
Yonge Reef, Great Barrier Reef Australia	-52 - -366	Gattuso, et al., 1996
Moorea, Tiahura Barrier Reef, French Polynesia	-1.5 - -2.0	Gattuso, et al., 1993
Fanning Island Lagoon	0 (+/- 0.06)	Smith 1974
Fanning Island Lagoon	-47.0	Smith and Pesret 1974
Canton Atoll	-1 - -12	Smith and Jokiel, 1976
Waipuilani, Maui, Hawaii	-238.3 - 393.6	This study
Ukumehame, Maui, Hawaii	-148.9 - 41.5	This study

4.8 LITERATURE CITED

Almgren, T., D. Dyrssen, and S. Fonselius. 1983. Determination of alkalinity and total carbonate, p. 99-123. In K. Grasshoff, M. Ehrhardt and K. Kremling [eds.], Methods of seawater analysis. Verlag Chemie, New York.

Aspila, K. I., H. Agemian, and S. Y. Chau. 1976. A semi-automated method for the determination of inorganic, organic and total phosphate in sediments. Analyst 101: 187-197.

Atkinson, M. J., and R. W. Bilger. 1992. Effects of water velocity on phosphate uptake in coral reef-flat communities. Limnology and Oceanography 37: 273-279.

Atkinson, M.J. and J.L. Falter. 2003. Coral Reefs. In: K.B.G. Shimmield (Editor), Biogeochemistry of marine systems. CRC Press, Boca Raton, Florida.

Atkinson, M.J. and S. V. Smith. 1983. C:N:P ratios of benthic marine plants. Limnology and Oceanography, 28(3): 568-574.

Bilger, R.W. and M.J. Atkinson. 1992. Anomalous mass transfer of phosphate on coral reef flats. Limnology and Oceanography, 37(2): 261-272.

Boudreau, B. P. 2000. The mathematics of early diagenesis: from worms to waves. Reviews of Geophysics 38: 389-416.

Capone, D., and J. Slater. 1990. Inter-annual patterns of water table height and groundwater derived nitrate in nearshore sediments. Biogeochemistry 10: 277-288.

Capone, D.G. and M.F. Bautista. 1985. A groundwater source of nitrate in nearshore marine sediments. Nature, 317: 214-216.

Cesar, H. et al. 2002. Economic valuation of the coral reefs of Hawai'i. Cesar Environmental Economics Consulting. Final Report. Arnhem , Netherlands, pp.

Chalker, B.E. D.L. and Taylor. 1978. Rhythmic variations in calcification and photosynthesis associated with the coral *Acropora cervicornis* (Lamarck). Proceedings of the Royal Society of London. Series B, Biological Sciences, 201(1143): 179-189.

Chisholm, J.R.M. and J.-P. Gattuso. 1991. Validation of the alkalinity anomaly technique for investigating calcification and photosynthesis in coral reef communities. Limnol. Oceanogr., 36(6): 1232-1239.

Crossland, C.J. et al. 2005. The Coastal Zone - a Domain of Global Interactions. In: C.J. Crossland, H.H. Kremer, H.J. Lindeboom, J.I. Marshall Crossland and M.D.A. Le Tissier (Editors), Coastal Fluxes in the Anthropocene. Springer-Verlag, Berlin Heidelberg, pp. 239.

Dailer, M. et al. 2010. Using $d^{15}N$ values in algal tissue to map locations and potential sources of anthropogenic nutrient inputs on the island of Maui, Hawai‘i, USA. Marine Pollution Bulletin, 60(5): 655-671.

De Goeij, J. M. et al. 2008. Organic matter cycling in tropical coral reef ecosystems: the role of the reef framework and its biota, dominated by encrusting sponges, Abstract 19-14. 11th International Coral Reef Symposium. Ft. Lauderdale, Florida.

Dickson, A. G. 1990. Standard potential of the reaction: AgCl(s)+1/2H2(g)-AG9s)+HCl(aq), and the standard acidity constant of the ion HSO4 in synthetic seawater from 273.15 to 318.15 K. J. Chem. Thermodyn. 22: 113-127.

---. 2001. Reference materials for oceanic CO2 measurements. Oceanography 14: 21-22.

Dickson, A. G., and F. J. Millero. 1987. A comparison of the equilibrium constants for the dissociation of carbonic acid in seawater media. Deep Sea Research 34: 1733–1743.

DOE. 1994. Handbook for the analysis of the various parameters of the carbon dioxide system in sea water, version 2, A. G. Dickson & C. Goyet, eds., ORNL/CDIAC-74

Dollar, S. J., and C. Andrews. 1997. Algal blooms off West Maui: Assessing causal linkages between land and the coast ocean. National Oceanic and Atmospheric Administration Coastal Ocean Program Office, Honolulu.

Dore, J. E. et al. 1996. Freezing as a method of sample preservation for the analysis of dissolved inorganic nutrients in seawater. Marine Chemistry 53: 173-185.

Dulaiova, H., and W. C. Burnett. 2007. Evaluation of the flushing rates of Apalachicola Bay, Florida via natural geochemical tracers. Marine Chemistry doi:10.1016/j.marchem.2007.09.001.

Falter, J. L., and F. J. Sansone. 2000a. Hydraulic control of porewater geochemistry within the oxic-suboxic zone of a permeable sediment. Limnology and Oceanography 45: 550-557.

---. 2000b. Shallow pore water sampling in reef sediments. Coral Reefs 19: 93-97.

Falter, J. L. 2002. Mass transfer limits to nutrient uptake by shallow coral reef communities. Ph.D. Dissertation, University of Hawaii, pp. 126.

Firing, Y.L. and M.A. Merrifield. 2004. Extreme sea level events at Hawaii: Influence of mesoscale eddies. Geophysical Research Letters, 31(L24306): 1-4.

Fletcher, C. H. et al. 2001-2003. Erosion hazard maps of the Kihei, Maui coastline, http://www.co.maui.hi.us/departments/Planning/erosion.htm, 1:3000. Accessed June 1, 2008.

Froelich, P.N. et al. 1979. Early oxidation of organic matter in pelagic sediments of the eastern equatorial Atlantic: suboxic diagenesis. Geochimica et Cosmochimica Acta, 43: 1075-1090.

Gesell, T.F. 1983. Background atmospheric ^{222}Rn concentrations outdoors and indoors: a review. Health Physics 45(2): 289-302.

Giambelluca, T.W., M.A. Nullet, and T.A. Schroeder. 1986. Rainfall Atlas of Hawai‘i, Report R76, Hawai‘i Division of Water and Land Development, Department of Land and Natural Resources, Honolulu. 267 pp.

Gordon, D.C.J. et al. 1996. LOICZ Biogeochemical modeling guidelines. LOICZ/R&S/95-5, LOICZ Core Project Netherlands Institute for Sea Research. Netherlands. 96 pp.

Gordon, L. I. et al. 1994. A suggested protocol for continuous flow automated analysis of seawater nutrients (phosphate, nitrate, nitrite and silicic acid) in the WOCE Hydrographic Program and the Joint Global Ocean Fluxes Study. In WOCE Operations Manual. WHP Office Report WHPO 91-1. WOCE Report No. 68/91. Revision 1. Woods Hole, Mass., U.S.A.

Hearn, C.J., M.J. Atkinson and J.L. Falter (2001) A physical derivation of nutrient-uptake rates in coral reefs: effects of roughness and waves. Coral Reefs, 20: 347-356.

Hebert, A.B., F.J. Sansone, and G.R. Pawlak. 2007. Tracer dispersal in sandy sediment porewater under enhanced physical forcing. Continental Shelf Research, 27(17): 2278-2287.

Herzfeld, I. et al. 2006. Diurnal Nutrient Dynamics Associated With a Nuisance Algal Bloom on South Maui, Hawaii. Eos Trans. AGU, 87(36), Ocean Sci. Meet. Suppl., Abstract OS54J-05, Hawaii.

Ho, David T. et al. 2006. Measurements of air-sea gas exchange at high wind speeds in the Southern Ocean: Implications for global parameterizations. Geophysical Research Letters, 33(L16611): 1-6.

Huettel, M. and G. Gust. 1992. Impact of bioroughness on interfacial solute exchange in permeable sediments. Marine Ecology Progress Series, 89: 253-267.

Huettel, M. et al. 2003. Hydrodynamical impact on biogeochemical processes in aquatic sediments. Hydrobiologia 494: 231-236.

Huettel, M., and I. T. Webster. 2001. Porewater flow in permeable sediments, p. 144-179. In B. P. Boudreau and B. B. Jorgensen [eds.], The benthic boundary layer. Oxford University Press. New York

Huettel, M., W. Ziebis, and S. Forster. 1996. Flow-induced uptake of particulate matter in permeable sediments. Limnology and Oceanography 41: 309-322.

Huettel, M. et al. 1998. Advective transport affecting metal and nutrient distributions and interfacial fluxes in permeable sediments. Geochimica et Cosmochimica Acta 62: 613-631.

Hunt , C. D. J. 2006. Ground-water nutrient flux to coastal waters and numerical simulation of wastewater injection at Kihei, Maui, Hawaii, p. 69. U.S. Geological Survey Scientific Investigations Report 2006–5283. Honolulu, Hawaii.

Ingall, E.D. and R.A. Jahnke. 1994. Evidence for enhanced phosphorus regeneration from marine sediments overlain by oxygen depleted waters. Geochimica et Cosmochimica Acta, 58(11): 2571-2575.

Ingall, E.D. and R.A. Jahnke. 1997. Influence of water-column anoxia on the elemental fractionation of carbon and phosphorus during sediment diagenesis. Marine Geology, 139: 219-229.

Keeling, C.D., H. Brix, and N. Gruber. 2004. Seasonal and long-term dynamics of the upper ocean carbon cycle at Station ALOHA near Hawaii. Glob. Biogeochem. Cycles, 18. GB4006, doi:10.1029/2004GB002227: 1:26.

Kinsey, D.W., 1978. Alkalinity changes and coral reef calcification. Limnol. Oceanogr., 23: 989-991.

Kobayashi, Noboru. 1970. Kihei Civic Development Plan. Prepared for Maui County Planning Commission. Wailuku, Maui. February.

Laws, E. A., D. Brown, and C. Peace. 2004. Coastal water quality in the Kihei and Lahaina districts of the island of Maui, Hawaiian Islands: Impacts from physical habitat and groundwater seepage: Implications for water quality standards. International Journal of Environment and Pollution 22: 531-546.

Lee, R.E. 2008. Phycology. Cambridge University Press, New York, 547 pp.

Leichter, J. and S.L. Miller. 1999. Predicting high-frequency upwelling: Spatial and temporal patterns of temperature anomalies on a Florida coral reef. Continental Shelf Research, 19: 911-928.

Lewis, E. and D. W. R. Wallace. 1998. Program Developed for CO2 System Calculations. ORNL/CDIAC-105. Carbon Dioxide Information Analysis Center.

Li, L., D.A. Barry, F. Stagnitti, and J.-Y. Parlange. 1999. Submarine groundwater discharge and associated chemical input to a coastal sea. Water Resources Research, 35(11): 3253-3259.

Liss, P., and L. Merlivat. 1986. Air-sea gas exchange rates: Introduction and synthesis, p. 113-127. In P. Buat-Menard [ed.], The role of air-sea exchange in geochemical cycling. NATO Science Series C, D. Reidel Pub. Co., Norwell, MA, U.S.A. 549 pp.

Millero, F. and M.L. Sohn. 1992. Chemical Oceanography. CRC Press. Boca Raton. 531pp.

Mehrbach, C. et al. 1973 Measurements of the apparent dissociation constants of carbonic acid in seawater at atmospheric pressure. Limnology and Oceanography 18:897-907.

Menge, B.A. et al. 2003. Coastal oceanography sets the pace of rocky intertidal community dynamics. Proceedings of the National Academies of Science, 100(21): 12229-12234.

Moore, W. S. 1976. Sampling 228Ra in the deep ocean. Deep Sea Research 23: 647-651.

---. 2000a. Ages of continental shelf waters determined from 223Ra and 224Ra. Journal of Geophysical Research 105: 22,117-122,122.

---. 2000b. Determining coastal mixing rates using radium isotopes. Continental Shelf Research 20: 1993-2007.

---. 2008. Fifteen years experience in measuring 224Ra and 223Ra by delayed-coincidence counting. Marine Chemistry 109: 188-197.

Moore, W. S., and R. Arnold. 1996. Measurement of 223Ra and 224Ra in coastal waters using a delayed coincidence counter. Journal of Geophysical Research 101: 1321-1329.

Moya, A. et al. 2006. Study of calcification during a daily cycle of the coral Stylophora pistillata: implications for 'light-enhanced calcification'. Journal of Experimental Biology, 209: 3413-3419.

Nightingale, P.D., P.S. Liss, and P. Schlosser. 2000a. Measurements of air-sea gas transfer during an open ocean algal bloom. Geophysical Research Letters, 27(14): 2117-2120.

Nightingale, P.D. et al., 2000b. In situ evaluation of air-sea gas exchange parameterizations using novel conservative and volatile tracers. Global Biogeochemical Cycles, 14(1): 373-387.

Oldham, C. E., and P. S. Lavery. 1999. Porewater nutrient fluxes in a shallow fetch-limited estuary. Marine Ecology Progress Series 183: 39-47.

Patrick, W.H., Jr. and R.A. Khalid. 1974. Phosphate release and sorption by soils and sediments: Effect of aerobic and anaerobic conditions. Science, 186(4158): 53-55.

Paytan, A. et al. 2006. Submarine groundwater discharge: An important source of new inorganic nitrogen to coral reef ecosystems. Limnology and Oceanography, 51(1): 343-348.

Pigott, J. D., and J. E. Laughlin. 1988. Carbon dioxide budget of a modern tropical lagoon. In Choat, J.H., Barnes, MA. Borowitzka, J.C. Coll, P.J.Davies, P. Flood, B.G. Hatcher, D. Hopley, P.A. Hutchings, D. Kinsey, G.R. Orme, M. Pichon, P.F. Sale, P. Sammarco, C.C. Wallace, C. Wilkinson, E. Wolanski and O. Bellwood (eds.) Proceedings of the 6th International Coral Reef Symposium: Vol. 2: Contributed Papers. Townsville, Australia. p. 569-575.

Precht, E., and M. Huettel. 2003. Advective pore-water exchange driven by surface gravity waves and its ecological implications. Limnology and Oceanography 48: 1674-1684.

---. 2004. Rapid wave-driven advective pore water exchange in a permeable coastal sediment. Journal of Sea Research 51: 93-107.

Rama, and W. S. Moore. 1996. Using the radium quartet for evaluating groundwater input and water exchange in salt marshes. Geochimica et Cosmochimica Acta 60: 4645-4652.

Rii, Y.M. et al. 2008. The transient oasis: Nutrient-phytoplankton dynamics and particle export in Hawaiian lee cyclones. Deep Sea Research Part II: Topical Studies in Oceanography, 55: 1275-1290.

Redfield, A.C. 1934. On the proportions of organic derivates in seawater and their relation to the composition of plankton. Woods Hole Oceanographic Institution. Contribution No. 30.

Reimers, C. E. et al. 2004. In situ measurements of advective solute transport in permeable shelf sands. Continental Shelf Research 24: 183-201.

Rooney, J. J. B., and C. H. Fletcher. 2005. Shoreline change and Pacific climatic oscillations in Kihei, Maui, Hawaii. Journal of Coastal Research 21: 535-547.

Rusch, A., and M. Huettel. 2000. Advective particle transport into permeable sediments-evidence from experiments in intertidal sandflats. Limnology and Oceanography 45: 525-533.

Rusch, A. et al. 2006. Benthic oxygen consumption and organic matter turnover in organic-poor, permeable shelf sands. Aquatic Geochemistry 12: 1-19.

Shum, K.T. 1993. The effects of wave-induced pore water circulation on the transport of reactive solutes below the rippled sediment bed. Journal of Geophysical Research, 98(C6): 10,289-10,301.

Slater, J.M. and D.G. Capone. 1987. Denitrification in aquifer soil and nearshore marine sediments influenced by groundwater nitrate. Applied and Environmental Microbiology, 53(6): 1292-1297.

Smith, C. M. and J.E. Smith. 2006. Algal blooms on Maui. A final report to the City and County of Maui and the Environmental Protection Agency. 75 pp.

Smith, S.V. and G.S. Key. 1975. Carbon dioxide and metabolism in marine environments. Limnol. Oceanogr., 20: 493-495.

Storlazzi, C. D. et al. 2004. Wave- and tidally-driven flow and sediment flux across a fringing coral reef: Southern Molokai, Hawaii. Continental Shelf Research 24: 1397-1419.

Tribble, G. W. et al. 1992. Hydraulic exchange between a coral reef and surface sea water. Geological Society of America Bulletin 104: 1280-1291.

Umezawa, Y. et al. 2008. Potential effects of terrestrial nutrients in submarine groundwater discharge on macroalgal blooms in a fringing reef ecosystem. In M. Taniguchi [ed.], From headwater to the ocean: Hydrological change and water management - Hydrochange 2008. CRC Press. Boca Raton, Florida. 696 pp.

U.S. Census Bureau. 2000. http://www.census.gov/main/www/cen2000.html. Accessed April 2009.

Valiela, I. et al. 1980. On the measurement of tidal exchanges and groundwater flow in salt marshes. Limnology and Oceanography, 25(1): 187-192.

Valiela, I. et al. 1990. Transport of groundwater-borne nutrients from watersheds and their effects on coastal waters. Biogeochemistry, 10: 177-197.

Valiela, I. et al. 1997. Nitrogen loading from coastal watersheds to receiving estuaries: New method and application. Ecological Applications, 7(2): 358-380.

van Beukering, P. J. H. and H. S. J. Cesar. 2004. Ecological economic modeling of coral reefs: Evaluating tourism overuse at Hanauma Bay and algae blooms at the Kihei Coast, Hawai'i. Pacific Science 58: 243-260.

Van Der Loeff, M. M. R. 1981. Wave effects on sediment water exchange in a submersed sand bed. Netherlands Journal of Sea Research 15: 100-112.

Van Der Loeff, M. M. R. et al. 1981. Sediment water exchanges of nutrients and oxygen on tidal flats in the EMS-Dollard estuary. Netherlands Journal of Sea Research 15: 113-129.

Wanninkhof, R. 1992. Relationship between wind speed and gas exchange over the ocean. Journal of Geophysical Research 97: 7373-7382.

Wanninkhof, R. and W.R. McGillis. 1999. A cubic relationship between air-sea CO_2 exchange and wind speed Geophysical Research Letters 13: 1889-1892.

Webb, J. E., and J. Theodor. 1968. Irrigation of submerged marine sands through wave action. Nature 220: 682-683.

Webster, I. T. 2003. Wave enhancement of diffusivities within surficial sediment. Environmental Fluid Dynamics 3: 269-288.

Webster, I. T. et al. 1996. Solute exchange by convection within estuarine sediments. Estuarine, Coastal and Shelf Science 42: 171-183.

Webster, I. T., and J. H. Taylor. 1992. Rotational dispersion in porous media due to fluctuating flows. Water Resources Research 28: 109-119.

Wild, C. et al. 2004a. Degradation and mineralization of coral mucus in reef environments. Marine Ecology Progress Series 267: 159-171.

Wild, C., R. Tollrian, and M. Huettel. 2004b. Rapid recycling of coral mass-spawning products in permeable sediments. Marine Ecology Progress Series 271: 159-166.

CHAPTER V – OVERALL CONCLUSIONS

The relationship between nutrient dynamics at the land-ocean interface and nearshore macroalgal blooms is complex. For example, episodic *Cladophora sericea* macroalgal blooms observed along northwest Maui, Hawaii, appear to be the result of sedimentary and fresh groundwater nutrient loads exacerbated by relatively long water residence times along the coast. Results from our studies suggest that, during the 2001 *C. sericea* bloom, sediment porewater nutrients delivered to coastal waters could have accounted for all of the P required by the macroalgae, but only <5% of the N. Macroalgal N requirements must have been met by external nutrient sources (i.e., either N_2-fixation or wastewater inputs).

Changing oceanic circulation along the main Hawaiian Islands can affect water residence times along different local embayments, resulting in episodes of optimal conditions for macroalgal growth due to increased nutrient retention within the coastal zone. Hypothesized interactions between wind, waves, and rainfall, and their effect on coastal zone nutrient loads and residence time, were tested using historical datasets (Chapter 2). Historical data (waves and rainfall, wind) were used as proxies for nutrient inputs and water residence time. A simple model (Bloom Index) constructed from a hypothesized relationship between these variables appears to predict periods of high macroalgal overgrowth along the West Maui coastal zone (Chapter 2). Our results suggest that natural and anthropogenic factors increase the probability for optimal macroalgal growth conditions to develop along this region, resulting in episodic blooms. Thus, although nitrogen loading to the coastal zone, and the regional effects of local water circulation, may control the extent and episodic nature of biomass buildup

observed during blooms, reductions in phosphorus loading to the coastal zone may be critical in the ultimate reduction of regional eutrophication (Tyrrell 1999).

Simultaneous time-series observations of surface water chemistry along different Maui coastal sites indicate that interactions between physical factors (i.e., waves, tides, wind, and currents) and coastal geomorphology regulate the temporal variability of dissolved nutrients, whereas anthropogenic factors appear to control the spatial variability of nutrient enrichment along the coast (Chapter 3). Results presented in this dissertation indicate that the northern Kihei sites (NWAI, WAI, and KAL) experience higher nutrient-rich submarine groundwater discharge compared to sites further north or south. Chronic occurrence of macroalgal blooms along southwest Maui seem to result from frequent optimal growth conditions maintained by periodic groundwater nutrient loads to a region experiencing greater apparent water residence times (Chapter 4).

This work further indicates that, although groundwater-derived nutrient enrichments and their interactions with coastal water circulation can determine the spatiotemporal variability of macroalgal blooms, difficulties still arise when one attempts to assess the net metabolic state of the coastal zone (Chapter 4). For example, physical factors affect the interactions between land-ocean-atmosphere CNP reservoirs, profoundly affecting non-conservative nutrient fluxes and their impact on the metabolic function of the Maui coastal zone. Spatiotemporal variability of the physicochemical interactions along the proximal coastal zone can result in drastically different coastal water nutrient regimes on time scales of hours and, on average, during different parts of the year. It is concluded that, in order to best detect change in the metabolic state of a coastal zone, the mean metabolic state should be established a priori. Time-series measurements of more than a

few days in duration, simultaneously capturing the physical, biological, and chemical conditions interacting within the coastal zone, are required in order to fully characterize the true mean net metabolic state of this coastal zone.

LITERATURE CITED

Tyrrell, T., 1999. The relative influences of nitrogen and phosphorus on oceanic primary production. Nature, 400: 525- 531.

APPENDIX A – Photo Plates


1

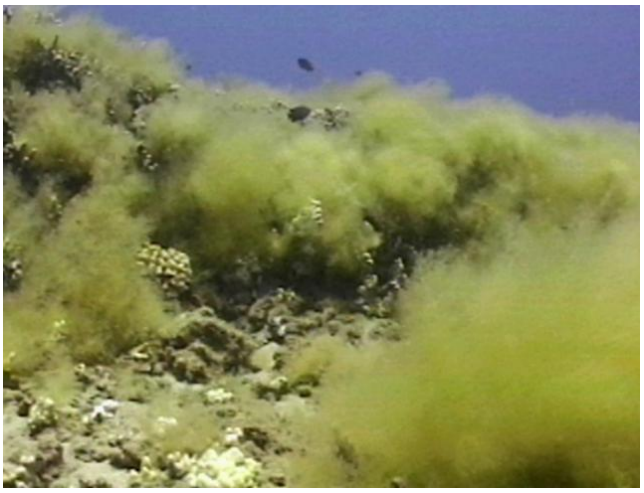
2

Plate A1 - Reef before (1) and during (2) the 1998 *C. sericea* bloom off Honokowai, Maui. Photographs 1 and 2 were taken at approximately the same location. Photo credits: Peter Bennett and Ursula Keuper-Bennett.

Plate A2 - Diver swimming through *Halimeda incrassata* meadows during summer 1989 *C. sericea* bloom at Honokowai, Maui. Photo credits: Peter Bennett and Ursula Keuper-Bennett.

Plate A3 - Honokowai Halimeda meadows covered with *C. sericea* during the summer 2000 bloom. Photo credits: Peter Bennett and Ursula Keuper-Bennett.

Plate A4 - Diver under *C. sericea* bloom during summer 2000 bloom off Honokowai, Maui. Photo credits: Peter Bennett and Ursula Keuper-Bennett.

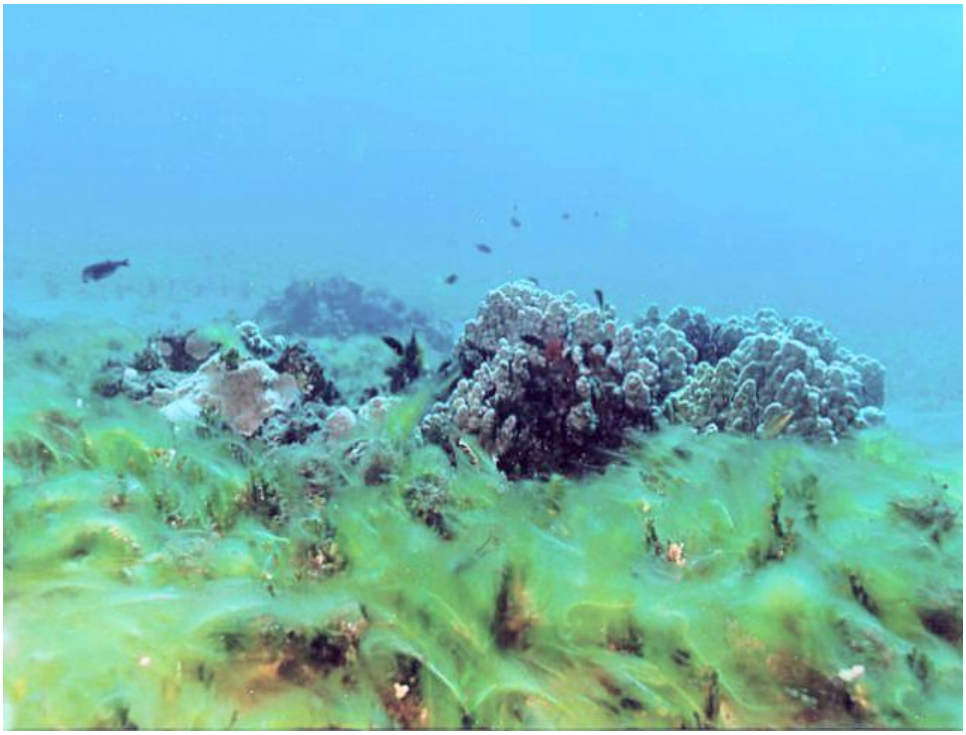

Plate A5 - Honokowai reef covered with *C. sericea* during the summer 1999 bloom. Photo credits: Peter Bennett and Ursula Keuper-Bennett.

APPENDIX B – Ancillary Correlation Plots

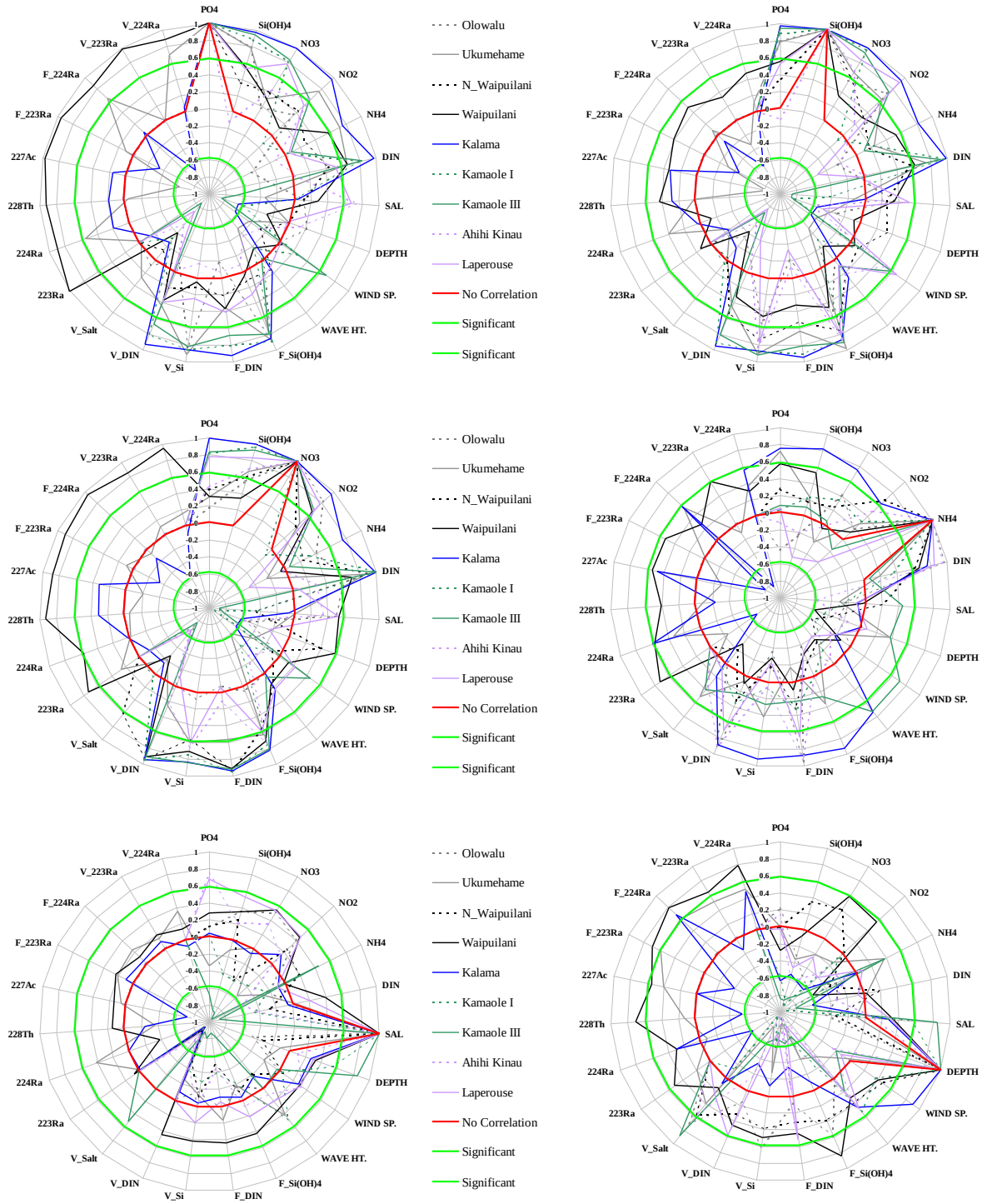

Figure AB2.1 – Correlation coefficient for all sites. Red arrow points to parameter being correlated with all others. Region between inner and outer green circles represent correlations not significant at the alpha 0.05 level of significance.

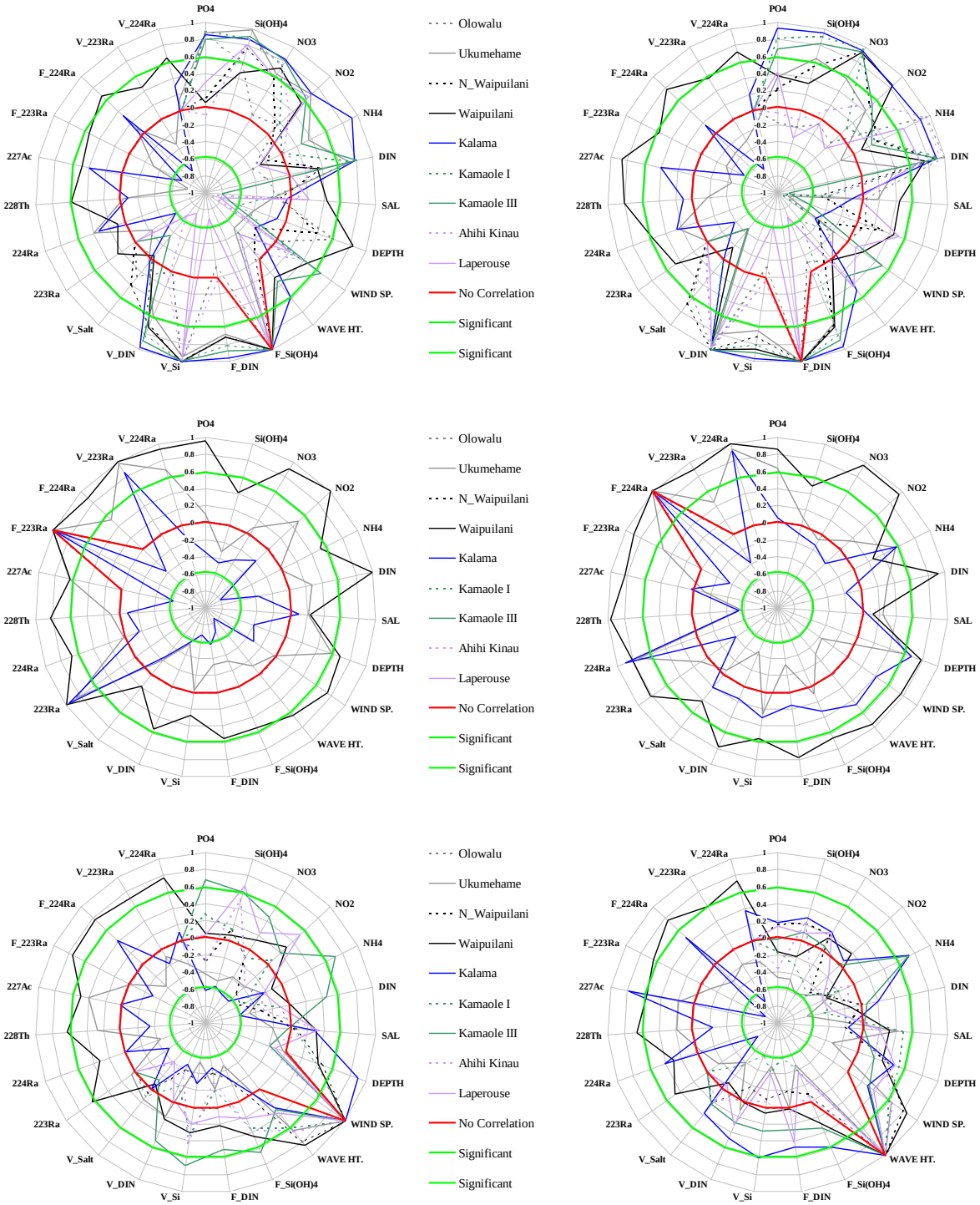

Figure AB2.2 – Correlation coefficient for all sites. Red arrow points to parameter being correlated with all others. Region between inner and outer green circles represent correlations not significant at the alpha 0.05 level of significance.

APPENDIX C

Table AC-1 - Summary of all spatiotemporal data collected at WAI and UKU.

	Waipulani					Ukumehame
	March 2005	**June 2005**	**January 2006**	**February 2006**	**March 2007**	**March 2007**
General						
Sampling dates	3/25-26/2005	6/22-24/2005	1/25-27/2006	2/1-3/2006	3/11-13/2007	3/17-19/2007
Season	Winter	Summer	Winter	Winter	Winter	Winter
Start time	18:00	15:00	12:00	12:00	13:00	12:00
Stop time	18:00	15:00	12:00	12:00	13:00	12:00
Total sample time (hrs)	24	48	48	48	48	48
Discrete sampling period (hrs)	2	3	3	3	3	3
Site water column sampled (WC)	A and B	A and B	A, B, C (bottom/top), D (bottom/top)	A and B	A, B, C (bottom/top), D (bottom/top)	A, B, C (bottom/top), D (bottom/top)
Site porewater sampled (PW) (-7 and -25 cm)	A	A and B	A and B	A and B	A and B	A and B
Discrete sample analyses (WC and PW)						
DIC (mmol/kg)		✓	✓	✓	✓	✓
Total alkalinity (mmol/kg)		✓	✓	✓	✓	✓
PO_4	✓	✓	✓	✓	✓	✓
Si	✓	✓	✓	✓	✓	✓
NO_3	✓	✓	✓	✓	✓	✓
NO_2	✓	✓	✓	✓	✓	✓
NH_4	✓	✓	✓	✓	✓	✓
223, 224, 226, 228Ra			20L (A, and B)		100L (A), 20L (B, C, and D)	100L (A), 20L (B, C, and D)
Pigments (Chla and Phaeo)		✓	✓			
TSS (mg/L)		✓ A and B	✓ A and B	✓ A and B		
Mn fiber field equilibrations (24 hr)			A, B, C, and D		A, B, C, and D	A, B, C, and D
Continuous data						
Salinity (PSU)	✓ 2hrs (A and B)	✓ 30s (B only)		✓ 10 min (A and B)	✓ 10 min (B and C)	✓ 10 min (B only)
Temperature (ºC)	✓ 2hrs (A and B)	✓ 30s (B only)		✓ 10 min (A and B)	✓ 10 min (B and C)	✓ 10 min (B only)
Dissolved oxygen (% and mg/l)	✓ 2hrs (A and B)	✓ 30s (B only)		✓ 10 min (A and B)	✓ 10 min (B and C)	✓ 10 min (B only)
pH	✓ 2hrs (A and B)	✓ 30s (B only)		✓ 10 min (A and B)	✓ 10 min (B only)	✓ 10 min (B only)
Turbidity (NTU)		✓ 30s (B only)		✓ 10 min (A and B)		
Rn timeseries					✓ 30 minutes (A only)	✓ 30 minutes (A only)
Chla					✓ 10 min (B only)	✓ 10 min (B only)
Tide height (cm)	✓	✓	✓	✓	✓	✓
Water depth (cm)		✓ 30s			✓	✓
Wind speed (m/s)		✓ 5min	✓ 5min	✓ 5min	✓ 5min	✓ 5min
Wind direction (degrees)		✓ 5min	✓ 5min	✓ 5min	✓ 5min	✓ 5min
Quanta ($\mu mol\ m^{-2}\ s^{-1}$), PAR		✓ 5min	✓ 5min	✓ 5min	✓ 5min	✓ 5min
Current velocity (m/s)		✓ 5 sec, C and Fish Pond	✓ B and C. 30min/60sec/1Hz	✓ B and C. 30min/60sec/1Hz	✓ B, C, and D 30min/60sec/1Hz	✓ B, C, and D 30min/60sec/1Hz
Current direction (degrees)		✓ 5 sec, C	✓ B and C. 30min/60sec/1Hz	✓ B and C. 30min/60sec/1Hz	✓ B, C, and D. 30min/60sec/1Hz	✓ B, C, and D. 30min/60sec/1Hz
Wave height (m)		✓ 2-3 Hz	✓ B and C. 1hr/20min/1Hz	✓ B and C. 1hr/20min/1Hz	✓ B, C, and D. 1hr/20min/1Hz	✓ B, C, and D. 1hr/20min/1Hz
Wave period (s)		✓ 2-3 Hz	✓ B and C. 1hr/20min/1Hz	✓ B and C. 1hr/20min/1Hz	✓ B, C, and D. 1hr/20min/1Hz	✓ B, C, and D. 1hr/20min/1Hz
Biological data						
Algal growth (mg dry/hr)		✓	✓		✓	✓
Tissue analysis (CNP)		✓	✓			
Algal biomass ($g\ m^{-2}$)		✓	✓			